Susan Elizabeth Critchley, B.Eng

Towards 3D bioprinting of anatomically accurate, mechanically reinforced cartilage templates for biological joint resurfacing

Trinity College Dublin, 2017

A thesis submitted to the University of Dublin in partial fulfilment of the requirements for the degree of

Doctor in Philosophy

Supervisor: Prof. Daniel J. Kelly

Internal examiner: Assoc. Prof. Bruce Murphy

External examiner: Prof. Lorenzo Moroni

Declaration

I declare that this thesis has not been submitted as an exercise for a degree at this or any other university and is entirely my own work. I agree to deposit this thesis in the University's open access institutional repository or allow the library to do so on my behalf, subject to Irish Copyright Legislation and Trinity College Library conditions of use and acknowledgement.

_____

Susan Critchley

Summary

Osteoarthritis (OA) is a pervasive disease worldwide which affects the articular cartilage and the underlying bone in synovial joints such as the knee. Currently, the only treatment for a severely degenerated knee joint is a total or partial joint replacement with a metal and polymer prosthesis. Whilst these procedures are well established, failures are not uncommon resulting in a more complicated revision surgery. The aging worldwide population and the increase in the instances of younger patients being diagnosed with OA are primary motivations behind the pursuit of new treatment options. Tissue engineering approaches have been gaining traction in recent years, having being successfully translated to the clinic to treat small focal defects. These therapies combine cells, scaffolds and signalling molecules to drive tissue formation and maturation to regenerate damaged tissues. 3D printing technology can be used in tandem with tissue engineering strategies to fabricate constructs that mimic the shape and function of a joint and to accurately position cells and biological cues within such biological implants.

The overall objective of this thesis is to tissue engineer an anatomically accurate, mechanically reinforced biological implant for total joint regeneration. To this end, this thesis set out to investigate the following; 1) whether a developmentally inspired cartilage template formed through *in vitro* priming of bone marrow derived stem/stromal cells (BMSCs) in an alginate hydrogel can be used to regenerate a critically sized osteochondral defect; 2) to identify suitable cell sources derived from OA joints for hyaline cartilage tissue engineering; 3) to identify a suitable thermopolymer that can be 3D printed to mechanically reinforce cartilage templates and subsequently engineer bi-layered cartilage templates with a top chondral layer containing a co-culture of mesenchymal stromal/stem cells (MSCs) and chondrocytes and a bottom endochondral layer of BMSCs, and to then evaluate these constructs *in vivo* subcutaneously in nude mice and within caprine osteochondral defetcs; 4) to develop a technique to biofabricate an anatomically accurate, mechanically reinforced, bi-layered cartilage template for whole joint resurfacing.

The thesis began by investigating if a tissue engineered cartilage template could undergo spatially defined differentiation to form bone and cartilage in a critical sized osteochondral defect in a rabbit model. The osteochondral unit develops postnatally from a cartilaginous precursor that undergoes endochondral ossification during skeletal maturation. Evaluation after 3 months demonstrated that the engineered cartilage template can enhance osteochondral repair, although consistent hyaline cartilage regeneration was not observed, suggesting room for further improvement.

Co-cultures of chondrocytes and MSCs are commonly used to enhance chondrogenesis. Recognising that the proposed biological implant is targeted toward patients with OA, the next part of the thesis examined the potential to use co-cultures of cells derived from osteoarthritic joints for cartilage tissue engineering. A co-culture of freshly isolated or culture expanded chondrocytes and infrapatellar fat pad derived MSCs underwent robust chondrogenesis when maintain in low oxygen.

The next stage of the thesis examined mechanically reinforcing the cartilage templates with 3D printed thermopolymers, specifically either PCL, PLA, PLGA (85:15 and 65:35). Whilst

all of the polymers supported the chondrogenic phenotype, only PCL maintained its mechanical properties over the 4 weeks of *in vitro* culture and therefore was chosen as the reinforcing network for the remainder of this thesis. PCL reinforced bi-layered engineered cartilage templates, consisting of a top layer of MSCs and CC co-culture in either alginate or agarose, and bottom layer of BMSCs in alginate, were capable of supporting hyaline cartilage and vascularised bone respectively. The top cartilage layer formed with agarose best suppressed mineralisation and therefore, was chosen as the material to support cartilage formation in a goat model.

Prior to evaluating the reinforced bi-layered cartilage template in a goat model, expansion and differentiation conditions of goat BMSC were optimised. 5% oxygen tension and high glucose availability were identified as the optimal conditions for expanding and differentiating goat BMSCs. Using these culture conditions the bi-layered template was primed *in vitro* preceding implantation in a critical sized defect in both the medial femoral condyle and the trochlear ridge. After 6 months the bi-layered scaffold supported hyaline-like repair, however, there was some animal to animal variability in the quality of bone repair pointing to areas for improvement in the design of future implants.

Finally a strategy using 3D printing was implemented to develop a tissue engineered, anatomically accurate biological implant for knee joint regeneration. An implant mimicking the geometry of a rabbit medial femoral condyle was printed using the geometrical information obtained from a CT scan of a rabbit knee. BMSC encapsulated in a GelMA bioink were used to engineer a hypertrophic cartilage tissue within the osseous layer. To cover the curved surface of the scaled-up implant, GelMA containing a co-culture of BMSCs and CCs was deposited in droplets on the uneven surface of the osseous region of the implant. The reinforcement frame had mechanical properties exceeding the compressive loads assumed to exist in a rabbit joint. However, three months after implantation of the scaled-up implant, it was observed that the scaffolds had failed mechanically. In most cases it appeared that this was due to delamination of the body of the implant from the stem.

To conclude this thesis describes a novel approach for the regeneration of whole joints by utilising developmental processes to direct repair of both articular cartilage and bone. Additionally, a suitable cell source for engineering articular cartilage using cell derived from OA joints has been identified. This work demonstrates how a combination of 3D printing and tissue engineering strategies can be used to engineer biological implants for synovial joint regeneration.

Acknowledgements

I would like to express my gratitude to Prof. Danny Kelly who has been the most wonderful and encouraging supervisor. Through his constant guidance, support, positivity and advice he has helped to navigate me through this, often stormy journey. On many an occasion I would arrive to his office feeling gloomy and frustrated with my heels dragging, and without fail I would leave it feeling energised ready to begin a new study or excited about my current data. I very much valued those meetings and from them I have learned to remain positive which is a quality which will benefit me greatly. I could not have imagined having a better advisor and mentor.

I would like to thank my funding Science foundation Ireland, without it none of this work would have been possible. I would also like to thank my examiners Professor Bruce Murphy and Professor Lorenzo Moroni for their taking the time to read my thesis and for their comments and suggestions.

I would also like to acknowledge the members of the TCBE whom have been part of my journey. They made the lab environment exciting and stimulating to work in, both academically and personally. Everyone was so willing to help or to share their knowledge, and on a personal level, 'up for a bit of craic' at lunch or after work. Having been at this lab for just over 4 years I have seen some wonderful people come and go, it has been a privilege to learn from them and their academic successes have driven me to strive for more. I would especially like to thank Dr. Masooma Naqvi, my coffee buddy for the greater part of my PhD, whose exuberance, opinions and chats were certainly the highlight of my morning…afternoon….and tea break!

Within the Kelly lab I would especially like to thank a number of people, the newly crowned Dr Tommy Gonzalez-Fernandez whose Latino flair and humour were always welcomed! Pedro, the animal whisperer, who without exception always had sound advice, a constant willingness to help and the most thought-provoking conversations. Rossana, who put up with my barrage of banter and was a wonderful support during my final few months especially from her Italian packages that kept me well fed and watered. Deviating slightly from the Kelly lab; to 'The Squad' members, Dinorath and Jenny, thank you for all of your support, enjoyable nights together and delightful company that made my days in the lab much brighter and more enjoyable. I would also like to acknowledge *newbie* Sophia, who has been a great confident and always had a good story to tell. Finally, thank you to Bruce, who put in a 'monster' effort to help in the end, his positivity and readiness to help without complaint was a god-send. I am lucky to have met such great people during my PhD.

I would particularly like to acknowledgement to Dr. Gráinne Cunniffe whose guidance, support, encouragement, positivity, and advice kept me above water on many occasions. She was always on-hand to help me work through issues and problems, never giving up until a solution was found, she gave me sound advice on how to formulate my studies and encouraged me greatly when things weren't going so well. The effort she put in to help organise the animal studies is unparrelled and much of this thesis would not have been possible without her.

Outside of the lab I would like to thank my housemates Michael and Paddy for listening to my presentation rehearsals and for putting up with both my excitement and grumpiness (depending on the day). Thank you too for making my transition to Dublin easier and making it feel like home.

I would finally like to thank my family whose unwavering support has made it possible for me to do this PhD. Their positive influence and sacrifices made for me throughout my entire life has allowed me to arrive to this point. Particularly to my dad, whose career in research inspired me to pursue this path, I know that he would be proud of me, and that whilst he is no longer physically here, his spirit has enshrouded me with a curtain of strength, solace and love. I am very grateful to my sister, Jenny, who encouraged me throughout the challenges I have faced both personally and academically and for bringing me on some wonderful holidays. I would like to thank my mum for giving me the tools to overcome obstacles, she has been an inspiration displaying great strength. She always put my needs first and gave me the space and encouragement to explore what it was I wanted to do. Lastly, I would like to thank my boyfriend Eoin, whose daily insurmountable patience and encouragement was and is much appreciated. He kept my spirits during the rough long evenings in the lab with spontaneous, kind, thoughtful gifts or surprise dinners. His belief in me and the level of support he gave to me cannot be transcribed, I hope to one day repay him in kind.

Table of Contents

SUMMARY ..... **I**

ACKNOWLEDGEMENTS ..... **III**

TABLE OF CONTENTS ..... **V**

LIST OF FIGURES ..... **X**

LIST OF TABLES ..... **XV**

NOMENCLATURE ..... **XVI**

PUBLICATIONS ..... **XVIII**

CONFERENCE ABSTRACTS ..... **XIX**

1 INTRODUCTION **1**

1.1 THE CLINICAL NEED FOR NEW THERAPIES TO TREAT OSTEOARTHRITIS 1

1.2 TISSUE ENGINEERING FOR SYNOVIAL JOINT REGENERATION 2

1.3 3D BIOPRINTING FOR BONE AND JOINT REGENERATION 3

1.4 THESIS OBJECTIVES 5

2 LITERATURE REVIEW **8**

2.1 INTRODUCTION 8

2.2 THE KNEE JOINT 8

2.3 ARTICULAR CARTILAGE 8

2.3.1 Extracellular Matrix Components *10*

2.3.2 Fluid *12*

2.3.3 Mechanical Properties *12*

2.3.4 Confined Compression *13*

2.3.5 Unconfined Compression *15*

2.3.6 Indentation Testing *15*

2.4 STRUCTURE AND COMPOSITION OF SUBCHONDRAL BONE 15

2.5 INJURY TO ARTICULAR CARTILAGE AND SUBCHONDRAL BONE 18

2.5.1 Pathogenesis of OA *18*

2.6 CLINICALLY AVAILABLE THERAPIES FOR TREATING FOCAL CARTILAGE DEFECTS 19

2.7 TISSUE ENGINEERING 22

2.8 TISSUE ENGINEERING ARTICULAR CARTILAGE 22

2.8.1 Cell Sources *22*

2.8.2 Biomaterials *23*

2.8.3 Growth Factors *25*

2.9 ENDOCHONDRAL BONE TISSUE ENGINEERING 26

2.9.1 Cell Sources 26
2.10 3D BIOPRINTING 26
2.10.1 Bioinks and Printability 28
2.10.2 Bioprinting Articular Cartilage 29
2.10.3 3D Printing Biological Whole Joints 33
2.11 SUMMARY 35
3 GENERAL METHODS 36
3.1 BONE MARROW MESENCHYMAL STEM/STROMAL CELLS (BMSCS) ISOLATION AND CULTURE 36
3.2 INFRAPATELLAR FAT-PAD STEM CELLS (FPSCS) ISOLATION AND CULTURE 36
3.3 CHONDROCYTE (CCS) ISOLATION AND CULTURE 37
3.4 CHONDROGENIC PRIMING 37
3.5 FORMATION OF PELLETS 37
3.6 ENCAPSULATION IN RGD-Γ-IRRADIATED ALGINATE 37
3.7 GELATIN METHACRLYDE (GELMA) SYNTHESIS 38
3.8 HISTOLOGY AND IMMUNOCHEMISTRY 38
3.9 QUANTITATIVE BIOCHEMICAL ANALYSIS 39
3.10 3D PRINTING PROCESS 40
3.11 STATISTICS 40
4 REGENERATION OF OSTEOCHONDRAL DEFECTS BY SPATIALLY RESTRICTING ENDOCHONDRAL OSSIFICATION WITHIN ENGINEERED CARTILAGE GRAFTS 41
4.1 INTRODUCTION 41
4.2 MATERIALS AND METHODS 43
4.2.1 Cell isolation and expansion 43
4.2.2 Engineering of the Cartilage Template 43
4.2.3 Biochemical, histological and Immunohistochemical analysis 43
4.2.4 Cartilage template implantation 43
4.2.5 Histological Scoring 44
4.2.6 Mechanical Testing 46
4.2.7 Micro-computed tomography 46
4.2.8 Statistical Analysis 46
4.3 RESULTS 47
4.3.1 RGD functionalized, γ-irradiated alginate hydrogels support the development of a cartilage template in vitro 47
4.3.2 Treatment of OC defects with an engineered cartilage template results in the development of a stiffer repair tissue 48
4.3.3 Engineered cartilage templates promote the development of a more hyaline cartilage-like repair tissue in osteochondral defects 50

4.4 DISCUSSION 52
4.5 CONCLUDING REMARKS 53

5 LOW OXYGEN CONDITIONS PROMOTE SYNERGISTIC INCREASES IN CHONDROGENESIS DURING CO-CULTURE OF HUMAN OSTEOARTHRITIC STEM CELLS AND CHONDROCYTES 54

5.1 INTRODUCTION 54
5.2 MATERIALS AND METHODS 56
5.2.1 Cell isolation and expansion 56
5.2.2 Chondrogenesis in pellet culture 56
5.2.3 Biochemical, histological and immunohistochemistry analysis 56
5.2.4 Interaction index 57
5.2.5 Immunohistochemistry quantification 57
5.2.6 Statistics 57
5.3 RESULTS 58
5.3.1 Cartilage matrix synthesis is enhanced within hypoxic co-cultures 58
5.3.2 Oxygen levels determine the specific types of collagen produced in a co-culture 60
5.3.3 Combining BMP-7 with TGF-β3 does not significantly enhance the cartilage matrix 61
5.4 DISCUSSION 63
5.5 CONCLUDING REMARKS 66

6 ENGINEERED SOFT TISSUE TEMPLATES REINFORCED BY 3D PRINTED THERMOPLASTICS FOR OSTEOCHONDRAL TISSUE ENGINEERING 67

6.1 INTRODUCTION 67
6.2 MATERIALS AND METHODS 70
6.2.1 3D printing process 70
6.2.2 Cell isolation and expansion 70
6.2.3 Formation of the reinforced soft tissue templates 71
6.2.4 Cartilage template implantation 72
6.2.5 Mechanical testing 72
6.2.6 Fibre swelling analysis 73
6.2.7 Biochemical, histological and immunohistochemistry analysis 73
6.2.8 Statistics 73
6.3 RESULTS 73
6.3.1 Mechanical properties of 3D printed PCL, PLA and PLGA scaffolds 73
6.3.2 Chondrogeneis within alginate hydrogels reinforced with networks of 3D printed PCL, PLA and PLGA 74
6.3.3 Chondrogenesis within bi-layered hydrogels reinforced with networks of 3D printed PCL 75
6.3.4 In vivo development of chondrogenically primed bi-layered hydrogels 77
6.4 DISCUSSION 81

6.5 CONCLUDING REMARKS 84

7 ENGINEERED SOFT TISSUE TEMPLATES REINFORCED BY 3D PRINTED PCL FOR OSTEOCHONDRAL REGENERATION 85

7.1 INTRODUCTION 85

7.2 MATERIALS AND METHODS 87

7.2.1 3D printing process 87

7.2.2 Cell isolation, expansion and CFU-F 87

7.2.3 Formation of the reinforced soft tissue cartilage templates 88

7.2.4 Surgical Procedure 89

7.2.5 Macroscopic and histological ICRS scoring 89

7.2.6 Safranin-O Quantification and Polarised Light Microscopy 91

7.2.7 Statistics 91

7.3 RESULTS 92

7.3.1 Oxygen tension and glucose availability regulate colony formation 92

7.3.2 Oxygen tension and glucose availability regulate the proliferation kinetics of goat BMSCs in pellet culture 93

7.3.3 Expansion and differentiation at 5% oxygen enhances chondrogenesis of goat BMSCs 95

7.3.4 Tissue engineering of reinforced, bi-layered cartilage templates for large osteochondral defect repair 99

7.3.5 Macroscopic repair appeared comparable in empty and treated osteochondral defects 101

7.3.6 Bi-layered scaffold supports the development of hyaline tissue in the chondral region 102

7.4 DISCUSSION 106

7.5 CONCLUDING REMARKS 108

8 TISSUE ENGINEERING AN ANATOMICALLY SHAPED KNEE CONDYLE FOR WHOLE JOINT REPLACEMENT 109

8.1 INTRODUCTION 109

8.2 MATERIALS AND METHODS 111

8.2.1 3D printing process and construct formation 111

8.2.2 Mechanical Testing 112

8.2.3 Surgical Procedure 112

8.2.4 Analysis of in vitro engineered implants 112

8.3 RESULTS 113

8.3.1 Development of bi-layered constructs for osteochondral tissue engineering using multi-tool biofabrication 113

8.3.2 Tissue engineered anatomically accurate knee condyle 115

8.3.3 In vivo failure of anatomically accurate prosthesis 117

8.4 DISCUSSION 118

8.5 Concluding Remarks 120

9 DISCUSSION 121

9.1 Summary 121

9.1.1 Cartilage templates for osteochondral defect repair 122

9.1.2 Co-cultures for engineering hyaline cartilage 123

9.1.3 Strategies to mechanically reinforce engineered tissues 123

9.1.4 Scaled-up biological implants for joint resurfacing 125

9.2 Limitations and Future Directions 126

9.3 Conclusions 129

REFERENCES 131

SUPPLEMENTARY FIGURES ..... A

List of Figures

Figure 1-1|Summary of the Aims of the Thesis (a) Schematic of Aim 1 whereby a chondrogenically primed cartilage template will be implanted into the medial condyle of a rabbit to assess the functionality, immune response and ability to incite spatial repair, (b) schematic of Aim 2, evaluating the use of cells derived from OA joints (c) schematic of Aim 3 in which bilayered scaffolds are mechanically reinforced with a 3D printed polymeric support and assessed subcutaneously and in situ for spatial repair, and (d) schematic of Aim 4 whereby an anatomically accurate rabbit knee condyle will be 3D printed using a reinforcement PCL scaffold, subsequently a hydrogel bioink will be co-printed to facilitate spatial distribution of endochondral bone and hyaline cartilage to repair a joint. 7

Figure 2-1|Articular Cartilage a) location of articular cartilage within the knee joint b) hierarchal structure and orientation of collagen fibers in articular cartilage (Mow et al., 1992b) c) graphs displaying how the ECM components vary with depth/in each zone (Mow and Guo, 2002) 9

Figure 2-2|Proteoglycans 'bottle brush analogy': a) organisation of the proteoglycan monomer and the PG aggregating structure (Mow et al., 1992a) 11

Figure 2-3| The swelling pressure which causes collagen fibres to be in a pre-stressed state (Mow et al., 1992b) 12

Figure 2-4 | Mechanical testing of cartilage samples: experimental set-up for a) unconfined compression b) confined compression (Lu and Mow, 2008) c) uniaxial confined compression of cartilage, where the horizonal bars depict the distribution of strain, O-B during the compression phase and C-D the relaxation phase, followed by the corresponding strain-time curve and stress-time curve (Mow et al., 1999) 14

Figure 2-5|Structure of subchondral bone: layers of the osteochondral unit from the articular cartilage, tidemark, calcified cartilage, cement lone subchondral bone plate and subarticular spongiosa 16

Figure 2-6 |Endochondral ossification process: a) condensation of MSCs b) MSCs become chondrocytes forming a cartilage template c) chondrocytes in the centre become hypertrophic d) osteoblasts form creating a bone collar and hypertrophic cartilage form a mineralised matrix, blood vessels invade e)the primary spongiosa is formed f) chondrocytes proliferate lengthening the bone g) a secondary ossification centre and growth plate is formed 17

Figure 2-7| Structure of normal and osteoarthritic cartilage: Polarised light light images of normal and diseased cartilage, the dashed line shows the boundary of the cartilage zones (Bi et al., 2005) 19

Figure 2-8| ACI procedure: ACI procedure, cells are isolated from healthy cartilage, digested and expanded and the re-injected into the joint under periosteal flap (Brittberg et al., 1994) 21

Figure 2-9| Bioink printer heads: a) types of inkjet printing, thermal and piezoelectric b) types of microextrusion printer heads, pneumatic, piston and screw driven (Murphy and Atala, 2014) 27

Figure 2-10| Bioinks for bioprinting: A) The biofabriaction window, finding a balance between printability and biocompatibility (Chimene et al., 2016), B) Graph depicting the shear-thinning behaviour (viscosity decreasing with shear rate) of a gellan gum-alginate bioink (Kesti et al., 2015), C) Extrusion of gelatin-alginate strand illustrating printability, with under-gelation

resulting in a droplet morphology and a lattice with truncated corners, ideal-gelation results a smooth uniform strand with square lattice and over-gelation results in an inconsistent strand thickness (Ouyang et al., 2016a). 29

Figure 2-11| Bioinks: a) direct repair for cartilage tissue engineering, ink-jetting PEGDMA laden with chondrocytes directly into the b) implant (Cui et al., 2012b) c) composite printing of multimaterial methacylated bioinks printed through a photopermeable lumen resulting in a core–shell when both inks are extruded and the UV is switched on, heterogeneous structure when each ink is extruded simultaneously and a hollow structure (Ouyang et al., 2016b), d) ECM bioink can be printed alone and reinforced with PCL (Pati et al., 2014) 31

Figure 2-12| Whole joint applications: a) A, Scan of the rabbit humeral head B, with the proposed implant, C, the top surface and the D, bottom surface of the 3D printed replacement joint, E, a native shoulder with immunoflurescence for collagen type II and aggrecan, F, 3D printed replacement with TGF-β3 and immunoflurescense (Lee et al., 2010), b) 3D printed meniscus graft, with spatial distribution of collagen type I and type II, histological sections after implantation in vivo (Lee et al., 2014) 34

Figure 4-1| Tissue engineering a cartilage template: (a) The process by which the cartilage template was formed (b) Young's Modulus for the acellular RGD-ɣ-alginate day 0 and after 28 days in culture pre-implantation, n=3 **p<0.01 (c) Histology for chondrogenic markers sGAG (alcian blue-aldehyde fuchsin) collagen (picro-sirius red) and collagen type II, hypertrophic marker collagen type X, fibrocartilage collagen type I and calcium (alizarin red), scale bar = 100μm, insert scale bar = 1000μm. 47

Figure 4-2| In vivo repair: Macroscopic repair of best and worst for (a) control empty defects and (b) cartilage template, scale bar = 2000μm. Macroscopic scoring (n=6) for (c) surface integration and (d) surface smoothness. (e-g) Mechanical testing at 3 months, (n=6 ***p<0.001, **p<0.01, t-test) 48

Figure 4-3| Bone repair: (a) 3D reconstruction of the microCT scans of the untreated and the treated condyles. The insert image in the top-left of each shows the cross-sectional plane through the defect. Quantitative analysis of c) the ratio of bone volume to total volume within a defined cylinder within the defect site and d) total bone volume (scale bar = 4mm) 49

Figure 4-4| Histological Staining: Alcian blue staining depicting the two best and two worst observed repair for two different a) empty and b) cartilage template (scale bar 2mm). Immunohistochemical staining for collagen type II, I and X portraying the worst, intermediate and best repair for c) empty and d) cartilage template (scale bar 200μm) 50

Figure 4-5: Histological Scoring: Histomorphometric analysis of cartilage repair parameters, demonstrating significant differences in (a) overall score, (b) % hyaline repair tissue, (f) integration of cartilage and (h) a lack of degenerative changes to adjacent cartilage. (n=6, *p<0.05, t-test) 51

Figure 5-1| Biochemical analysis at day 28: Freshly isolated chondrocytes (fresh CC), expanded chondrocytes (exp CC), expanded FPSC (FPSC), co-culture of freshly isolated chondrocytes and expanded FPSC (fresh co-culture) and co-culture of expanded chondrocytes and expanded FPSC (exp co-culture). a) DNA at day 0 is represented by the dashed line, b) sGAG content c) collagen content, d) collagen to sGAG ratio. *significance to fresh co-culture 5%, #significance to FPSC 5% and FPSC 20%, !significance to exp co-culture 5% and exp co-culture 20%, &significance to FPSC 20% only, ᴸsignificance to expanded co-culture 20% only, ᵂsignificance to exp CC 20% only, %significance to all other groups presented on the graph, (p<0.05), n=3, 2-way ANOVA, Tukey post-test. 59

Figure 5-2| Interaction index: a) sGAG accumulation and b) collagen accumulation, where a value of 1 indicates the expected levels of matrix component were found within the co-culture,

and a value >1.0 indicates chondro-induction. The expected levels of sGAG in the 25:75 co-culture are defined as the sum of 25% of the chondrocyte only levels and 75% of the FPSC only levels (see Equation 1 and 2 for further details). ***indicates a significant difference to the expected levels of sGAG or collagen (p<0.05). 60

Figure 5-3| Immunohistochemical staining day 28: a) collagen type II and b) collagen type I (scale bar 100μm) c) percentage of the total pellet area staining positive for collagen type I d) percentage of the total pellet area staining for collagen type II. *significance to fresh co-culture 5%, #significance to FPSC 5% and FPSC 20%, !significance to exp co-culture 5% and exp co-culture 20%, ᴸsignificance to expanded co-culture 20% only, @significance to fresh co-culture 20% (p<0.05)., 2-way ANOVA..... 61

Figure 5-4| Effect of growth factos on expanded co-cultures: Biochemical analysis a) DNA b) sGAG, c) collagen, d) Picro-sirius red for collagen e) alcian blue for sGAG f) immunohistochemisty for collagen type II and g) collagen type I after 28 days of culture (Scale bar 100μm) *significance (p<0.05), t-test..... 62

Figure 6-1| Schematic of the experimental design: a) 3D printed PCL and PLGA reinforcing networks. b) Mould used to cast the hydrogels into the reinforcement thermoplymer and macroscopic image of either a PCL or PLGA reinforced alginate. c) The experimental groups reinforced alginate with PCL, PLA, PLGA 85:15 or 65:35. d) Second step in which a bi-layered construct was mechanically reinforced. e) Details of the experimental groups used in the study; Alg PCL was used as a control to the bi=layered scaffolds Alg-Alg and Ag-Alg, both contained a co-culture of infrapatellar stem/stromal cells (FPSC) and chondrocytes in a (3:1) ratio, respectively..... 72

Figure 6-2|Macroscopic and mechanical assessment: a) Representative image of how the reinforced polymers changed over time in culture b) the change in fiber diameter overtime c) Young's modulus of each construct over time (n=3/4), #each group is significant from each other within the same time point, &significance of the same group when compared across all time points, ^significant to day 14 of the same group, *significance as shown, p<0.05 2-way-ANOVA. 74

Figure 6-3|Chondrogenesis of reinforced cartilage templates: Biochemical and histological analysis after 28 days in vitro a) DNA, b) sGAG and c) collagen content, (n=3/4, *p<0.05, #significant to day 0, p<0.05, ANOVA) d) histology for sGAG deposition (aldehyde fuchsin), collagen (picrosirius red) (scale bar 1000μm) and immunohistochemistry for collagen type 2 and X (scale bar 100μm). 75

Figure 6-4|Quantitative analysis of the bi-layered cartilage template: a) Young's modulus of an acellular alginate, agarose, PCL frame and native porcine cartilage (n=3/4) !!significance to all other groups except where specified by ns, p<0.05, ANOVA) b) DNA/ww, and c) sGAG/ww (*significance p<0.05, #significance to the corresponding osseous layer, p<0.05, ANOVA n=6) d) calcium content, (nd=not detected)..... 76

Figure 6-5|Histolgy staining: a) alginate-PCL control, b) alginate-alginate bilayer and c) agarose-alginate bilayer for H&E, sGAG (aldehyde fucshin), collagen (picrosirius red), calcium (alizaran red) and immunohistochemical staining for collagen type II, I and X (scale bar 100μm) 77

Figure 6-6|In vivo characterisation of the cartilage template: a) macroscopic images post-implantation (scale bar 1000μm), b) μCT 3D render of the mineral deposition in each group, the red box signifies where the chondral region is located (scale bar=1000μm), c) quantification of the bone volume from μCT sections (*p<0.05, ANOVA) d) Young's modulus after 6 weeks subcutaneous implantation, insert bar represents the mean±SD of the values pre-implantation, !significance compared to pre-implanted values, t-test e) calcium accumulation

measured pre-implantation and post-implantation (nd=not detected), #significance compared to alginate chondral region, & significance compared to alginate chondral region, *significance, 1-way ANOVA p<0.05 78

Figure 6-7|Histological staining: a) Alg PCL, b) Alg alg bi-layer, c) Ag alg bi-layer stained for H&E (scale bar=1000μm), sGAG (aldehyde fuchsin) and immunohistochemical staining for collagen type II, I and X (all scale bars 100μm) 79

Figure 6-8|High magnification of H&E sections: a) chondral region for the alginate-alginate bilayer, the arrows point to bone, each image represents a different sample and b) chondral region for the agarose-alginate bilayer, arrow points to bone and possibly a vessel forming around the PCL, this is from one section only, the image with green arrows show PCL fibers in the that has not the same artefact (c) the interface between the chondral and the osseous region, (d) arrows point to bone formation at the interface (scale bar=100μm)..... 80

Figure 7-1| Overview of the experimental groups: 16 in total, alternating oxygen, glucose in both expansion and differentiation phases. 2 donors were maintained in all 16 conditions, 1 donor in all the mentioned expansion phases, but only differentiated in HG CDM 88

Figure 7-2| Expansion Analysis a) representative CFU-F for each of the expansion conditions, 20% oxygen high glucose, 20% oxygen low glucose, 5% oxygen high glucose, 5% oxygen low glucose b) average colony diameter and c) number of colonies, n=4, 3 donors, ***significance compared to all groups, *significance, P<0.05..... 92

Figure 7-3|Levels of DNA after 28 days: a) 20% O_2 low glucose differentiation b) 20% O_2 high glucose differentiation c) 5% O_2 high glucose differentiation d) 5% O_2 low glucose differentiation, bars represent the mean values from 2 or 3 donors, #significance compared to all other groups, *significance, p<0.05, 2-way ANOVA, e) Pareto chart, anything right of the red bar denotes significance p<0.05, f) interaction plot where 'blocks' refers to donor..... 94

Figure 7-4| Biochemical levels of sGAG after 28 days: a) 20% O_2 low glucose differentiation b) 20% O_2 high glucose differentiation c) 5% O_2 high glucose differentiation d) 5% O_2 low glucose differentiation, bars represent the mean values from 2 or 3 donors, #significance compared to all other groups, *significance, p<0.05, 2-way ANOVA, e) Pareto chart, anything right of the red bar denotes significance p<0.05, f) interaction plot where 'blocks' refers to donor..... 96

Figure 7-5| Staining for cartilage specific markers: a) Day 28 safranin-O staining for sGAG, scale bar=500μm, b) immunohistochemistry for collagen type II, the magnified images were taken at the centre of the pellet, scale bar 100μm..... 98

Figure 7-6| Summary of the experimental plan and pre-implantation analysis: a) 3D printed PCL scaffold, macroscopic and SEM images, b) outline of the components of the 6x6mm bi-layered scaffold c) summary of the in vivo experiment in a caprine model in both the medial condyle and the trochlear ridge, comparing an empty defect to the bilayer at a timepoint of 6 month, d) macroscopic, sGAG, collagen (scale bar 1mm) and collagen type II staining after 4 weeks of in vitro priming (scale bar100μm), e) biochemical analysis for each layer *significance p<0.05, t-test, f) the Youngs Modulus of an unreinforced hydrogel, day 0 reinforced and 4 week in vitro primed scaffold, *significance p<0.05, 1-way ANOVA..... 100

Figure 7-7| 6-month analysis: a) macroscopic images detailing the repair by the bi-layer or spontaneously in the defects left untreated, b) the corresponding macroscopic scores, c) bone regeneration from microCT scans, d) peak force at a depth of 100μm..... 102

Figure 7-8| Safranin-O staining for sGAG deposition and collagen type II in the treated joints: histolgical sections detailing the repair by the bi-layered scaffold and the empty controls in a) the medial condyle and b) trochlear ridge, c) quantification of positive saf-o staining in the chondral (upper 1.5mm) and the bone region (lower 3.5mm) *p<0.05, t-test 104

Figure 7-9|Histological scoring and PLM analysis: a) ICRS scoring, for repair of the TR and MC combined, b) PLM images of the defect area, with directionality analysis 105

Figure 8-1| Summary of the printing process and mechanical characterisation: a) the stages of forming the bi-layered construct, first the PCL frame is printed, then gelMA containing BMSC is injected into the scaffold and UV'ed for 10 minutes, followed by ink-jetting of the chondral layer, which is then UV'ed for 10 minutes to form a homogenous surface, b) Macroscopic image of the cylindrical PCL scaffold, scale bar =1mm, c) stress-strain curve, for 6 samples, d) representative cyclic loading curve, each colour represents another cycle. 114

Figure 8-2| In-vitro analysis: a) macroscopic image, b) sGAG deposition in the whole construct, scale bar 1mm c)magnified images of sections of either the chondral or the osseous layer, scale bar 100μm d) collagen deposition in the entire construct, scale bar 1mm e) deposition of immunohistochemical staining for collagen type II and X in chondral and osseous layers, scale bar 100μm, biochemical analysis for half the construct f) DNA, g) sGAG, h) collagen, i) calcium, *significance $p<0.05$, t-test. 115

Figure 8-3|Fabrication process and pre-implantation analysis: a) 3D reconstruction of the microCT scan of a rabbit knee b) 3D reconstruction of the condyle that was converted to an STL file for printing c) the printed scaffold in the mould prior to injection of BMSC laden gelMA d) printed scaffold in the mould prior to ink-jetting the chondral layer, e) schematic of forming the osseous layer f) schematic of forming the chondral layer g) macroscopic images of the construct after 4 weeks in culture, h) alcian blue staining showing deposition of sGAG with magnified images of sections from the two layers, scale bar =100μm, i) pricosirius red staining for collagen, j) collagen type II deposition and k) collagen type X in chondral and osseous layers, scale bar =100μm. 116

Figure 8-4| Scaffold implantation and post-implantation images: a) image of the scaffold prior to implantation, black arrow shows the scaffold in the joint b) 3 months after implantation the repair was analysed, red arrow points to the repair tissue and the black arrow to the opposing condyle c) an implant which had been displaced in the joint d) red arrow points to a failed scaffold and the black again to the opposing condyle. 117

List of Tables

Table 2-2-1| Values for Equilibrium modulus (Ha), permeability (k) and height (h) of cartilage. Adapted from (Athanasiou et al., 1991) 14

Table 4-1| Macroscopic Scoring 44

Table 4-2|Histological Scoring 45

Table 6-1 | Printing parameters for reinforcing polymers 70

Table 7-1| Macroscopic scoring parameters 90

Table 7-2|Histology scoring parameters 91

Table 8-1| Summary of printing parameters 111

Nomenclature

%w/w	% wet weight
ACI	Autologous chondrocyte implantation
ANOVA	Analysis of variance
BMP	Bone morphogenetic protein
BMSC	Bone marrow derived mesenchymal stem/stromal cell
$CaCl_2$	Calcium chloride
CC	Chondrocyte
CFU-F	Colony forming unit-fibroblast
ECM	Extracellular matrix
EDTA	Ethylenediaminetetraacetic acid
FBS	Fetal bovine serum
FGF	Fibroblast growth factor
FPSC	Infrapatellar fat pad derived stem cell
H&E	Haematoxylin and Eosin
HCL	Hydrochloric acid
IL	Interleukin
MACI	Matrix-induced autologous chondrocyte implantation
MSC	Mesenchymal stem/stromal cell
OA	Osteoarthritis
PBS	Phosphate buffered saline
PCL	Polycaprolactone
PEG	Polyethylene-glycol
PLGA	Poly (lactic-co-glycolic acid)

RGD	Argininеglycineaspartic acid
sGAG	Sulphated glycosaminoglycan
TGF-β	Transforming growth factor-β
μCT	Micro-computed tomography
VEGF	Vascular endothelial growth factor
γ	Gamma irradiated

Publications

This is a list of publications generated from the work presented in this thesis.

Critchley S.E., Kelly D.J., 2017. Bioinks for bioprinting functional meniscus and articular cartilage. Journal of 3D Printing in Medicine 1 (4), 269-290.

Critchley S.E., Eswaramoorthy R., Kelly D.J., 2017. Low oxygen conditions promote synergistic increases in chondrogenesis during co-culture of human osteoarthritic stem cells and chondrocytes. Journal of Tissuen Engineering and Regenerative Medicine (in press)

Conference Abstracts

SE Critchley, DJ Kelly, Engineering phenotypically stable, mechanically functional articular cartilage grafts using adult stem cells. 20th Annual Conference of the Bioengineering Section of the Royal Academy of Medicine in Ireland, January 24th - 25th, 2014. Castletroy Park Hotel, Hotel, Co. Limerick, Ireland.

SE Critchley, AO' Reilly, GM Cunniffe, PJ Diaz Payno, A McAlinden, H Almeida, DJ Kelly, Regeneration Of Osteochondral Defects By Spatial Modulation Of Endochondral Ossification Within Engineered Cartilage Grafts, Bioengineering in Ireland 22, January 2016

SE Critchley, AO'Reilly, GM Cunniffe, P Diaz-Payno, A McAlinden, H Almeida, DJ Kelly, Regeneration of osteochondral defects by spatial modulation of endochondral ossification within engineered cartilage grafts. Tissue Engineering and Regenerative Medicine International Society (TERMIS), EU Chapter, June 28 – July 1, 2016, Uppsala, Sweden

SE Critchley, GM Cunniffe, E Alsberg, BN Sathy, DJ Kelly, Incorporation of 3d printed pcl fibres to reinforce bilayered tissue engineered osteochondral constructs. Bioengineering in Ireland 23, January 20-21, 2017, Belfast, United Kingdom

SE Critchley, GM Cunniffe, E Alsberg, DJ Kelly, Biofabrication of mechanically reinforced and spatially distinct tissues using 3D printing for osteochondral tissue engineering. ORS Annual Meeting, March 2017, San Diego, USA

SE Critchley, R Eswaramoorthy, DJ Kelly, Low oxygen conditions promote synergistic increases in chondrogenesis during co-culture of human stem cells with osteoarthritic chondrocytes. ORS Annual Meeting, March 2017, San Diego, USA

SE Critchley, AO'Reilly, GM Cunniffe, P Diaz-Payno, A McAlinden, D Withers, H Almeida, E Alsberg, DJ Kelly, Mimicking endochondral ossification for enhanced osteochondral defect repair. ORS Annual Meeting, March 2017, San Diego, USA

1 Introduction

1.1 The clinical need for new therapies to treat osteoarthritis

Osteoarthritis (OA) is a disease of the joints such as the hip and the knee. It affects the entire joint, which in the knee includes the cartilage, synovium, meniscus, infrapatellar fat pad and the subchondral bone (Mobasheri et al., 2017). After the onset of OA the joint damage generally becomes progressively worse until the patient is debilitated by pain. OA is generally associated with the older and obese population, however, early symptoms/markers are increasingly being seen in younger patients (Amoako et al., 2014). In 2004 the World Health Organisation (WHO) positioned OA in the top ten diseases which cause work loss due to disability. Subsequent studies have demonstrated that incidences of OA had increased by 32.9% since that WHO report (Vos et al., 2016). When a joint is severely compromised the common surgical intervention is to replace the entire joint with a metal and polymer prosthesis, termed *total joint replacement* (TJR). However, there are a number of well documented limitations associated with this treatment (Wylde et al., 2007) such as aseptic loosening and a limited lifespan of 10-15 years, after which a more complicated revision surgery is required (Kurtz et al., 2009). The aging worldwide population, and the associated increase in the instances of joint degeneration are motivating the need for new treatment options for damaged and diseased joints.

The knee is a diarthrodial joint, opposite bone ends are lined with hyaline articular cartilage. Articular cartilage is an anisotropic, highly organised, and durable tissue which is responsible for frictionless motion and load transmission within synovial joints (in this case between the femur and tibia in the knee joint). Due to its location in a high load bearing environment, it is imperative that articular cartilage maintains its mechanical function. The mechanical functionality of this hydrated tissue arises from the depth dependant organisation and alignment of the collagen network and its interaction with negatively charged sulphated glycosaminoglycans (sGAG) (Mow et al., 1992a). These sGAGs molecules function to generate a swelling pressure, which draws in fluid that pressurises to supports loads within the tissue. Damage can occur due to disease, trauma or altered biomechanics from the removal of an injured meniscus (Gelber et al., 2000; Martinez et al., 2006; Moskowitz et al., 1973; Papalia et al., 2011; Shiomi et al., 2012). Owing in part to the lack of vasculature, articular cartilage has a poor regenerative capacity. One of the associated outcomes of a compromised joint is the

degenerative disease, OA (Gelber et al., 2000). The process is not completely understood, but it includes the disruption of the metabolic equilibrium with increased catabolic activity causing the degradation of the cartilage matrix (Goldring and Goldring, 2010; Hunziker, 2002). The breakdown in extracellular matrix (ECM) structure impairs the tissue's mechanical function.

1.2 Tissue Engineering for Synovial Joint Regeneration

Microfracture was one of the earliest surgical options for treating damaged cartilage, and involves recruiting endogenous cells from the underlying bone marrow into the defect. The surgeon drills or perforates the subchondral bone to allow an influx of bone marrow cells into the site. The recruited mesenchymal stem/stromal cells (MSCs) from the bone marrow stimulate a repair process (Kalson et al., 2010). The short term results are promising, however, this technique generally results in the formation of mechanically inferior fibrocartilage (Mithoefer et al., 2009). Tissue engineering and cell-based therapies are attractive treatments as they promise to regenerate the joint by employing the use of living cells and/or biomaterials and/or growth factors to grow a living tissue. These principles have already been applied for treating focal cartilage defects with reasonable clinical success (Abdel-Sayed and Pioletti, 2015; Behrens et al., 2006; McNickle et al., 2008). One of the first examples of tissue engineering principles being used in the clinic was autologous chondrocyte implantation (ACI). It is two stage approach, whereby cells are isolated from a non-load bearing region of the joint, expanded *in vitro* and subsequently implanted into the defect site beneath a periosteal flap or a collagen membrane (Brittberg et al., 1994; Dewan et al., 2014). Patients have reported improvements in pain and mobility (Harris et al., 2010; Kreuz et al., 2007; Peterson et al., 2002). However, there has been some reports of a mixture of hyaline and fibrocartilage being formed (Nehrer et al., 1999). ACI is often used as a secondary repair option to microfracture, however in these cases the outcome is generally inferior (Minas et al., 2009). Second generation ACI included a final step of seeding the expanded chondrocytes onto a collagen matrix prior to implantation, and is aptly named matrix-assisted autologous chondrocyte implantation (MACI). A five-year follow-up study reported increased activity and ICRS scoring with histological biopsies staining for collagen type II and sGAGs (Behrens et al., 2006). There were instances of abnormality, such as chondrocyte clustering and positive collage type I staining (a marker of fibrous or fibrocartilage development), however this occurred in the minority of cases. These current approaches only target injures/degeneration of the articular cartilage, whereas treating OA joints requires targeting other joint tissues, particularly the underlying subchondral bone intervention.

In addition to cell-based strategies, several biomaterial based approaches have also been developed to treat focal cartilage and osteochondral defects (Dewan et al., 2014; Kon et al., 2010, 2013). For example, MaioRegen™ is a flexible, degradable, off-the-shelf tri-layered biomimetic scaffold designed for osteochondral applications. The cartilage phase is composed of collagen type I, the transitional and bone region a mixture of hydroxyapatite and collagen I of differing percentages (Kon et al., 2010). These approaches suggest that tissue engineering strategies can potentially be used to treat different tissues in the joint, however they have yet to be developed to the point where they can be considered a potential treatment for OA. Specifically, none of the current treatments options can be used to biologically resurface the entire joint, with TJR remaining the only viable option for patients with advanced OA.

1.3 3D Bioprinting for Bone and Joint Regeneration

Engineering functional joint tissues requires recapitulating their native mechanical properties and re-establishing the spatial complexity of the bone to cartilage interface. An emerging technique with the potential to enable the engineering of such complex tissues is three-dimensional (3D) printing, which allows for the accurate positioning of different cell types, growth factors, genes and other biological cues within 3D biomaterials. In this way it may be possible to engineer constructs that mimic the shape, structure, composition and ideally the function of specific tissues and organs (Daly et al., 2016a; Hockaday et al., 2012; Mandrycky et al., 2016; Murphy and Atala, 2014; Visser et al., 2013). Thermoplastic polymers can be printed alongside cell-laden hydrogels (bioinks) to form hybrid scaffolds with mechanical properties tailored to specific applications (Cunniffe et al., 2017; Kang et al., 2016; Kim et al., 2016; Kundu et al., 2015; Shim et al., 2016; Visser et al., 2015a). For example, by reinforcing methacrylated gelatin bioink (gelMA) with melt-electrospun PCL it has been possible to engineer constructs with mechanical properties that mimic articular cartilage (Visser et al., 2015b). The melt-electrospinning technique enabled the production of small (<100 μm) diameter fibres with scaffold porosities of 93-98%. Synergistic increases in the mechanical properties of the composite material compared to the PCL scaffold alone were observed, whereby the deformation of the fibres under axial loads were supported by the gelMA. By manipulating the fibre diameter and pore size the authors could generate constructs with stiffness and elasticity approaching native cartilage. The potential application of 3D printing for whole joint orthopaedic applications was demonstrated in a study which replaced an entire rabbit shoulder joint with a 3D printed PCL-hydroxyapatite scaffold infused with growth factor, TGF-β3 (Lee et al., 2010). The TGF-β3 was responsible for recruiting large numbers of host cells and

4 months after implantation a layer of cartilage positive for collagen type II and sGAG was visible over the implant surface.

Key to realising the promise of a bioprinted implant for joint regeneration is selecting an appropriate hydrogel bioink, cell type and reinforcing polymer which will support cell proliferation, differentiation and tissue specific ECM deposition. Hydrogels are water swollen, cross-linkable materials that are used extensively in cartilage tissue engineering (Lee and Mooney, 2001; Orth et al., 2014). They can support and promote chondrogenesis by facilitating matrix deposition and by providing physical and chemical cues mimicking specific cell niches. Important hydrogel design parameters include matrix stiffness, degradation rate, provision of cell adhesion motifs and biocompatibility (Lee and Mooney, 2001). Articular cartilage specific chondrocytes are an obvious choice however OA joints contain a limited amount of available tissue, yielding low numbers of chondrocytes with a limited chondrogenic potential. For a whole joint application, this would require their expansion *in vitro* to increase the cell number. However, studies have shown that repeated expansion through numerous passages causes them to dedifferentiate and lose their phenotype (Benya et al., 1978).

The mesenchymal stem cell/stromal (MSC) is commonly used as an alternative cell type for cartilage and bone tissue engineering as it is capable of differentiating along multiple lineages. These cells are found in numerous locations such as in adipose tissue (ADSC), bone-marrow (BMSC) and the infrapatellar fat-pad (FPSC). The use of BMSCs for cartilage tissue is promising, as when supplemented with growth factors such as transforming growth factor (TGF-β3) they can produce cartilage-like constructs (Johnstone et al., 1998; Mackay et al., 1998; Ng et al., 2017; Pittenger et al., 1999; Vinardell et al., 2012a). However, these are often reported to be unstable *in vivo*, eventually expressing the hypertrophic marker collagen type X and undergoing endochondral ossification (the conversion of cartilage into bone) (Chen et al., 2015; Pelttari et al., 2006; Vinardell et al., 2012a). This endochondral phenotype can potentially be leveraged as novel bone tissue engineering strategies that aim to mimic the developmental process by which our long bones form (Scotti et al., 2010). Furthermore, spatially regulating the process of endochondral ossification has been proposed as a strategy to engineer osteochondral tissues. FPSCs are less inclined to undergo hypertrophy, however they have a tendency to promote the development of a more fibrocartilagenous tissue (Dragoo et al., 2003; Khan et al., 2007). To engineer a more stable articular cartilage phenotype, co-culturing MSCs and chondrocytes has been shown to supress hypertrophy whilst addressing the limitations of chondrocyte numbers (Acharya et al., 2012; Bian et al., 2011; Fischer et al., 2010; Hendriks et al., 2007). Co-cultures have been reported to synergistically enhance cartilage ECM synthesis compared to MSC only controls (Giovannini et al., 2010). The mechanism by which this occurs is unclear but it is thought to be as a result of either MSC

secreting factors which drive chondrocyte proliferation (Wu et al., 2011) or that chondrocytes are modulating the lineage and resultant phenotype of the differentiating MSC (Ahmed et al., 2007). What remains unclear is whether co-cultures of chondrocytes and stem cells from OA patients will produce hyaline-like cartilage. Regardless, appropriate co-cultures of chondrocytes and MSCs represent a promising cell combination to use with bioinks for 3D bioprinting of functional articular cartilage.

1.4 Thesis Objectives

The overall goal of this thesis is to develop a 3D bioprinting strategy to engineer scaled-up functional osteochondral implants for whole joint resurfacing. A central hypothesis of this thesis is that cartilage templates engineered or bioprinted using BMSCs can be used to regenerate the bony component of an osteochondral defect. The specific objectives of the thesis are to:

1. **Investigate whether a cartilage template engineered using BMSCs can be used to regenerate a critically sized osteochondral defect (Fig.1-1 a).** Engineered cartilage templates will be implanted into the medial condyle of a rabbit. The defect regeneration will be assessed mechanically, histologically and using μCT to determine if spatially defined regeneration can occur.
2. Motivated by firstly, the need to engineer phenotypically stable articular cartilage and secondly, the fact that an autologous cell based therapy for treating OA will involve the use of cells from diseased patients (Fig.1-1 b), the second objective is to **evaluate the capacity of a co-culture of FPSCs and chondrocytes derived from osteoarthritic patients for tissue engineering hyaline cartilage. Furthermore, to explore if a specific growth factor supplementation regime is more suitable for driving chondrogenesis of these co-cultures.**
3. Recognising that engineered soft tissue templates may lack the mechanical strength and integrity to use for the regeneration of a large load bearing defects, this thesis next sought **to mechanically reinforce such cartilage templates using 3D printed polymeric supports.** Firstly, an optimal reinforcing polymer will be chosen by assessing the mechanical properties and chondrogenesis by comparing PCL, PLA and PLGA. On selecting the reinforcing polymer, bi-layered hydrogels consisting of a top chondral region containing a co-culture of MSCs and chondrocytes and a bottom osseous layer consisting of BMSCs, integrated with polymeric supports will be evaluated. The ability to spatially regulate endochondral ossification within such

constructs to engineer osteochondral tissues was assessed both subcutaneously and subsequently in a caprine osteochondral defect (Fig.1-1 c).

4. The final part of this thesis will attempt to scale up the biofabrication process to tissue engineer an osteochondral construct capable of whole joint resurfacing (Fig.1-1 d).

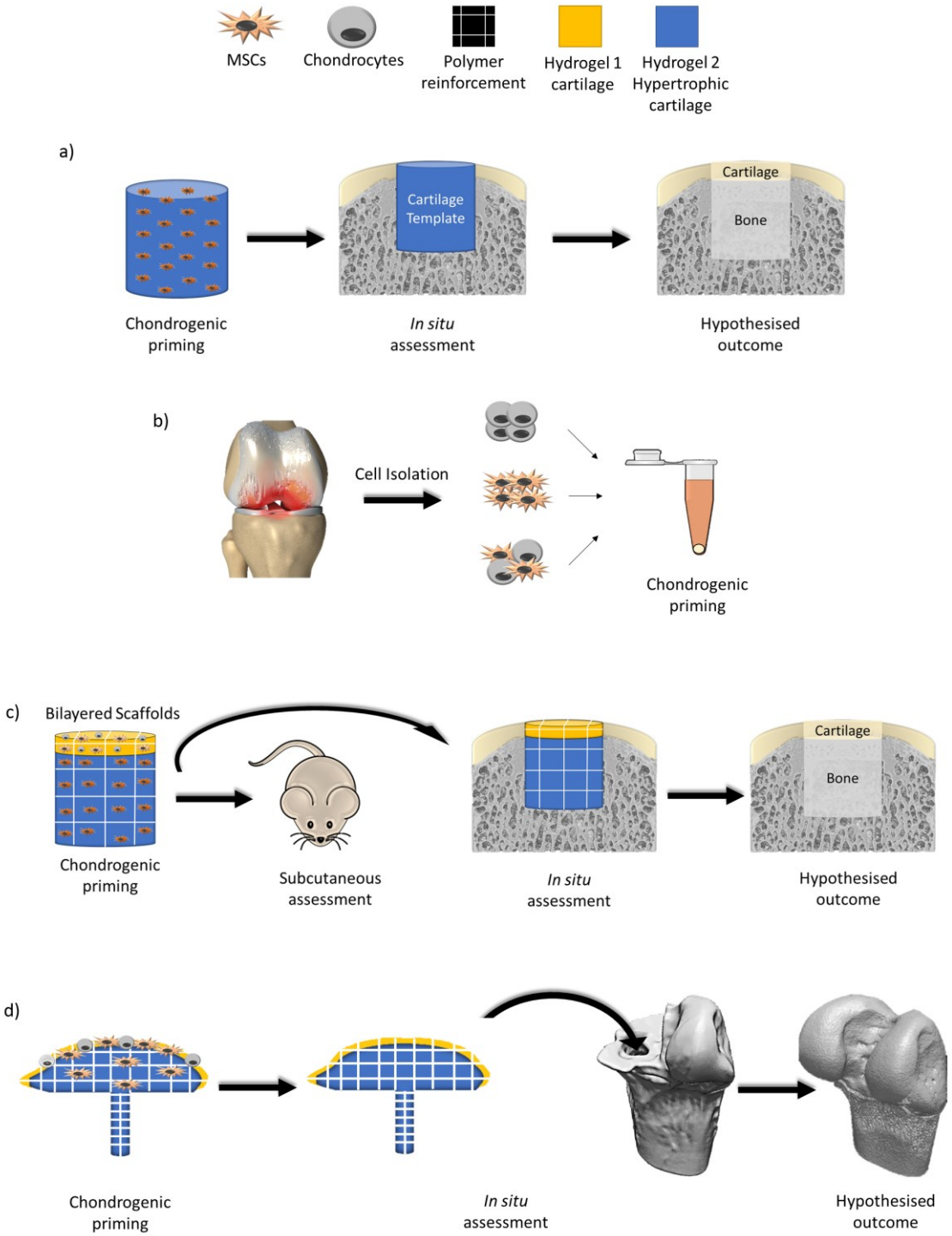

Figure 1-1|Summary of the Aims of the Thesis *(a) Schematic of Aim 1 whereby a chondrogenically primed cartilage template will be implanted into the medial condyle of a rabbit to assess the functionality, immune response and ability to incite spatial repair, (b) schematic of Aim 2, evaluating the use of cells derived from OA joints (c) schematic of Aim 3 in which bilayered scaffolds are mechanically reinforced with a 3D printed polymeric support and assessed subcutaneously and in situ for spatial repair, and (d) schematic of Aim 4 whereby an anatomically accurate rabbit knee condyle will be 3D printed using a reinforcement PCL scaffold, subsequently a hydrogel bioink will be co-printed to facilitate spatial distribution of endochondral bone and hyaline cartilage to repair a joint.*

2 Literature Review

2.1 Introduction

Regenerating the knee joint will require engineering both the articular cartilage and the subchondral bone, mimicking the native shape and spatial distribution of ECM components. To achieve this premise, the structure and function of each tissue must be examined. Additionally, current cell-based strategies used clinically will be reviewed to examine the translatability to whole joint size implants. Numerous researchers have attempted to grow functional cartilage and/or osteochondral constructs in the laboratory using several different methods, cells, materials and growth factors, these will be reviewed, with the different approaches presented. Finally, 3D bioprinting can potentially enable the engineering of a biological construct mimicking the complex geometry, architecture and mechanical properties. This new and exciting technique will be examined highlighting key design parameters, bioinks and current successes.

2.2 The Knee Joint

The knee joint exists at the interface between the femur and the tibia, it facilitates flexion, extension and slight internal and external rotation of the limb. It is categorised as a diarthrodial joint meaning that a layer of cartilage lines opposing bone surfaces and the joint cavity is filled with synovial fluid. In the case of the knee, the meniscus, a fibrocartilaginous tissue separates the hyaline articular cartilage lined femoral condyle and tibial plateau. This thesis will focus on strategies to regenerate the articular cartilage and the underlying subchondral bone.

2.3 Articular Cartilage

Articular cartilage is a hyaline cartilage and covers the surface of synovial joints. It is responsible for load transmission and lubrication for smooth articulation of the joint. It is a thin, dense layer of tissue (2-4mm) covering the femoral condyle in the knee joint (Fig.2-1 a). It is lined by a lubricant membrane allowing for frictionless movement. The tissue is water-swollen consisting of a highly organised organic porous ECM in which a small number of chondrocytes (cartilage forming cells) are embedded. Articular cartilage being both avascular

and aneural lacks regenerative capabilities. The intricate zonal structure and anisotropic ECM composition is integral to the mechanical function of the tissue (Gannon et al., 2015). The architecture and composition of the ECM components change with depth and is often categorised as having four zones, the superficial tangential zone (STZ), the middle zone (MZ), the deep zone (DZ) and the calcified zone (Fig.2-1 b). Common to each zone are chondrocytes, water, glycosaminoglycans (sGAG) and type II collagen. The composition of each ECM component changes with zonal location through the tissue (Fig.2-1 c). This in turn determines the mechanical properties and the function of cartilage. As will be described later, sGAG and collagen work synergistically to provide mechanical function to articular cartilage.

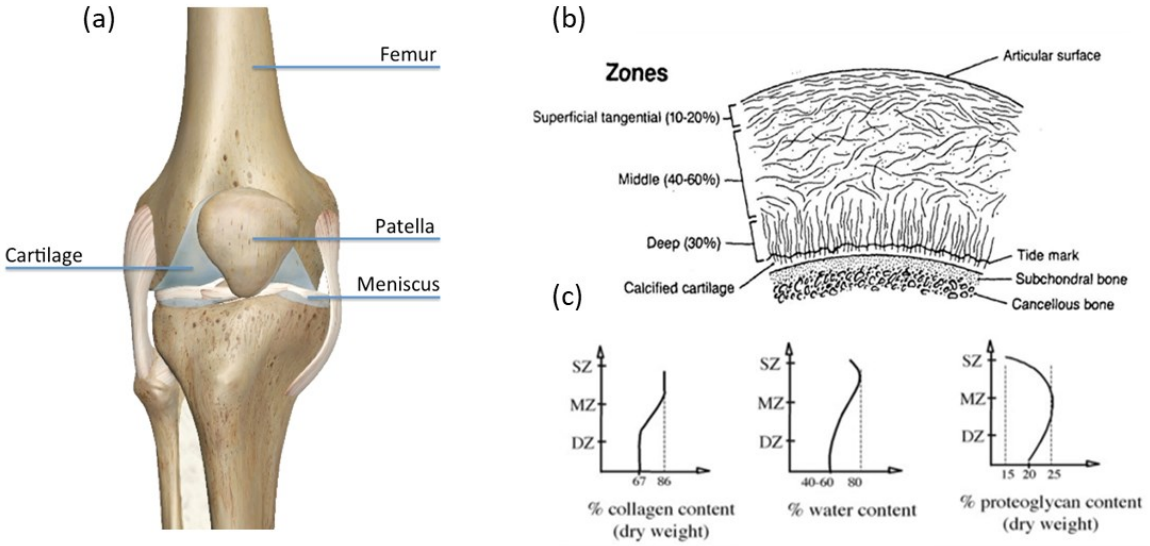

Figure 2-1|Articular Cartilage *a) location of articular cartilage within the knee joint b) hierarchal structure and orientation of collagen fibers in articular cartilage* (Mow et al., 1992b) *c) graphs displaying how the ECM components vary with depth/in each zone* (Mow and Guo, 2002)

The STZ makes up 10-20% of the overall tissue thickness. It contains a high number of chondrocytes that have a flattened morphology. They secrete a boundary lubricant called lubricin or PRG-4 into the surrounding synovial fluid, reducing friction (Schumacher et al., 1994). There is a low sGAG concentration but high a content of collagen fibers which are densely packed and orientated parallel to the surface giving high tensile properties. Water content within the tissue is also highest in this region, reaching 80%. This layer protects against high shear stresses and tensile forces from articulation. The MZ is a transitional region between superficial and deep zones. The chondrocytes are spherical and there is an increased level of proteoglycans compared to the STZ. The collagen fibres transition in orientation from their parallel form in the STZ to perpendicular, thus resulting in a random orientation. The fibers are

larger and less packed to entrap the sGAG molecules. Water content decreases slightly from the level in the STZ (Buckwalter and Mankin, 1997). The DZ has thick bundles of collagen fibres that are perpendicular to the surface and anchor the tissue to the underlying calcified cartilage. The chondrocytes are sparsely distributed in a columnar fashion and are larger and rounder than the ones located in the superficial zone. The calcified region, or tidemark, is where cartilage transitions to bone (Poole, 1997). The inhomogeneity of matrix causes depth-dependent mechanical properties. The zones of cartilage have individual mechanical properties that are essential to functional cartilage.

2.3.1 Extracellular Matrix Components

Proteoglycan macromolecules (PG) comprise 4-7% of the wet weight of articular cartilage (Lu and Mow, 2008). The aggregating PG, aggrecan constitutes up to 90% of PGs in articular cartilage (Mow and Huiskes, 2005). Aggrecan monomers non-covalently bind to hyaluronan (HA), this is supported by a link protein (Fig.2-2 b). This link protein is essential to the prevention of the components of the molecule escaping the tissue, and therefore stabilises the PG and anchors it within the matrix. Aggrecan itself is composed of glycosaminoglycan (GAG) chains which are covalently bound to a core protein (Fig.2-2 a). The GAG chains consist of negatively charged suphate and/or carboxyl groups, such as chondroitin sulphate (cs) and keratan sulphate (ks) (Hardingham and Fosang, 1992; Schaefer and Schaefer, 2010). The PG structure can be depicted using a bottle-brush analogy (Fig.2-2 b). The negative charge gives hydrophilic properties and water retention is possible as the high negative charge attracts counter ions, this high osmotic imbalance attracts water from the surrounding area (Mow and Guo, 2002). The density of the negative charge in sGAGs (sulphated GAGs), also known as the fixed charge density (FCD) is responsible for governing and regulating the hydration, rate of fluid transport and other electrochemical responses (Mow and Guo, 2002; Mow et al., 1980).The molecular confirmation of PG causes it to become trapped in the collagen network. Due to the ECM components being densely packed the negative GAG charge creates a charge-to-charge repulsion, but they are restrained by collagen fibres, thus creating compressive stiffness within the tissue (Mow and Huiskes, 2005). To maintain electoneutrality counter-ions such as Na^+ cause a swelling pressure known as the Donnan osmotic pressure (Mow et al., 1992a).

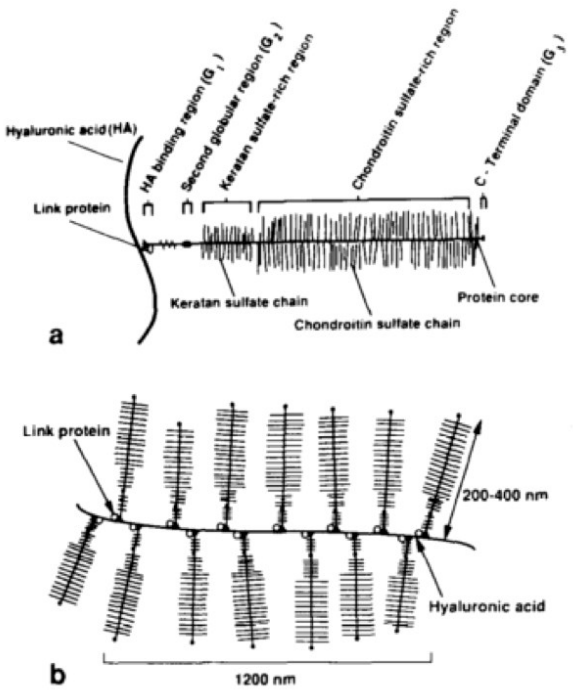

Figure 2-2|Proteoglycans 'bottle brush analogy': *a) organisation of the proteoglycan monomer and the PG aggregating structure* (Mow et al., 1992a)

Collagen type II (10-20% of tissue wet weight) is the most abundant collagen (90-95% of all collagens present) in articular cartilage (Mow and Huiskes, 2005). Other forms of collagens also exist, such as types VI, IX, XI and XII but in much smaller quantities (Buckwalter and Mankin, 1997). Collagen has a high tensile strength due to the triple helix arrangement of polypeptides (tropocollagen molecule) of the amino acid alpha chains. However, the high length to thickness ratio results in weak compressive properties. In skeletally mature cartilage collagen fibres have an arcade like structure. The perpendicular fibres in the DZ transition in an arc to residing parallel in the STZ, this observation was first noted by Benninghoff in 1925, thus it is referred to as the 'Benninghoff architecture'. The collagen functions to restrain the swelling pressure associated with the negatively charged PG resulting in a pre-stressed collagen network, providing compressive stiffness (Figure 2-3) (Mow et al., 1992a).

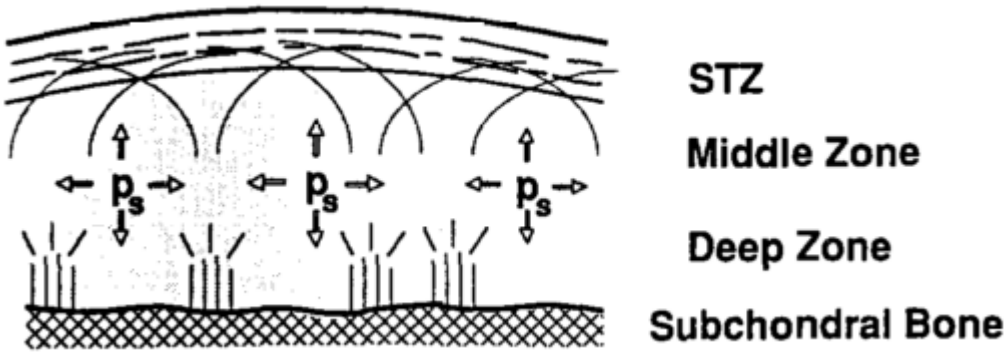

Figure 2-3| *The swelling pressure which causes collagen fibres to be in a pre-stressed state* (Mow et al., 1992b)

Chondrocytes make up less than 10% of the tissue (Alford and Cole, 2005) and are embedded in the ECM. They are responsible for secreting, maintaining and synthesising the matrix. Due to the avascular nature of cartilage, the chondrocytes rely on nutrient diffusion from the surrounding synovial fluid (located in the joint capsule) for metabolism. Nutrients are acquired from the synovial fluid at the surface of the tissue. The successive diffusion of nutrients results in a hypoxic environment. They are spherical in shape, but have a more flattened morphology in the STZ. They surround themselves in matrix and do not experience direct cell-to-cell contact. Collectively the chondrocyte and the pericellular matrix is called a chondron. Poole described the morphology of the chondron as having an outside surface of fibrillar collagens, primarily collagen VI which encapsulates a single chondrocyte that is linked to a pericellular glycocalyx (Bekkers et al., 2013a; Poole, 1997).

2.3.2 Fluid

Fluid is one of the primary components of articular cartilage, constituting 65-80% (Buckwalter and Mankin, 1997; Chen et al., 2017). In addition to playing a key role in determining the compressive properties of cartilage it circulates nutrients, proteins and cations throughout the tissue and removes waste. It primarily resides in the intrafibrillar space.

2.3.3 Mechanical Properties

Articular cartilage undergoes physiological loading daily, with forces ranging from 0 to 10 times that of body weight. The dominant force experienced by articular cartilage is compression, however there exists tensile and shear forces at the articulating surfaces. As it is a porous, permeable and deformable material that contains both a fluid and a solid phase, and flow-dependent, the mechanical properties of articular cartilage are best represented by a

biphasic model. In compression, the solid matrix deforms and there is an increase in fluid pressure forcing it to exude through the pores of the tissue. Frictional drag is generated by the fluid flowing through the solid matrix causing both compaction of the ECM and preventing too excessive fluid loss.

There are two well-practiced compressive mechanical tests of articular cartilage, confined and unconfined compression. In confined compression, the cartilage sample is restricted on all sides except the side being compressed (Fig.2-4 b). This does not allow for bulging of the tissue. Unconfined, restricts the tissue top and bottom, while allowing for lateral bulging (Fig.2-4 a). In both cases a stress relaxation test is preformed, a pre-defined strain is applied at a constant rate and then held until the tissue relaxes and reaches equilibrium.

2.3.4 Confined Compression

This is a uniaxial test involving a confined cylindrical cartilage plug in an impermeable chamber of identical diameter. The specimen is compressed using a porous platen using a pre-defined strain rate. The confinement chamber prevents the bulging of cartilage in the radial direction, thus fluid is forced out in the vertical direction only. In confined compression the compressive force is applied until the desired displacement is reached, at which point it is held until the sample reaches equilibrium. Initially the fluid bears up to 90% of the load (Soltz and Ateshian, 1998). As the permeability of the tissue is low (approx. $10^{-14}m^4/Ns$ bovine cartilage (Mow et al., 1980) a pressure gradient is created causing the fluid to flow and exude uniaxially through the pores (Fig.2-4 c). Fluid from the top of the cartilage effluxes first, followed by movement from deeper regions. As fluid flows from the tissue, more of the compressive load is borne by the solid matrix (Fig.2-4 c). A non-homogenous strain field is created in the solid matrix with the stress at cartilage-platen interface highest. When the desired displacement is reached, this point correlates to peak stress in the test. At this point fluid begins to redistribute throughout the sample (Fig.2-4 c C) and stress in the sample and from the porous platen deteriorates exponentially (Fig.2-4 c D) until equilibrium is reached (Fig.2-4 c E). Equilibrium in the sample refers to the point at which the stress in the matrix balances the applied stress, no fluid flow or pressure gradient exists (Mow and Guo, 2002). The equilibrium force can be used to calculate the aggregate modulus (H_a) of articular cartilage (Table 2-2-1). The permeability may also be determined.

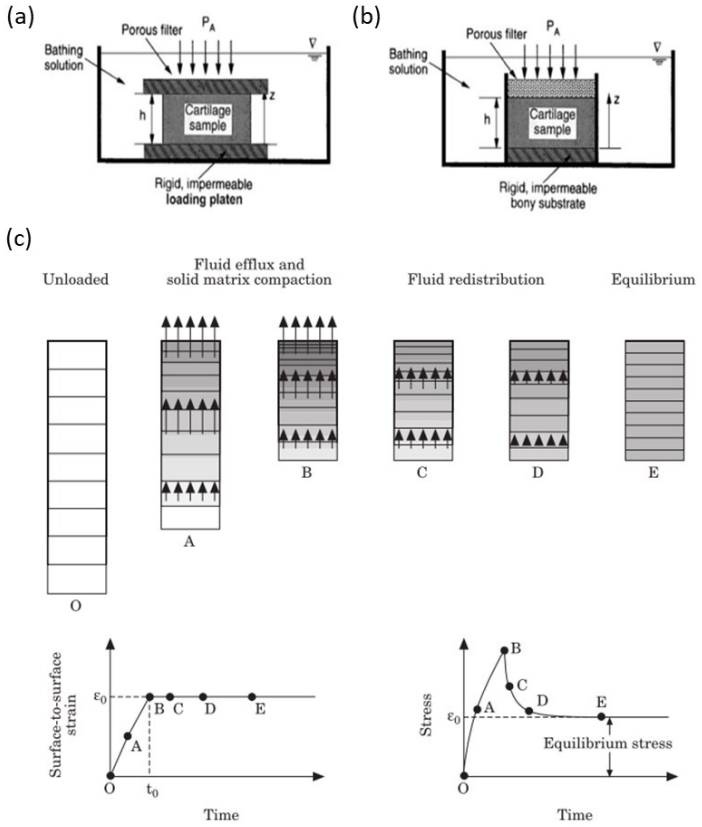

Figure 2-4 | Mechanical testing of cartilage samples: *experimental set-up for a) unconfined compression b) confined compression* (Lu and Mow, 2008) *c) uniaxial confined compression of cartilage, where the horizonal bars depict the distribution of strain, O-B during the compression phase and C-D the relaxation phase, followed by the corresponding strain-time curve and stress-time curve* (Mow et al., 1999)

Table 2-2-1| *Values for Equilibrium modulus (Ha), permeability (k) and height (h) of cartilage. Adapted from* (Athanasiou et al., 1991)

Location	Species	H_a	K (m^4 Ns^{-1})x10^{15}	h (mm)
Medial Condyle	Human	0.588±0.114	1.137±0.160	2.21±0.59
	Bovine	0.899±0.427	0.455±0.332	1.19±0.24
	Rabbit	0.741±0.101	2.019±1.621	0.41±0.1
Patellar Groove	Human	0.530±0.094	2.173±0.730	3.57±1.12
	Bovine	0.472±0.147	1.422±0.580	1.38±0.19
	Rabbit	0.516±0.202	3.842±3.260	0.20±0.04

2.3.5 Unconfined Compression

Unconfined compression (Fig.2-4 a) is an alternative mechanical test to confined compression; in this case the cartilage sample is confined between two non-porous smooth platens, one, which is responsible for the applied force. The sample is submersed in a fluid bath allowing for fluid exchange. The tissue is allowed to bulge, considering properties in the radial direction. The tissue experiences both perpendicular and parallel strains (to the applied force) thereby more accurately simulating physiological loading conditions. The Young's modulus can be determined from this approach.

2.3.6 Indentation Testing

Indentation testing is commonly used when assessing the mechanical properties of repair or native tissue of curved surfaces such as the condyle, or *in situ* (Julkunen et al., 2009; Korhonen et al., 2002; Lu and Mow, 2008; Roemhildt et al., 2006). Unconfined and confined approaches are more suited to testing samples with a defined geometry, such as a cylindrical sample, or when the cartilage layer can be separated from the bone layer. The set-up of an indentation test requires the sample to be held in place by a clamp or similar, and, in general, a constant load is applied via a porous or a non-porous platen of variable diameter (usually greater than 0.8mm (Mansour, 2009)). It is often thought that this type of testing is more relevant as the test is undertaken in a more 'natural' environment. The aggregate modulus, Poisson's ratio, and permeability can be determined by fitting the data to a biphasic model (Mansour, 2009). The Young's modulus can be determined when a value for the cartilage thickness is obtained. A study which presented data for the mechanical properties of bovine cartilage obtained by using indentation, unconfined and confined compression concluded that values for Young's modulus differed depending on the test with indentation resulting in higher values than unconfined (Korhonen et al., 2002).

2.4 Structure and Composition of Subchondral Bone

Bone is a dynamic tissue, undergoing continuous remodelling in response to loading. It provides a framework and protects some of the major organs in the body. It is also responsible for storing bone marrow and forming blood cells. Osteoblasts, osteocytes and osteoclasts are the three types of cells resident in bone, the balance of osteoblast and osteoclast activity is critical to maintain bone homeostasis. Bone can be described as a composite material consisting of inorganic mineral (~70%), organic (~30%) that includes 2-5% cells, and water phases (5%) (Sommerfeldt and Rubin, 2001). Hydroxyapatite (inorganic), collagen type 1,

osteocalcin, gylcoproteins and proteoglycans (organic) are the primary ECM components. Synergistically these components render bone a stiff and tough yet flexible material. There are two types of bone structures, cortical and cancellous/trabecular bone, the former is denser and encloses the trabecular bone in vertebrae or in long bones (Wolfram and Schwiedrzik, 2016). Cancellous/trabecular bone consists of an interconnected network of bone struts with a central marrow cavity.

The subchondral bone is the area of calcified tissue immediately below the articular cartilage tidemark (Madry et al., 2010). Characteristically, the thickness, density and composition are highly varied between individuals. However, it can be categorised by two components, the subchondral plate or cortical end plate and the subarticular spongiosa (cancellous bone) (Fig.2-5) The collagen type II fibres from the articular cartilage cross the tidemark into the calcified cartilage but they do not penetrate the cortical endplate. The subchondral bone is highly vascularised, with some vessels and nerves branching into the calcified cartilage region (Imhof et al., 1999). The vesselised canals from the subchondral bone perforate the subchondral plate and supply nutrients from the marrow to the calcified and deeper regions of cartilage (Imhof et al., 1999; Madry et al., 2010; Malinin and Ouellette, 2000). In addition to nutrient supply the subchondral plate plays a role in absorbing forces from movement. Both the articular cartilage and the subchondral bone work as a unit to absorb compressive stresses.

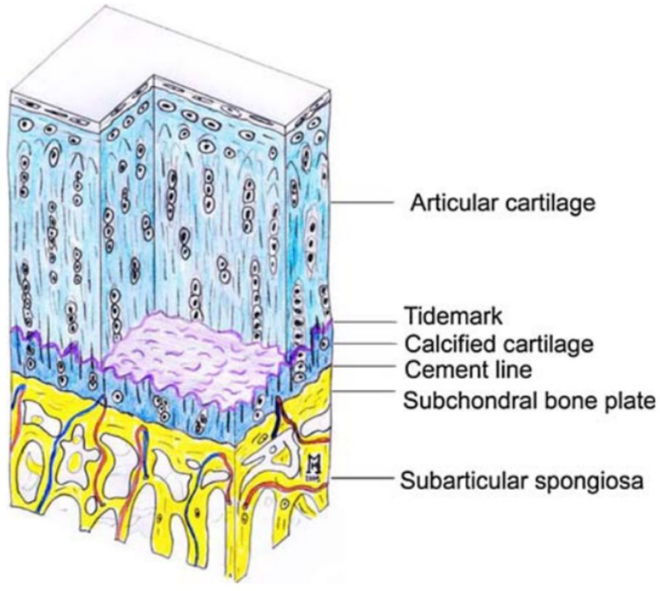

Figure 2-5|Structure of subchondral bone: *layers of the osteochondral unit from the articular cartilage, tidemark, calcified cartilage, cement lone subchondral bone plate and subarticular spongiosa*

There are two mechanisms by which bone is formed, endochondral ossification and intramembranous ossification. Intramembranous bone is formed via direct differentiation of mesenchymal cell condensation into osteoblasts. The endochondral ossification process includes an intermediate step of mesenchymal cell differentiation into chondrocytes and form a cartilage template (Fig.2-6 a-g). The chondrocytes eventually enlarge and become hypertrophic secreting collagen type X and angiogenic factors (Fig.2-6 c). Adjacent cells lining the immature bone become osteoblasts and form a bone collar, this is invaded by vasculature supplying oxygen and other nutrients (Fig.2-6 d). The hypertrophic chondrocytes eventually die and allow recruited osteoblasts to secrete bone ECM. As bone matrix is being formed in the centre, the chondrocytes at each apex is proliferating elongating the bone. A second ossification region is created sandwiching the proliferating chondrocytes (Fig.2-6 f), these will later form the growth plate. In the epiphysis region, there is evidence to suggest that the cartilage acts as a growth plate for bone development in the radial and longitudinal directions (Hunziker et al., 2007). This supports the hemispherical shape of the condyles.

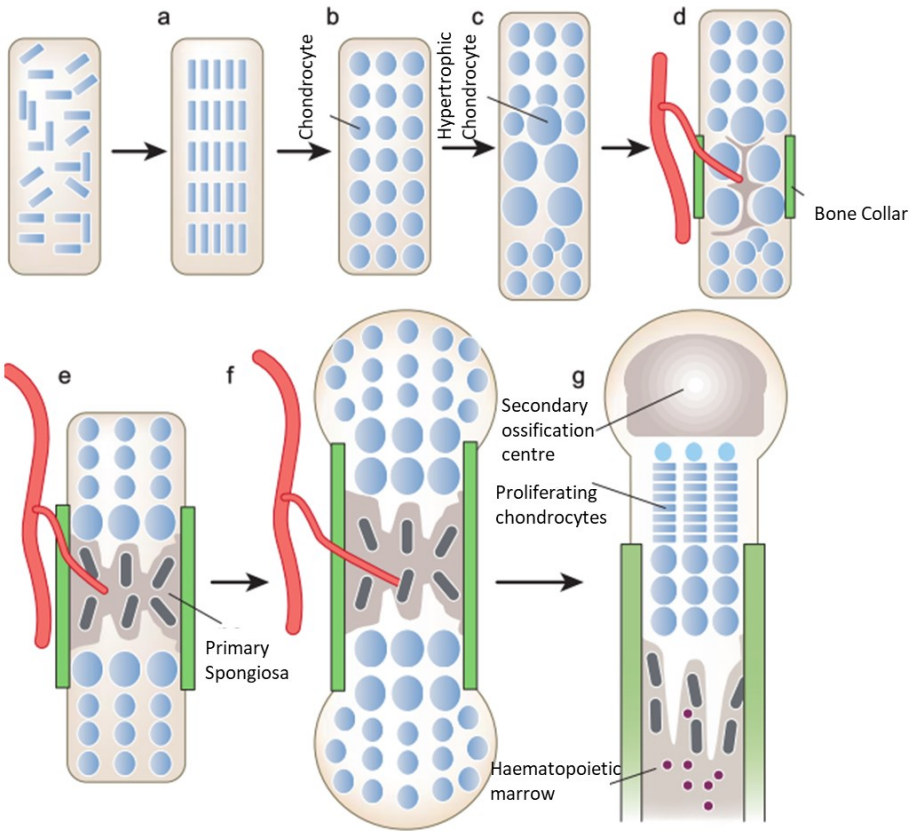

Figure 2-6 |Endochondral ossification process: *a) condensation of MSCs b) MSCs become chondrocytes forming a cartilage template c) chondrocytes in the centre become hypertrophic d) osteoblasts form creating a bone collar and hypertrophic cartilage form a mineralised matrix, blood vessels invade e)the primary spongiosa is formed f) chondrocytes proliferate lengthening the bone g) a secondary ossification centre and growth plate is formed*

2.5 Injury to Articular Cartilage and Subchondral Bone

When cartilage becomes damaged by trauma, disease, metabolic/inflammatory disorders or degeneration the protection against shear and compressive stresses is reduced causing pain and inhibiting mobility. Damage can range from a focal lesion to complete degeneration of the tissue resulting in a bone-bone interface. Additionally, injury to the meniscus or the cruciate ligaments can result in altered joint biomechanics with increased contact stresses (Andriacchi et al., 2006; Fithian et al., 1990; Martinez et al., 2006; Shiomi et al., 2012) and a concomitant increase in the risk of developing osteoarthritis (OA) (Moskowitz et al., 1973, 1979; Papalia et al., 2011; Wu et al., 1990). OA is one of the most prevalent degenerative diseases that affects 915,000 adults in Ireland alone (Arthritis Ireland, 2015). In 2004 the World Health Organisation (WHO) positioned OA in the top ten diseases which cause work loss due to disability. Subsequent investigations have shown that incidences of OA had increased by 32.9% since the WHO report (Vos et al., 2016). Due to the more active lifestyle of younger people, there is a rise in cases of OA amongst younger generations (Amoako et al., 2014).

2.5.1 Pathogenesis of OA

The aetiology of OA is poorly understood; however, the primary concept involves an unbalanced homeostasis, (i.e. secretion and degradation of ECM components). There are two phases associated with OA, a biosynthetic phase and a degradative phase (Sandell and Aigner, 2001). During the biosynthetic phase, the tissue attempts to repair itself increasing chondrocyte proliferation, anabolic and catabolic activity. However, the OA chondrocytes produce more degradative cytokines and factors than usual causing a catabolic response to dominate. For example, the production of cytokine interleukin-1 (IL-1) is increased, IL-1 stimulates metalloproteases that degrade the molecules of the matrix (Goldring, 2000). There is failure to stabilise the tissue, and eventually there is a decline in response of the chondrocytes and the tissue degrades. In later stage of OA the number of PG present in affected cartilage is decreased (Barbero et al., 2004; Tallheden et al., 2005) . The water content is increased which coupled with the reduced PG chain length leads to increased permeability and lower frictional drag, thus, a decreased matrix stiffness. This can be due to inflammation and/or reduced chondrocyte metabolism. These changes have a cascade affect decreasing the FCD and hence, the swelling pressure, while the hydrolytic permeability increases. As a result, the matrix deforms more than it would originally and there is increased fluid flow, lessening the load bearing properties. Additionally, changes to and/or loss of the parallel structure of the STZ occurs (Fig.2-7), without the tensile and shear resistant properties of the articulating surface further wear and degradation occurs (Mow and Huiskes, 2005). This degradation

continues causing degeneration of the entire cartilage surface until subchondral bone is exposed. Because cartilage and the bone function as a unit the subchondral bone also undergoes a number of degenerative changes. The articular cartilage-subchondral bone interface is remodelled during OA and in some cases the thickening of the subchondral plate occurs (Madry et al., 2010). Additionally, the calcified cartilage is invaded by vasculature from the underlying bone causing alternations to the cartilage homeostasis (Walsh et al., 2007). Additional markers or features of OA include the formation of osteocytes and synovial inflammation (Goldring and Goldring, 2010; Walsh et al., 2007).

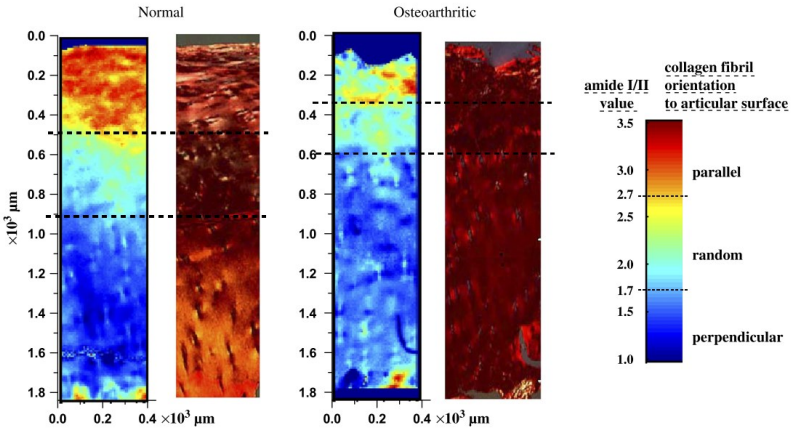

Figure 2-7| Structure of normal and osteoarthritic cartilage: *Polarised light light images of normal and diseased cartilage, the dashed line shows the boundary of the cartilage zones (Bi et al., 2005)*

2.6 Clinically Available Therapies for Treating Focal Cartilage Defects

The clinical treatment for OA includes pain management, anti-inflammatory medications and physiotherapy. A total joint replacement (TJR) is necessary when injury to the cartilage and bone is severely compromised. A TJR consists of metal femoral and tibial components with a plastic insert between the two. This prosthesis has a limited lifespan, after which time a further, more complicated surgery is required. Therefore, this is suboptimal for younger patients as they may require multiple invasive surgeries. Additionally, there are issues such as stress shielding, implant loosening, wear and integration with the underlying bone. A 2017 report on knee replacement surgeries carried out by the Norwegian National Advisory Unit on arthroplasty and hip fractures detailed the survival rates of implants (Norwegian National Advisory Unit on Arthoplasty and Hip Fractures, 2017). This report showed that whilst the there was an improvement in the longevity of implants from 2005 onwards, this was not true of unicondylar implants. Additionally, it highlighted that younger patients (<=60 years) had a lower prosthesis survival rate compared to older patients. To date there is no cell based

approach for OA. However there has been success in utilising tissue engineering strategies to treat cartilage lesions. Tissue engineering strategies for focal defects include microfracture, autologous chondrocyte implantation (ACI), matrix-assisted chondrocyte implantation (MACI) and osteochondral grafting.

Microfracture involves the penetration of the subchondral bone to cause bleeding which in turn forms a blood clot filled with bone marrow stem cells (BMSC). The concept is that these cells will stimulate repair, however, this procedure often results in inferior fibrocartilage (Harris et al., 2010; Lee et al., 2013) that does not compare mechanically to articular hyaline cartilage. Microfracture is considered a temporary repair and more suited to smaller defects (Kalson et al., 2010; Mithoefer et al., 2009).

ACI is a two-step procedure; firstly, chondrocytes are harvested from a non-load bearing area of the knee. They are digested and expanded in monolayer *in vitro* until a suitable number of cells are obtained. The cells, in a subsequent procedure, are then injected into the lesion beneath a periosteal flap (Figure 2-8) (Brittberg et al., 1994). The concept is that the chondrocyte suspension will secrete new matrix thus, regenerating the cartilage. However, chondrocytes when expanded on plastic in monolayer culture tend to de-differentiate (Benya and Shaffer, 1982a; Diaz-Romero et al., 2005; Marlovits et al., 2004; Schnabel et al., 2002). This can result in an inferior fibrocartilage or a mixture of hyaline and fibrocartilage (Gikas et al., 2009). Another disadvantage with this procedure is that two surgeries are required thereby increasing the chance of infection. ACI is recommended for lesions for larger (>2cm^2) lesions (Abdel-Sayed and Pioletti, 2015). However, there have been positive reports of athletes being able to return to activities 18-36 months after surgery (Harris et al., 2010). MACI is a 'next generation' ACI, as it includes similar steps except the cultured cells are encapsulated into, or seeded onto a biomaterial. The MACI product is secured using a fibrin based glue which eliminates the need for stitching (Kalson et al., 2010).

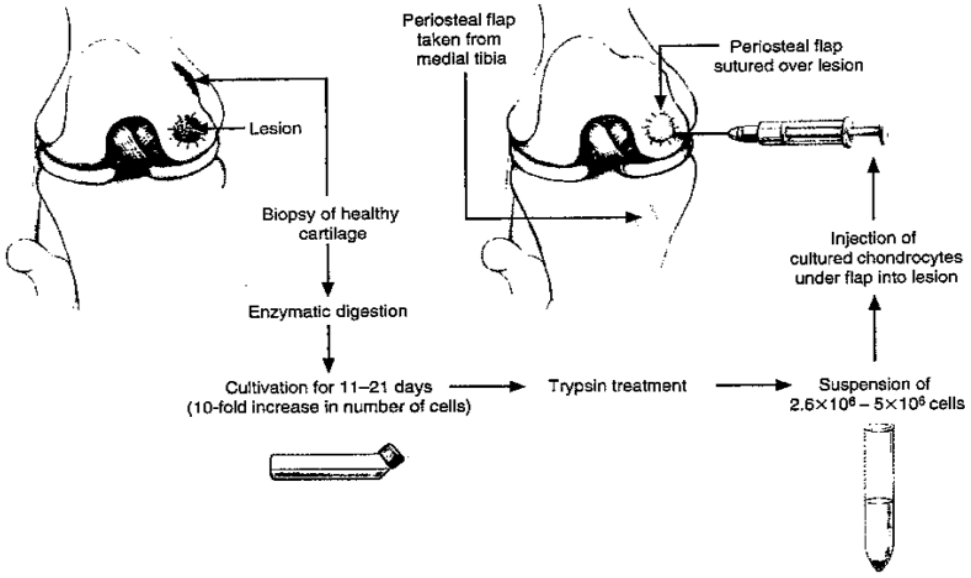

Figure 2-8| ACI procedure: *ACI procedure, cells are isolated from healthy cartilage, digested and expanded and the re-injected into the joint under periosteal flap* (Brittberg et al., 1994)

More severe defects which affect both the articular cartilage and the subchondral bone require different treatment approaches. Osteochondral grafting is often referred to as mosaicplasty or osteochondral autograft transplantation (OATS) and involves the transplantation of one or more osteochondral plugs into the defect site. The plug is harvested from an undamaged, non- or low weight bearing area. Disadvantages with this approach include harvest site morbidity and given that the graft originated in a low weight bearing area, when implanted in an area which experiences much higher and more frequent loads, it can be overloaded and degenerate (Hunziker, 2002). To overcome this allogenic cadaver plugs can also be used, however biocompatibility and immunological problems can be an issue and cryopreservation can lead to chondrocyte death and tissue deterioration (Hunziker, 2002). It has been also noted in a number of cases, that fibrocartilage forms between the gaps of the cylindrical plugs (Gudas et al., 2005). Despite these limitations, clinical successes with the OATS method has been reported. In one study on athletes it stated that 93% of patients returned to activities at preinjury level after undergoing the OATS procedure compared to 52% who received microfracture (Gudas et al., 2005).

Harris et al., 2010 reviewed 11 studies on the treatment of chondral defects in athletes' knees. They concluded that of the available treatments, OATS had the best recovery and chance of returning to sports followed by ACI, but microfracture had mixed results and its effectiveness was inconclusive (Harris et al., 2010). Donor site morbidity was cited as one of the major problems with these approaches. Also many of the reported successes were for a younger population (Harris et al., 2010) with no obvious signs of degeneration.

2.7 Tissue Engineering

Tissue engineering is an interdisciplinary field combining information from many backgrounds such as engineering, chemistry, biology and material science. The overall goal is to regenerate damaged tissues or to develop adequate substitutes. The typical approach involves three portions; cells, biomaterials and signals, this often referred to as the tissue engineering triad. The cells are responsible for secreting the tissue specific matrix. Scaffolds, house the cells and provide a temporary environment until the cells have laid down matrix. In general, these scaffolds will degrade over time. Signals can be mechanical, chemical or biological and are chosen and tailored depending on the tissue to be regenerated. The following section will examine each element in the triad in relation to cartilage tissue engineering.

2.8 Tissue Engineering Articular Cartilage

2.8.1 Cell Sources

Chondrocytes are the first cell choice for cartilage regeneration as they are the tissues native cell. They form cartilaginous like tissues both *in-vitro* and *in-vivo* (An et al., 2001; Aulthouse et al., 1989; B.R. et al., 2015; Hu and Athanasiou, 2006; Mesallati et al., 2013, 2015a) and are used clinically in ACI treatment. Despite the attractiveness of chondrocytes, there are several limitations associated with their use, these include:

- Only a limited number of chondrocytes are available upon isolation from a joint (Tallheden et al., 2005).
- Removing cartilage from undamaged areas, may cause site morbidity and further lesions and degradation
- The number of chondrocytes per gram of tissue decreases with age (Barbero et al., 2004)
- Chondrocytes gradually lose their phenotype and de-differentiate when passaged *in vitro* (Benya et al., 1978)

Mesenchymal stem/stromal cells (MSCs) are a multipotent cell source with the capacity to proliferate extensively and differentiate along a number of lineages. The differentiation pathway of an MSC depends on the source, chemical, environmental and physical cues. Importantly, there have been numerous studies demonstrating that MSCs undergo chondrogenesis in the presence of TGF-β3 and ideally in low oxygen conditions (Almeida et al., 2016; Daly et al., 2016b; Johnstone et al., 1998; Kanichai et al., 2008; Robins et al., 2005; Vinardell et al., 2012a). Adult MSCs can be isolated from tissues such as bone marrow (BMSC),

synovium (SDSC), infrapatellar fat-pad (FPSC) and adipose tissue (ADSC) (Ando et al., 2008; Awad et al., 2004; Dragoo et al., 2003; Johnstone et al., 1998; Liu et al., 2014; Pittenger et al., 1999; Shimomura et al., 2010; Vinardell et al., 2012a; Zuk, 2001).

The number of BMSC decreases with age (Muschler et al., 2001) and if the donor is >50years, the differentiation capabilities dramatically reduces (Mendes et al., 2002). Unlike chondrocytes, however, they can be passaged in-vitro without de-differentiation occurring. BMSC can be primed using growth factors such as TGF-β3 to differentiate into chondrocytes. A potential limitation of chondrogenically primed MSCs is their inherent tendency to undergo endochondral ossification and form bone (Pelttari et al., 2006; Vinardell et al., 2012a).

Fat-Pad derived stem cells (FPSC) are another promising MSC cell source. They are isolated from the fat-pad which lies behind the patella in the knee joint. FPSC have been shown synthesize chondrogenic markers sGAG and collagen type II using porcine cells (Buckley et al., 2010a; Mesallati et al., 2014) when supplemented with growth factor TGF-β3. Human cells derived from the FP of OA patients (Khan et al., 2007; Liu et al., 2014) have also been shown capable of synthesizing a cartilage specific matrix.

An alternative approach is to use a co-culture of a small number of primary cells with a larger number of stem cells (Hendriks et al., 2007; Paschos et al., 2014). The mechanism is not fully understood but thought that either MSC differentiation (as stimulated by the CC), chondroinduction (MSCs promoting CC proliferation) or a combination of the two (de Windt et al., 2014). An advantage of co-culture is it only uses a small number of chondrocytes, thus, eliminating the need to expand or acquire large quantities from the donor for a large joint resurfacing application. Co-culture has successfully enhanced the chondrogenic potential of BMSCs (Giovannini et al., 2010) and ADSCs (Wu et al., 2011) isolated from OA patients.

2.8.2 Biomaterials

3D scaffolds are widely used in the tissue engineering field for the encapsulation of cells to serve as a temporary extracellular matrix (Drury and Mooney, 2003) until the cells can secrete their own. The topography and stiffness of a scaffold can control stem cell fate (Engler et al., 2006). They can be fabricated materials such as decellurised ECM, synthetic or natural polymers. There are several considerations when choosing a biomaterial for cartilage tissue engineering. The biocompatibility of the material is paramount, it must not cause an adverse immune reaction or an inflammatory response (O'Brien, 2011). Additionally, having a similar elasticity and mechanical properties to the native tissue can help to maintain the chondrocyte phenotype or to direct the stem cells along the chondrogenic lineage. This can also prevent scaffold failure when implanted *in situ*. Cartilage is a load bearing material, scaffolds with

inferior mechanical properties may delaminate or become damaged. It must also support the characteristic round cell morphology of the chondrocyte.

Hydrogels are water swollen polymer networks that are commonly used as matrices/scaffolds. Hydrogels can be modified to incorporate ligands which the cells can bind to aiding in proliferation, differentiation and/or chondrogensis. There are numerous materials which can form hydrogels. These can be categorised as natural or synthetic. Natural hydrogels include collagen, agarose, alginate, fibrin and gelatin, while synthetic biomaterials commonly used in tissue engineering include polyetholene glycol (PEG), polyethylene oxide (PEO) and polyvinyl alcohol (PVA) or composites thereof. The advantage of naturally derived hydrogels is that they have molecular or structural similarities to the native ECM. Synthetic biomaterials can be attractive due to their reproducibility and tailorability (Drury and Mooney, 2003). Agarose, alginate and gelatin will be explored in more detail as they will feature in later chapters of this thesis.

Agarose is a naturally derived polysaccharide polymer from seaweed and forms a thermoreversible hydrogel. In solution at high temperatures agarose resembles a coil-like structure and during gelation (cooling) these form bundles and finally double helices. The structure can be controlled by the material concentration, with lower concentrations yielding hydrogels with larger pores and lower mechanical properties. Agarose has been shown to support chondrogenesis of adipose derived stem cells (Awad et al., 2004), BMSC (Huang et al., 2004), FPSC (Buckley et al., 2010a) and chondrocytes (Benya and Shaffer 1982). An advantage of agarose is that due to the low cell-adhesion properties it maintains the round cell shape of chondrocytes (Benya and Shaffer, 1982a) and promotes it in BMSC encapsulated in agarose (Mauck et al., 2006).

Alginate is a natural water-soluble material primarily derived from brown seaweed. It is a linear polysaccharide copolymer of 1,4-linked β-ᴅ mannuronic acid (M) and α-ʟ-guluronic acid (G) monomers (Drury and Mooney, 2003; Drury et al., 2004). It is a biocompatible material with low toxicity levels, is easily available and fabricated. Ionically cross-linked alginate hydrogels can be formed with calcium ions such as calcium chloride, calcium phosphate or calcium carbonate (Lee and Mooney, 2012). The stiffness can therefore be tailored based on the degree of crosslinking and the material concentration. One disadvantage is that it is non-degradable as mammals lack the appropriate enzyme. Dissolution of the gel is however possible, occurring when the ions are released to the surrounding medium (Lee and Mooney, 2012). Alginate has been extensively used in the field of tissue engineering, and has been shown to support chondrogenesis of stem cells and chondrocytes both *in vitro* and *in vivo* (Awad et al., 2004; Daly et al., 2016b; Igarashi et al., 2010; Mo et al., 2009; Sukegawa et al., 2012)RGD modified alginate has incorporated cell adhesion ligands to enhance cellular

adhesion. The degradation rate of alginate depends on the cross-linking density and the molecular weight.

Gelatin is derived from denatured and partially hydrolyzed collagen, therefore it retains some of the bioactive cues such as the arginylglycylaspartic acid (RGD) sequence which facilitates cellular adhesion, while matrix metalloproteinase (MMP) degradation sites allows for cellular remodelling (Klotz et al., 2016). Gelatin is a thermoreversible hydrogel, gelling at temperatures below 25-35˚C (Hoch et al., 2013). Methacrylated gelatin (gelMA) is commonly used as it overcomes the limitation of reversible thermal crosslinking by allowing covalent crosslinking in the presence of UV light. Properties such as stiffness can be tailored by altering the amount of methacrylation during fabrication (Yue et al., 2015). GelMA is widely used for cartilage applications as it supports both cell proliferation, migration and matrix production (Li et al., 2016; Schuurman et al., 2013). GelMA has also been combined with digested cartilage tissue in an attempt to promote tissue specific ECM production, although no significant improvement was observed over gelMA alone (Visser et al., 2015c).

2.8.3 Growth Factors

Growth factors are biological polypeptides which activate/stimulate the growth, differentiation or proliferation of active cells. They bind to specific receptors on the cell surface, some are versatile and some are cell-type specific. Many growth factors are present in articular cartilage and they work synergistically to regulate and promote cartilage growth and metabolism (Goldring et al., 2006). Key growth factors associated with chondrogenesis include members of transforming growth factor (TGF) family, which includes bone morphogenetic proteins (BMPs), fibroblastic growth factors (FGF) and insulin growth factor (IGF). These growth factors are used alone or in tandem to promote cartilage growth of stem cells.

Transforming Growth Factor β (TGF- β) is a family of growth factors, of which TGF- β1, TGF- β2 and TGF- β3 are extensively used in cartilage tissue engineering. They have been shown to maintain the chondrocyte phenotype (Giovannini et al., 2010) promote proliferation and chondrogenesis of BMSC micromass pellet cultures (Giovannini et al., 2010; Yoo et al., 1998) as defined by collagen type II and proteoglycan staining or incorporated into scaffolds supporting controlled release of TGF- β3 with subsequent chondrogenesis of human derived FPSC (Almeida et al., 2014) . Additionally, they have been shown to counteract the catabolic activity of OA (Blaney Davidson et al., 2007). The use of TGF must be controlled as direct injections into the joint have shown adverse responses from surrounding tissues, such as osteophyte formation at the synovial-chondral interface and fibrosis (Bakker et al., 2001; Blaney Davidson et al., 2007).

Bone Morphogenetic Proteins (BMPs) are members of the TGF-β superfamily. The use of BMP-7 alone on stem cells is not enough to induce robust chondrogenesis in a 3D model (Iwakura et al., 2013). However, when used in combination with a member of the TGF family it plays a supportive role (Weiss et al., 2010).

2.9 Endochondral Bone Tissue Engineering

2.9.1 Cell Sources

In general, MSCs are the most widely used cell type to recapitulate endochondral ossification Originating in marrow cavity BMSCs are an inherent choice to mimic endochondral ossification as they can be stimulated to undergo chondrogenesis and osteogenesis (Pittenger et al., 1999). As highlighted earlier, a disadvantage of BMSC for cartilage tissue engineering is the tendency to undergo hypertrophy (Pelttari et al., 2006), a key step in endochondral ossification. Several studies have investigated this as a method to tissue engineer bone (Dang et al., 2017; Farrell et al., 2009; Mesallati et al., 2015b; Scotti et al., 2010; Sheehy et al., 2015a, 2015b). Jukes *et. al* demonstrated that chondrogenically primed embryonic stem cells in the presence of TGF-β3 can form bone *in vivo* in a rat cranial defect (Jukes et al., 2008). Interestingly, they also demonstrated that at least 14 days of chondrogenic priming was required for bone to form within the template. Also of note, when mature chondrocytes themselves synthesized the chondrogenic template matrix, it did not mineralise. A number of other papers have confirmed this finding (Bahney et al., 2016; Gawlitta et al., 2010; Pelttari et al., 2006), however chondrocytes from transient cartilage (Oliveira et al., 2009a, 2009b), and modified chondrocytes (passage 5/6 stimulated with TGF-β3 and BMP-4) (Bahney et al., 2016) can undergo hypertrophy.

2.10 3D Bioprinting

3D printing of biomaterials with living cells, biomolecules and extracellular matrix (ECM) components is emerging as a powerful technique to engineer new tissues and organs to replace those lost due to trauma or disease (Daly et al., 2016a; Hockaday et al., 2012; Mandrycky et al., 2016; Moroni et al., 2017; Murphy and Atala, 2014; Visser et al., 2013). This technology allows for the accurate positioning of different cell types, growth factors, genes and other biological cues within 3D biomaterials to mimic the shape, structure, composition and ideally the function of different tissues and organs. The current technologies facilitate hybrid printing of cell

suspensions or cell encapsulated hydrogels (bioinks) and polymers such as polycaprolactone (PCL) or polylactic-co-glycolic acid (PLGA).

In commercially available bioprinters, there are two primary approaches to 3D printing, extrusion (via pneumatic, piston or screw) and inkjet (thermal or piezoelectric) (Fig.2-10 a, b). The extrusion based method involves applying a force to extrude the material through a needle in the form of a strand. The strand size can be controlled by the diameter of the needle and by varying the magnitude of extrusion force. The forces can be applied by one system or with multiple, usually, pneumatically or mechanically (by a piston or a screw)(Murphy and Atala, 2014). In many cases, the printer heads can be surrounded by heating or cooling jackets to facilitate printing of thermoreversible bioinks. One of the advantages of extrusion based printing is it can print a large variety of materials including PCL (Schuurman et al., 2011), bioinks such as gelMA (Klotz et al., 2016) and alginate (Kundu et al., 2015; Tabriz et al., 2015) and even more complex, 'tissue strands', which are self-assembled tissues in the shape of a strand/string (Yu et al., 2016).

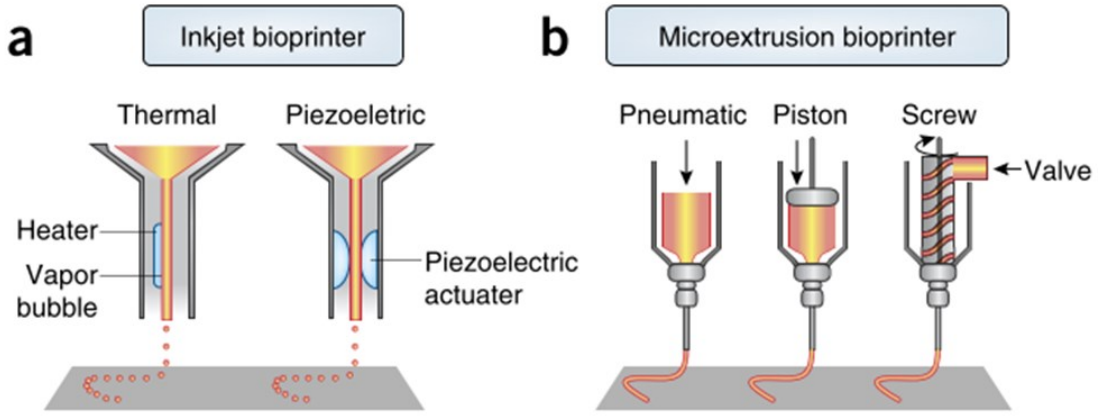

Figure 2-9| Bioink printer heads: *a) types of inkjet printing, thermal and piezoelectric b) types of microextrusion printer heads, pneumatic, piston and screw driven* (Murphy and Atala, 2014)

Inkjet printing technology deposits controlled volumes of cell suspensions or bioinks using piezoelectric or thermal affects onto a desired location. This technology offers high resolution, however, bioinks require a very low viscosity to be extruded (Hoch et al., 2013; Moroni et al., 2017; Murphy and Atala, 2014). Thermal inkjet printers function by heating the print head to produce small air bubbles, these collapse and provide a pressure pulse forcing droplets from the nozzle (Cui et al., 2012a). The size of droplets varies depending on the temperature gradient, frequency of current pulse, and ink viscosity (Cui et al., 2012a). The piezolectric method functions by applying a voltage to a piezoelectric crystal that creates an

acoustic wave deforming the material to break the liquid into droplets at regular intervals (Cui et al., 2012a; Murphy and Atala, 2014).

2.10.1 Bioinks and Printability

Bioprinting an anatomically accurate, functional joint will involve utilising bioinks that are both printable and provide encapsulated cells with an appropriate environment to perform their desired function (Fig.2-10 a). Many of the hydrogels traditionally used in biofabrication have been explored as bioinks for 3D bioprinting. As mentioned previously, there a number of key hydrogel design parameters, these parameters directly translate to bioinks with one critical addition, printability. Printability is an umbrella term incorporating the resolution and the shape stability which is influenced by the bioink rheology, concentration and crosslinking mechanism.The printability is strongly dependent on the viscosity and the yield stress of the material. The ideal bioink has been defined as (Jungst et al., 2016):

- Solid gel before printing with a shear thinning but not a thixotropic behaviour (time-dependent change in viscosity) to the viscosity that permits printing with the selected technology,
- Rapid gelation after printing to obtain high shape fidelity,
- Minimum or no swelling during or after extrusion.

In general, inkjet printer heads are more suited to depositing low viscosity materials which do not clog the print head. When using an extrusion based printer head, bioinks that exhibit non-Newtonian, shear thinning behaviour print with good shape fidelity. Shear thinning is the phenomenon that causes the polymer chains to align when a force is applied, thus decreasing the viscosity with increased shear strain (Fig.2-10 b). At the tip of the needle, when the strain is removed, the chains reassemble resulting in a stable strand. Potentially one of the more overlooked parameters is determining printability is the yield stress of bioinks. Yield stress is defined as the point at which the material begins to flow. It has been shown that bioinks with high yield stresses print filaments with greater shape fidelity than bioinks with the same viscosity but lower yield stress (Mouser et al., 2016). This occurs due to a steep viscosity drop after the yield stress has been overcome.

Parameters that can alter the viscosity of a bioink include biomaterial concentration (Chang et al., 2011), temperature or the number of encapsulated cells (Blaeser et al., 2016; Ouyang et al., 2016a). Several different techniques can be used to enhance the printability of bioinks without shear thinning properties. Such approaches include combining components such as nanoparticles to tailor the rheological properties, printing sacrificial bioinks to act as a

mould, printing into a bath of suitable cross-linking material, or by pre-crosslinking prior to dispensing (Tabriz et al., 2015). A number of simple methods have been used to gauge printability, such as comparing the printed geometry to the target geometry obtained from the original CT scans both immediately post-printing and after 24hours in PBS (Hockaday et al., 2012) or to the area of the inputted design (Duan et al., 2014). Alternatively, the ratio between the nozzle diameter the extruded filament diameter can be measured, with a value of 1 considered ideal (Fig.2-10 c) (Ouyang et al., 2016a).

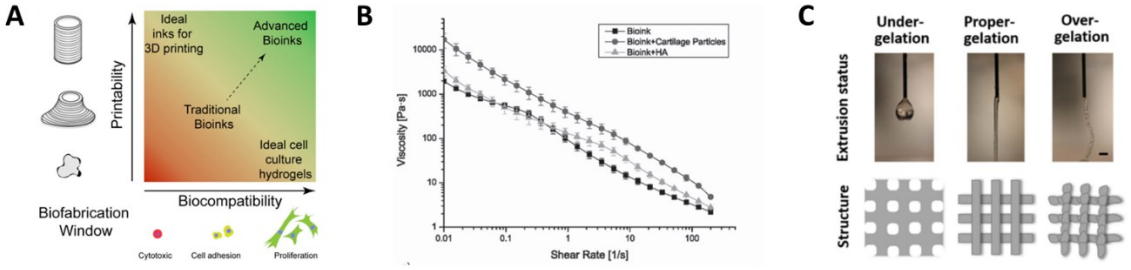

Figure 2-10| Bioinks for bioprinting: *A) The biofabriaction window, finding a balance between printability and biocompatibility* (Chimene et al., 2016)*, B) Graph depicting the shear-thinning behaviour (viscosity decreasing with shear rate) of a gellan gum-alginate bioink* (Kesti et al., 2015)*, C) Extrusion of gelatin-alginate strand illustrating printability, with under-gelation resulting in a droplet morphology and a lattice with truncated corners, ideal-gelation results a smooth uniform strand with square lattice and over-gelation results in an inconsistent strand thickness* (Ouyang et al., 2016a).

2.10.2 Bioprinting Articular Cartilage

The first studies bioprinting articular cartilage used traditional hydrogels as bioinks. These studies validated the use of 3D printing technology with the primary focus of these early studies on cell viability, the effects of shear and temperature on cellular function and modifications to hydrogels to ensure stable fibres could be printed.

Cui *et al.* (Cui et al., 2012b) demonstrated a 'direct repair' of a chondral defect by inkjetting a chondrocyte laden PEGDMA bioink into a defect in the cartilage of an osteochondral plug (Fig.2-11 a, b). They demonstrated that a viable homogenous distribution of cells could be obtained by simultaneously UV crosslinking. The construct was cultured for 6 weeks, after which time the chondrocytes had synthesised cartilage specific matrix. Schuurman *et al.* (Schuurman et al., 2013) demonstrated an 83% cell viability post printing a gelMA bioink. They also showed the concept of reinforcing a co-printing structure with two gelMA hydrogels inside a PCL frame. Several other early studies demonstrated modified solutions to extruding low viscosity bioinks. For example, alginate (hydrogel concentrations are usually between 1-4% which are typically not viscous enough to be printable), can be printed using a co-axial needle that surrounds the bioink with calcium chloride, thereby co-extrusion causes immediate

crosslinking to form a stable fibre (Costantini et al., 2016). Other papers have described methods to print gelMA which at 37˚C is in liquid form. They describe how blending gelMA with viscous components such as HA, gellan gum, fibrin or PEGDA result in more stable constructs at such temperatures (Melchels et al., 2014; Schuurman et al., 2013; Wei Xu et al., 2007; Zhou et al., 2017). An alternative approach involves the application of UV light directly to the extruding filament during the printing process, rather than post-printing, as this allows immediate crosslinking of the GelMA fiber as it is extruded from the needle orifice (Ouyang et al., 2016b) (Fig.2-11 c). This concept has facilitated spatial control over two different methacrylated materials to print complex shapes such as hollow tubes, core-shell structures and composites (Ouyang et al., 2016b).

Later papers have explored incorporating ECM into bioinks. One of the advantages of ECM derived scaffolds is they maintain some of the biological, chemical and signally cues to direct cell fate. In general, they are not rejected by the body and cell proliferation, migration and differentiation is observed on these scaffolds (Almeida et al., 2015). Incorporation of ECM into bioinks has been successfully executed in a number of ways; either ECM particles (cartilage pieces, or ECM components HA, CS and collagen) are added into a bioinks such as alginate or gelMA or the ECM is itself directly printed (Garreta et al., 2017; Kim et al., 2017; Pati et al., 2014). The benefits of the former approach were nicely demonstrated in a seminal study by Pati et al. (Pati et al., 2014), who demonstrated that decellurised and solubilised cartilage, heart and adipose ECM could be used to develop printable bioinks that provide tissue specific cues to direct the differentiation of encapsulated MSCs.

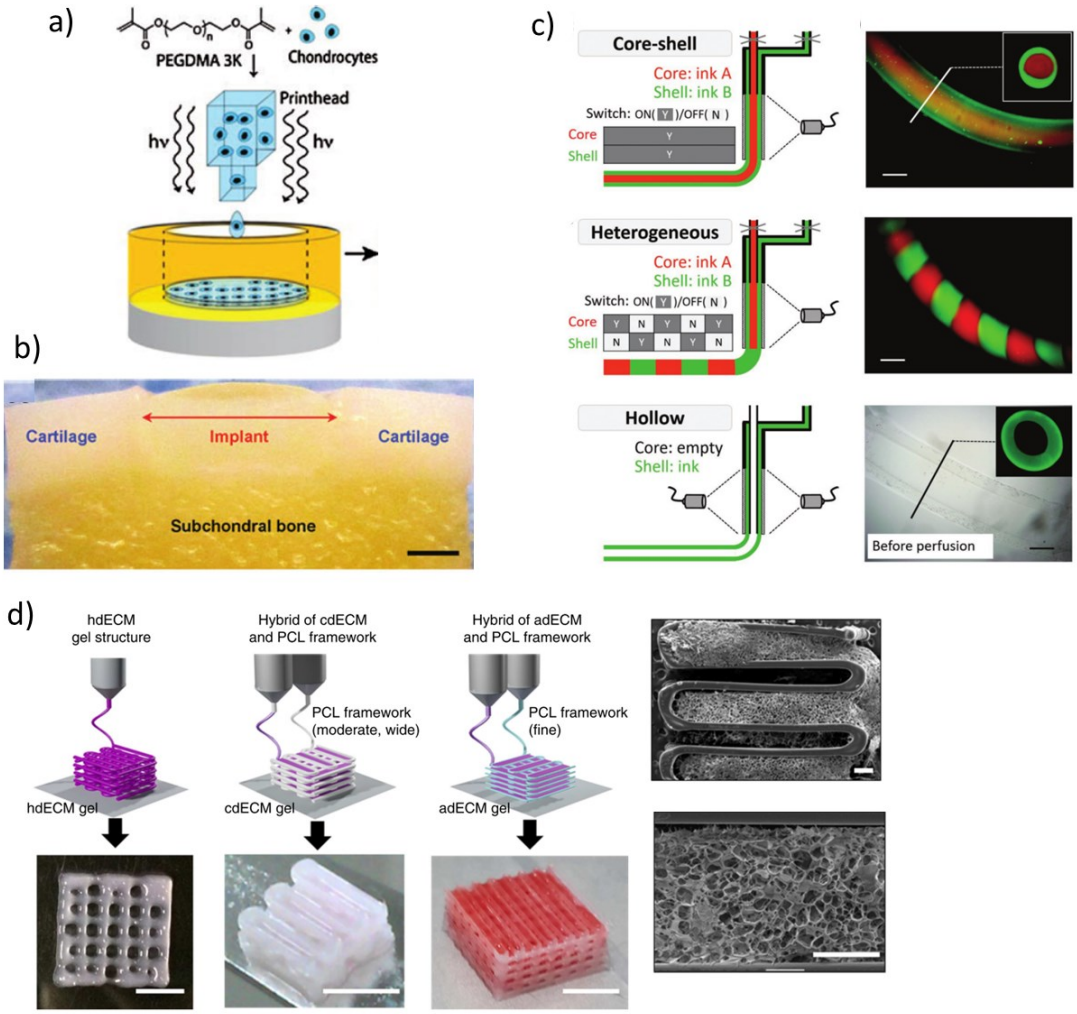

Figure 2-11| Bioinks: *a) direct repair for cartilage tissue engineering, ink-jetting PEGDMA laden with chondrocytes directly into the b) implant* (Cui et al., 2012b) *c) composite printing of multimaterial methacylated bioinks printed through a photopermeable lumen resulting in a core–shell when both inks are extruded and the UV is switched on, heterogeneous structure when each ink is extruded simultaneously and a hollow structure* (Ouyang et al., 2016b)*, d) ECM bioink can be printed alone and reinforced with PCL* (Pati et al., 2014)

Typically, low concentration hydrogels are used for cartilage tissue engineering which on their own generally lack sufficient mechanical integrity for implantation into high load bearing environments. The Young's modulus of cartilage is in the range of 0.2 to 2 MPa (Gannon et al., 2015; Gao et al., 2014; Wang et al., 2002) and the meniscus is 0.1-0.3 MPa (Sweigart et al., 2004), whereas the modulus of hydrogels that have been shown to support chondrogenesis are in the range of 0.2-40 kPa (Buckley et al., 2010a; Daly et al., 2016b; Lee et al., 2001; Nichol et al., 2010). Increasing the material concentration will increase the hydrogel stiffness, however the permeability will decrease and the matrix density will increase, which can negatively impact nutrient transport and waste removal. Furthermore, the hydrogel itself can become a barrier to extracellular matrix development (Erickson et al., 2009; Sridhar et al.,

2015). Additionally, it has been demonstrated that stiffer substrates direct stem cell fate to the undesired hypertrophic or osteogenic lineage (Engler et al., 2006). One of the advantages of 3D printing is the ability to reinforce these bioinks with a stiff polymer such as PCL or PLGA, thereby not impeding the niche or cues provided by the hydrogel.

Polycaprolactone (PCL) is a polymer that is used clinically for drug delivery. It is a hydrophobic, biocompatible polymer with degradation kinetics spanning 3-4 years (Woodruff and Hutmacher, 2010). PCL is widely used in 3D printing; its low melting temperature (59-64˚C) enables it to be extruded alongside bioinks without negatively affecting cell viability (Kim et al., 2016). The mechanical properties of a 3D printed PCL scaffold can be controlled by the material molecular weight and the filament pattern, spacing and diameter (Olubamiji et al., 2016). Hypothetically, this enables the development of a scaffold mimicking the bulk properties of native meniscus or articular cartilage. An excellent example of this involved the use of a gelMA composite reinforced by melt-electrospun PCL. The melt-electrospinning technique enabled the production of small (<100μm) diameter fibres with scaffold porosities of 93-98%. The authors observed synergistic increases in the mechanical properties of the composite material compared to the PCL scaffold alone, whereby the deformation of the fibres under axial loads were supported by the gelMA. By manipulating the fibre diameter and pore size they were able to generate constructs with stiffness and elasticity approaching native cartilage (Visser et al., 2015b).

To date, 3D printing of PCL has found use in the development of scaffolds for osteochondral defect repair. For example, MSC seeded 3D printed PCL scaffolds have been used to treat osteochondral defects in a rabbit femoral condyle, with no evidence of implant failure and improved joint repair compared to empty defects (Shao et al., 2006). A similar study was conducted but with the PCL as the support for a bilayered collagen (bone region) and HA (cartilage region) based bioinks. 8 weeks after implantation in the trochlear groove, the cartilage region demonstrated significantly improved repair compared to empty, PCL only and a bilayered alginate, based on histological scores (Shim et al., 2016). While such studies are promising, it should be noted that these focal osteochondral defects are much simpler to regenerate compared to treating a diseased joint where tissue damage is more diffuse.

Poly(D,L Lactic-Co-Glycolic Acid) (PLGA) is another biodegradable polymer that is widely used in the medical field (Middleton and Tipton, 2000). One of the many advantages to PLGA is the ability to tailor the degradation (Middleton and Tipton, 2000; Pan and Ding, 2012). This can be achieved by altering the ratio of lactic to glycolic acid. For example, 65:35 PLGA refers to the weight fractions of lactic acid and glycolic acid which are 65% and 35% respectively (Pan and Ding, 2012). A 50:50 PLGA degrades in approximately 1–2 months, 65:35 3-4, 85:15 in 5–6 months (Middleton and Tipton, 2000). Park *et al.* compared a 3D printed PCL

and a 50:50 PLGA scaffold to repair 1.5cm defect in the tibia. After 8 weeks, there was little to no evidence remaining of the PLGA, whereas the PCL frame was still visible (Park et al., 2012). PLGA has also been used to repair an osteochondral defect in the patellar groove of a rabbit, using a chondrogenically primed porous PLGA scaffold seeded with BMSC (Seung et al., 2008). PLGA can be printed using the extrusion process, it requires higher temperatures than PCL, from 95 to 145 degrees celcius. The printing temperature is dependent on the LA:GA ratio, the molecular weight and the end cap (Guo et al., 2006).

2.10.3 3D Printing Biological Whole Joints

Regenerating an entire functioning joint is the holy grail of tissue engineering. 3D printing technology has increased this prospect exponentially with 3D printed PCL playing an integral part of several new therapies for regenerating whole joint surfaces. There have been two seminal papers depicting the recreation of a rabbit shoulder and in a separate paper the meniscus. The geometries were obtained through CT scans. In the case of meniscus regeneration (Lee et al., 2014), a 3D printed PCL scaffold loaded with growth factor releasing microspheres was grafted in place of a resected meniscus in an ovine model (Fig.2-12 b). The scaffold had a dynamic modulus slightly exceeding the native value. No dislocation was reported, and the growth factor releasing scaffold was found to facilitate spatially defined meniscus tissue deposition and to restore mechanical functionality after 3 months (Lee et al., 2014). In the case of synovial joint regeneration (Lee et al., 2010), a PCL-hydroxyapatite composite was printed to mimic the geometry of rabbit shoulder, with TGF-β3 infused into the construct to recruit host cells and to promote cartilage repair (Fig.2-12 a). After 4 months, animals were reported to have a normal gait and histological sections demonstrated bone growth and the beginnings of cartilage repair. These studies demonstrate the potential of bioprinting strategies for whole joint regeneration, and provide a template upon which more complex strategies can be developed to treat diseased joints. Another pivotal paper demonstrated the capacity to print tissues on a human-scale. They combined several printing strategies to achieve an ear, muscle, a cranial defect and a mandible using strategies such as PCL reinforcement, and sacrificial fibers.

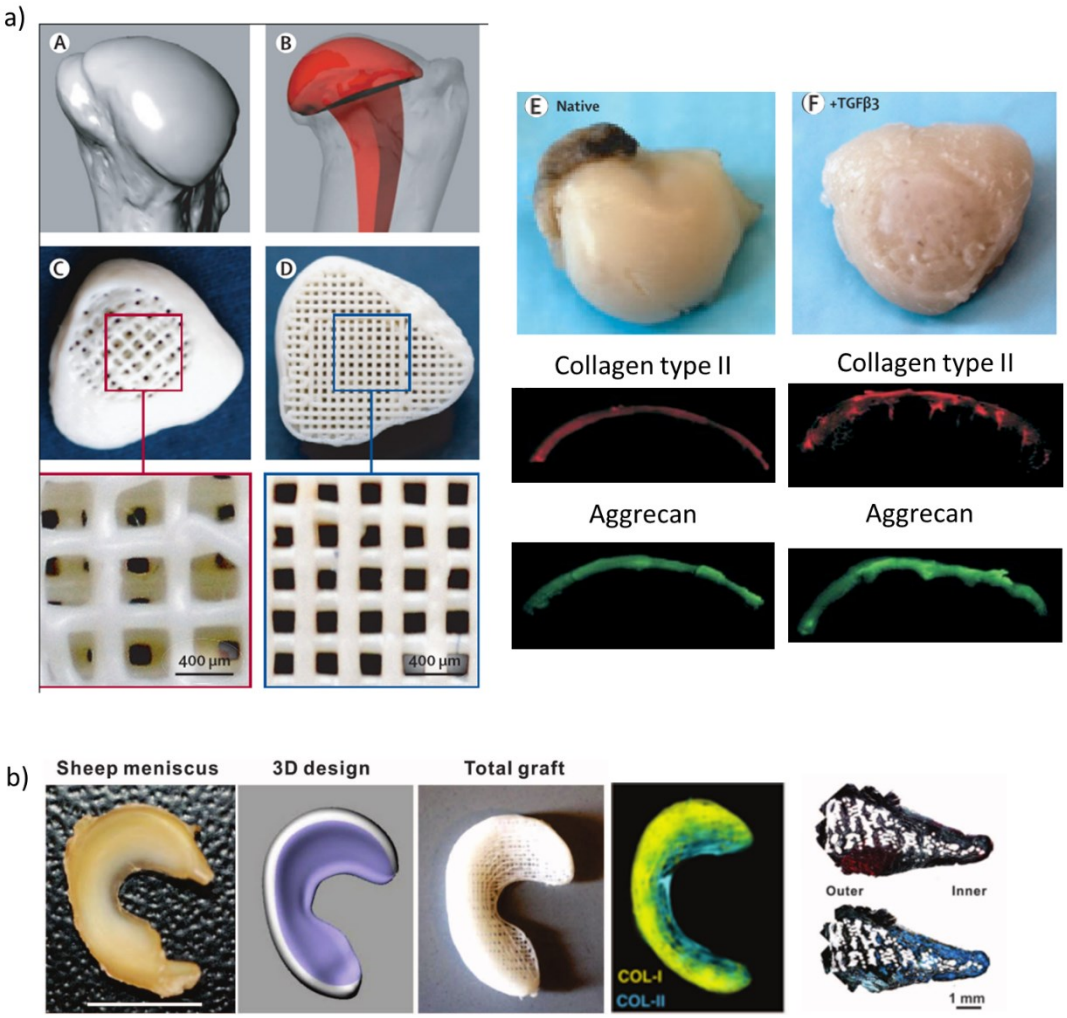

Figure 2-12| Whole joint applications: *a) A, Scan of the rabbit humeral head B, with the proposed implant, C, the top surface and the D, bottom surface of the 3D printed replacement joint, E, a native shoulder with immunoflurescence for collagen type II and aggrecan, F, 3D printed replacement with TGF-β3 and immunoflurescense* (Lee et al., 2010)*, b) 3D printed meniscus graft, with spatial distribution of collagen type I and type II, histological sections after implantation in vivo* (Lee et al., 2014)

2.11 Summary

In recent years, there have been impressive advances in the field of tissue engineering cartilage and bone. In parallel, developments in additive manufacturing has resulted in the use of 3D bioprinting as a promising technique to engineer anatomically accurate whole joints. The literature review has discussed the potential of recapitulating endochondral ossification to form mature bone tissue and the use of co-cultures to generate cartilaginous tissues. In general, the focus of these studies were on engineering implants for focal defects, with only a few seminal papers on engineering a whole joint. Transitioning from repairing focal defects to an entire joint will require ensuring sufficient mechanical properties of the tissue engineered construct, additionally it will require amplified cell numbers. The most promising study, from the Lancet, demonstrated repairing the shoulder joint of a rabbit using a 3D printed polymer frame containing a growth factor (designed to recruit host cells). This study has laid the groundwork for other synovial joints, however, additional steps of elucidating suitable cell sources and biomaterials for both cartilage and bone tissue are required to engineer a biological knee joint. In addition, as highlighted in the literature review, the chosen materials must comply with the limitations of bioinks used in conjunction with 3D bioprinting strategies.

It is first hypothesised in this thesis that a cartilage template can be formed through *in vitro* priming of BMSCs in a low molecular weight alginate hydrogel. This cartilage template will then mimic the process of endochondral ossification and regenerate both the bone and the cartilage in a critically sized osteochondral defect in a rabbit. It is next hypothesised that BMSCs alone are not sufficient to engineer phenotypically stable hyaline cartilage, therefore a co-culture of fat-pad stem cells (FPSCs) and articular chondrocytes derived from clinically relevant cells (from diseased patients) will support robust chondrogenesis. Next, recognising that hydrogels do not have sufficient mechanical properties for load bearing applications, a 3D printed polymer will be selected to reinforce bi-layered cartilage templated to form articular cartilage and endochondral bone. These templates will be evaluated *in vitro* and *in vivo*. Finally, having validated that reinforced bi-phasic cartilage templates can form the tissues analogous to osteochondral unit, a 3D bioprinting strategy will be developed to print an anatomically accurate polymer scaffold containing the bi-phasic cartilage templates that will undergo spatial tissue formation *in vivo*.

3 General methods

3.1 Bone marrow mesenchymal stem/stromal cells (BMSCs) isolation and culture

Bone marrow was removed from the femoral shaft and washed in high-glucose Dulbecco's Modified Eagle Medium (hgDMEM) (GlutaMAX™; Biosciences, Ireland) supplemented with 10% foetal bovine serum (FBS), (Biosciences, Ireland), 1% penicillin (100 U ml-1)-streptomycin (100 µg ml-1) (Biosciences, Ireland) and amphotericin B (0.25µg/mL) (Sigma-Aldrich, Ireland) hereafter, named XPAN. A homogenous cell suspension was achieved by triturating with a 18G needle. The solution was centrifuged twice at 650g for 5 min, with removal of the supernatant. The resultant cell pellet was triturated and the cell suspension was filtered through a 40 µm cell sieve (Falcon, Sarstedt, Ireland). Cell counting was performed with trypan blue and acetic acid before plating at a density of 5 x 10^3 cells/cm^2 and maintained in a humidified chamber. Following colony formation, cells were trypsinized, counted and re-plated for a further passage at a density of 5 x 10^3 cells/cm^2, FGF-2 (Prospec-Tany TechnoGene Ltd., Israel) was added to the XPAN media which was changed twice weekly.

3.2 Infrapatellar fat-pad stem cells (FPSCs) isolation and culture

The tissue was washed in sterile PBS (Sigma-Aldrich, Germany), weighed and then finely diced. The tissue was digested in hgDMEM containing 1% penicillin-streptomycin and 4ml per gram of tissue of collagenase type II (750 U ml^{-1}, Worthington Biochemical, LanganBach Services, Ireland) for 4 hrs under constant rotation at 37°C. The resulting cell suspension was filtered through a sieve with a pore size of 40µm and centrifuged at 650*g* for 5 mins. The supernatant was removed and cell number and viability were determined using a haemocytometer and 0.4% trypan blue staining (Sigma-Aldrich, Dublin, Ireland). Cells were plated at a density of 5 x 10^3 cells/cm^2 and maintained in XPAN media a humidified chamber. Following colony formation, cells were trypsinized, counted and re-plated for a further passage at a density of 5 x 10^3 cells/cm^2, FGF-2 was added to the XPAN media which was changed twice weekly.

3.3 Chondrocyte (CCs) isolation and culture

The cartilage tissue was rinsed with PBS, weighed and finely diced. Chondrocytes were isolated by digestion in hgDMEM containing 1% penicillin (100 U ml^{-1})-streptomycin (100 µg ml^{-1}) and 8ml per gram of collagenase type II (350 U ml^{-1}) for 12-14hr under constant rotation at 37°C. The resulting cell suspension was passed through a 40µm cell filter, and the filtrate centrifuged and rinsed with PBS twice. Cell number and viability were determined using a haemocytometer and 0.4% trypan blue staining.

3.4 Chondrogenic priming

Chondrogenic media containing hereafter CDM, consisting of hgDMEM supplemented with penicillin (100 U ml^{-1})-streptomycin (100 µg ml^{-1}), 100 µg ml^{-1} sodium pyruvate, 40 µg ml^{-1} l-proline, 50 µg ml^{-1} l-ascorbic acid-2-phosphate, 1.5 mg ml^{-1} BSA, 1× insulin-transferrin-selenium, 100 nM dexamethasone (all from Sigma-Aldrich, Ireland) and 10 ng ml^{-1} recombinant human growth factor-β3 (TGF-β3; ProSpec-Tany TechnoGene Ltd, Israel). Unless stated otherwise all chondrogenic priming was maintained in 5% oxygen in a humidified chamber with media change twice weekly.

3.5 Formation of pellets

Cells were lifted from plastic culture flasks using trypsin and counted. Pellets were formed by centrifuging 250,000 cells in 1.5 ml Eppendorf tubes at 2000rpm for 5 min. Pellets were maintained in CDM with 1ml supplied to each pellet and the medium was exchanged twice weekly.

3.6 Encapsulation in RGD-γ-irradiated alginate

The cartilage template was prepared by dissolving RGD-γ alginate in sterile hgDMEM to make up a final concentration of 1.5% w/v. RGD-γ alginate was made as follows;

Low-molecular-weight sodium alginate (52,000 g/mol) was prepared by irradiating Protanal LF 20/40 (196,000 g/mol; FMC Biopolymer, Philadelphia, PA) at a gamma dose of 5 Mrad (Alsberg et al., 2003). RGD-modified alginates were prepared by coupling the GGGGRGDSP to the alginate by carbodiimide reaction chemistry. Alginate (10 g) was dissolved

at 1% (w/v) in MES Buffer (pH 6.5). Sulfo-NHS (274 mg, Pierce, Rockford, IL), 1-Ethyl-3-(3-dimethylaminopropyl)carbodiimide (EDC, 484 mg, Sigma), and GGGGRGDSP peptide (100 mg, AIBioTech, Richmond, VA) were then added into alginate solution. After reacting for 24 h at 48C, the reaction was stopped by addition of hydroxylamine (0.18 mg/mL; Sigma), and the solution was purified by dialysis against ultrapure deionized water (diH2O) (MWCO 3500; Spectrum Laboratories, Rancho Dominguez, CA) for 3 days, treated with activated charcoal (0.5 mg/100 mL, 50–200 mesh; Fisher, Pittsburgh, PA) for 30 min, filtered (0.22 mm filter), and lyophilized (Jeon and Alsberg, 2013; Jeon et al., 2010, 2011).

The constructs were formed by combining BMSCs, counted and spun to form a cell pellet, with the alginate, using a 16G needle to mix the suspension with a final density of 2 x 10^7 cells/ml. The alginate/cell suspension was poured into a specifically designed 4% agarose mould containing 50 mM $CaCl_2$, and allowed to cross-link for 30 min at 37°C to produce 4 x 4 mm cylindrical constructs.

3.7 Gelatin methacrlyde (gelMA) synthesis

GelMA was synthesised by reaction of porcine type A gelatin (Sigma Aldrich) with methacrylic anhydride (Sigma Aldrich) at 50 °C for four hours. Methacrylic anhydride was added to a 10% solution of gelatin in PBS under constant stirring. To achieve a high degree of functionalization, 0.6 g of methacrylic anhydride was added per gram of gelatin. The functionalized polymer was dialyzed against distilled water for 7 days at 40 °C to remove methacrylic acid and anhydride, freeze-dried and stored at−20 °C until use. NMRwas used to confirm functionalisation of the GelMA hydrogels. The constructs were formed by combing a cell pellet with the final concentration of gelMa 10% and Irgacure 2959, 0.05%, in hgDMEN (Irgacure 2959 0.05%). The suspension was poured into a mould and subjected to UV light complete the cross-linking.

3.8 Histology and immunochemistry

In vitro samples were fixed in 4% PFA, before being embedded in paraffin, and sliced. Slices were rehydrated through graded alcohols before staining with 1% alcian blue 8GX in 0.1 M HCl, PH1 or Alician blue/Aldehyde Fuschin or safranin-o for sGAG, picrosirius red for collagen deposition, Alizarin Red pH 4.1 and Haematoxylin and Eosin (H&E) (all Sigma, Ireland).

I*n vivo* samples were fixed in 10% formalin (Sigma, Ireland) for 3 days under agitation at room temperature. The samples were decalcified using 'Decalcifying Solution-Lite' (Sigma-

Aldrich) for 1-6 weeks. Samples were frequently x-rayed to determine if any mineral content remined. When no mineral was visible the sample was considered decalcified. The samples were cut along the plane to be visualised and paraffin wax embedded. Histological sections were cut to a thickness of 10μm and stained as mentioned above.

Collagen types I and II were identified through immunohistochemistry. Paraffinised samples were rehydrated and antigen retrieval was performed using chondroitinase ABC, 0.25 U/ml, (Sigma) at 37°C for 1 h. This was followed by incubation in a blocking buffer (10% goat serum and 1% BSA in PBS) to prevent binding of non-specific sites. Rinses were performed in-between each step in PBS. The primary anti-body was applied for 1hr at room temperature in the following dilutions in blocking buffer, mouse monoclonal anti-collagen type I (Abcam) 1:400 (ab90395, 1:400) and mouse monoclonal anti-collagen type II (Abcam) 1:100 II (ab3092, 1:100) or collagen type X (ab49945, 1:100) were applied overnight at 4°C. Endogenous peroxidase activity was blocked by submersing the sides in 3% hydrogen peroxide solution for 20 minutes in the dark. Then, the secondary antibody, collagen type I and II, 1.5:200 (B7151, anti-mouse IgG biotin conjugate; Sigma-Aldrich) and collagen type X, ab49760, 1:200 was added for another hour. Colour was developed using the Vectastain ABC reagent (Vectastain ABC kit: Vector Laboratories) for 45 min and exposure to peroxidase DAB substrate kit (Vector laboratories) for 5 min. Slides were dehydrated and mounted with Vectamount medium (Vector Laboratories). Ligament, cartilage and growth plate were included as controls for collagen type I, type II and type X respectively.

3.9 Quantitative biochemical analysis

Samples were digested in papain (125 μg mL^{-1}) in 0.1 M sodium acetate, 5 mM cysteine HCl, and 0.05 M EDTA (pH 6.0) (all from Sigma-Aldrich) at 60 °C under constant rotation for 18h. Total DNA content was quantified using the Hoechst Bisbenzimide 33258 dye assay (Sigma-Aldrich). Proteoglycan content was estimated by quantifying the amount of sulfated glycosaminoglycan (sGAG) in constructs using the dimethylmethylene blue dye-binding assay (Blyscan, Biocolor Ltd.) pH 1.35, with a chondroitin sulfate standard. Total collagen content was determined by measuring the hydroxyproline content. Samples were hydrolyzed at 110°C for 18 h in concentrated HCL (38%) and assayed using a chloramine-T assay with a hydroxyproline-to-collagen ratio of 1:7.69. Calcium content was analysed by digesting the samples in 1M of HCL at 60 °C under constant rotation until sample is fully dissolved. Calcium was detected using the sentinel calcium kit (Alpha Labs, UK)

3.10 3D Printing Process

A 3D bioplotter from RegenHU (3D Discovery) was used for 3D printing. Scaffold architectures were designed using the accompanying software, BioCAD (RegenHU, Switzerland). Polycaprolactone (PCL), Mw=45 000, (Sigma-Aldrich and Capa) was melted in the printing chamber. A screw driven piston (screw diameter 1 cm) extruded the PCL onto a coverslip. Parameters for printing are described in the individual results section.

3.11 Statistics

Results are presented as mean + standard deviation. Statistical analysis was performed with GraphPad Prism 6 software package (GraphPad, USA). Experimental groups were analyzed for significance differences using either a t-test or a general linear model for analysis of variance (ANOVA) and preforming Tukey's post-test, significance was accepted at a level of $p < 0.05$.

4 Regeneration of osteochondral defects by spatially restricting endochondral ossification within engineered cartilage grafts

4.1 Introduction

Successfully treating osteochondral defects involves regenerating both the damaged articular cartilage and the underlying subchondral bone, in addition to the complex interface that separates these tissues. Current treatments such as mosaicplasty are limited by complications such as donor site morbidity, matching the topography of the damaged site and poor graft integration (Bowland et al., 2015; Koh et al., 2004; Nakagawa et al., 2007). This has motivated the development of tissue engineered implants to treat these clinically challenging defects (Grässel and Lorenz, 2014; Martin et al., 2007). To this end there has been increased interest in recapitulating aspects of tissue or organ development when designing new regenerative strategies. All long bones, including their epiphyses, are formed, in part, by the process of endochondral ossification (Hunziker et al., 2007; Scotti et al., 2010). Their development involves the condensation of stem cells, which differentiate into chondrocytes to form a cartilage model/template. The chondrocytes enlarge and become hypertrophic, secreting collagen type X and angiogenic factors, and their surrounding extracellular matrix (ECM) is invaded by vasculature (Kronenberg, 2003). The subsequent delivery of oxygen, growth factors and other regulatory cues through this vasculature, as well as the recruitment of osteo-progenitor cells, promotes osteogenesis and bone formation (Hu et al., 2017). During postnatal development, articular cartilage also acts as a surface growth plate for the longitudinal, radial and lateral growth of the epiphyseal bone (Hunziker et al., 2007). Therefore, cartilage acts as the precursor tissue to the cancellous bone, subchondral bone, calcified cartilage and articular cartilage that make up a mature long bone organ. Bone marrow derived mesenchymal stem cells (BMSCs) have been used to engineer both articular cartilage (Liu et al., 2008; Mackay et al., 1998; Ng et al., 2017) and hypertrophic cartilage templates for endochondral bone tissue engineering (Daly et al., 2016a; Dang et al., 2017; Farrell et al., 2009; Scotti et al., 2010). Under appropriate environmental conditions, this suggests that cartilage tissue engineered using BMSCs could provide a template for the development of the different components of the osteochondral unit. To date, no tissue engineering strategy exists to successfully regenerate the complex bone, articular and calcified cartilage interface within damaged joints.

While it is well established that cartilaginous tissues engineered using BMSCs can progress along the endochondral pathway and mineralize (Farrell et al., 2009; Scotti et al., 2010; Sheehy et al., 2015a; Vinardell et al., 2012a), certain environmental factors such as oxygen (Chen et al., 2015; Leijten et al., 2014; Sheehy et al., 2012), or the application of joint-like mechanical loading (Carroll et al., 2014; Luo et al., 2015; Vinardell et al., 2012b) can modulate this process and promote the development of a more stable chondrogenic phenotype. *In situ,* the oxygen tension of bone ranges from 5 - 12.5% pO_2, whereas cartilage resides in a more hypoxic environment with levels ranging from 1 - 5% pO_2 (Lafont, 2010). BMSC-laden constructs maintained at or below 5% pO_2 undergo enhanced chondrogenesis with a suppression of hypertrophy, whereas culture at higher oxygen concentrations tends to direct BMSCs towards an osteogenic lineage (Kanichai et al., 2008; Robins et al., 2005; Sheehy et al., 2012). Physiological levels of hydrostatic pressures increases TGF-β expression, regulates ECM synthesis (Ikenoue et al., 2003; Luo et al., 2015; Steward et al., 2012; Takahashi et al., 1997) and suppresses calcium deposition within BMSC laden constructs (Carroll et al., 2014; Thorpe et al., 2013a), however, application of levels outside the physiological range can have negative effects (Takahashi et al., 1997). Other mechanical cues such as dynamic compression can also enhance chondrogenesis of MSCs and suppress their tendency to progress along an endochondral pathway (Li et al., 2010; Luo et al., 2015; Thorpe et al., 2013b; Yao et al., 2010). *In vivo* it seems clear that such environmental cues will also play a central role in determining the fate of tissues engineered using BMSCs.

The objective of this study was to tissue engineer a cartilage template using BMSCs and to then evaluate its capacity to repair a critically sized osteochondral (OC) defect in the femoral condyle of skeletally mature rabbits. The hypothesis is that this cartilage template would undergo spatially defined differentiation *in vivo* in response to the unique environmental conditions within an OC defect, resulting in the development of a repair tissue consisting of hyaline articular cartilage overlying a layer of bone formed *via* endochondral ossification.

4.2 Materials and methods

4.2.1 Cell isolation and expansion

Bone marrow derived mesenchymal stem cells (BMSCs) were obtained from the femur of 4-6 month old lapine donors. The isolation of bone marrow is described in Chapter 3 section 3.1 with one differentiation, all expansion media was supplemented with 8% foetal bovine serum and 2% rabbit serum (Sigma, Ireland). All expansion was conducted at 5% oxygen tension and media was changed twice weekly. Cells were embedded within the alginate gel at the end of passage 2.

4.2.2 Engineering of the Cartilage Template

The cartilage template was prepared by dissolving RGD-γ alginate in sterile hgDMEM to make up a final concentration of 1.5% w/v. The preparation of RGD-γ alginate is described in Chapter 4 section 3.6. The constructs were formed by combining BMSCs, counted and spun to form a cell pellet, with the alginate, using a 16G needle to mix the suspension with a final density of 2 x 10^7 cells/ml. The alginate/cell suspension was poured into a specifically designed 4% agarose mould containing 50 mM $CaCl_2$, and allowed to cross-link for 30 min at 37°C to produce 4 x 4 mm cylindrical constructs. Constructs were maintained CDM (Chapter 3, section 3.4). Constructs were cultured at 37°C with 5% oxygen for 4 weeks and 20% oxygen for 5 days with medium exchange twice weekly.

4.2.3 Biochemical, histological and Immunohistochemical analysis

Cartilage templates were either digested in 500µl of papain or fixed in 4% PFA, and analysed as described in Chapter 3, sections 3.8 and 3.9

4.2.4 Cartilage template implantation

New Zealand white (6-8 months) rabbits were anesthetized with ketamine-medatomidine maintained using isofluorane and oxygen. The defect sites were prepared by shaving and washing with chlorhexidine surgical scrub and alcohol. Surgical drapes were used to cover the non-incision area. Defects (4 x 4 mm in diameter) were introduced in the medial femoral condyle of the hind leg of using a biopsy punch and a dental drill with a burr. The defects were cleaned with saline prior to implanting the cartilage template. Two defects were made per rabbit (one in each femur), constructs were implanted (n=6) by press-fitting and empty defects

served as controls (n=6). Post-surgery, rabbits were permitted free activity with post-operative analgesia buprenorphine hydrochloride, given for three days. Animals were sacrificed after 3 months using Pentobarbital. This protocol and study was reviewed and approved by the ethics committee of Trinity College Dublin, Ireland and Health Products Regulatory Authority (HPRA), Ireland.

4.2.5 Histological Scoring

Histological and macroscopic blind scoring was conducted by 6 impartial people in groups of 2 (n=3 scores). The wax embedded sample was cut down the centre and sliced from the centre of the defect. Two histological slides (one from each side of the sample) were included in the randomly selected histological slides for scoring, and an average score was calculated. Histological and macroscopic images were scored using a modified version of the O'Driscoll score (Table 4-1 & 4-2).

Table 4-1| Macroscopic Scoring

Parameter	Points
Surface Smoothness of the Cartilage	
Smooth	0
Moderate	1
Irregular	2
Severe	3
Edge Integration with Native Cartilage	
Completely Integrated	0
Partial	1
None	2

Table 4-2| Histological Scoring

Parameter	Points
% Repair Tissue that is Hyaline	
80-100%	8
60-80%	6
40-60%	4
20-40%	2
0-20%	0
Articular Surface Continuity	
Continuous and Smooth	2
Continuous but Rough	1
Discontinuous	0
Thickness of Repair Tissue Compared to Host Cartilage	
81-120% of normal cartilage	2
51-81% of normal cartilage	1
0-50% of normal cartilage	0
Tidemark	
Present	2
Incomplete	1
Absent	0
Integration of Cartilage	
Complete (integrated on both sides)	2
Partial	1
Poor (not integrated)	0
Degenerative Changes in the Repair Tissue	
Normal cellularity	2
Slight to moderate hypocellularity or hypercellularity	1
Severe hypocellularity or hypercellularity	0
Degenerative Changes in Adjacent Cartilage	
Normal cellularity, no clusters, no fibrillations	3
Normal cellularity, mild clusters, superficial fibrillations	2
Mild cellularity, moderate fibrillations	1
Severe changes in cellularity, moderate fibrillations	0
Chondrocyte Clustering	
No clusters	2
<25% of cells	1
25-100% cells	0
Total Score	23

4.2.6 Mechanical Testing

Indentation tests were performed using a single column Zwick (Zwick, Roell, Germany) with a 5 N load cell. Unconfined compression tests were carried out as previously described (Olvera et al., 2015). Briefly, the repaired tissue was indented using an impermeable metal indenter of 1 mm diameter to a depth of 50μm into the tissue and held until relaxation. Subsequently, a dynamic test was performed at 1 Hz, from this the amplitude of the dynamic stress was extracted by dividing the cross-sectional area by the average force between the peak and trough of ten cycles. The mechanics of the repair tissue was assessed at the centre point, unless there was an uneven surface; in such cases preference was given to the region with the most repair tissue slightly left or right of the centre of the defect site.

4.2.7 Micro-computed tomography

Micro-computed tomography (μCT) scans were performed on the femoral condyle explants using a Scanco Medical 40 μCT system (Scanco Medical, Bassersdorf, Switzerland) to visualise and quantify mineral deposition. Six condyles were scanned per experimental and control group after 3 months *in vivo*. Constructs were scanned in 50% EtOH, at a voxel resolution of 30 μm, a voltage of 70 kVp, and a current of 114 μA. Reconstructed 3D images were generated to visualise the repaired bone. Quantification of mineralization within the defect site was performed by setting a threshold of 210 (corresponding to a density of 399.5 mg hydroxyapatite/cm^3) and calculating the bone volume (BV) within a 3.5 x 3.5 mm cylinder, which excluded the original bone.

4.2.8 Statistical Analysis

Results are presented as mean ± standard deviation. Statistical analysis was performed with GraphPad Prism 5 software package (GraphPad, USA). Experimental groups were analyzed for significant differences using either a t-test or a general linear model for analysis of variance (ANOVA). Significance was accepted at a level of $p < 0.05$.

4.3 Results

4.3.1 RGD functionalized, γ-irradiated alginate hydrogels support the development of a cartilage template in vitro

Over 32 days of *in vitro* culture the RGD γ-irradiated alginate hydrogels supported the development of a cartilage-like tissue that stained positive for collagen type II and sGAG (Fig.4-1 c). sGAG and collagen accumulation were measured to be 166 ± 28 µg and 123 ± 10 µg respectively. There was some positive staining for collagen type X, indicating the early stages of hypertrophy in some areas of the cartilage template (Fig.4-1 c), although negative staining for alizarin red (for calcium deposition) and collagen type I demonstrated that the tissue had not ossified to any extent *in vitro* (Fig.4-1 c). There was a significant increase in mechanical properties of the template over time in culture, from 2.39 ± 0.94 kPa to 7.35 ± 1.25 kPa (Fig.4-1 b).

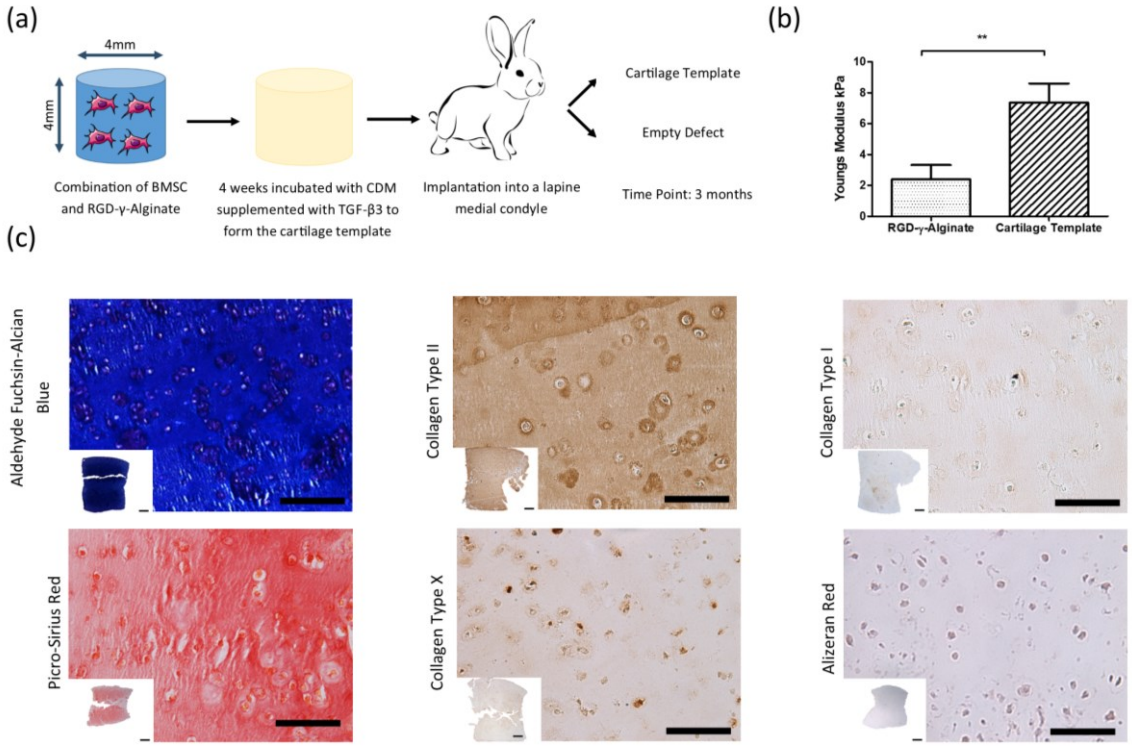

Figure 4-1| Tissue engineering a cartilage template: *(a) The process by which the cartilage template was formed (b) Young's Modulus for the acellular RGD-γ-alginate day 0 and after 28 days in culture pre-implantation, n=3 **p<0.01 (c) Histology for chondrogenic markers sGAG (alcian blue-aldehyde fuchsin) collagen (picro-sirius red) and collagen type II, hypertrophic marker collagen type X, fibrocartilage collagen type I and calcium (alizarin red), scale bar = 100µm, insert scale bar = 1000µm.*

4.3.2 *Treatment of OC defects with an engineered cartilage template results in the development of a stiffer repair tissue*

Macroscopically, there was no difference apparent between the treated group and empty control group (Fig.4-2 a, b), as quantified using macroscopic scoring (Fig.4-2 c, d). In both groups, there were instances of what appeared to be both complete and partial filling of the defects. However, mechanical testing identified that repair tissue was significantly stiffer in defects treated with the cartilage template compared to the empty controls (Fig.4-2 e-g).

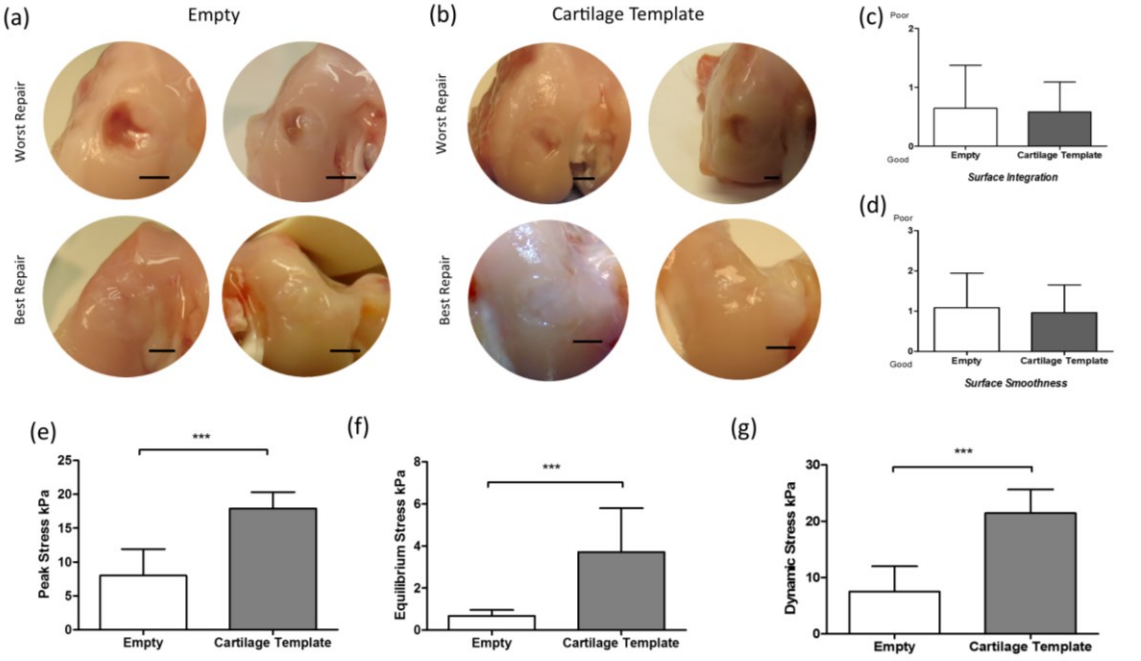

Figure 4-2 | In vivo repair: *Macroscopic repair of best and worst for (a) control empty defects and (b) cartilage template, scale bar = 2000µm. Macroscopic scoring (n=6) for (c) surface integration and (d) surface smoothness. (e-g) Mechanical testing at 3 months, (n=6 ***p<0.001, **p<0.01, t-test).*

De novo bone tissue was observed within the osteochondral defects. The reconstructed 3D scans demonstrated mineralized tissue within the centre of the defect, with trabecular struts evident in the deeper regions of the repair tissue (Fig.4-3 a, b). Complete bone repair was not detected in either the empty or treated defects, and even in the best examples of repair there was some evidence of incomplete subchondral bone regeneration at the bone-cartilage interface. Quantitative analysis of the defect area revealed no significant difference in overall levels of bone fill between empty and treated defects (Fig.4-3 c, d).

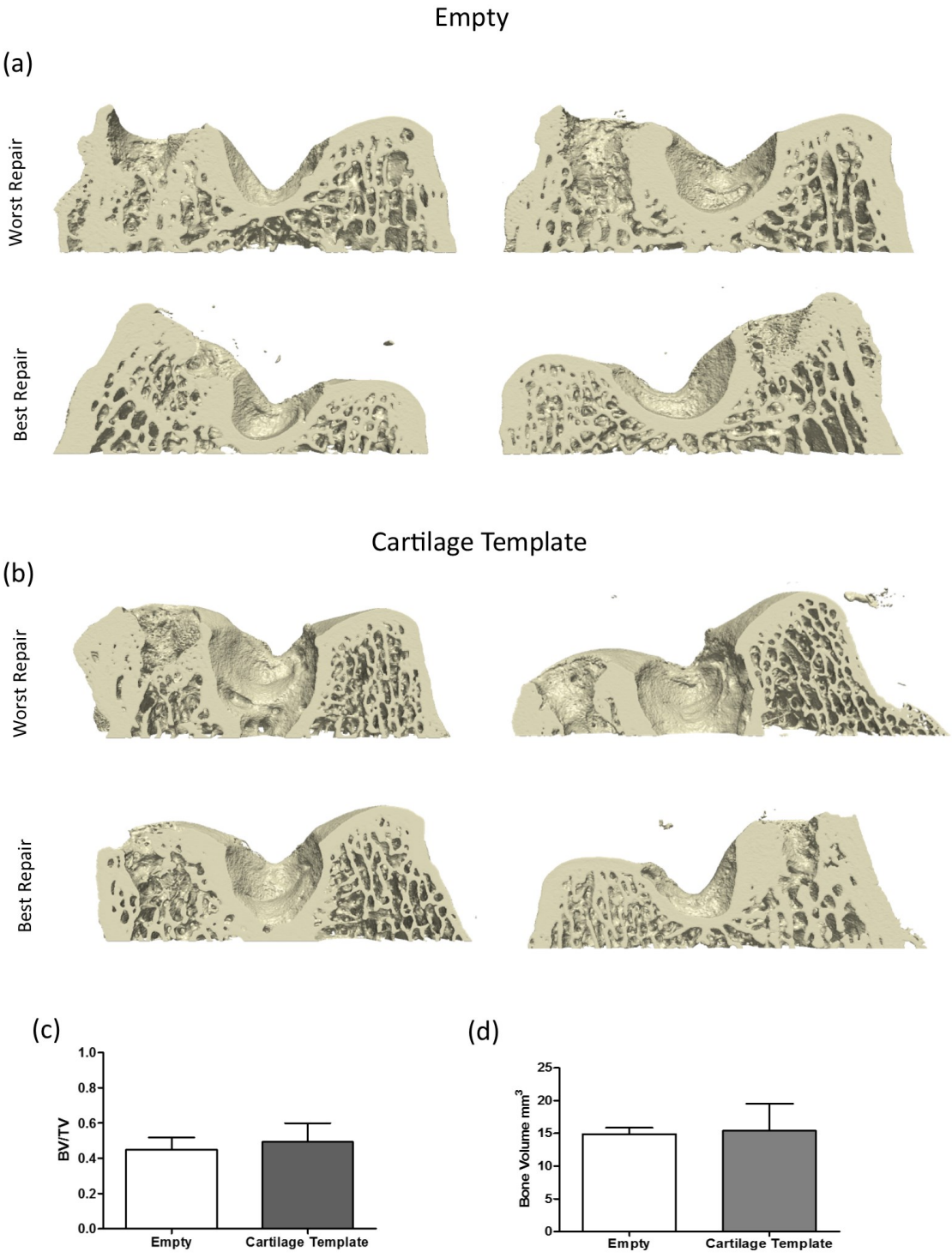

Figure 4-3| Bone repair: *(a) 3D reconstruction of the microCT scans of the untreated and the treated condyles. The insert image in the top-left of each shows the cross-sectional plane through the defect. Quantitative analysis of c) the ratio of bone volume to total volume within a defined cylinder within the defect site and d) total bone volume (scale bar = 4mm).*

4.3.3 *Engineered cartilage templates promote the development of a more hyaline cartilage-like repair tissue in osteochondral defects*

All defects treated with engineered cartilage templates stained intensely with alcian blue, indicating the development of proteoglycan-rich tissue, with more variable staining observed within the empty controls (Fig.4-4 a, b). The best repair observed in the empty defects was fibrocartilaginous in nature, staining positively for type I and type II collagen, whilst the corresponding cartilage template treated defects displayed a more hyaline-like tissue with only minimal type I collagen staining (Fig.4-4 a-d). The repair tissue stained weakly for type X collagen, a marker for hypertrophy, in the best repair both empty and treated defects. However, there appeared to be pericellular staining of the collagen type X in the poorer repair empty defects.

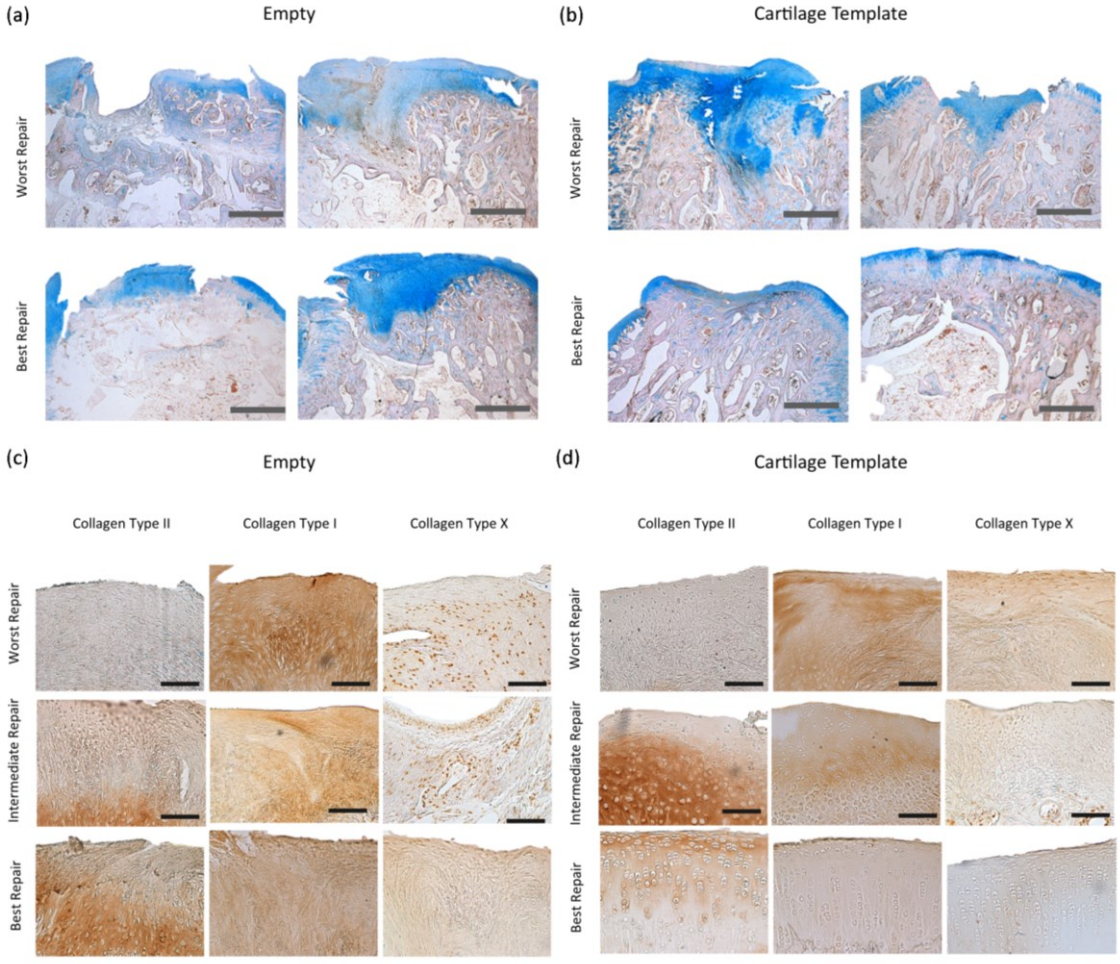

Figure 4-4| Histological Staining: *Alcian blue staining depicting the two best and two worst observed repair for two different a) empty and b) cartilage template (scale bar 2mm). Immunohistochemical staining for collagen type II, I and X portraying the worst, intermediate and best repair for c) empty and d) cartilage template (scale bar 200μm)*

Following blind evaluation of histological sections, a significant difference was found in the overall histological scores of empty and treated defects, with superior repair observed in treated defects (Fig.4-5 a, b). Additionally, a lack of cellular alignment is observed within the empty controls when compared to native cartilage. The cartilage template treated group generally exhibited more normal cell morphology and alignment more like that of native articular cartilage (Fig.4-5 d). Overall, the histomorphometric analysis demonstrated that the cartilage template trended towards improved repair in all parameters evaluated, with significant differences observed for percentage tissue that is hyaline (Fig.4-5 b), integration of newly formed cartilage with surrounding cartilage (Fig.4-5 f) and a lack of degenerative changes in the adjacent tissue (Fig.4-5 h).

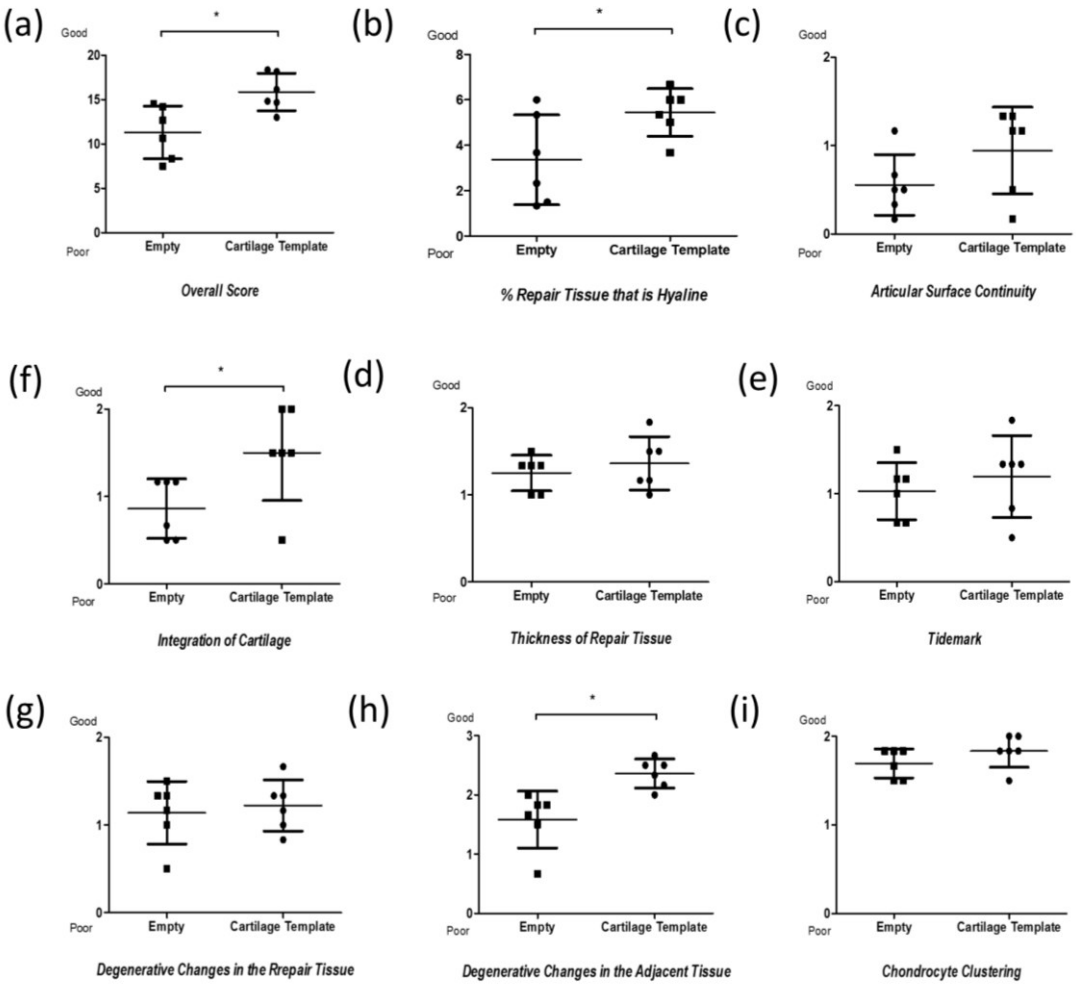

Figure 4-5: Histological Scoring: *Histomorphometric analysis of cartilage repair parameters, demonstrating significant differences in (a) overall score, (b) % hyaline repair tissue, (f) integration of cartilage and (h) a lack of degenerative changes to adjacent cartilage. (n=6, *p<0.05, t-test)*

4.4 Discussion

The osteochondral unit develops postnatally from a cartilaginous precursor that undergoes endochondral ossification during skeletal maturation (Hunziker et al., 2007; Worthley et al., 2015). Inspired by this developmental process, herein this study has demonstrated that cartilaginous templates engineered using BMSCs encapsulated within RGD-modified and gamma irradiated alginate hydrogels can be used to regenerate critically-sized osteochondral defects. While empty osteochondral defects are capable of undergoing spontaneous repair (Orth et al., 2012; Wei and Messner, 1999), more hyaline-like cartilage tissue was observed in defects treated with engineered soft tissue templates. Furthermore, the repair tissue in treated defects was stiffer than in empty controls.

Cartilage templates were engineered *in vitro* by encapsulating BMSCs within RGD modified and *γ*-irradiated alginate hydrogels and by stimulating these constructs with TGF-β3 over 32 days *in vitro*. Such alginate hydrogels have previously been shown to support endochondral bone formation subcutaneously (Daly et al., 2016a), and in this study cartilaginous tissues engineered within these gels also facilitated bone regeneration and remodeling within the osseous phase of the osteochondral defect. Biomaterials are commonly used for bone tissue engineering; however, a key factor is tailoring the material degradation rate to synchronize with tissue formation, and to facilitate vascular invasion. Previously it has been shown that unmodified alginate can support the development of a hypertrophic cartilage template *in vitro* (Mesallati et al., 2015b) and endochondral bone formation subcutaneously (Sheehy et al., 2015a), but permitted only limited bone formation *in vivo* in a cranial defect model due to the slow degradation rate of the hydrogel (Cunniffe et al., 2015). However, using this modified alginate, in 4 out of the 6 defects there was no evidence of significant amounts of residual material 3 months post-implantation.

Defects treated with the engineered cartilage template were found to contain a more hyaline-like repair tissue as demonstrated by histological staining, superior mechanical properties and a statistically significant histomorphometric scores. The inferior mechanical properties of the repair tissue within the empty control defects, coupled with positive collagen type 1 staining, suggests the development of a fibrocartilaginous tissue. The integration of the *de novo* cartilage with existing cartilage is also paramount for joint stability, and in often reported to be difficult to achieve with bioengineering strategies (Obradovic et al., 2001; Wakitani et al., 1994). For example, integration with the host tissue was one of limiting factors reported to affect complete of repair of osteochondral defects using bone marrow derived stem cells in a collagen gel (Wakitani et al., 1994). In this study, a significantly more integrated repair tissue is observed in the treated group, however consistent integration with the host cartilage

was not obtained. In addition, hyaline repair was not observed in all treated defects, demonstrating that further optimization of the tissue engineering strategy is warranted.

Ideally the mechanical properties of the engineered template would more closely mimic that of the native tissue prior to implantation, or the oxygen environment within the template could be altered through the incorporation of hypoxia inducing factors (Park and Gerecht, 2014). Potentially, a stiffer implant is required to sustain the harsh loading, however, it must not compromise the chondrogenic capacity of the implant. This could be achieved, for example, using 3D biofabrication technology to reinforce the alginate hydrogel with printed polymer fibres (Visser et al., 2015a). Polycaprolactone (PCL) has previously been used in articular cartilage defects to some degree of success (Martinez-Diaz et al., 2010).

In summary, tissue engineered cartilage templates in some cases were found to undergo spatially defined differentiation in response to local environmental cues within OC defects. This engineered template prompted the development of a more hyaline-like cartilage repair tissue compared to empty controls, there was, however, variability between animals.

4.5 Concluding Remarks

This chapter examined the potential of an engineered cartilage template to mimic the developmental process of endochondral ossification, and thereby continue towards osteochondral defect regeneration. Inspired by the potential of the cartilage template to regenerate the osteochondral unit, but recognising that hyaline cartilage repair was not consistent, the next chapter will seek to develop a chondral layer which is designed to specifically support the development if stable hyaline cartilage. Many studies in the literature have detailed that a co-culture of MSCs and CC result in more stable chondrogenesis over that observed with MSCs alone. Furthermore, co-cultures provide the large numbers of cells required for engineering scaled-up cartilaginous tissues. It will next be assessed if this concept is viable clinically by evaluating chondrogenesis using co-cultures of cells isolated from osteoarthritic joints.

5 Low oxygen conditions promote synergistic increases in chondrogenesis during co-culture of human osteoarthritic stem cells and chondrocytes

5.1 Introduction

Autologous chondrocyte implantation (ACI) is a well-established technique for treating cartilage defects which involves filling the defect site with high numbers of autologous chondrocytes harvested from non-load bearing areas (Brittberg et al., 1994). In order to obtain sufficient numbers of chondrocytes, *in vitro* expansion of cells is required which results in de-differentiation and a loss of phenotype as evidenced by the development of a more elongated fibroblastic cell morphology and increased collagen type 1 synthesis (Benya and Shaffer, 1982b; Diaz-Romero et al., 2005; Marlovits et al., 2004; Schnabel et al., 2002). Such limitations have led to increased interest in the use of co-cultures of chondrocytes and mesenchymal stem cells (MSCs), where small numbers of chondrocytes are combined with larger numbers of stem cells for the purposes of engineering stable articular cartilage (Hendriks et al., 2007; Leijten et al., 2013; de Windt et al., 2014). The putative benefits of such co-cultures are multi-faceted. They may limit or prevent the need for culture expansion of chondrocytes thereby enabling the development of single stage therapies (Bekkers et al., 2013a, 2013b; McNickle et al., 2008). They promote proliferation and the reestablishment of a chondrocyte phenotype (Acharya et al., 2012; Wu et al., 2011). In addition, they enable the engineering of scaled-up tissues that could be used for resurfacing of entire joints (Mesallati et al., 2015b). Realising the full potential of this co-culture approach will require identifying the optimal combinations of cell types and environmental conditions for promoting robust chondrogenesis.

The mechanism by which a co-culture enhances chondrogenesis is not completely understood. It has been established that MSCs secrete factors such as FGF-1 and FGF-2 (Wu et al., 2013) that promote proliferation of chondrocytes (Jakob et al., 2001; Tsuchiya et al., 2004). MSCs have also been shown to secrete TGF-β and TIMP-2 which is an anti-inflammatory cytokine inhibiting metalloproteinase activity (van Buul et al., 2012; Doorn et al., 2012; Schinkothe et al., 2008). Furthermore, there is evidence to suggest that chondrocytes can in turn promote chondrogenesis of MSCs (or at least a subset of MSCs within the co-culture)(Liu et al., 2010), supress hypertrophy (Bian et al., 2011) and increase matrix synthesis (Acharya et

al., 2012; Bian et al., 2011; Giovannini et al., 2010; Sabatino et al., 2012; Wu et al., 2011). Growth factors such as TGF-β3, IGF-1, and BMP-2 (Chen et al., 2009; Liu et al., 2010) have been detected in the media of co-cultures. All three have been reported to be involved in the chondrogenic process and synergistically enhance ECM production (Fortier et al., 2011; Indrawattana et al., 2004; Sailor et al., 1996).

The benefit of such co-cultures has been established for different courses of stem cells, including bone marrow and adipose derived stem cells (Awad et al., 2004; Estes et al., 2006; Johnstone et al., 1998; Mackay et al., 1998). More recently, pre-clinical and clinical studies (NCT01041885) have been undertaken to establish the efficacy of such cell combinations for repairing focal cartilage defects (Bekkers et al., 2013b). For example, pre-clinically it has been shown that a combination of freshly isolated chondrocytes (i.e not culture expanded) and BMSCs leads to statistical significant higher macroscopic regeneration compared to microfracture in goat focal cartilage defects (Bekkers et al., 2013b). Such freshly isolated chondrocytes appear particularly responsive to the factors secreted by MSCs in a co-culture, and are particularly attractive for the development of single-stage or point-of-care cell based therapies for treating focal cartilage defects. However, as there is a shift towards engineering tissues of scale for treating severely damaged or osteoarthritic joint surfaces, it is likely that large numbers of expanded chondrocytes will be required, even when using co-cultures to engineer such tissues. It remains unclear if such expanded chondrocytes will respond differently to freshly isolated chondrocytes in co-culture with MSCs. It also unclear if such co-cultures will lead to enhanced chondrogenesis using cells isolated from osteoarthritic patients.

Previously it has been demonstrated that a co-culture of chondrocytes with either bone marrow or infrapatellar fat pad derived stem cells can promote the development of phenotypically stable cartilage *in vivo* (Mesallati et al., 2015b). These cells were isolated from young porcine donors, which may not be representative of clinically relevant cell sources. The goal of this study was to explore the potential of co-cultures of chondrocytes and infrapatellar fat pad derived stem cells (FPSCs) isolated from osteoarthritic donors for promoting robust chondrogenesis. Given that chondrocytes de-differentiate into a more fibroblastic-like cell during *in vitro* expansion (Darling and Athanasiou, 2005), it was sought to compare the capacity of freshly isolated and culture expanded chondrocytes to generate robust cartilage in co-cultures with diseased FPSCs. Given the importance of oxygen in regulating chondrogenesis (Buckley et al., 2010b; Leijten et al., 2014; Meyer et al., 2010; Schrobback et al., 2012; Sheehy et al., 2012; Thorpe et al., 2013a), these co-cultures were maintained in both normoxic (20% pO2) and low oxygen (5% pO2) culture conditions.

5.2 Materials and methods

5.2.1 Cell isolation and expansion

Ethical approval for the use of human fat-pad (FP) and cartilage tissue was obtained from the institutional review board of the Mater Misericordiae University Hospital. FP and cartilage tissue was obtained from 5 patients undergoing total joint arthroplasty for degenerative OA. The cells were isolated following the protocol outline in Chapter 3, section 3.2 and 3.3. The cells from the 5 donors were pooled to form a 'superlot' (Bodle et al., 2014). The FPSC and CC were plated separately at a seeding density of 5×10^3 cells cm^{-2} and supplemented with 5 ng/ml FGF-2. Cells were expanded in 20% oxygen for 2 passages prior to differentiation. Media changes were performed twice weekly.

5.2.2 Chondrogenesis in pellet culture

Pellets were formed by centrifuging 250,000 cells in 1.5 ml eppendorf tubes at 2000rpm for 5 min. 'Fresh' (non-expanded) cells were used after digestion of cartilage tissue. 'Expanded' cells were lifted from plastic culture flasks using trypsin. Co-cultures were formed with 25% CCs and 75% FPSCs. Pellets were maintained in chondrogenic medium (CDM), consisting of hgDMEM supplemented with penicillin (100 U ml^{-1})-streptomycin (100 µg ml^{-1}), 100 µg ml^{-1} sodium pyruvate, 40 µg ml^{-1} l-proline, 50 µg ml^{-1} l-ascorbic acid-2-phosphate, 1.5 mg ml^{-1} BSA, 1× insulin-transferrin-selenium, 100 nM dexamethasone (all from Sigma-Aldrich, Ireland) and 10 ng ml^{-1} recombinant human growth factor-β3 (TGF-β3; ProSpec-Tany TechnoGene Ltd, Israel). Pellets were cultured at 37°C with 5% O_2 or 20% O_2 for 28 days with medium exchange twice weekly. Additional pellets were also supplemented with 10 ng/ml recombinant human bone morphogenic protein-7 (ProSpec-Tany TechnoGene Ltd, Israel). Pellets were cultured at 37°C with 5% O_2 for a period of 28 days. 1ml of CDM was supplied to each pellet and the medium was exchanged twice weekly.

5.2.3 Biochemical, histological and immunohistochemistry analysis

Pellets were either digested in 300µl of papain or fixed in 4% PFA, and analysed as described in Chapter 3, sections 3.8 and 3.9

5.2.4 Interaction index

The interaction index was calculated using the method as described by Acharya *et al*. 2012. Briefly the expected value was calculated by using the following equation:

$$sGAG\ expected = (sGAG_{100\%\ Chondrocyte}\ x\ 25\%) + (sGAG_{100\%\ FPSC}\ x\ 75\%)$$

…Equation 1

$sGAG_{100\%\ Chondrocyte}$ = Level of sGAG measured in chondrocyte only pellet

$sGAG_{100\%\ FPSC}$ = Level of sGAG measured in FPSC only pellet

The interaction index was calculated by:

$$\frac{sGAG_{measured\ from\ co-culture}}{sGAG_{expected}}$$

…Equation 2

A value of 1 denotes that the sGAG measured from the co-culture is equal to the expected level of sGAG determined from equation 1 above. A value greater than 1 signifies synergistic increases in ECM accumulation (chondro-induction) i.e. MSC-induced chondrocyte proliferation and/or chondrocyte-enhanced MSC chondrogenesis.

5.2.5 Immunohistochemistry quantification

Quantification of the immunohistochemistry sections was conducted using the open source software Image-J. The number of positive DAB pixels was determined using an established protocol (Varghese et al., 2014). Briefly, a colour deconvolution was preformed separating the colours on the DAB spectrum from the rest of the image, background staining was negated with threshold values obtained from the control image. The number of positive particles was analysed and normalised to the size of the slice to obtain a percentage area positive for a specific type of collagen. A minimum of two samples with 2-3 slices from each sample were analysed per group.

5.2.6 Statistics

Results are presented as mean ± standard deviation. Statistical analysis was performed with GraphPad Prism 6 software package. Experimental groups were analyzed for significance differences using either a t-test or a general linear model for analysis of variance (ANOVA) and

preforming Tukey's post-test. All graphs are presented with error bars + standard deviation, significance was accepted at a level of $p < 0.05$.

5.3 Results

5.3.1 Cartilage matrix synthesis is enhanced within hypoxic co-cultures

Pellets were formed using CCs (freshly isolated or culture expanded) or FPSCs alone or in co-culture. After 28 days of culture, DNA levels were highest in the co-cultures, suggesting that cells were more proliferative in this environment (Fig.5-1 a). The DNA content of such co-cultures was higher than FPSC only cultures at both 5% O_2 and 20% O_2, using either freshly isolated or culture expanded chondrocytes. Fresh chondrocytes secreted the highest levels of sGAG in both oxygen environments; however, collagen accumulation was lower in chondrocyte only pellets compared to other groups. A co-culture of fresh chondrocytes and FPSCs contained at least twice as much sGAG as FPSCs alone (21.795 µg *vs* 7.71 µg at 5%; 15.6128 µg *vs* 8.32 µg at 20% O2; $p<0.05$). Furthermore, both sGAG and collagen accumulation within the co-culture containing fresh chondrocytes was significantly higher when maintained in low oxygen conditions (Fig.5-1 b, c). As expected, expanded chondrocytes secreted dramatically lower levels of sGAG than freshly isolated chondrocytes in both normoxic and low oxygen environments (36.15µg *vs* 11.54µg at 5% O_2; 29.28µg *vs* 14.34µg at 20% O_2). Using such expanded chondrocytes, it was found that the highest levels of collagen were observed in the co-culture. Both co-cultures were also found to promote the development of a tissue with a collagen-sGAG ratio closer to native articular cartilage (~2:1) (Fig.5-1 d) (Mesallati et al., 2013; Mwale et al., 2004; Plumb and Aspden, 2005; Whitney et al., 2012, 2017). Histological staining for sGAG and collagen deposition confirmed these findings (Supplementary Fig. S1).

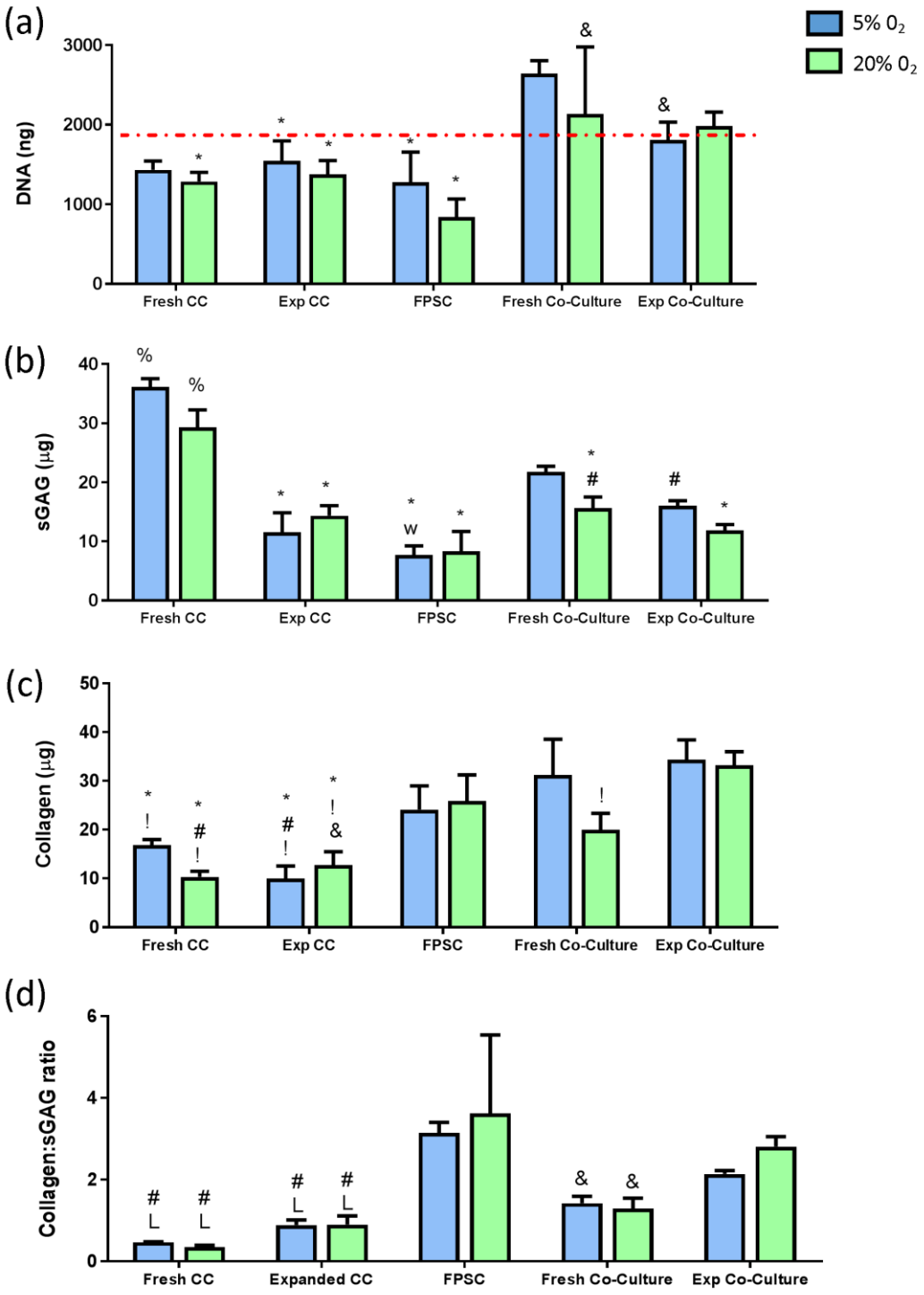

Figure 5-1| Biochemical analysis at day 28: *Freshly isolated chondrocytes (fresh CC), expanded chondrocytes (exp CC), expanded FPSC (FPSC), co-culture of freshly isolated chondrocytes and expanded FPSC (fresh co-culture) and co-culture of expanded chondrocytes and expanded FPSC (exp co-culture). a) DNA at day 0 is represented by the dashed line, b) sGAG content c) collagen content, d) collagen to sGAG ratio. *significance to fresh co-culture 5%, $^{\#}$significance to FPSC 5% and FPSC 20%, $^{!}$significance to exp co-culture 5% and exp co-culture 20%, $^{\&}$significance to FPSC 20% only, ^{L}significance to expanded co-culture 20% only, ^{w}significance to exp CC 20% only, $^{\%}$significance to all other groups presented on the graph, ($p<0.05$), n=3, 2-way ANOVA, Tukey post-test.*

To determine if a co-culture was leading to a synergistic increase in matrix accumulation, expected levels of sGAG and collagen accumulation within the co-cultures (the sum of 25% of the chondrocyte only values and 75% of the FPSC only values) were calculated and compared to actual measured levels by way of an interaction index (Eqn. 2, Fig.5-2 a, b). Co-cultures were only found to lead to synergistic increases in ECM accumulation in low oxygen conditions. For example, the sGAG levels in co-cultures expanded chondrocytes and FPSCs were 0.8 times higher than would be expected based on the levels observed in the chondrocyte only and FPSC only cultures. Similarly, collagen levels were 0.69 times higher than expected in these co-cultures.

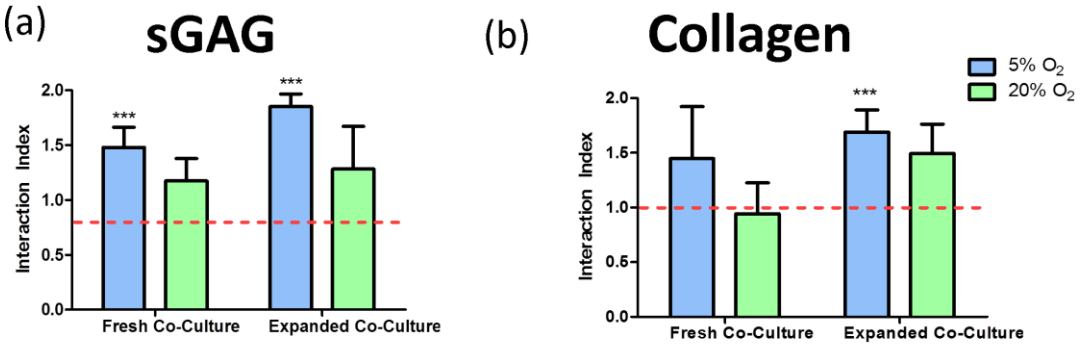

Figure 5-2| Interaction index: *a) sGAG accumulation and b) collagen accumulation, where a value of 1 indicates the expected levels of matrix component were found within the co-culture, and a value >1.0 indicates chondro-induction. The expected levels of sGAG in the 25:75 co-culture are defined as the sum of 25% of the chondrocyte only levels and 75% of the FPSC only levels (see Equation 1 and 2 for further details). ***indicates a significant difference to the expected levels of sGAG or collagen (p<0.05).*

5.3.2 Oxygen levels determine the specific types of collagen produced in a co-culture

All groups stained positive for collagen type II (Fig.5-3 a). There was little evidence of collagen type I deposition in the chondrocyte monocultures (either fresh or expanded) maintained at 5% O_2 (Fig.5-3 b). However, positive staining for type I collagen was observed in chondrocyte pellets maintained in 20%, especially for expanded cells. The biochemical and histological analysis of FPSC pellets demonstrated high levels of collagen accumulation, however immunohistochemistry confirmed that the development of a fibrocartilage like tissue, as evident by strong staining for both collagens type I and type II (Fig.5-3, a, b). Combining FPSCs with chondrocytes appeared to supress the deposition of type I collagen, especially in low oxygen environments. Semi-quantitative analysis of immunohistological sections confirmed these general observations (Fig.5-3 c, d), with a significant reduction in collagen type I deposition observed in co-cultures of expanded chondrocytes and FPSCs maintained at 5% O_2 compared to mono-cultures of FPSCs.

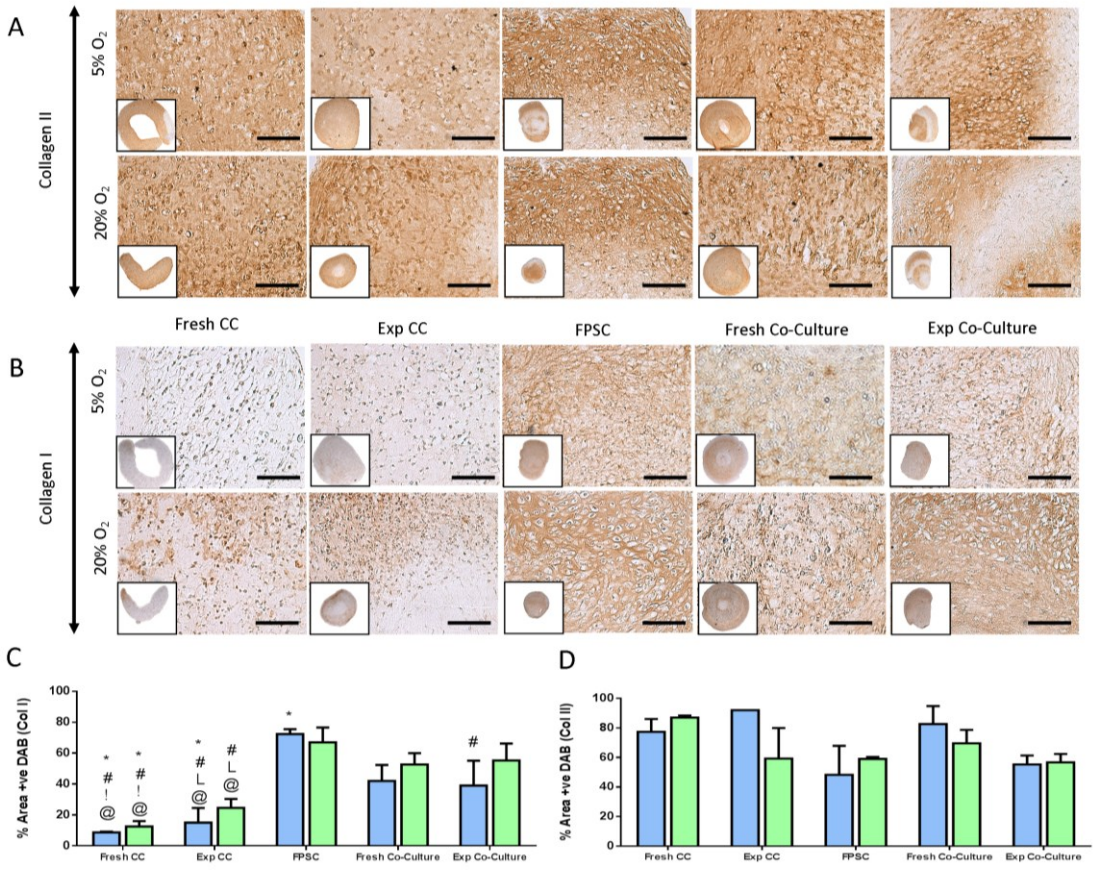

Figure 5-3| Immunohistochemical staining day 28*: a) collagen type II and b) collagen type I (scale bar 100µm) c) percentage of the total pellet area staining positive for collagen type I d) percentage of the total pellet area staining for collagen type II. *significance to fresh co-culture 5%, #significance to FPSC 5% and FPSC 20%, !significance to exp co-culture 5% and exp co-culture 20%, ˪significance to expanded co-culture 20% only, @significance to fresh co-culture 20% (p<0.05)., 2-way ANOVA*

5.3.3 Combining BMP-7 with TGF-β3 does not significantly enhance the cartilage matrix

It is clear from this study and others that freshly isolated chondrocytes secrete a more chondrogenic matrix compared to expanded chondrocytes. Since large numbers of expanded chondrocytes will be required for tissue engineered cartilaginous constructs of scale, even in a co-culture, it was next sought to determine if incorporating BMP-7 into the chondrogenic media would enhance chondrogenesis in a co-culture of FPSCs with expanded chondrocytes. sGAG and DNA levels were not affected by the additional growth factor supplementation (Fig.5-4 a, b). There was a significant drop in collagen accumulation within pellets maintained in TGF-β3 and BMP-7 (Fig.5-4 c). Histologically tissues engineered in TGF-β3 of TGF-β3 and BMP-7 appeared similar (Fig.5-4 d-g).

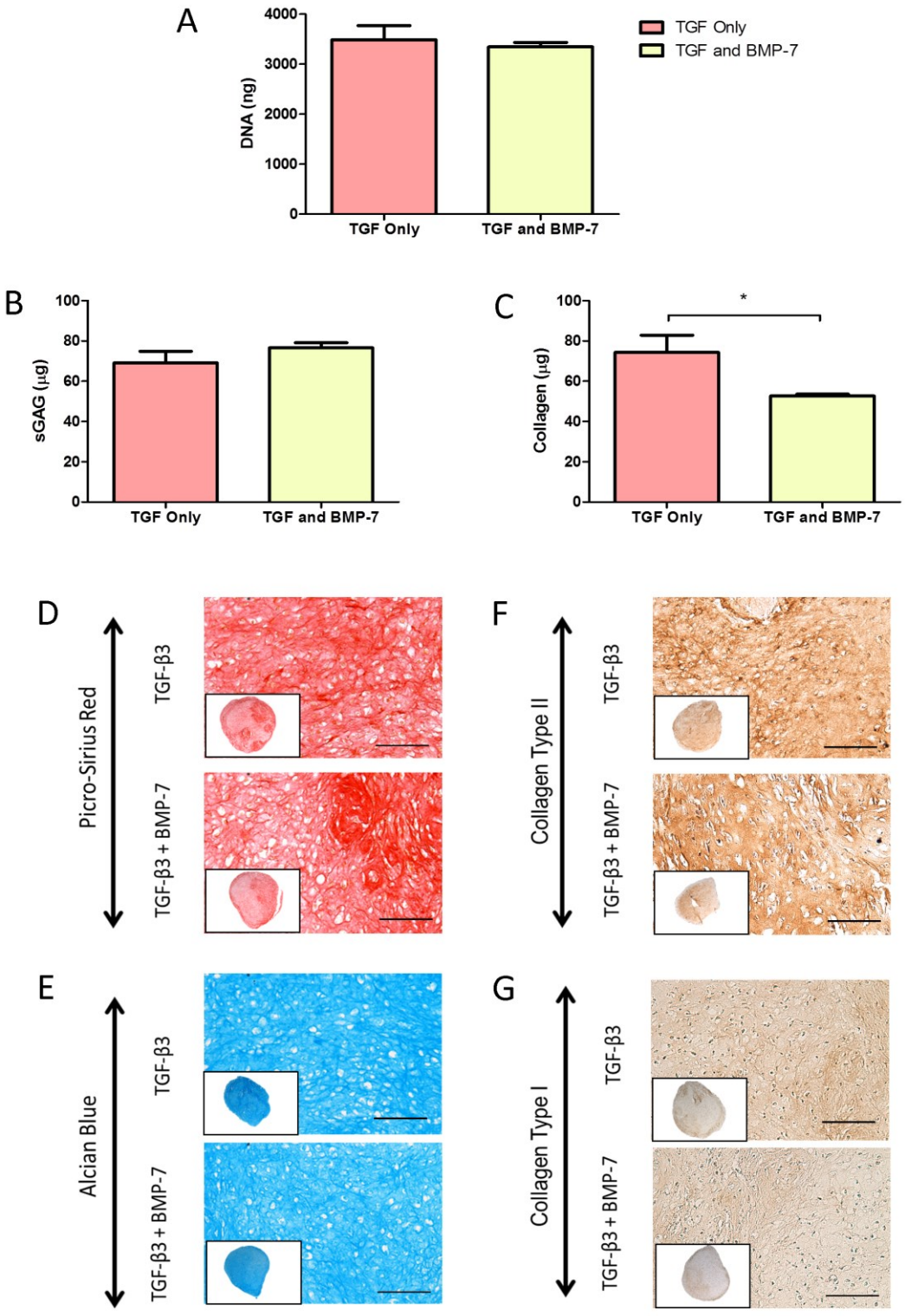

Figure 5-4| Effect of growth factos on expanded co-cultures: *Biochemical analysis a) DNA b) sGAG, c) collagen, d) Picro-sirius red for collagen e) alcian blue for sGAG f) immunohistochemisty for collagen type II and g) collagen type I after 28 days of culture (Scale bar 100µm) *significance ($p<0.05$), t-test.*

5.4 Discussion

While MSCs are abundant in number and possess the ability to differentiate into different specialised cell types, they tend to form a phenotypically instable cartilaginous tissue with inferior biochemical and biomechanical properties to the native tissue. This has led to increased interest in the use of co-cultures for cartilage tissue engineering, including the use of freshly isolated chondrocytes in combination with MSCs for the treatment of focal cartilage defects (Bekkers et al., 2013b). However, when attempting to engineer tissues of scale for whole joint resurfacing, large numbers of cells will be required, suggesting that MSCs will have to be combined with culture-expanded chondrocytes. Furthermore, if autologous cells are to be used in the treatment of osteoarthritic patients, it will require engineering cartilage tissues using diseased cells. Therefore, the primary objective of this study was to determine if a co-culture of diseased FPSCs and either freshly isolated or culture expanded chondrocytes would lead to enhanced chondrogenesis. It was found that a co-culture of either freshly isolated or culture expanded chondrocytes and FPSC was more chondrogenic than stem cells only. The collagen to sGAG ratio was also closer to that of the native tissue (Mwale et al., 2004). This positive interaction between chondrocytes and FPSCs was generally enhanced in a low oxygen environment. Furthermore, the deposition of type I collagen was supressed in a low oxygen co-culture. Together these results demonstrate that a combination of chondrocytes and FPSCs from diseased human joints represent a promising population of cells for driving cartilage regeneration.

A co-culture of either fresh or expanded chondrocytes with FPSCs was found to enhance matrix accumulation, particularly in low oxygen conditions. The mechanism by which this occurs is not yet fully understood. Previous studies have demonstrated that MSCs secrete factors that drive proliferation of the chondrocyte population (Acharya et al., 2012; de Windt et al., 2014; Wu et al., 2011), including FGF-1, FGF-2, TGF-β3 and IGF-1 (van Buul et al., 2012; Chen et al., 2009; Schinkothe et al., 2008). There have also been reports of increases in chondrogenic markers through soluble paracrine signalling (Ahmed et al., 2007; Aung et al., 2011). One study which investigated the co-culture of nucleus pulpous (NP) cells and BMSC showed a large increase in the DNA of NP cells while the 'supporting' BMSC population decreased in number (Naqvi and Buckley, 2015a). Other studies have observed a similar phenomenon of 'chondro-induction' mediated by two concomitant effects: MSC-induced chondrocyte proliferation and chondrocyte-enhanced MSC chondrogenesis (Acharya et al., 2012). This study demonstrates that human chondrocytes and stem cells also interact synergistically in disease. It has also demonstrated that human stem cells isolated from the infrapatellar fat pad of the knee form robust cartilage when co-cultured with human

chondrocytes. Thus, it can be said that diseased human FPSCs and chondrocytes represent a suitable cell source for cartilage tissue engineering.

In addition to promoting higher levels of total matrix accumulation, a co-culture was also found to supress type I collagen deposition. Chondrocytes in monoculture, specifically those maintained in low oxygen conditions, were found to secrete negligible levels of type I collagen. Based on the assumption that chondrocytes are rapidly dividing in co-culture, a simple explanation for this result it the tissue becomes dominated by a chondrocyte population that does not express type I collagen over time in low oxygen conditions. Alternatively, it may be that chondrocytes are secreting factors that are supressing the production of type I collagen by FPSCs within the co-culture.

An interesting result was that both freshly isolated and expanded chondrocytes expressed type I collagen in normoxic conditions. The differences in ECM deposition between fresh chondrocyte pellets maintain at 5% and 20% suggest that the dedifferentiation of chondrocytes *in vitro* may not simply be due to expansion in monolayer culture, but also due to exposure to a non-physiological (i.e. hyperoxic) oxygen environment. The fresh chondrocytes were not exposed to any monolayer culture, however pellets of these cells maintained at 20% oxygen produced significantly lower levels of sGAG (indicative of a loss in chondrogenic phenotype) compared to those maintained at 5%. Additionally, there was no evidence of collagen type I deposition in fresh chondrocyte pellets maintained at 5%, while there was some deposition observed at 20%, although levels were still low. Chondrocytes normally reside in low oxygen or hypoxic conditions and the oxygen environment plays a key role in maintaining or re-establishing the chondrogenic phenotype (Murphy and Polak, 2004). Markway conducted a study in which he compared the chondrogenic capabilities of healthy and OA chondrocytes in both hypoxic and normoxic environments. Irrespective of the cell source, hypoxia upregulated aggrecan and type II collagen mRNA expression after two weeks of culture. Furthermore, hypoxia supressed the expression of both levels of col1A1 and col10A1 (Markway et al., 2013). In FPSC only cultures, increased regions of type II collagen deposition were observed in the central core region of pellets maintained at 20% O2, while increased staining for type II staining was observed around the periphery of pellets maintained at 5% O2. Lower oxygen conditions likely develop in the core of pellets which explains these findings. Maintaining the chondrocyte phenotype is critical for engineering tissues with comparable mechanical function to articular cartilage.

A key finding of this study was that a co-culture of FPSCs and either freshly isolated or culture expanded chondrocytes synergistically enhanced chondrogenesis in low oxygen conditions. The importance of low oxygen conditions for maintaining a chondrogenic phenotype have already been discussed above. In addition to this, the local oxygen

environment likely regulates the secretome of MSCs. For example, MSCs maintained in low oxygen conditions have been shown to secrete significantly higher levels of Grem1, DKK1 and FRZB compared to normoxic cultures (Leijten et al., 2014). Grem1 and DKK1 are enhanced in articular hyaline cartilage and are associated with preventing chondrocyte hypertrophy (Chen et al., 2015; Leijten et al., 2012). The expression of all these proteins is also down regulated in OA (Leijten et al., 2014, 2012). The stronger interaction between MSCs and chondrocytes is therefore likely due to their altered secretome in low oxygen conditions.

While freshly isolated chondrocytes produce the most hyaline cartilage-like tissue, it is not feasible to use unexpanded cells in isolation for tissue repair clinically, and the results of this study support the use of combining freshly isolated chondrocytes and adult stem cells for the treatment of focal cartilage defects. While combining fresh chondrocytes with FPSCs lead to the development of a slightly inferior cartilage tissue compared to the use of fresh chondrocytes only, this was not observed with expanded chondrocytes. Here a co-culture in low oxygen conditions lead to the development of a cartilage tissue at least comparable to that generated by the use of expanded chondrocytes only. It may be that expanded and dedifferentiated chondrocytes are more receptive to the factors secreted by FPSCs within these co-cultures. This result strongly supports the use of this combined cell population for engineering tissues of scale.

As might be expected, the co-culture containing fresh CCs produced higher overall levels of sGAGs than that generated using expanded CCs. In an attempt to improve the levels of cartilage-specific extracellular matrix deposition, additional growth factor supplementation was explored during co-culture of expanded CCs and FPSCs. It is known that BMP-7 is present in cartilage, however the concentration is said to vary with age (Chubinskaya et al., 2002). No significant increase in sGAG was observed with the addition of BMP-7 to the co-culture. Previous studies have demonstrated that combining TGF-β1 with BMP-7 enhanced collagen type II synthesis compared to TGF-β1 alone for synovial explants (Iwakura et al., 2013). Compared to this study a considerably higher dose of BMP-7 was used (3000ng/ml). It is possible that a higher concentration of BMP-7 is needed to induce such an effect, as physiological levels are reported to be as high as 50-200ng/ml (Chubinskaya et al., 2007). A transient approach was also attempted, in which pellets were supplemented with TGF-β3 for 2 weeks, at which point it was removed and they were supplemented with BMP-7 (data not shown). No benefit was observed with this temporal growth factor stimulation strategy. Further studies are required to identify if additional growth factor stimulation will result in further increases in chondrogenesis within co-cultures of CCs and stem cells, with qPCR analysis to determine changes at both the gene and protein level.

There are limitations to the current study. The benefit of co-culture was only demonstrated in pellet culture. For further tissue engineering applications, it will be important to assess the validity of these results in scaled-up tissues, where dramatic oxygen gradients will exist (Buckley et al., 2012). Likewise, the effect of co-culture and oxygen conditions on mechanical functionality was not determined, which is an important consideration for engineering cartilage tissues. Further assessment of other important extracellular matrix markers present in normal articular cartilage also need to be assessed. Finally, this study focused on the use of FPSCs, however how these findings will translate to other sources of diseased stem/progenitor cells has not been explored.

In conclusion, the results of this study demonstrate that a relatively small number of osteoarthritic chondrocytes combined with FPSCs result in the development of hyaline cartilage-like tissue. While unexpanded chondrocytes, in isolation, still produce the most articular cartilage-like tissue, a strong positive interaction still occurs between adult stem cells and both freshly isolated and culture expanded chondrocytes when maintained in low oxygen conditions. The results of this study support the use of co-cultures of expanded chondrocytes and stem/progenitor cells for engineering large cartilage tissues of scale.

5.5 Concluding Remarks

This chapter has demonstrated the potential for OA derived cells to be used for cartilage tissue engineering applications. By co-culturing FPSCs and CCs, the levels of cartilage ECM deposition can be greatly enhanced over FPSCs alone, identifying it as a suitable as a cell source for engineering the chondral layer of a bi-layered cartilage template targeting osteochondral defect healing. The next chapter will build on this information by analysing the tissue synthesised within such a bi-layered template in a subcutaneous environment. Additionally, since the overall goal is to engineer a mechanically functional biological implant for knee joint regeneration, and given the poor mechanical properties of hydrogels, a suitable polymer for reinforcing the cartilage template will be identified.

6 Engineered soft tissue templates reinforced by 3D printed thermoplastics for osteochondral tissue engineering

6.1 Introduction

Treating an osteochondral (OC) defect requires supporting subchondral bone regeneration whilst simultaneously prohibiting vascularisation and hypertrophy of the overlying chondral layer. Hydrogels are commonly used for tissue engineering both articular cartilage and bone (Alsberg et al., 2003; Awad et al., 2004; Cunniffe et al., 2015; Mesallati et al., 2013, 2015a, Sheehy et al., 2015a, 2015b; Spiller et al., 2011). Their high-water content allows for the diffusion of nutrients and other regulatory signals such as growth factors. Altering the material content, synthesis, and material selection can provide control over of the mechanical and degradative properties of the hydrogel as well as cell adhesion and interaction (Alsberg et al., 2003; Drury and Mooney, 2003; Jeon et al., 2010; Kim et al., 2011; Wang et al., 2017). It has been previously shown in the lab that a bilayered hydrogel consisting of agarose and alginate with distinct cell populations can support either endochondral ossification or the development of phenotypically stable articular cartilage in spatially distinct regions of the constructs, thereby enabling the development of the osteochondral unit (Mesallati et al., 2015b). The 'chondral' region consisted of a MSC-chondrocyte co-culture which has been shown to promote the development of a cartilage tissue (Hubka et al., 2014; Meretoja et al., 2012) that is resistant to hypertrophy and mineralisation (Bian et al., 2011; Mesallati et al., 2015b). However, this proof-of-principle study was performed in a subcutaneous environment, and consequently the engineered construct was not subjected to high levels of mechanical load that they would experience in an orthotopic location. Therefore, strategies are required to develop composite mechanically reinforced hydrogels that have bulk mechanical properties compatible with implantation into high load bearing defects, but which possess a cellular environment that support robust differentiation and matrix synthesis.

Strategies to enhance the mechanical properties of hydrogels include increasing the concentration of the bulk material (Bryant and Anseth, 2002; Kim et al., 2011), the degree or type of crosslinker (Duong et al., 2009; Freeman and Kelly, 2017; Homenick et al., 2011; Lee et al., 2001) or the creation of interpenetrating polymer networks (IPNs) (Ingavle et al., 2013).

Increasing hydrogel concentration to increase implant stiffness can have a negative impact on cellular activity, degradation kinetics, permeability, the diffusion of nutrients and waste removal (Bensaïd et al., 2003; Deorosan and Nauman, 2011; Kim et al., 2011; Wu et al., 2009). Furthermore, the hydrogel itself can become a barrier to ECM development (Erickson et al., 2009; Sridhar et al., 2015). Increasing hydrogel stiffness by altering crosslinking density can have a similar effect on encapsulated cells. Furthermore, such changes can impact the fate of encapsulated cells, with stiffer hydrogels more conducive to osteogenesis or endochondral phenotype, which is undesirable in the context of cartilage tissue (Chaudhuri et al., 2015; DeForest and Anseth, 2012; Engler et al., 2006). IPNs are independent networks that are physically interlocked, resulting in mechanical properties of the sum of the materials or higher. In some cases, the mechanical properties are still too low compared to native cartilage (Kutty et al., 2007) or the cell viability is compromised (Ingavle et al., 2013). In other cases cell viability or chondrogenesis is not assessed (Gong et al., 2003; Wei et al., 2015). In recent years, multiple tool biofabrication has been used to engineer composite constructs consisting of cell laden hydrogels mechanically reinforced with polymer networks (Daly et al., 2016a; Kang et al., 2016; Kundu et al., 2015; Malda et al., 2013). For example, reinforcing gelatin methacrylate (gelMA) hydrogels with melt-electrowritten polycaprolactone (PCL) fibres (<100 μm diameter) results in the development of constructs with mechanical properties superior to that of the hydrogel or the scaffold alone, which furthermore could be tailored to be in the range of native cartilage (Visser et al., 2015a). The advantage of such approaches is that the hydrogel phase can be engineered to provide a stiffness and composition compatible with supporting a specific cellular phenotype, which can be decoupled from the reinforcing polymer phase which provides bulk strength and stiffness to the composite implant.

Identifying a suitable reinforcing polymer network material will be integral to the success of such composite engineered tissues. PCL is a widely used polymer for 3D printing due to its low printing temperature (59-64 degrees Celsius) (Middleton and Tipton, 2000), biocompatibility, elasticity and mechanical properties (Woodruff and Hutmacher, 2010). The mechanical properties can be tailored by modulating the molecular weight, strand size, printed architecture and strand spacing (Olubamiji et al., 2016). However, PCL has a long degradation time, approx. 2-3 years (Sun et al., 2006), during which time matrix deposition could be inhibited by the persistence of material at the site of injury. Poly(lactic acid) (PLA) and poly(lactic-co-glycolic acid) (PLGA) are also widely used in the medical field, both are biocompatible with good mechanical properties with PLGA having a much faster degradation rate than PCL (Nair and Laurencin, 2007; Pan and Ding, 2012; Shasteen and Choy, 2011). They have been used for drug delivery, growth factor delivery, as porous scaffolds (Hickey et al., 2002; Lee et al., 2014; Middleton and Tipton, 2000; Wang et al., 2010) and can be 3D printed

(Guo et al., 2006). One drawback to PLA/PLGA are the melting temperatures are much higher than PCL (~130 degrees Celsius for PLGA and ~180 degrees Celsius for PLA), which can render co-printing live cells and PLA/PLGA a challenge. The degradation of PLGA is defined by the ratio of lactic acid to glycolic acid, with PLGA 50:50 having a degradation time of 1-2 months and 85:15 5-6 months (Middleton and Tipton, 2000). A significant concern is the releases of acids as degradation products that can induce inflammation (Dawson et al., 2008; Kim et al., 2007; van Sliedregt et al., 1992). PLGA has been combined with osteoinductive components such as β-TCP and hydroxyapatite nanocomposite (Kim et al., 2012), while more chondroinductive implants have been fabricated using MSCs and a gelatin/chondroitin/hyaluronate hybrid scaffold (Fan et al., 2006). 3D printed PCL and PLGA 50:50 scaffolds were compared in a 1.5cm rabbit tibia defect. No evidence of PLGA was detected after 8 weeks, whereas the PCL struts were evident. New bone formed in between the PCL fibres, while less structured bone formed within the PLGA treated groups (Park et al., 2012). The optimal polymer for reinforcing bilayered scaffolds for osteochondral applications is yet to be determined.

The objective of this study was to engineer a mechanically reinforced, bi-layered osteochondral construct capable of supporting stable hyaline cartilage in the chondral layer and endochondral bone development in the osseous layer of the implant. To this end the mechanical properties, swelling and levels of chondrogenesis within PLA, PLGA 65:35, PLGA 85:15 and PCL reinforced alginate hydrogels were first compared *in vitro*. The optimal reinforcing polymer was then used to produce composite bi-layered implants, whereby the chondral layer of the implant mimicked the compressive moduli of articular cartilage. To engineer an osteochondral tissue, the osseous region of the construct was primed, it consisted of a BMSC laden RGD-ɣ-alginate hydrogel, to undergo endochondral ossification. The overlying chondral layer, which consisted of a MSC-chondrocyte co-culture (3:1), was designed to support the development of stable hyaline cartilage. These reinforced constructs were assessed *in vitro* and *in vivo* in a subcutaneous environment for their capacity to support the development of vascularised bone-like tissue overlaid by phenotypically stable layer of hyaline cartilage.

6.2 Materials and methods

6.2.1 3D printing process

Comparison of polymers: A 3D bioplotter was used for printing (Chapter 3, section 3.10). The orthogonal architecture (6mm diameter, 4mm height, line spacing 1.5mm) was designed on the accompanying software, BioCAD. PCL, PLA, PLGA 85:15, PLGA 65:35 (all Sigma-Aldrich) were heated in the extruding tank at temperatures and extruded through a 25-guage needle (individual parameters are shown in Table 6-1). All reinforcement cages were then sterilised with ethylene oxide (EtO) for 12 hours (Anprolene, Andersen Products, USA).

Table 6-1 | Printing parameters for reinforcing polymers

Material	Molecular Weight	Tank Temp °C	Needle Temp °C	Pressure MPa	Screw Speed
PCL	45,000	70	70	0.1	9 rev/m
PLA	60,000	180	160	0.1	20 rev/m
PLGA 85:15	50-75,000	145	130	0.1	20 rev/m
PLGA 65:35	40-75,000	140	120	0.1	16rev/m

For the bilayered scaffolds: An orthogonal architecture (12mm diameter, 6mm height, line spacing 2mm) was printed with a tank and needle temperature of 70 degrees, screw speed of 18 rev/s and a 30guage needle. The PCL was then punch using a 6mm biopsy punch to form 6x6mm unconfined lattice shaped constructs.

6.2.2 Cell isolation and expansion

BMSCs, chondrocytes and FPSCs were obtained from a 3-month-old porcine donor and were isolated and expanded as per the procedure in Chapter 3, section 3.1, 3.2 and 3.3. or for the first experiment, a goat donor. All cells were maintained in XPAN and 5% oxygen tension during the expansion phase, media was changed twice weekly. BMSCs, FPSC, and chondrocytes were used at passage 2, 2 and 1 respectively.

6.2.3 Formation of the reinforced soft tissue templates

A summary of the experimental procedure is shown in Fig.6-1 a-e.

Comparison of polymers: Custom built negative Polylactic acid (PLA) moulds were fabricated using a 3D printer. 6% agarose was combined with 100mM $CaCl_2$, pH 7.2, in a 1:1 ratio (final concentration of 3% and 50mM respectively) and poured into the moulds to create cylindrical wells of diameter 6mm and a height of 4mm. A reinforcing polymer was placed into each mould and 1.5 % of RGD-γ alginate, 1% oxidised, containing $20x10^6$/ml of goat BMSCs was pipetted into the mould and allowed to cross-link at 37°C for 30 minutes. All constructs were maintained in chondrogenic medium (CDM), consisting of hgDMEM supplemented with penicillin (100 U ml^{-1})-streptomycin (100 μg ml^{-1}), 100 μg ml^{-1} sodium pyruvate, 40 μg ml^{-1} l-proline, 50 μg ml^{-1} l-ascorbic acid-2-phosphate, 1.5 mg ml^{-1} BSA, 1× insulin-transferrin-selenium, 100 nM dexamethasone (all from Sigma-Aldrich, Ireland) and 10 ng ml^{-1} recombinant human transforming growth factor-β3 (TGF-β3; ProSpec-Tany TechnoGene Ltd, Israel). Constructs were cultured at 37°C with 5% oxygen for 28 days with medium exchange twice weekly.

For the bilayered scaffolds: The agarose- $CaCl_2$ moulds were fabricated using the same method as described above. However, two separate moulds were made with height of either 6mm or 4mm. The groups were fabricated as follows;

Alg PCL: The PCL cage was placed into the 6x6mm agarose-$CaCl_2$ mould and 1.5% RGD-γ alginate, 1% oxidised containing $20x10^6$/ml BMSCs was pipetted into the mould up to the top and allowed to cross-link at 37°C for 30 minutes.

Alg-Alg Bilayer: The PCL cage was placed into the 6x4mm agarose-$CaCl_2$ mould. To form the 'endochondral layer' 1.5% of RGD-γ alginate containing $20x10^6$/ml BMSCs was pipetted to the 4mm height. The construct was left at 37°C to cross-link for 10 minutes before being cut free and placed into the 6x6mm agarose-$CaCl_2$ mould. To form the 'chondral layer' 1.5% of RGD-γ alginate containing $20x10^6$/ml of a 3:1 co-culture of FPSC:CC. The constructs crosslinked for a further 20 minutes before being cut free.

Ag-Alg Bilayer: The PCL cage was placed into the 6x4mm agarose-$CaCl_2$ mould. To form the 'endochondral layer' 1.5% of RGD-γ alginate containing $20x10^6$/ml BMSCs was pipetted up to the 4mm height. The construct was left to cross-link for 30 minutes before being cut free and placed into the 6x6mm agarose mould. To form the 'chondral layer' 3% of agarose type VI at a temperature of 42°C was combined with $40x10^6$/ml of a 3:1 co-culture of FPSC:CC for a final concentration of 1.5% and $20x10^6$ /ml agarose and cells respectively. The agarose crosslinked after 10 minutes at room temperature before being cut free. CDM with TGF-β3 at 37°C with 5% oxygen for 28 days with medium exchange twice weekly followed by 7 days in 20% oxygen.

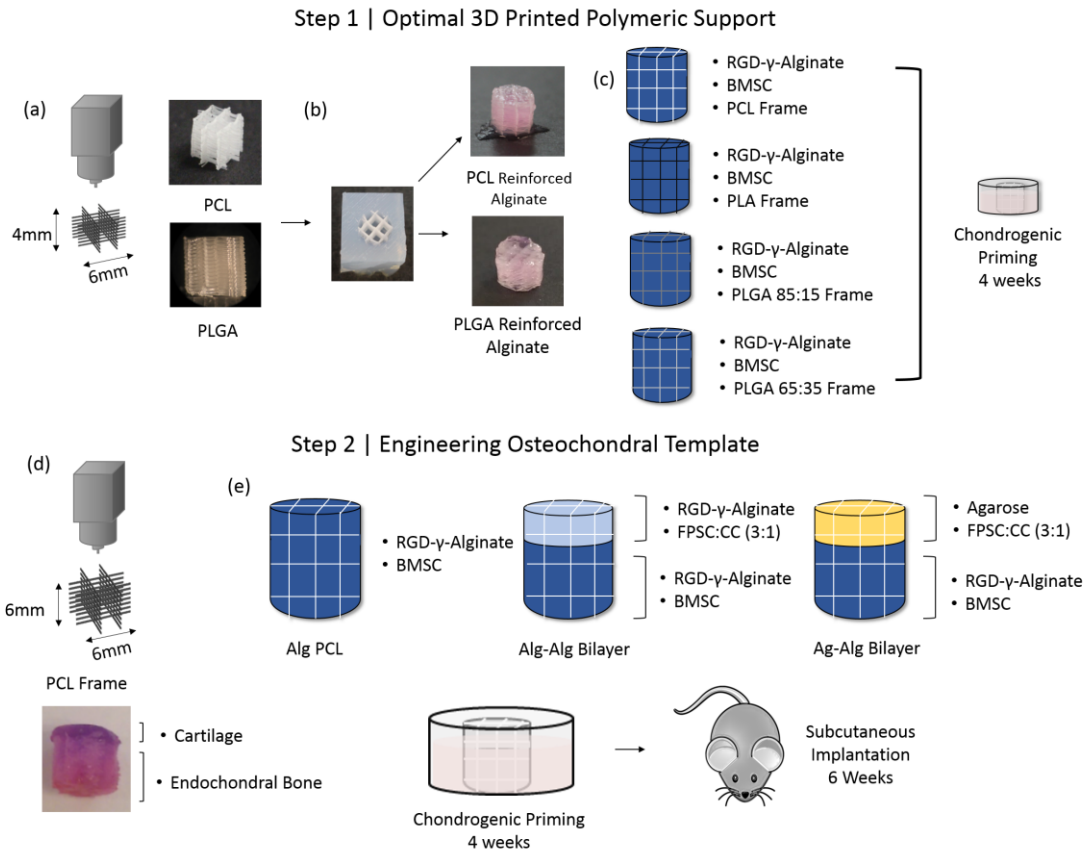

Figure 6-1 | Schematic of the experimental design: *a) 3D printed PCL and PLGA reinforcing networks. b) Mould used to cast the hydrogels into the reinforcement thermoplymer and macroscopic image of either a PCL or PLGA reinforced alginate. c) The experimental groups reinforced alginate with PCL, PLA, PLGA 85:15 or 65:35. d) Second step in which a bi-layered construct was mechanically reinforced. e) Details of the experimental groups used in the study; Alg PCL was used as a control to the bi=layered scaffolds Alg-Alg and Ag-Alg, both contained a co-culture of infrapatellar stem/stromal cells (FPSC) and chondrocytes in a (3:1) ratio, respectively*

6.2.4 Cartilage template implantation

Following 5 weeks in vitro priming, the bilayered constructs (n = 6 per group) were implanted subcutaneously into the back of nude mice (Balb/c; Harlan, UK). Two subcutaneous pockets were created at the shoulders and the hips three constructs were inserted per pocket. Mice were sacrificed 6 weeks post-implantation, by CO_2 inhalation. The animal protocol was reviewed and approved by the ethics committee of Trinity College Dublin and the Irish Medicines Board.

6.2.5 Mechanical testing

Mechanical tests were performed using a single column Zwick (Zwick, Roell, Germany) with a 5N load cell as previously described (Olvera et al., 2015; Vinardell et al., 2012a). Briefly, stress relaxation tests were performed using impermeable metal platens in XPAN media. The Youngs

modulus was determined by measuring the slope of the stress-strain graph. The equilibrium compressive modulus was determined from the equilibrium force following unconfined compression testing to 10% strain.

6.2.6 Fibre swelling analysis

To assess the fibre swelling, images were take of 3-4 samples and processed through image-J software. From which the diameter was taken at 18 points.

6.2.7 Biochemical, histological and immunohistochemistry analysis

Constructs were either digested in 500µl of papain or fixed in 4% PFA, and analysed as described in Chapter 3, sections 3.8 and 3.9

6.2.8 Statistics

Experimental groups were analyzed for significance differences using a general linear model for analysis of variance (ANOVA). All graphs are presented with error bars + standard deviation, significance was accepted at a level of $p < 0.05$.

6.3 Results

6.3.1 Mechanical properties of 3D printed PCL, PLA and PLGA scaffolds

MSC laden hydrogels were mechanically reinforced using networks of 3D printed PCL, PLA and PLGA (Fig.6-1 a, b). There was no change in the PCL filament diameter (0.22±0.03mm, day 0 and day 28) or in the mechanical properties of printed PCL networks over 28 days *in vitro* (data not shown). In contrast, the PLGA fibres were observed to swell over the time in culture (Fig.6-2 a), hence a more in-depth analysis was undertaken. By day 14 it was not possible to measure the fibre diameter of PLGA 65:35 constructs and by 28 the cylindrical geometry was unrecognisable from that originally printed (Fig.6-2 a). The construct lost all its reinforcing capabilities, the Young's modulus reducing from 7.17MPa to 0.0075MPa by day 21 (Fig.6-2 c). The mechanical properties of the PLA and the PLGA 85:15 scaffolds underwent less dramatic changes in mechanical properties over time in culture, reducing from 15.31MPa to 5.6MPa for the PLA scaffolds, and from 11.4MPa to 2.375MPa for the PLGA 85:15 scaffolds (Fig.6-2 c). PLGA 85:15 held its structure better, however the fibres did swell by 28% from day 3 to 28

(Fig.6-2 b). The final strut size was measured as 0.588mm which is almost 10% of the diameter of the original scaffold. The swelling effect corresponded with a decrease in mechanical properties (from 11.38 MPa to 2.37 MPa at day 21) (Fig. 3 c). Overall, PLA networks maintained their fibre diameter, however it had halved in mechanical reinforcement (Fig.6-2. b).

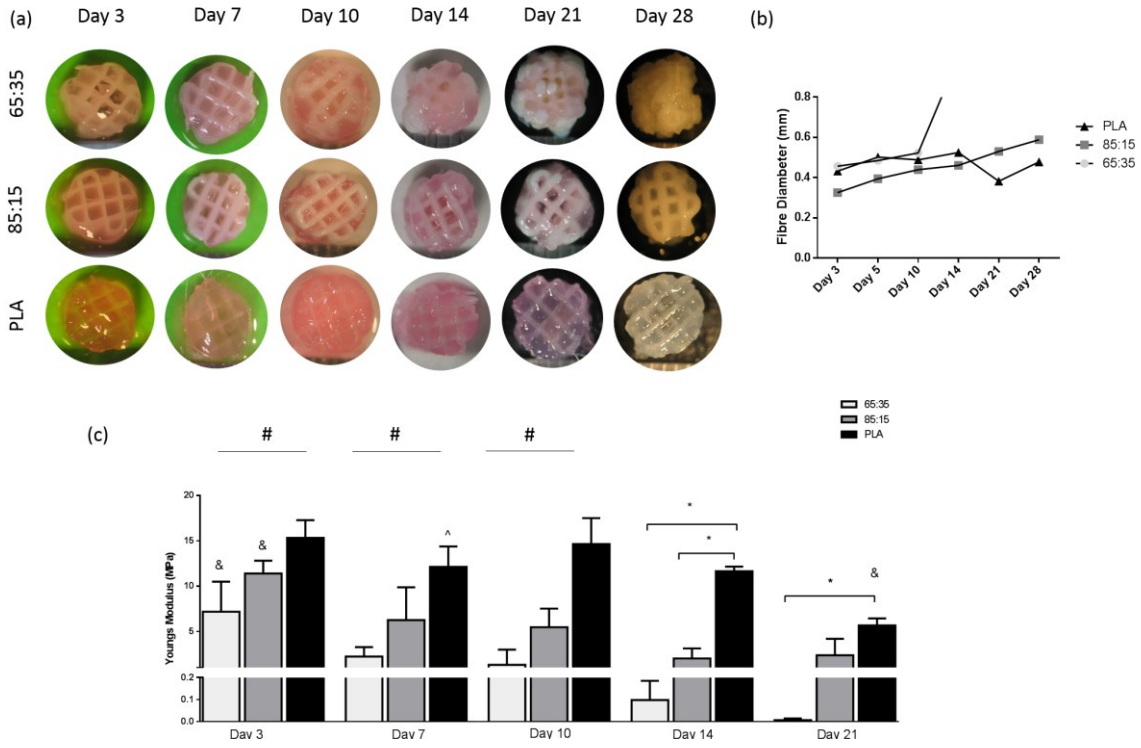

Figure 6-2|Macroscopic and mechanical assessment: *a) Representative image of how the reinforced polymers changed over time in culture b) the change in fiber diameter overtime c) Young's modulus of each construct over time (n=3/4), #each group is significant from each other within the same time point, &significance of the same group when compared across all time points, ^significant to day 14 of the same group, *significance as shown, p<0.05 2-way-ANOVA.*

6.3.2 Chondrogeneis within alginate hydrogels reinforced with networks of 3D printed PCL, PLA and PLGA

Chondrogenesis of MSCs encapsulated within alginate hydrogels mechanically reinforced with printed polymeric networks was next assessed over 28 days in culture (Fig.6-3 a-d). DNA levels significantly reduced in the PLGA 65:36 scaffolds with time in culture (Fig.6-3 a), suggesting a loss of cell viability within these constructs. However, histological sections and biochemical analysis showed that the cells had synthesised a cartilage tissue rich in sGAGs and collagen type 2 (Fig.6-3 d). Similar levels of chondrogenesis were observed in the PLGA 85:15 constructs (Fig.6-3 c), despite lower levels of swelling. No significant difference in DNA levels were observed over time in the PLA and PCL constructs, and both supported significantly higher

levels of sGAG synthesis than constructs reinforced with PLGA (Fig6-3 b). Only negligible staining for collagen type X was observed in all groups (Fig 3 d). PCL had higher DNA at day 0 (9137±931 ng) compared to the PLA and PLGA groups (6766±64 ng) because the fibre thickness of the PCL constructs were thinner, therefore there was more area for the hydrogel to infiltrate. As superior chondrogenesis was observed in the PLA and PCL scaffolds, and based on the fact that PCL could be printed at lower temperatures and hence is more compatible with bioprinting strategies, PCL was used as a reinforcing network for the remainder of this study.

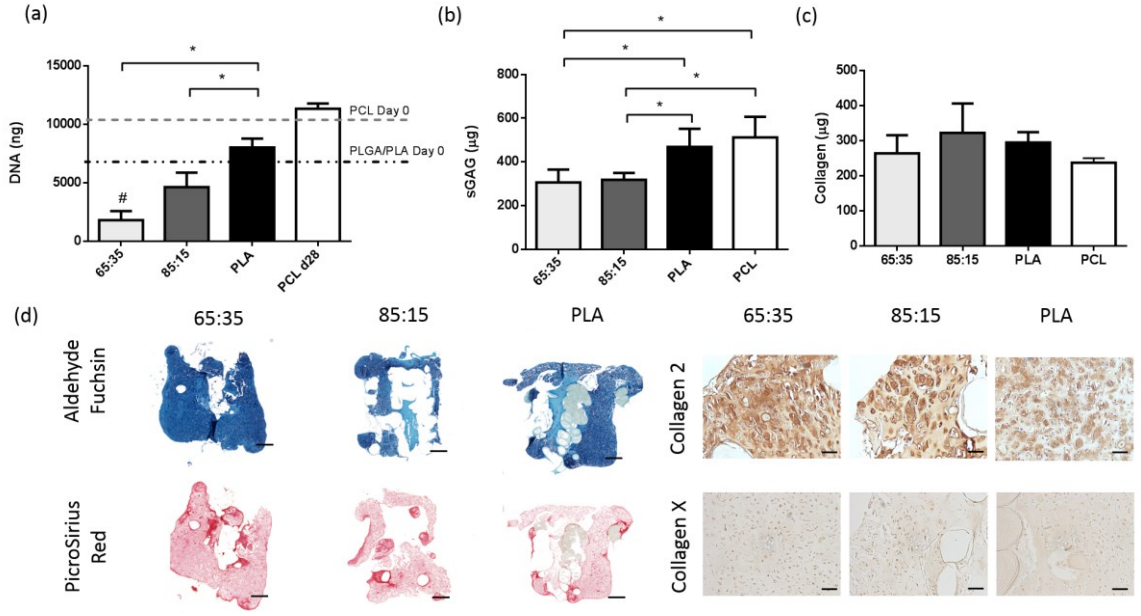

Figure 6-3|Chondrogenesis of reinforced cartilage templates: *Biochemical and histological analysis after 28 days in vitro a) DNA, b) sGAG and c) collagen content, (n=3/4, *p<0.05, #significant to day 0, p<0.05, ANOVA) d) histology for sGAG deposition (aldehyde fuchsin), collagen (picrosirius red) (scale bar 1000µm) and immunohistochemistry for collagen type 2 and X (scale bar 100µm).*

6.3.3 Chondrogenesis within bi-layered hydrogels reinforced with networks of 3D printed PCL

With a view to engineering reinforced hydrogels with mechanical properties mimicking that of articular cartilage, PCL scaffolds were printed with a larger filament spacing of 2 mm. The Young's modulus of these were dramatically higher than that of agarose and alginate but similar to that of native porcine cartilage (Fig.6-4 a). In an attempt to engineered bi-layered hydrogels capable of supporting osteochondral tissue development, the bottom osseous region of 3D printed scaffolds were seeded with BMSC, while the top *chondral* region was produced using either alginate or agarose hydrogels seeded with a co-culture of CC and FPSCs. Control constructs consisted of an alginate hydrogels seeded with BMSCs. After 5 weeks of *in vitro* culture all groups stained positively for sGAG and collagen type II deposition (Fig.6-5 a-c). While no dramatic differences in the spatial levels of chondrogenesis was observed throughout

the constructs, the osseous region of the bi-layered constructs appeared to stain more intensely for collagen type X and collagen type I than the corresponding chondral region (Fig.6-5 a-c). Alizarin red (calcium) was not detected in the chondral layer but there were small patches evident in the osseous layers of the bi-layers (Fig.6-5 a-c). DNA levels (normalised to tissue wet weight) were significantly higher in the chondral region of bi-layered implants compared to the corresponding osseous region and to the same region within homogenous alginate-PCL controls (Fig.6-4 b). No significant differences in overall levels of sGAG deposition were observed between the osseous and chondral region of bi-layered implants (Fig.6-4 c). Corresponding with histological staining for Alizeran red, calcium was detected in small amounts in the osseous layers and was not detected in the chondral (Fig. 6-4 d).

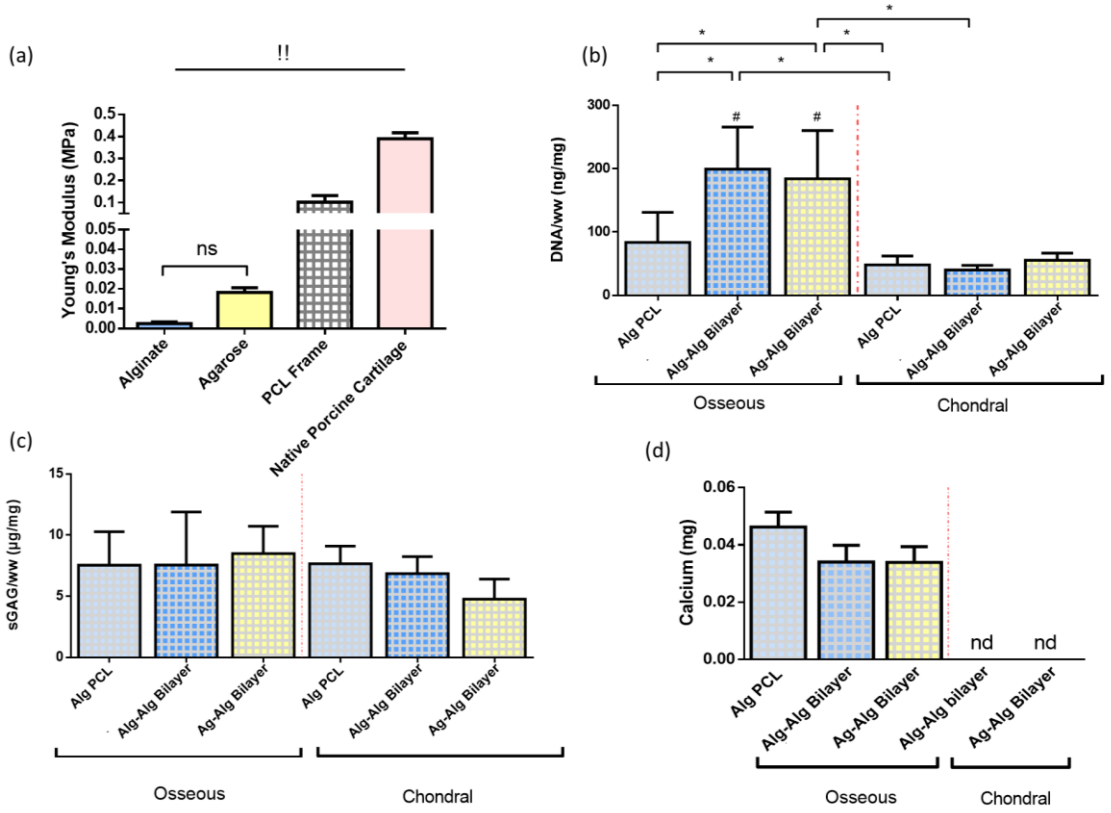

Figure 6-4|Quantitative analysis of the bi-layered cartilage template: *a) Young's modulus of an acellular alginate, agarose, PCL frame and native porcine cartilage (n=3/4) !!significance to all other groups except where specified by ns, p<0.05, ANOVA) b) DNA/ww, and c) sGAG/ww (*significance p<0.05, #significance to the corresponding osseous layer, p<0.05, ANOVA n=6) d) calcium content, (nd=not detected)*

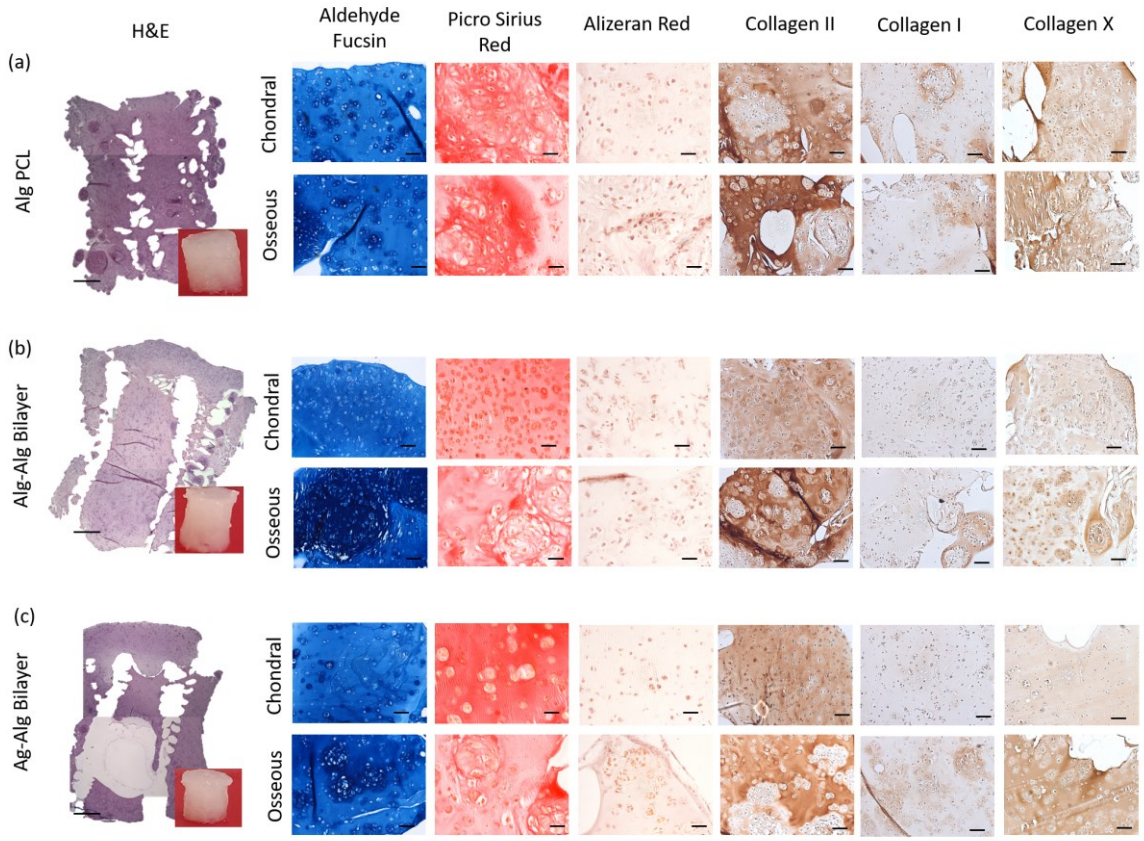

Figure 6-5|Histolgy staining: *a) alginate-PCL control, b) alginate-alginate bilayer and c) agarose-alginate bilayer for H&E, sGAG (aldehyde fucshin), collagen (picrosirius red), calcium (alizaran red) and immunohistochemical staining for collagen type II, I and X (scale bar 100µm)*

6.3.4 In vivo development of chondrogenically primed bi-layered hydrogels

Following 5 weeks of chondrogenic priming in media supplemented with TGF-β3, constructs were implanted subcutaneously into nude mice. 6 weeks after subcutaneous implantation, an obvious interface had formed between the osseous and chondral layers of the bi-layered constructs (Fig.6-6 a). The bone region contained visible vasculature, whereas the cartilage had a white hyaline cartilage-like appearance and appeared avascular. This observation was supported both by µCT analysis which demonstrated negligible mineral deposition in the chondral layers, and by the low calcium levels measured in this region of the bi-layered implant (Fig.6-6 b, c, e). The control homogenous PCL-alginate became significantly stiffer *in vivo* (pre-implantation = 0.097 MPa; post-implantation = 0.297 MPa), while the stiffness of the bi-layered alginate (pre-implantation = 0.01 MPa; post-implantation = 0.16 MPa) and agarose (pre-implantation = 0.0899 MPa; post-implantation = 0.11 MPa) increased slightly but not significantly. (Fig.6-6 d).

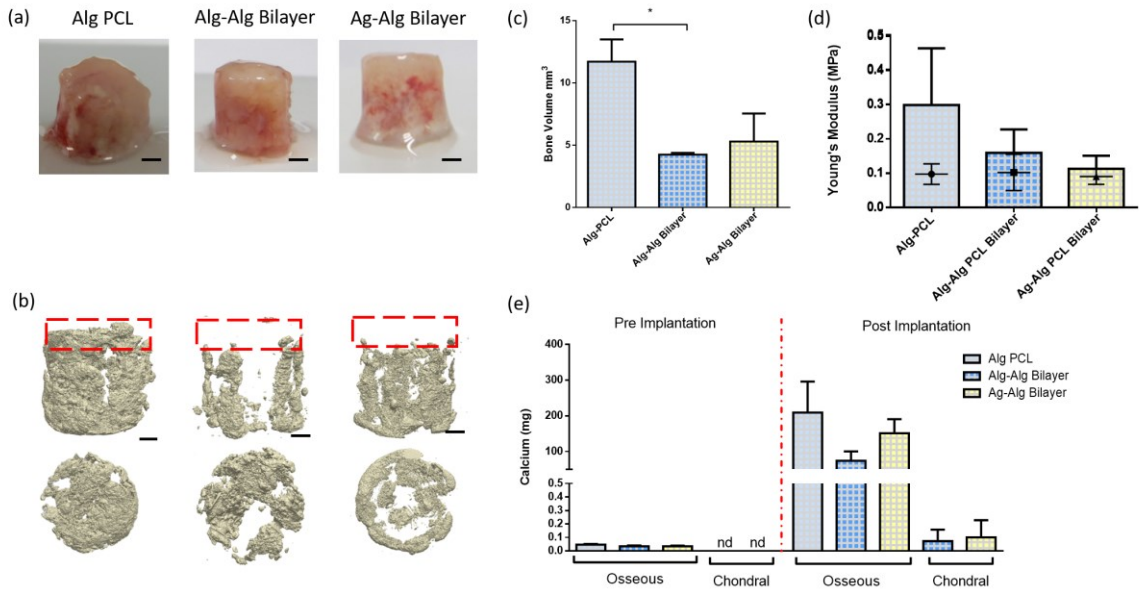

Figure 6-6|In vivo characterisation of the cartilage template: *a) macroscopic images post-implantation (scale bar 1000µm), b) µCT 3D render of the mineral deposition in each group, the red box signifies where the chondral region is located (scale bar=1000µm), c) quantification of the bone volume from µCT sections (*p<0.05, ANOVA) d) Young's modulus after 6 weeks subcutaneous implantation, insert bar represents the mean±SD of the values pre-implantation, !significance compared to pre-implanted values, t-test e) calcium accumulation measured pre-implantation and post-implantation (nd=not detected), #significance compared to alginate chondral region, & significance compared to alginate chondral region, *significance, 1-way ANOVA p<0.05*

Histological analysis confirmed that the bi-layered constructs supported spatially defined tissue types. H&E staining demonstrated the development of a vascularized, bone-like tissue within the osseous region of the bi-layered constructs, and in pockets throughout the control homogenous alginate-PCL constructs (Fig.6-7). While positive staining for sGAGs and collagen type II was observed throughout the constructs, collagen type I and X deposition was generally more intense in the osseous region of the bi-layered implants (Fig.6-7 a-c).

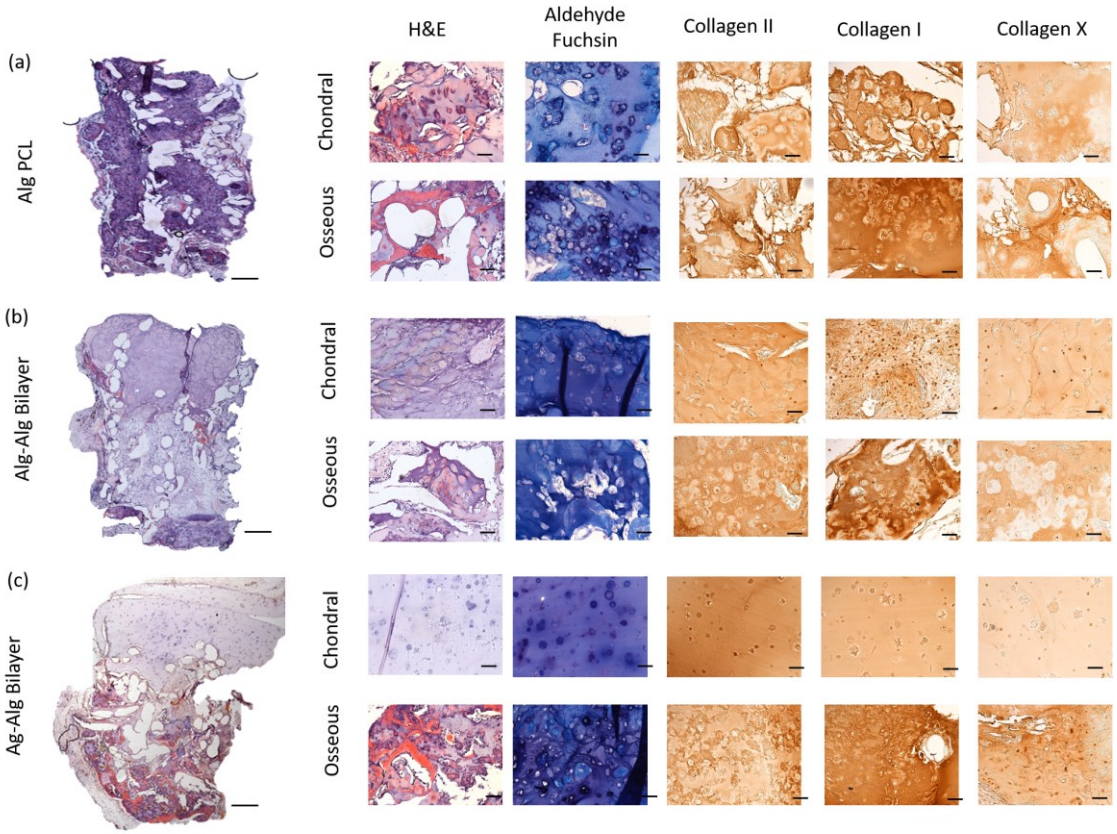

Figure 6-7|Histological staining*: a) Alg PCL, b) Alg alg bi-layer, c) Ag alg bi-layer stained for H&E (scale bar=1000µm), sGAG (aldehyde fuchsin) and immunohistochemical staining for collagen type II, I and X (all scale bars 100µm)*

Even though overall levels of calcification in the chondral regions of bi-layered implanted was very low, there was some early evidence for the onset of mineralization. This was more apparent in the chondral layer engineered using alginate (Fig.6-8 a, c black arrows). Evidence of mineral was present in all of the samples fabricated alginate chondral layers. Mineral was only detected in one agarose chondral layer, close to the PCL filaments (Fig.6-8 b, black arrows) and at the interface with the osseous alginate layer (Fig.6-8 d, black arrow). The green arrows in Fig.6-8 b, show a PCL filament in the agarose where no pink staining was detected.

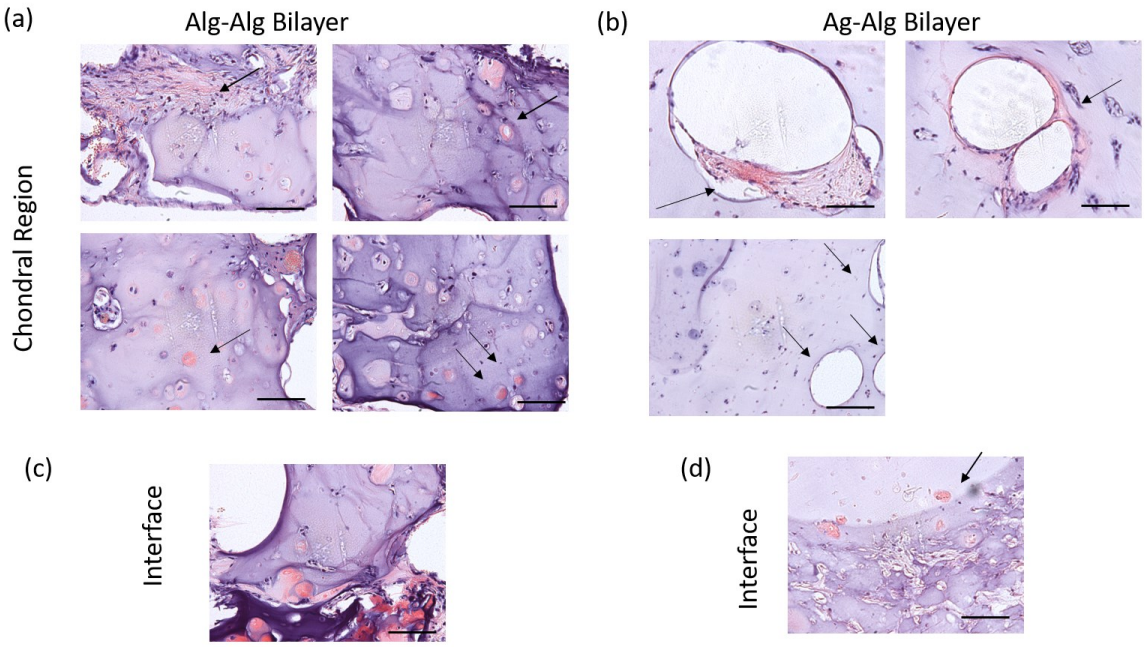

Figure 6-8|High magnification of H&E sections: *a) chondral region for the alginate-alginate bilayer, the arrows point to bone, each image represents a different sample and b) chondral region for the agarose-alginate bilayer, arrow points to bone and possibly a vessel forming around the PCL, this is from one section only, the image with green arrows show PCL fibers in the that has not the same artefact (c) the interface between the chondral and the osseous region, (d) arrows point to bone formation at the interface (scale bar=100µm).*

6.4 Discussion

Hydrogels have shown great promise for cartilage and bone tissue engineering. This has been attributed to several features, including providing a hydrated environment conducive to the native tissue, in addition to facilitating ECM deposition and modulating the cell shape. It was hypothesized that hydrogels could be mechanically reinforced using 3D printed thermoplastics, specifically PLA, PLGA 65:35, PLGA 85:15 and PCL, to generate composite constructs capable of supporting robust chondrogenesis. It was further hypothesised that it would be possible to engineer bi-layered constructs capable of supporting stable hyaline cartilage in the chondral layer and endochondral bone development in the osseous layer. PLA and PCL supported more robust chondrogenesis, as defined by overall levels of sGAG and collagen type II accumulation. PLGA was found to swell, particularly the 65:35 group which had lost all shape fidelity after 28 days *in vitro*. PCL was chosen as the optimal reinforcing polymer due to the lower melting temperature and more stable mechanical properties. Reinforced bilayered cartilage templates were engineered using different combinations of cells (either MSCs only or a bi-layered co-culture) and hydrogels (either alginate or agarose). In all cases, robust chondrogenesis was observed, although subtle differences in cartilage composition were observed between the osseous and chondral region of the bi-layered implants. The co-culture supressed collagen type I and calcium deposition in the chondral layer *in vitro*, whilst both were apparent throughout the homogenous alginate-PCL control. 6 weeks after subcutaneous implantation, a defined distinction between chondral and osseous layers was clear within the bilayered scaffolds, with blood vessels confined to the lower half of the construct. Microct, calcium and histological staining confirmed this finding with mineralised bone restricted to the osseous layers indicating that the co-culture was supressing hypertrophy and mineralisation of the chondral layer.

Scaffolds produced using 3D printed PLA, PLGA 85:15 and PLGA 65:35 all experienced a loss in mechanical properties over time. There has been a significant amount of literature on the degradation of PLA and PLGA describing how the mechanical properties can be tuned based on the method manufacturing and the molecular weight. For example, an ester end cap PLGA will degrade more slowly than an acid end cap (Middleton and Tipton, 2000). However, there are several other factors which probably caused the PLGA to degrade quicker. Forming scaffolds through printing has been shown to decrease the molecular weight, which can speed up the degradation process (Guo et al., 2006). Additionally, the sterilisation method can affect the surface of the PLGA creating cracks and pores (Holy et al., 2001; Shearer et al., 2006). In this case the scaffolds were sterilised by ETO gas. In a study comparing the effects of common sterilisation methods on PLGA 75:25, it was revealed that after ETO treatment, the scaffold had lost approximately 12% of its initial molecular weight. Ethanol sterilisation was deemed the

only method which did not alter the molecular weight, (γ-irradiation lost 54% and plasma gained 36%). A similar study compared the effects of ethanol, UV-light, peracetic acid and antibiotics on 50:50, 65:35 and 85:15 PLGA ratios (Shearer et al., 2006). They reported structural damage in all cases including the ethanol treated scaffolds. It must be noted that although ethanol may suffice for *in vitro* experiments it does not guarantee full sterilisation, which is critical for *in vivo* studies.

PLA and PCL supported the best chondrogenesis whilst maintaining mechanical and structural integrity. It is conceivable that the lower sGAG levels of PLGA 85:15 and 65:35 could be attributed to the significantly lower DNA values compared to day 0, PLA and PCL. One possibility is that the acidic environment created by the PLGA degradation products is causing the cell death (Kim et al., 2007). Contrastingly, several studies have reported that PLGA supports MSC proliferation over time (Fan et al., 2006; Tanaka et al., 2009; Xin et al., 2007). These studies did not assess the DNA up to day 28 and because our study did not measure the DNA over a number of timepoints it is not known at which stage the drop occurred. (Tanaka et al., 2009). Another potential reason could be that the swelling and subsequent degradation of both the PLGA constructs is causing cells to be released into the surrounding media. A comprehensive analysis of the media is required to elucidate if this is a factor.

PCL was chosen over PLA due to the lower printing temperature (for future co-printing potential) and more elastic mechanical properties. PLA has a high glass transition temperature (approximately 60-65˚C) causing it to be brittle (Kim and Cho, 2009; Middleton and Tipton, 2000). It has been reported that PLGA/PLA degrades faster *in vivo* than *in vitro*, therefore it may not be stable enough in a load bearing joint (Lu et al., 2000). Improvements can be made by increasing the molecular weight of the PLA/PLGAs or by blending it with PCL (Hiep and Lee, 2010; Kim and Cho, 2009; Shim et al., 2012; Vieira et al., 2011). PCL-PLGA-βTCP was used to promote bone formation in a lapine calvarial defect (Shim et al., 2012). Electrospun blends of PCL and PLGA, in tension had a reduced the strain at failure, however this could be modified based on the ratio of components. Importantly, elastic and plastic regions were increased (Hiep and Lee, 2010). However, further studies would need to be performed on the compressive properties of this material and the degradation over time *in vitro.*

A co-culture of FPSC and chondrocytes appeared to support the development of more hyaline-like cartilage *in vitro*. Whilst overall levels of sGAG accumulation did not increase in tissues engineered using such co-cultures, there was a significant increase in their DNA content. Several studies have demonstrated that MSCs secrete factors such as FGF-1, FGF-2, TGF-β3 and IGF-1 (van Buul et al., 2012; Chen et al., 2009; Schinkothe et al., 2008) that drive the proliferation of chondrocytes (Acharya et al., 2012; de Windt et al., 2014; Wu et al., 2011). Both calcium and collagen type I were present in the MSC laden osseous layers and in the

homogenous alginate-PCL controls, however there was no such staining observed in the chondral layers that were engineered using a co-culture of chondrocytes and MSCs.

Distinct tissues developed *in vivo* within the different regions of the bi-layered implants. Vasculature was clearly evident in the lower portion of the construct, with a white hyaline like appearance on top. The two layers were well integrated, appearing very much like an osteochondral plug. The co-culture supressed mineralisation *in vivo,* with the upper portion devoid of mineral in μCT scans, however there was no distinct difference between the chondral regions engineered using agarose or alginate hydrogels based on quantification of calcium. In fact, the only differences were noted when examining high resolution images of H&E staining where positive staining for bone was evident. It is hypothesised that small amounts of bone were detected in the alginate co-culture due to the degradation of the material. An RGD modified low molecular weight alginate was used which will degrade as opposed to agarose. The degradation would lead to vasculature infiltration and increased oxygen levels that have been shown to regulate hypertrophy of MSCS (Gawlitta et al., 2012; Sheehy et al., 2012). Additionally, the RGD peptide enhances cell adhesion and causes the cell to spread (Genes et al., 2004), directing the cells along a more osteogenic lineage (Park et al., 2010; Wang et al., 2013). Conversely, agarose has been shown to maintain the round cell morphology of chondrocytes (An et al., 2001; Aufderheide and Athanasiou, 2005; Aulthouse et al., 1989) which will promote a more stable chondrogenic phenotype. This result shows that not only are the cells important for stable chondrogenesis, but also the biomaterial.

There was little evidence of residual RGD-γ-alginate material within the implants after 6 weeks *in vivo*. Tailoring the material degradation rate to facilitate vascularization and host cell invasion is critical for robust bone formation. Materials which do not degrade quickly can delay bone formation by occupying space needed by the cells to deposit ECM (Cunniffe et al., 2015). The alginate in this system was γ-irradiated, which has been shown to support more and structurally superior bone tissue formation than non-irradiated alginate (Alsberg et al., 2003). One limitation to this approach is the incorporation of the PCL fibres will inhibit bone formation as it will be many years before it fully degrades, consequently the PCL cage was fabricated to be as porous as possible.

This work examined several reinforcement thermopolymers for tissue engineering 3D printed, mechanically reinforced soft tissue templates for the construction of a bilayer scaffold with spatially distinct regions capable of supporting the development of either endochondral bone and stable articular cartilage. All PLGA and PLA reinforced constructs were found lose mechanical integrity over time, with 3D printed PLGA fibres undergoing severe swelling. In spite of this all groups were found to support deposition of chondrogenic ECM when loaded with MSC-laden hydrogels. PCL was chosen as the reinforcing thermoplymer, and supported

endochondral bone formation in the osseous layer. Co-cultures embedded in alginate and agarose supressed mineralisation and supported a chondrogenic phenotype in the chondral region of bi-layered implants, although agarose was found to maintain a more stable cartilaginous tissue. These findings point to the potential of using such reinforced bilayered scaffolds as soft tissue templates for osteochondral regeneration.

6.5 Concluding Remarks

This chapter has demonstrated that tissue engineered cartilage templates can be mechanically reinforced with 3D printed polymers. Using this approach, mechanical properties similar to native articular cartilage can be achieved. Bi-layered cartilage templates can be tissue engineered within the PCL frame, using a co-culture of MSCs and CCs to form the cartilage layer and BMSCs the osseous layer. When these templates are implanted *in vivo*, distinct layers of tissue are formed, analogous to the osteochondral unit. The chondral layer formed within the agarose did not undergo mineralisation *in vivo* and therefore was chosen as the hydrogel with which to engineer the top chondral layer of an osteochondral implant that will be next evaluated in a goat model of osteochondral defect repair.

7 Engineered soft tissue templates reinforced by 3D printed PCL for osteochondral regeneration

7.1 Introduction

In vitro experiments can provide important information on cell-biomaterial interactions under controlled, repeatable conditions. In the previous chapter, initial *in vivo* evaluation in a subcutaneous environment provided a first insight into the behaviour of reinforced soft tissue templates *in vivo.* For engineered cartilaginous tissues, the phenotypic stability (inhibition of hypertrophic markers and/or tissue calcification) can be evaluated; while for endochondral bone tissue engineering strategies this in vivo model provides an assessment of the implant to promote vascularization and bone formation. However, evaluation *in situ* is critical for translating any new therapy/treatment to the clinic (Chu et al., 2010; Moran et al., 2016). Additionally, the construct can be evaluated for immune responses, host integration and regenerative capabilities that are not possible using *in vitro* or subcutaneous nude mouse models.

There are a number of animal models used to evaluate tissue engineered strategies for joint regeneration, including murine, lapine, ovine, caprine, porcine, equine and canine models (Ahern et al., 2009). The ideal animal model would closely resemble the geometry and range of movement of humans (Proffen et al., 2012), however external factors such as initial and maintenance costs and time to skeletal maturity play a significant role in the model selection. Human articular cartilage is thicker compared to any of the previously mentioned animal models, for example the average thickness of human articular cartilage is 2.35mm, would compares to 0.1mm in a mouse (Ahern et al., 2009). The closest thickness to human is an equine model which has an average thickness of 1.75mm (Ahern et al., 2009; Chu et al., 2010). Horses are, however, expensive both to buy and maintain. Rabbits (used earlier in this thesis) are a popular model for cartilage and osteochondral defect repair (Frenkel et al., 2005; Grande et al., 1995; Reyes et al., 2012; Shimomura et al., 2014; Sukegawa et al., 2012; Wakitani et al., 1998). The average cartilage thickness is only 0.3mm thick (Ahern et al., 2009), however the low cost, rapid reaching of skeletal maturity at 6-8 months, easy husbandry and larger joint size than either mice or rats make it a practical model for early stage or proof-of-concept *in situ*

evaluation (Chu et al., 2010; Grässel and Lorenz, 2014; Moran et al., 2016; Poole et al., 2010; Proffen et al., 2012). Goats are considered an excellent model as they have an anatomy and biomechanics similar to humans, are easily available and have low maintenance costs (Ahern et al., 2009; Moran et al., 2016). The cartilage is on average 1.1mm thick and the subchondral trabecular architecture is more similar to humans than rabbits (Moran et al., 2016). The large size of a goat condyle is beneficial as larger defects can be made. A 6mm cylindrical defect has been shown as a critical size to prevent spontaneous repair (Jackson et al., 2001). Therefore, a goat model was chosen to evaluate the mechanically reinforced bi-layered scaffold developed in the previous chapter for osteochondral repair.

Evaluation of any cartilage tissue engineering strategy involving MSCs in the goat requires optimization of the expansion and differentiation conditions of goat MSCs for chondrogenesis. There is, however, little information concerning the optimal expansion and differentiation conditions for goat BMSC reported in the literature. Previous studies have reported expanding goat BMSCs in both high and low glucose media and in hypoxic culture conditions (Gotterbarm and Spector, 2005; Murphy et al., 2003). Under such conditions it has been demonstrated that the sGAG synthesis by goat MSCs is strongly donor dependant, with some unable to synthesise a sGAG-rich tissue (Gotterbarm and Spector, 2005). A study refining the culture conditions of goat chondrocytes in pellet culture concluded that expanding in high glucose (4.5g/L), 5% oxygen and FGF-2 were optimal for chondrogenesis (Miot et al., 2006). The first objective of this study was to identify appropriate culture conditions for inducing robust chondrogenesis of goat BMSC. Having identified such conditions, reinforced bi-layered cartilage templates were then engineered using the strategy outlined in the previous chapter. These were then implanted into critically sized osteochondral defects in the trochlear ridge and the medial femoral condyle of goats.

7.2 Materials and methods

7.2.1 3D printing process

An orthogonal architecture (12mm diameter, 6mm height, line spacing 2mm) was printed with a tank and needle temperature of 70 degrees, screw speed of 18 rev/s and a 30-gauge needle. The PCL was then punch using a 6mm biopsy punch to form 6x6mm unconfined lattice shaped constructs.

7.2.2 Cell isolation, expansion and CFU-F

Bone marrow was obtained from 3 different goat donors, 2 male and 1 female (ages were 6months to 2 years) were isolated as per the procedure in Chapter 3, section 3.1. After cell counting, the cells were divided into 2 groups with XPAN media containing either low (1 g/L) or high glucose (4.5 g/L), hereafter will be referred to as LG and HG. All other supplements of the XPAN media kept constant (details in Chapter 3, section 3.1). BMSC were either expanded on T175s or plated onto petri dishes for CFU-F analysis. CFU-Fs were plated at a density of 43103 cells/cm^2. The groups were maintained in either 5% or 20% oxygen (Fig.7-1). After the first passage, the CFU-Fs were analysed (washed twice with PBS and fixed with 2% PFA for 15 minutes. They were stained with 1% crystal violet for 2 min at room temperature. The crystal violet was removed and washed twice under flowing tap water. FGF-2 was added to the media from P1 onwards. Pellets of BMSCs were formed at the end of passage 1, refer to Chapter 3, section 3.5 for details. The pellets were maintained in fully supplemented low or high glucose CDM (containing 10 ng/ml of TGF-β3; see Chapter 3, section 3.4 for details). A full overview of the pellet experimental groups is shown in figure 7-1, 2 donors were expanded and differentiated in the conditions in figure 7-1 (with the exception of one donor which was only differentiated in high glucose conditions). Chondrogenesis was assessed using the histological and biochemical techniques described in Chapter 3, sections 3.8 and 3.9.

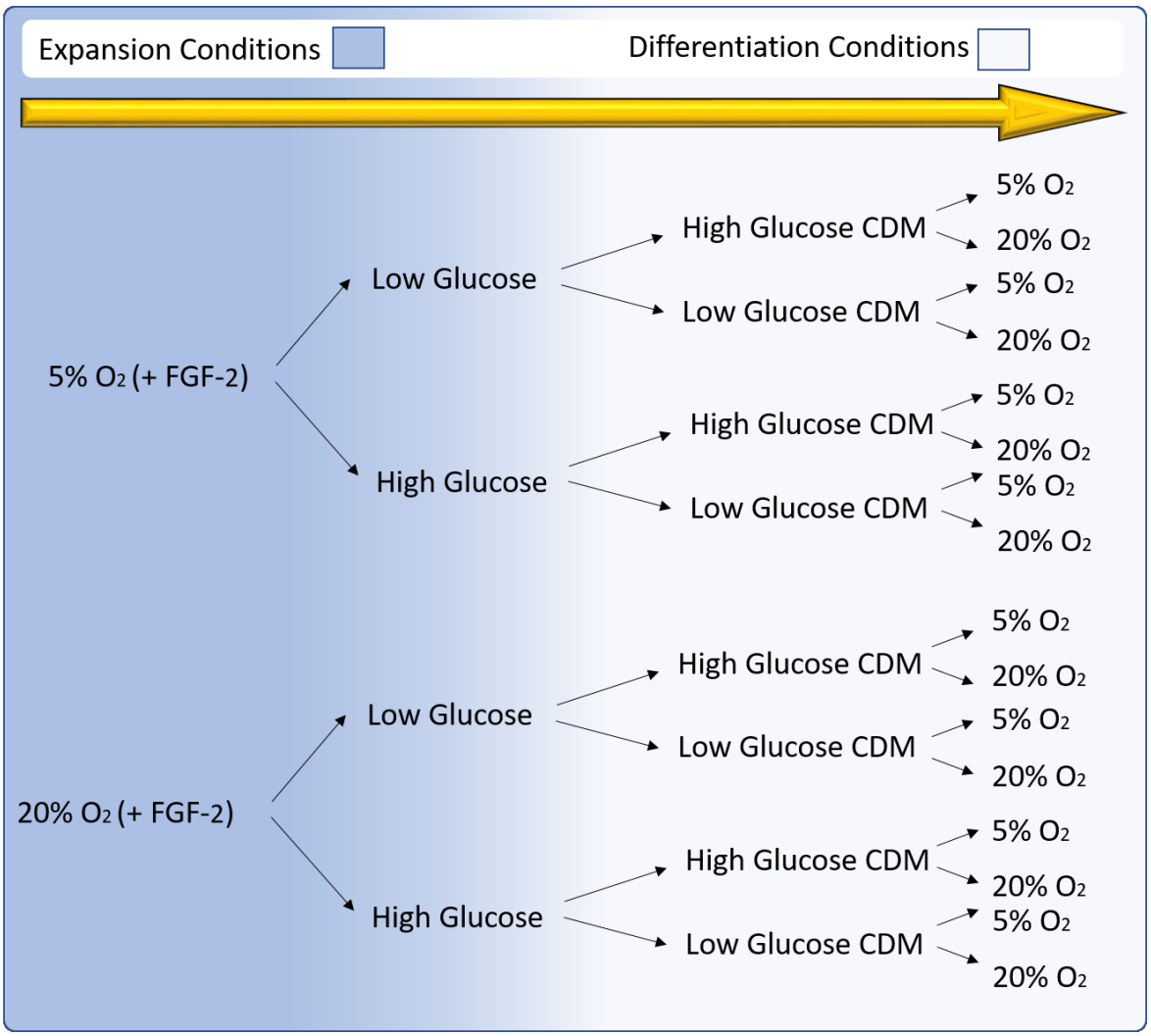

Figure 7-1| Overview of the experimental groups: *16 in total, alternating oxygen, glucose in both expansion and differentiation phases. 2 donors were maintained in all 16 conditions, 1 donor in all the mentioned expansion phases, but only differentiated in HG CDM*

7.2.3 Formation of the reinforced soft tissue cartilage templates

Cartilage templates were formed in the same manner as Chapter 6, briefly, a PLA mould was fabricated using a 3D printer. 6% agarose was combined with 100mM $CaCl_2$, pH 7.2, in a 1:1 ratio (final concentration of 3% and 50mM respectively) and poured into the mould to create cylindrical wells of diameter 6mm and a height of 4mm. A second mould was formed in similar fashion except the 6% agarose was combined with deionised water to create 3% agarose wells of diameter 6mm and height 6mm. The PCL cage was placed into the 6x4mm agarose-$CaCl_2$ mould. To form the 'osseous' 1.5% of RGD-γ alginate containing $20x10^6$/ml BMSCs was pipetted up to the 4mm height. The construct was left to cross-link for 30 minutes before being cut free and placed into the 6x6mm agarose mould. To form the 'chondral layer' 2% of agarose type VII at a temperature of 42°C was combined with $40x10^6$/ml of a 3:1 co-culture of BMSC:CC for a final concentration of 1% and $20x10^6$ /ml agarose and cells respectively. The agarose

crosslinked after 10 minutes at room temperature before being cut free. The constructs were maintained in CDM with TGF-β3 at 37°C with 5% oxygen for 28 days.

7.2.4 Surgical Procedure

Following 4 weeks *in vitro* priming, the bilayered constructs (n = 4 per group) were implanted into the medial femoral condyle and the trochlear ridge of skeletally mature goats. Surgical procedure in caprine model was performed as previously described (Levingstone et al., 2016). Briefly, following anaesthesia, an arthrotomy of each stifle joint was performed using the lateral para-patellar approach. A critically-sized defect, 6 mm in diameter x 6 mm in depth, was created in each medial femoral condyle using a hand drill, a flattened drill bit and a depth guide. The joint was flushed with fluids (0.9 % NaCl) and the stifle joints were assigned to be either empty or include the reinforced bi-layered scaffold. Euthanasia was carried out at 6 months to permit harvesting of the treated condyles. Ethical evaluation and approval was performed by University College Dublin (UCD) and the HPRA.

7.2.5 Macroscopic and histological ICRS scoring

Macroscopic evaluation of the joints was performed immediately upon opening the joint and assessed on the following parameters presented in table 7-1 (van den Borne et al., 2007);

Table 7-1| *Macroscopic scoring parameters*

Parameter	Points
Degree of defect repair	
In level with surrounding cartilage	4
75% repair of defect depth	3
50% repair of defect depth	2
25% repair of defect depth	1
0% repair of defect depth	0
Integration to border zone	
Complete integration with surrounding cartilage	4
Demarcating border < 1 mm	3
3/4th of graft integrated, 1/4th with a notable border > 1 mm width	2
1/2 of graft integrated with surrounding cartilage, 1/2 with a notable border > 1 mm	1
From no contact to 1/4th of graft integrated with surrounding cartilage	0
Macroscopic appearance	
Intact smooth surface	4
Fibrillated surface	3
Small, scattered fissures or cracs	2
Several, small or few but large fissures	1
Total degeneration of grafted area	0
Overall repair assessment	
Grade I: normal	12
Grade II: nearly normal	11–8
Grade III: abnormal	7–4
Grade IV: severely abnormal	3–1

Histological sections stained with H&E and safranin-O were blindly scored by 4 experts using ICRS scores presented in table 7-2 (Hoemann et al., 2011);

Table 7-2| *Histology scoring parameters*

Histological Parameter	Score	
	0%	100%
1. Tissue Morphology	Full Thickness Collagen Fibres	Normal Cartilage Birefringence
2. Matrix Staining	No Staining	Full Metachromasia
3. Cell Morphology	No round/oval cells	Mostly round/oval cells
4. Chondrocyte Clustering	Present	Absent
5. Surface Architecture	Delamination, or major irregularity	Smooth surface
6. Basal Integration	No integration	Complete integration
7. Formation of a Tidemark	No Calcification Front	Tidemark
8. Subchondral Bone Abnormalities/ marrow fibrosis	Abnormal	Normal Marrow
9. Inflammation	Present	Absent
10. Abnormal calcification/ossification	Present	Absent
11. Vascularization (within repaired tissue)	Present	Absent
12. Surface/Superficial Assessment	Total loss or complete disruption	Resembles intact articular cartilage
13. Mid/deep zone assessment	Fibrous Tissue	Normal Hyaline Cartilage
14. Overall Assessment	Bad (fibrous tissue)	Good (hyaline cartilage)

7.2.6 Safranin-O Quantification and Polarised Light Microscopy

Sections stained with safranin O staining were quantified using Photoshop. Picro-sirius red stained samples were imaged under polarised light microscopy to investigate collagen fibre orientation. Image J software was used to quantify the average orientation of the collagen fibres and provide a dispersion value for the distribution using the directionality function.

7.2.7 Statistics

Statistical analysis was performed with GraphPad Prism 6 software package. All graphs are presented with error bars + standard deviation, significance was accepted at a level of $p < 0.05$. Pareto charts and interaction plots were developed using Minitab 16. Briefly, a factorial design was created with 4 inputs. 6 or 9 corner points were chosen (2/3 donors; N=3), the donors were blocked.

7.3 Results

7.3.1 Oxygen tension and glucose availability regulate colony formation

The largest CFU-F colony diameter generated by goat bone marrow 19 days after plating was for cells maintained at 5% O_2 in HG media. There was a general trend towards HG supporting larger colony sizes (5% HG 1.03±0.04mm, 20% HG 0.869±0.03mm compared to 5% LG 0.76±0.02mm and 20% LG 0.645±0.02mm) (Fig.7-2 a, b), suggesting a more proliferative phenotype in these culture conditions. In contrast, it appeared that oxygen tension was regulating the number of colonies produced, with greater numbers of colonies observed at 5% O_2 (Fig.7-2 a, c). This suggests a higher yield of colony forming stem cells can be obtained by plating bone marrow at 5% O_2.

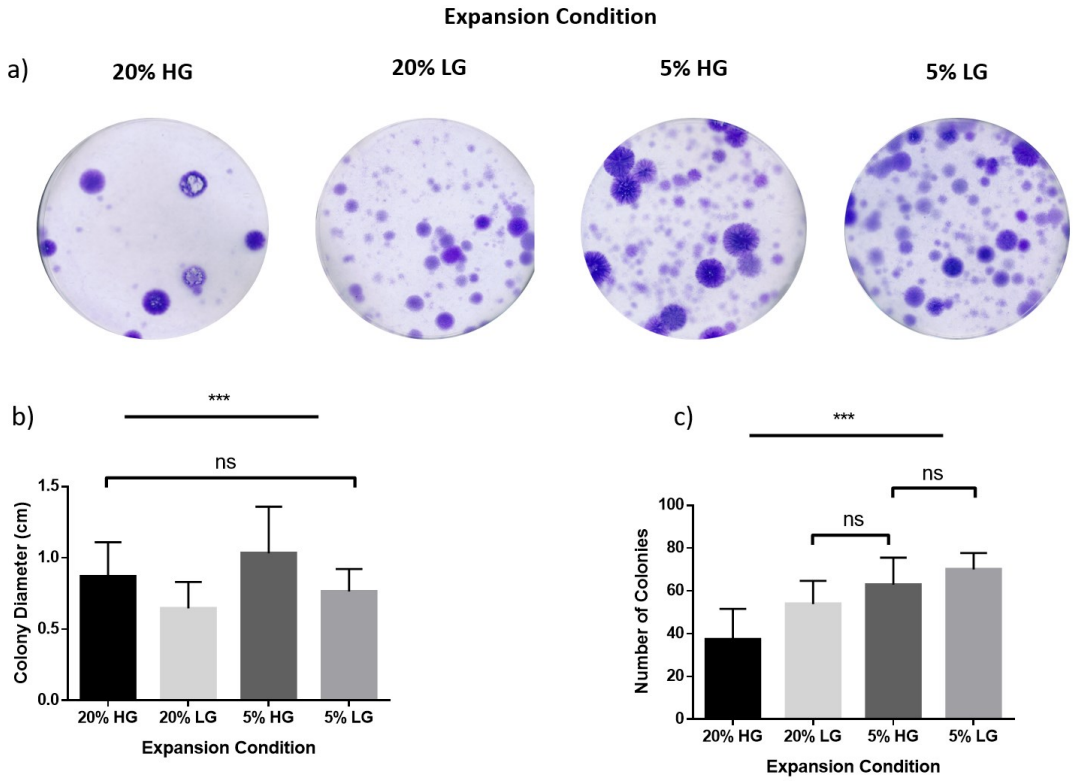

Figure 7-2| Expansion Analysis *a) representative CFU-F for each of the expansion conditions, 20% oxygen high glucose, 20% oxygen low glucose, 5% oxygen high glucose, 5% oxygen low glucose b) average colony diameter and c) number of colonies, n=4, 3 donors, ***significance compared to all groups, *significance, P<0.05*

7.3.2 Oxygen tension and glucose availability regulate the proliferation kinetics of goat BMSCs in pellet culture

After expansion to P1, goat MSCs from three donors were individually pelleted and maintained for 3 weeks in chondrogenic culture conditions. DNA and GAG levels in pellets (n=3) generated from each individual donor are provided in supplementary Figure S3-5, but are pooled here for statistical analysis. DNA level in pellets were used a marker of BMSC proliferation during chondrogenesis. DNA levels were reasonably similar between donors; however, one donor did appear to have higher levels then the other two across all conditions (Fig.7-2 a-d). Differentiating BMSCs at 5% O_2 in HG media resulted in lower levels of DNA (20% LG = 421ng, 20% HG = 571.53ng, 5% LG = 560ng, 5% HG 1000.6ng, Fig.2 c) compared to other differentiation conditions (for example differentiation at 5% O_2 in LG media resulted in the following mean DNA values: 20% LG = 1108.41ng, 20% HG = 890.52ng, 5% LG = 750.87ng, 5% HG 1101.63ng) (Fig.7-2 d). To elucidate the most potent factors affecting DNA levels in pellets, a more complex statistical model was employed in the form of a pareto chart (Fig.7-2 e). This demonstrated that the oxygen conditions during BMSC expansion has the largest effect on DNA levels, followed by glucose availability during expansion (Fig.7-2 e). From the corresponding interaction plot, it is evident that HG media had a positive effect on DNA levels in the expansion phase (Fig.7-2 f). Overall, the interaction plot suggests that 20% O_2 promotes a more proliferation phenotype during chondrogenesis, regardless of the expansion conditions (Fig.7-2 f), it is however, largely donor dependent. Similar results were observed when all three donors were assessed, however, since not all donors were differentiated in both LG and HG media, differentiation glucose was not taken into consideration (supplementary Fig S-2).

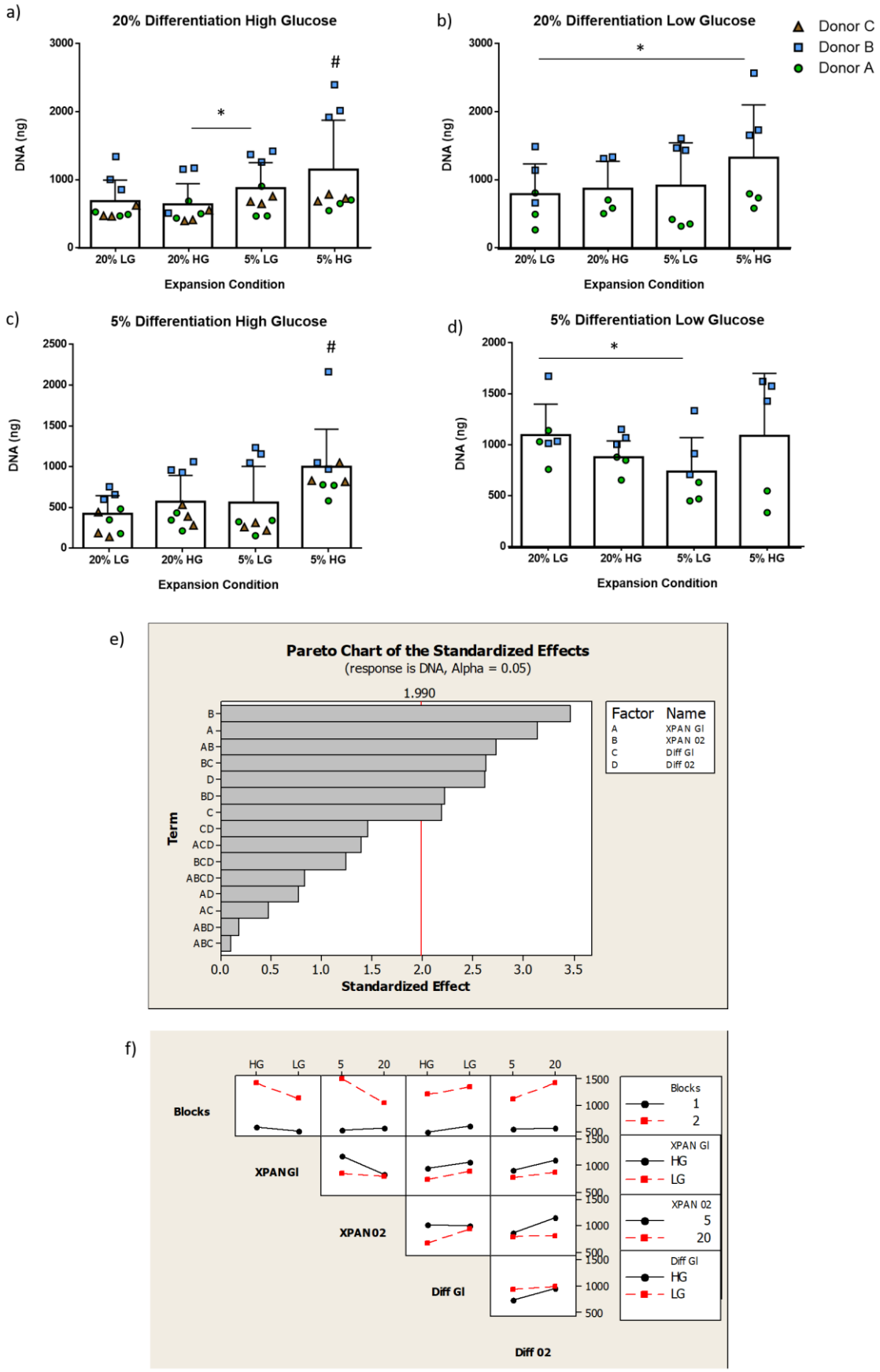

Figure 7-3|Levels of DNA after 28 days: *a) 20% O_2 low glucose differentiation b) 20% O_2 high glucose differentiation c) 5% O_2 high glucose differentiation d) 5% O_2 low glucose differentiation, bars represent the*

*mean values from 2 or 3 donors, #significance compared to all other groups, *significance, p<0.05, 2-way ANOVA, e) Pareto chart, anything right of the red bar denotes significance p<0.05, f) interaction plot where 'blocks' refers to donor*

7.3.3 Expansion and differentiation at 5% oxygen enhances chondrogenesis of goat BMSCs

Levels of sGAG deposition in pellets generated from BMSCs expanded and differentiated in altered oxygen and glucose conditions was donor dependent, with one donor outperforming the others (Fig.7-4 a-d). However, expansion and differentiation at 5% O_2 in HG media conditions consistently and significantly resulted in higher levels of sGAG deposition (Fig.7-4 a-d). Overall, expansion and differentiation at 20% O_2 in LG resulted in the lowest accumulated sGAG (Fig.7-4 b). Across all differentiation conditions, expansion at 5% O_2 in HG media resulted in highest levels of sGAG deposition (Fig.7-4 c). The pareto chart showed that glucose availability during differentiation has the most potent effect on sGAG synthesis, followed by oxygen levels during expansion phase and then the relationship between the glucose during differentiation and the oxygen level during expansion (Fig.7-4 e). On visualising the interaction between the variables, it confirmed that the donors were strongly affected by the 5% O_2 HG conditions during both expansion and differentiation (Fig.7-4 f). It also suggested that the glucose availability during differentiation interacted strongest with the other variables.

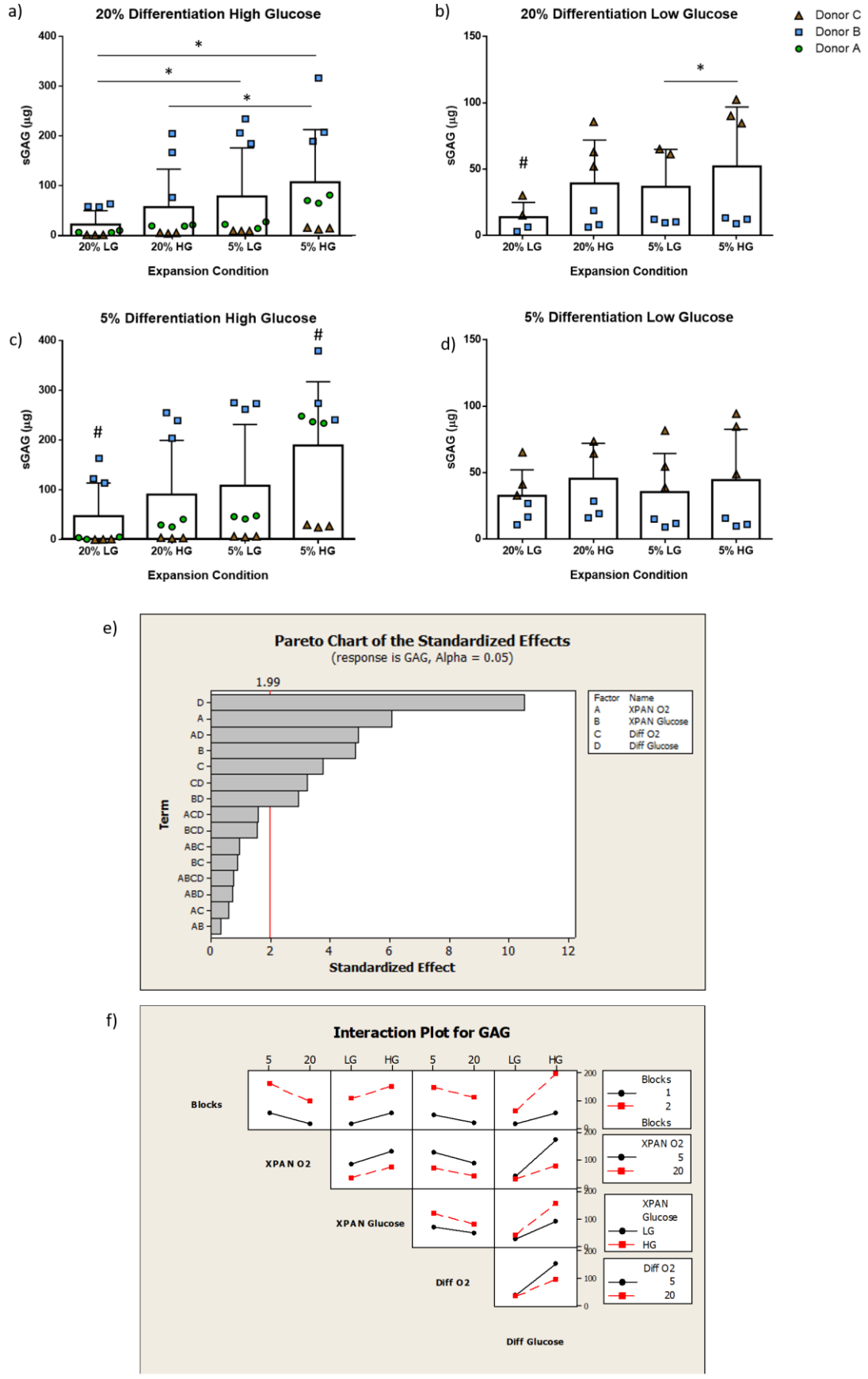

Figure 7-4| Biochemical levels of sGAG after 28 days: *a) 20% O_2 low glucose differentiation b) 20% O_2 high glucose differentiation c) 5% O_2 high glucose differentiation d) 5% O_2 low glucose differentiation, bars*

*represent the mean values from 2 or 3 donors, #significance compared to all other groups, *significance, p<0.05, 2-way ANOVA, e) Pareto chart, anything right of the red bar denotes significance p<0.05, f) interaction plot where 'blocks' refers to donor*

Staining with Safranin-O for sGAG deposition corresponded well with the biochemical analysis, with more intense stating for sGAG accumulation observed in the 5% O_2 in HG media expansion group (Fig.7-5 a). The weakest staining was observed in pellets generated using MSCs expanded at 20% O_2 in LG media (Fig.7-5 a). Regions absent of staining were usually in the centre of the pellet, this was especially apparent in the 5% O_2 LG expansion group (Fig.7-5 a). An interesting observation was the difference in the pellet size. BMSC expanded at 5% O_2 produced larger pellets. Overall, differentiation at 20% O_2 was least optimal for collagen type II synthesis, with BMSCs expanded and differentiated at 5% O_2 consistently generating tissues that stained intensely for type II deposition (Fig.7-5 b). Expanding in 20% O_2 and subsequently differentiating in 5% O_2 lead to predominately pericellular collagen type II deposition, as opposed to more homogenous deposition when cells were maintained at 5% oxygen throughout both the expansion and differentiation phases (Fig.7-5 b).

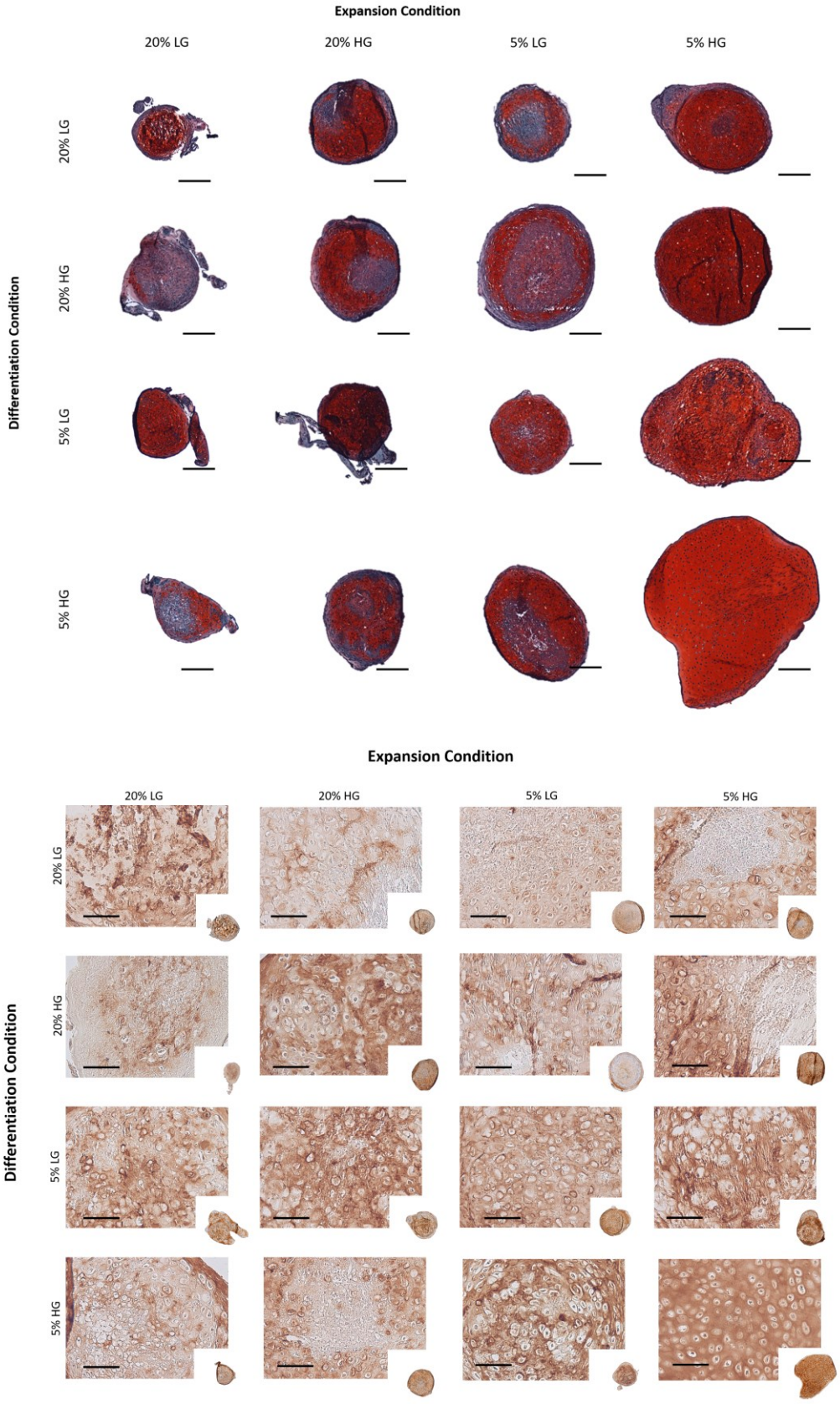

Figure 7-5| Staining for cartilage specific markers: a) *Day 28 safranin-O staining for sGAG, scale bar=500µm, b) immunohistochemistry for collagen type II, the magnified images were taken at the centre of the pellet, scale bar 100µm*

7.3.4 Tissue engineering of reinforced, bi-layered cartilage templates for large osteochondral defect repair

Reinforcing PCL templates (filament diameter = 0.156 ± 0.047 mm; filament spacing = 2 mm) were generated using fused deposition modelling (Fig.7-6 a). The osseous region (bottom 4 mm) of this PCL frame was filled with 1% oxidised, RGD-γ-alginate seeded with BMSCs, while the chondral region (top 2 mm) was filled with a co-culture of BMSC and CCs (Fig.7-6 b). BMSCs were expanded at 5% oxygen in HG, until passage 2. This construct was then maintained for 4 weeks *in vitro* in the optimised differentiation conditions identified above (5% oxygen, HG). Robust chondrogenesis was observed throughout the engineered template (Fig.7-6 d). The co-culture in the chondral layer promoted higher levels of sGAG and collagen deposition (Fig.7-6 e). The bi-layered scaffold maintained its mechanical properties over time in culture (day 0 = 0.273±0.05 MPa, day 28 = 0.278±0.04), and was significantly higher than the unreinforced hydrogel (0.012±0.002 MPa) (Fig.7-6 f).

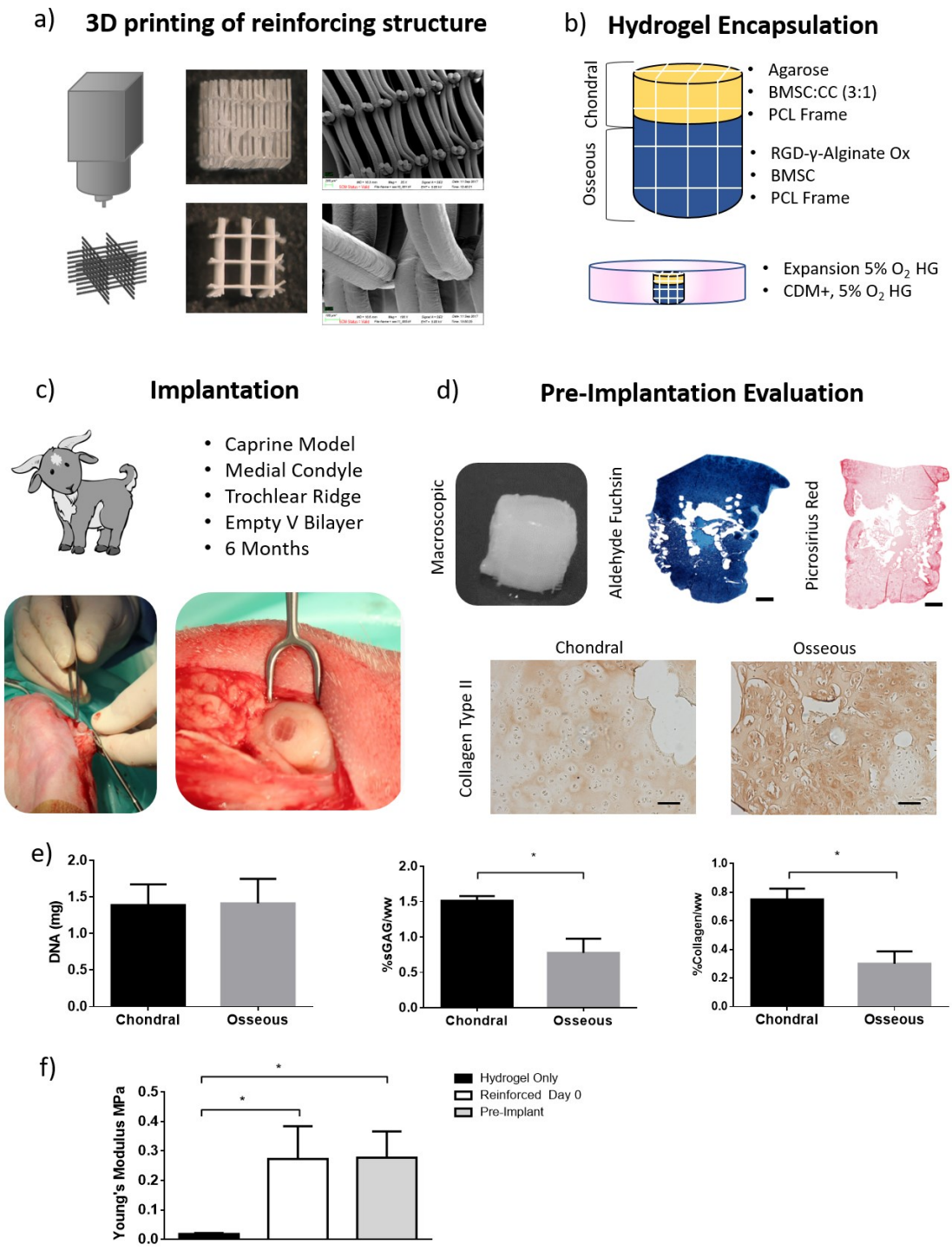

Figure 7-6| Summary of the experimental plan and pre-implantation analysis: *a) 3D printed PCL scaffold, macroscopic and SEM images, b) outline of the components of the 6x6mm bi-layered scaffold c) summary of the in vivo experiment in a caprine model in both the medial condyle and the trochlear ridge, comparing an empty defect to the bilayer at a timepoint of 6 month, d) macroscopic, sGAG, collagen (scale bar 1mm) and collagen type II staining after 4 weeks of in vitro priming (scale bar100µm), e) biochemical analysis for each layer *significance p<0.05, t-test, f) the Youngs Modulus of an unreinforced hydrogel, day 0 reinforced and 4 week in vitro primed scaffold, *significance p<0.05, 1-way ANOVA*

7.3.5 Macroscopic repair appeared comparable in empty and treated osteochondral defects

To evaluate their regenerative potential *in situ*, the tissue engineered bi-layered templates were implanted into critically-sized osteochondral defects created in the medial femoral condyle and the trochlear ridge of skeletally mature goats. 6 months after scaffold implantation, the quality of repair was compared to that of defects left empty. Macroscopic scoring did not highlight any significant differences between groups in either the medial condyle (bilayer =7.83±0.09, empty=9.67±1.64) or the trochlear ridge (bilayer=7.5±1.6, empty=8.17±1.8) (Fig.7 a,b). Both treatments resulted in large gaps in bone repair in the medial condyle groups, even those considered as 'best repaired' (Fig.7-7 c). The bone repair was marginally better in defects made in the trochlear ridge (Fig.7-7 c), however, both had areas where there was no bone detected. There was also no significant difference in mechanical properties of the repair tissue within empty and treated defects (Fig.7-7 d).

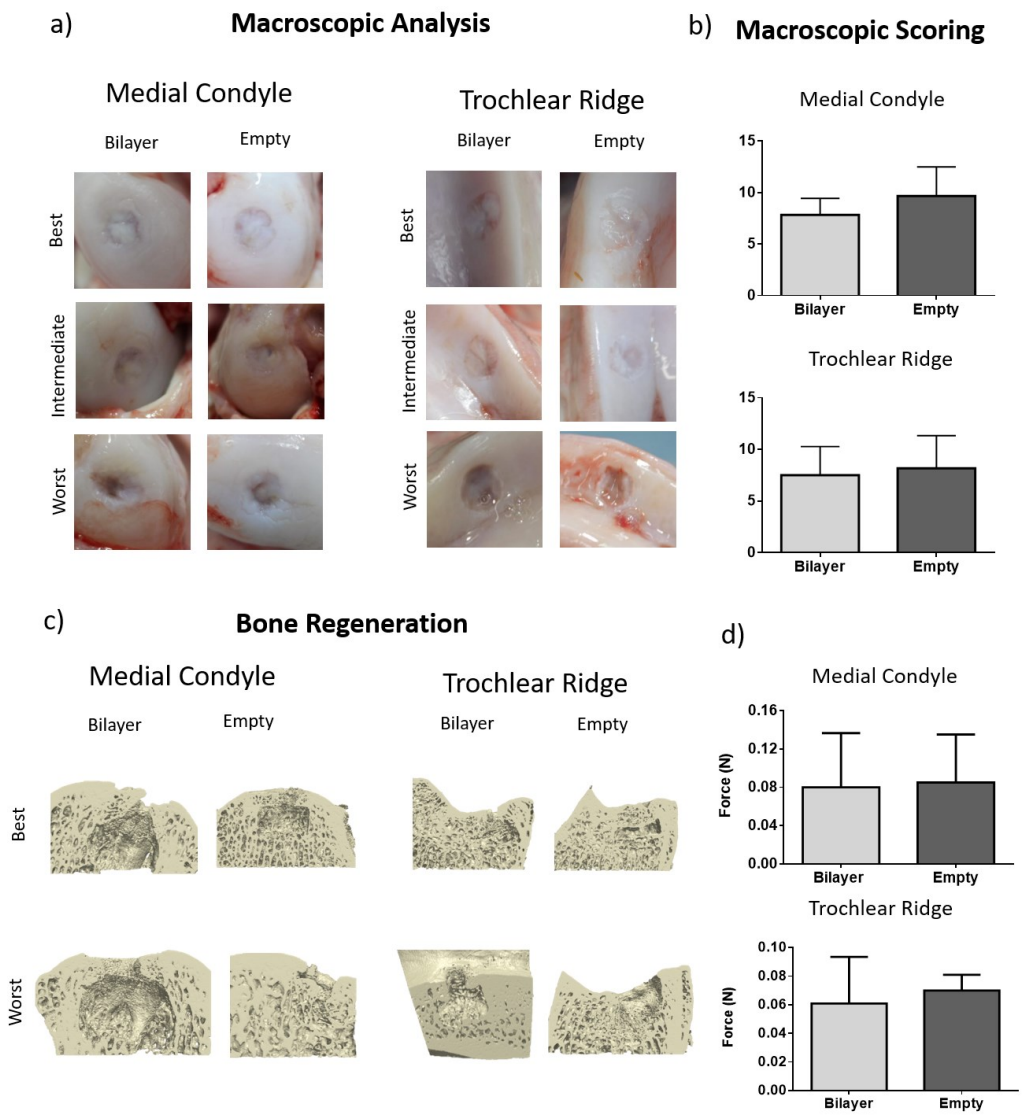

Figure 7-7| 6-month analysis: *a) macroscopic images detailing the repair by the bi-layer or spontaneously in the defects left untreated, b) the corresponding macroscopic scores, c) bone regeneration from microCT scans, d) peak force at a depth of 100µm.*

7.3.6 Bi-layered scaffold supports the development of hyaline tissue in the chondral region

The level of repair was examined in more detail *via* histological staining (Fig.7-8 a, b). Defects in the medial condyle that were left empty formed a layer of tissue staining positive for sGAG and collagen type II (Fig. 8a). Interestingly, however, the adjacent native cartilage stained weakly for collagen type II (Fig.8 a), suggesting that degeneration had progressed to the tissue surrounding the original defect. The treated group also formed a hyaline cartilage-like repair tissue, however the loss of type II collagen in the adjacent tissue was less apparent (Fig.8 a). The PCL struts were visible in the bone region, where they were surrounded by tissue, but in such cases no trabecular bone developed in the centre of the implant (Fig.8 a). Empty defects

within the trochlear ridge spontaneously repaired in a manner similar to that observed in the medial femoral condyle (Fig.8 a, b). Within the trochlear ridge, defects treated with engineered templates repaired with a more consistent hyaline-like tissue (Fig.8 b). The percentage of repair tissue staining positive for Safranin-O was also significantly higher in the chondral region of these defects (Fig.8 c). ICRS scoring did not highlight any significant differences in parameters such as tidemark formation, tissue morphology or cell morphology (Fig. 9 a). The directionality of the collagen fibers had a wide dispersion in the bottom of the articular cartilage, whereas less dispersion was observed in the top of the repair tissue (Fig.9 b).

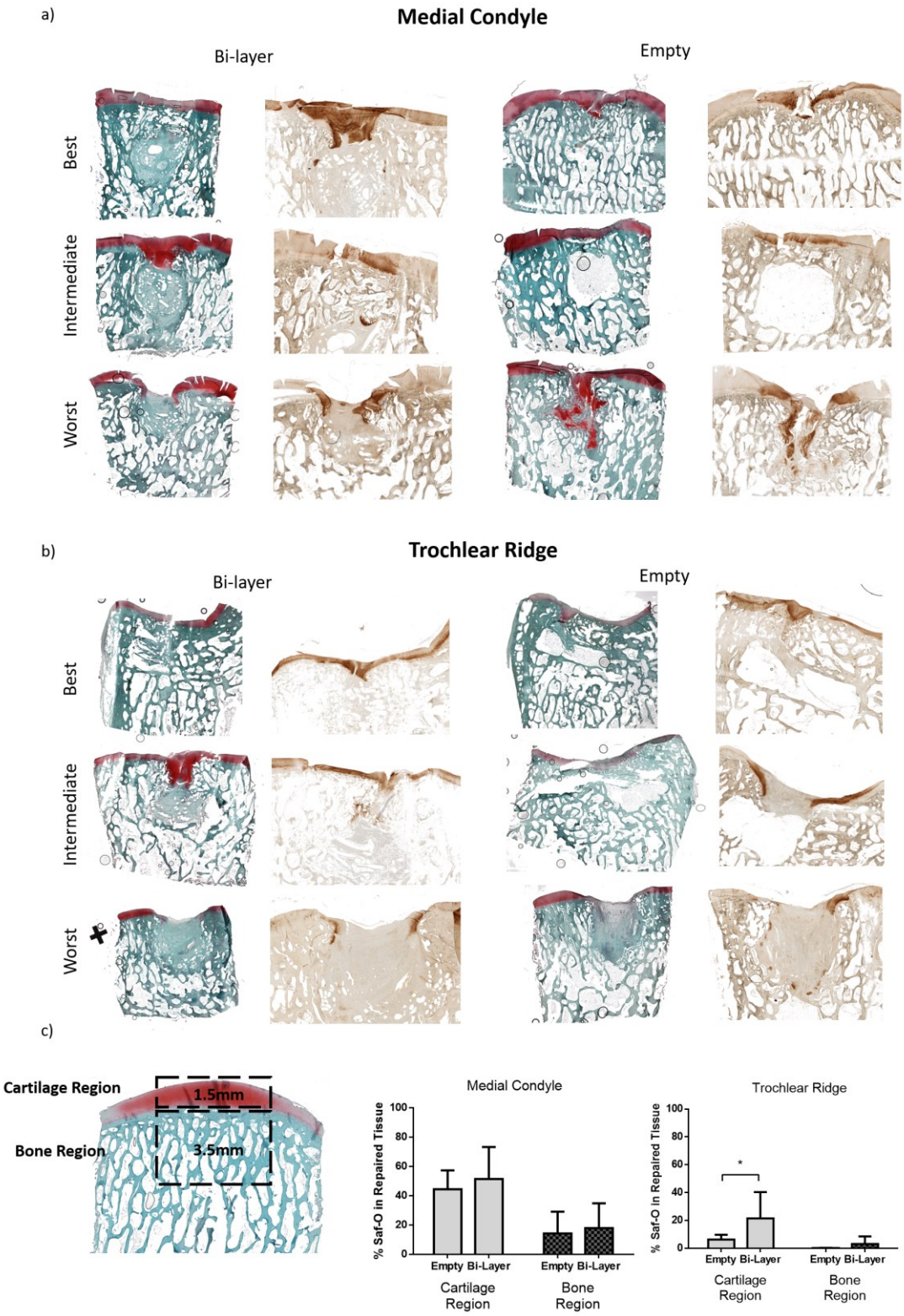

Figure 7-8| Safranin-O staining for sGAG deposition and collagen type II in the treated joints: *histolgical sections detailing the repair by the bi-layered scaffold and the empty controls in a) the medial condyle and b) trochlear ridge, c) quantification of positive saf-o staining in the chondral (upper 1.5mm) and the bone region (lower 3.5mm) *p<0.05, t-test*

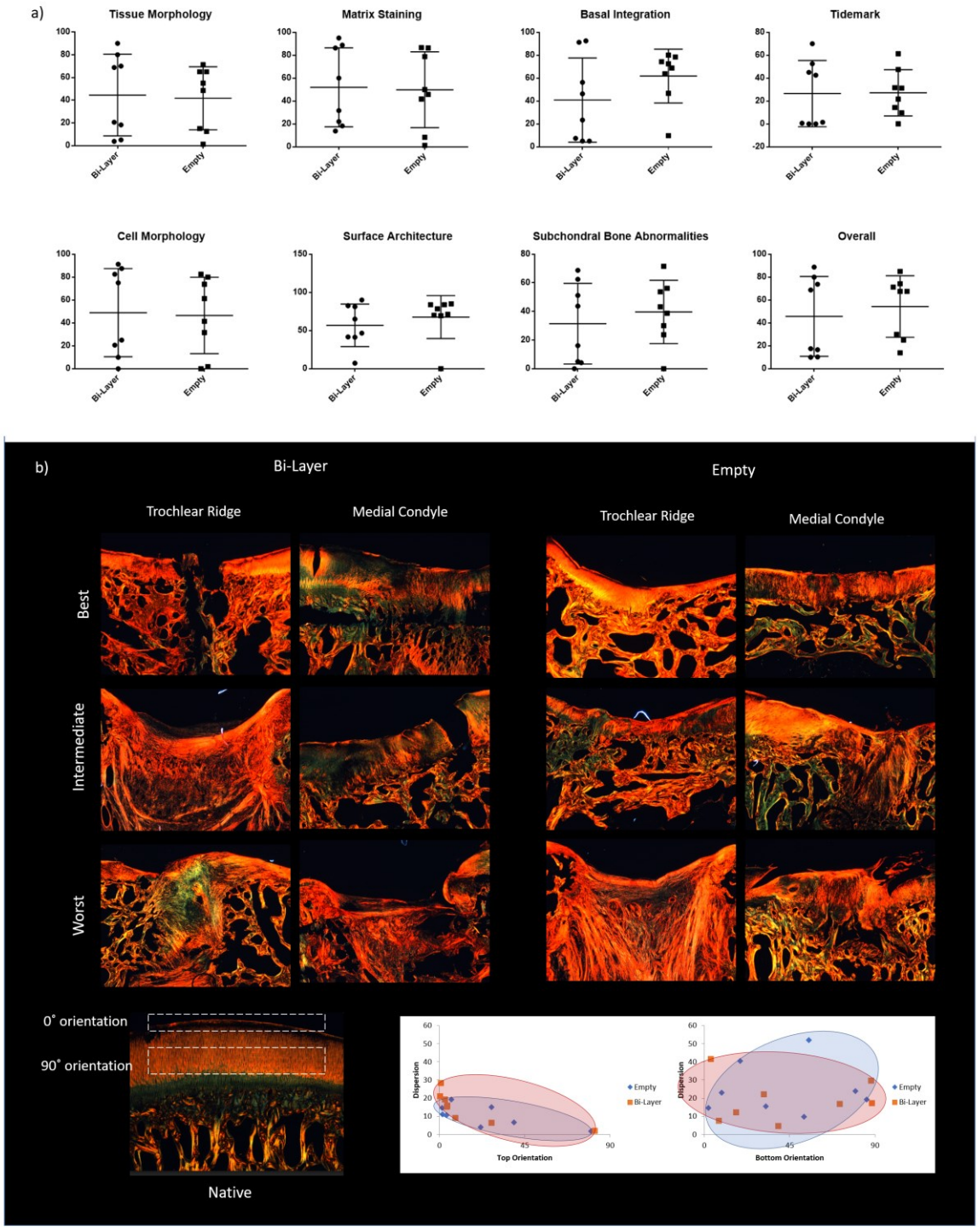

Figure 7-9|Histological scoring and PLM analysis: a) ICRS scoring, for repair of the TR and MC combined, b) PLM images of the defect area, with directionality analysis

7.4 Discussion

Animal models are a critical step in the development of new therapies for treating damaged or diseased joints. They provide insight into the safety and efficacy of the treatment and how the construct will interact with surrounding joint tissues. Here, a goat model was used to determine if a tissue engineered, bi-layered cartilage template can regenerate the osteochondral unit in a critically-sized defect. Goats are an applicable model due to their anatomical similarity to humans, the large size of their stifle and the thickness of their cartilage (Chu et al., 2010; Moran et al., 2016; Poole et al., 2010; Teeple et al., 2013). As a prerequisite to a goat model of osteochondral defect repair, an initial study examining the influence of oxygen and glucose availability during BMSC expansion and differentiation was undertaken with the aim of enhancing the chondrogenic potential of goat BMSCs. It was found that both factors had a significant effect on the levels of DNA, sGAG and collagen within cartilage pellets generated using goat BMSCs. BMSCs expanded and differentiated at 5% oxygen in HG media were found to best support sGAG and collagen type II deposition. Using these culture conditions, reinforced cartilage templates were engineered *in vitro* for 4 weeks before being implanted into both the trochlear ridge and the medial condyle of skeletally mature goats. The quality of the repair was assessed after 6 months. In this time, the bi-layered scaffold supported the formation of a hyaline-like tissue in the chondral layer, however some animal-to-animal variability in the quality of repair was observed. Bone healing was generally poor in both empty and treated defects, pointing to areas for improvement in the design of future implants. In summary, this study shows the potential of fibre reinforced, bi-layered cartilage templates for the repair of the osteochondral unit.

Oxygen and glucose levels during BMSC expansion and differentiation were found to modulate the DNA, sGAG and collagen levels within cartilage pellets. Glucose and/or oxygen have been shown to regulate the proliferation, viability and metabolism of BMSCs derived from murine (Deorosan and Nauman, 2011; Robins et al., 2005), porcine (Meyer et al., 2010; Naqvi and Buckley, 2015b, 2016; Sheehy et al., 2012), rat (Kanichai et al., 2008) and ovine (Krinner et al., 2009) donors. However, it is not clear if all mammalian cells respond to oxygen tension or metabolise glucose in the same way. It is generally accepted that lower oxygen tensions promote a more cartilaginous phenotype (Anderson et al., 2017; Chen et al., 2015; Krinner et al., 2009), which is correlated by the findings in this study. In fact, MSCs can remain viable in harsh oxygen conditions (0.2%), provided there is glucose available to the cells (Deschepper et al., 2011). In this study, BMSCs from the three donors favoured high glucose expansion and differentiation for promoting sGAG synthesis. It has been shown previously that 5mM glucose (approx. 0.9g/L) during differentiation in alginate hydrogels promotes significantly higher sGAG per wet weight and per DNA when compared to 25mM (approx. 4.5g/L) (Naqvi and

Buckley, 2015b). This result was only applicable for constructs maintained in 5% oxygen. In contrast to this study, the cells were encapsulated in alginate hydrogels where the diffusivity of nutrients would differ compared to pellets. As mentioned earlier, several studies using goat BMSC have expanded their cells in low glucose media. This study found that the 1g/L of glucose was sufficient to induce chondrogenesis especially when combined with 5% oxygen. However, the donors in this study were shown to react more favourably towards the high glucose conditions. For this study, it was assumed that three donors were sufficient to make this assumption, however increasing the number of donors would yield a more accurate determination of the factors which affect the fate of goat BMSCs. A further limitation of this study is only chondrogenic markers were evaluated. A more in-depth analysis could be undertaken to evaluate the deposition of hypertrophic markers such as collagen type X. Should a specific expansion condition promote a more hypertrophic cartilage phenotype it could lead to the possibility of engineering a spatially distinct osteochondral construct based solely on the expansion conditions of the cells.

The bi-layered, PCL reinforced engineered cartilage template promoted variable hyaline-like repair in both the medial condyle and the trochlear ridge. For both the empty and treated defects the levels of bone repair was generally poor. Both the PCL and alginate materials used in the development of this tissue engineered implant have been used previously *in vivo* and proven to be biocompatible (Alsberg et al., 2003; Varoni et al., 2012). Previously in this thesis it was shown that the RGD gamma irradiated hydrogel supports bone formation *in vivo.* In this study, the alginate had been further oxidised which would enhance the degradation of the material, thereby limiting any inhibition of angiogenesis and bone formation due to slow degradation. There was no evidence of residual alginate, so it was not thought that this was a contributing factor to the poor levels of bone repair. In may be that the implant is not completely integrating with the surrounding host tissue, with bone or cartilage tissue forming around the construct. If this is the case, it may be because the implanted tissue is too dense to facilitate new bone formation inside the construct. It is conceivable that channels are needed for the vascularization and nutrient diffusion required to promote bone formation(Cunniffe et al., 2015; Sheehy et al., 2014). Another possibility for the poor bone repair is that allogenic cells were not suitable and caused an adverse immune reaction. In spite of these limitations, a promising finding is that hyaline cartilage can be generated at the articular surface using this approach.

Future studies could focus on enhancing the osteogenic potential of the osseous layer, by inducing channels or canals (Sheehy et al., 2014) which would more closely mimic and direct the endochondral ossification paradigm (Blumer et al., 2008; Gawlitta et al., 2010). Canals are formed during endochondral ossification and are thought to serve three primary

functions; metabolic exchange, the supply of osteogenic cells and to act as a reservoir of cells for cartilage growth (Blumer et al., 2008). Such channels could be formed using the 3D printing software, whereby sacrificial materials such as gelatin, sucrose or pluronic could be printed in the desired canal architecture and subsequently washed away following cross-linking of the cell seeded bioink (Jin et al., 2016; Kesti et al., 2015; Visser et al., 2013). Another approach is to incorporate growth factors such as BMP-2 or VEG-F through loading onto polymers or encapsulated into degradable microspheres (Place et al., 2009). A further more complex strategy is to utilise the concept developed as the 'bone bioreactor' (Stevens et al., 2005) to enable maturation of engineered osteochondral unit in an ectopic location prior to implantation into an orthotopic defect. This system was described in a seminal paper by Stevens *et al.,* and functions by using a space between the periosteum and the tibia to stimulate growth of a cell-seeded hydrogel. After 6 weeks, mature bone had been formed, it could be harvested from the 'bioreactor' and used as a graft to repair a bone defect. The process was also demonstrated as viable for the engineering of articular cartilage (Stevens et al., 2005).

To conclude, it has been demonstrated that oxygen and glucose levels affect the synthesis of cartilage specific ECM components by goat BMSC. 5% oxygen and high glucose during expansion and differentiation promotes the robust chondrogenesis of goat BMSCs. Bi-layered, mechanically reinforced engineered cartilage templates stimulate some repair of the chondral region of osteochondral defects, however the repair was donor dependent. Further work is needed to optimise this regenerative implant to ensure integration with the surrounding tissue, enhanced subchondral bone repair and re-establishment of the cartilage-bone interface.

7.5 Concluding Remarks

Having identified that a reinforced bi-layered cartilage template has the potential to engineer stable hyaline cartilage, the next chapter sought to develop a strategy to 3D bioprint an anatomically accurate, functional, biological knee prosthesis. Previously, there have been reports of difficulties 3D printing RGD-γ alginate (Daly et al., 2016a) and it can be challenging to achieve a high degree of resolution with agarose bioinks (Daly et al., 2016b). GelMA, therefore, was selected as the bioink to print cells in the appropriate location within such a geometrically complex implant. Similar to the previous chapters, a co-culture be used for the chondral layer, and BMSCs for the osseous layer.

8 Tissue Engineering an Anatomically Shaped Knee Condyle for Whole Joint Replacement

8.1 Introduction

Osteoarthritis (OA) is a significant problem worldwide, with the world health organisation in 2004 citing it as the 5th largest cause of years lost to disability in high-income countries and 9th in low income countries (Wittenauer et al., 2013). Since then, the prevalence of OA has increased by 32% (Vos et al., 2016). While OA is usually associated with the elderly or obese, it is also becoming more prevalent in the younger more active population (Gioe et al., 2007), which demands new treatment options that delay or ideally replace the need for total joint arthroplasty. This highly invasive procedure requires surgical replacement of the diseased joint with a metal and polymer prosthesis. While total knee arthroplasty (TKA) is usually successful, failures are not uncommon, resulting in a more complicated revision surgery (Schiavone Panni et al., 2009). Factors triggering a revision include aseptic loosening, wear and osteolysis (Keeney et al., 2011). Younger patients are more at risk of requiring a revision operation (Gioe et al., 2007; Keeney et al., 2011). Additionally, it has been reported that after TKA not all patients return fully to exercise or are pain free (Schiavone Panni et al., 2009; Wylde et al., 2007). The aging worldwide population and the increasing instances of joint degeneration are motivating the need for new treatment options. Consequently, there has been an increased interest in regenerative approaches to delay or prevent the need for TKAs.

In recent years there have been attempts to biofabricate biological constructs for whole joint regeneration (Ding et al., 2013; Hung et al., 2003; Lee et al., 2009, 2010; Sheehy et al., 2015a; Woodfield et al., 2009). Critical to the success of such an implant is the capability to mimic both the native geometry and mechanical properties with the aim of maintaining congruency of the joint. One of the most successful studies to date attempted to repair the humeral head of a rabbit (Lee et al., 2010). The authors 3D printed an anatomically accurate porous prosthesis using a PCL-HA blend, with a filament spacing of 200μm and 400μm in the bone and cartilage regions respectively. TGF-β3 was infused into the scaffold to promote stem cell homing, using collagen as a delivery vector. 4 months after implantation *in situ,* the scaffold had been infiltrated with new tissue. The chondral layer stained positive for sGAG and collagen type II and blood vessels were observed in the osseous layer. However, it remains unclear if a cell homing concept would translate from healthy young rabbits to OA human joints. The first

attempt to regenerate the entire knee using tissue engineering involved 3D printing scaffolds mimicking the geometry of both the femoral head and the tibial plateau (both containing a fixation stem) using poly(ethylene glycol)-terephthalate/poly-(butylene terephthalate) (PEGT/PBT) (Woodfield et al., 2009). The constructs were directly seeded with chondrocytes and cultured for 5 weeks *in vitro* prior to implantation. The rabbits were described as having compromised mobility, however, upon excision after 6 weeks the constructs were reported as stable. Tissue had infiltrated the scaffold but it was observed to be fibrous in nature and there was no indication of a hyaline cartilage layer, suggesting the implant was not supportive of stable chondrogenesis in the joint environment. There have been several other studies concerned with tissue engineering anatomically accurate synovial joints such as the femoral head, tibial plateau and femoral condoyle (Ding et al., 2013; Lee et al., 2009; Mesallati et al., 2015b), however they were all evaluated in a non-loaded subcutaneous environment. Despite promoting the development of a spatially inhomogenous tissue mimicking the osteochondral unit, it is unknown how these constructs would perform in an orthotopic environment. In particular, it is uncertain if many of the hydrogel based strategies for osteochondral tissue engineering would have sufficient mechanical strength for whole joint resurfacing applications.

Some of the limitations associated with previous whole joint tissue engineering strategies could potentially be resolved by using multiple-tool bioprinting strategies. In particular, it enables the simultaneous bioprinting of cell laden hydrogels conducive to specific tissues phenotypes alongside reinforcing thermoplastics that provide mechanical strength to the implant (Daly et al., 2016b; Kundu et al., 2015; Visser et al., 2015a). In this study, gelatin methacrylate (gelMA) based bioinks will be used to print the different components of a scaled up, anatomically accurate biological implant for punitive joint resurfacing applications. To engineer functional articular cartilage a gelMA bioink containing a co-culture of BMSCs and chondrocytes (CCs) will be ink-jetted on top of a BMSC laden gelMA osseous layer which is designed to undergo endochondral ossification *in vivo* (Mesallati et al., 2015b). The concept will be assessed *in vitro*, followed by scaling-up the process to print an anatomically accurate biological implant designed to regenerate the entire medial femoral condyle. The final phase of this study will assess the efficacy of this approach in a rabbit model of femoral condyle regeneration.

8.2 Materials and methods

8.2.1 3D printing process and construct formation

The PCL scaffolds, cylindrical disc of (diameter 8mm, height 5mm), the anatomically accurate knee construct and the stem were printed with the parameters outlined in Table 8-1.

Table 8-1| *Summary of printing parameters*

Parameter	Body of the Scaffolds	Stem
Needle gauge	25	25
Tank temperature	67˚C	67˚C
Print head temperature	67˚C	67˚C
Layer thickness	0.22 mm	0.22 mm
Printing rate	14 revs/mm	14 revs/mm
Spacing	1 mm	0.8 mm
Pressure	0.1 MPa	0.1 MPa

The printed PCL scaffolds were sterilised in ETO and allowed to air dry in a sterile environment for 3 hours. The scaffolds were then placed in a custom-built mould. The mould was designed to fit into the printing platform of the 3D printer (RegenHu). To form the osseous layer, 10% GelMA containing 0.05% irgacure 2959 was combined with BMSC, for a final concentration of $20x10^6$ cells per ml. Using an 18G needle, the cell-gelMA-irgacure solution was injected into the PCL scaffold. It was placed under UV light for 10 minutes. Next, 10% gelMA containing 0.05% irgacure 2959 was combined with a co-culture of BMSCs and CCs (3:1) in a syringe. The syringe was screwed into the inkjet printhead and was surrounded with a heating jacket that maintained a temperature of 37˚C. The following parameters were inputted into the software; Dosing distance = 20mm, valve opening time = 500µs, pressure = 0.01MPa. The scaffold containing the osseous layer was removed from the mould and placed under the inkjet valve. The program was run until 2 layers (approximately 400-600µm thick) has been deposited on top of the scaffold. UV light was then applied for a further 10 minutes (summarised in Fig.8-1 a, b). The constructs were cultured *in vitro* in 5% oxygen with fully supplemented CDM.

8.2.2 Mechanical Testing

A 10kN load cell was used to compress the samples. A 1N preload was applied, followed by 15% strain at a speed of 1mm/min. On separate samples dynamic testing was conducted after first applying a 5N preload. Cyclic strain at 10% offset strain was applied for 5 cycles at 1mm/min

8.2.3 Surgical Procedure

The rabbits were anaesthetised with xylazine and buprenorphine. The condyle was resected using a surgical saw. The hole for the stem was drilled using a surgical drill with a diameter of 3mm. The cavity was washed with sterile PBS prior to the scaffold being placed. The incision was closed using Ethicon, 4-0 vicryl rapide sutures. The rabbits were free to move immediately after surgery and were given buprenorphine for 7 days. This protocol and study was reviewed and approved by the ethics committee of Trinity College Dublin, Ireland and Health Products Regulatory Authority (HPRA), Ireland.

8.2.4 Analysis of in vitro engineered implants

Constructs were either digested in 500µl of papain or fixed in 4% PFA, and analysed as described in Chapter 3, sections 3.8 and 3.9

8.3 Results

8.3.1 Development of bi-layered constructs for osteochondral tissue engineering using multi-tool biofabrication

To assess the feasibility of ink-jetting gelatin onto the surface of a 3D printed implant, a simple cylindrical scaffold was first printed using PCL (Fig.8-1 b). By altering the filament spacing and the needle gauge size, it was possible to print PCL scaffolds with a Young's Modulus of 32.24±0.7 MPa, which was much higher than frames used previously in this thesis (chapter 5, 2.7±0.8 MPa and chapter 6, 0.27±0.05 MPa). The elastic limit at a strain rate of 1mm/min was reached just before 10% strain (Fig.8-1 c). Cyclic testing showed that the scaffold deformed permanently after the first cycle to 10% strain, with significant hysteresis observed during the unloading cycle. For subsequent cycles, the loading and unloading curves were more comparable (Fig.8-1 d). After printing of these PCL scaffolds, the osseous region was filled with gelMA laden with BMSC, followed by inkjet printing of a co-culture of BMSC and CC.

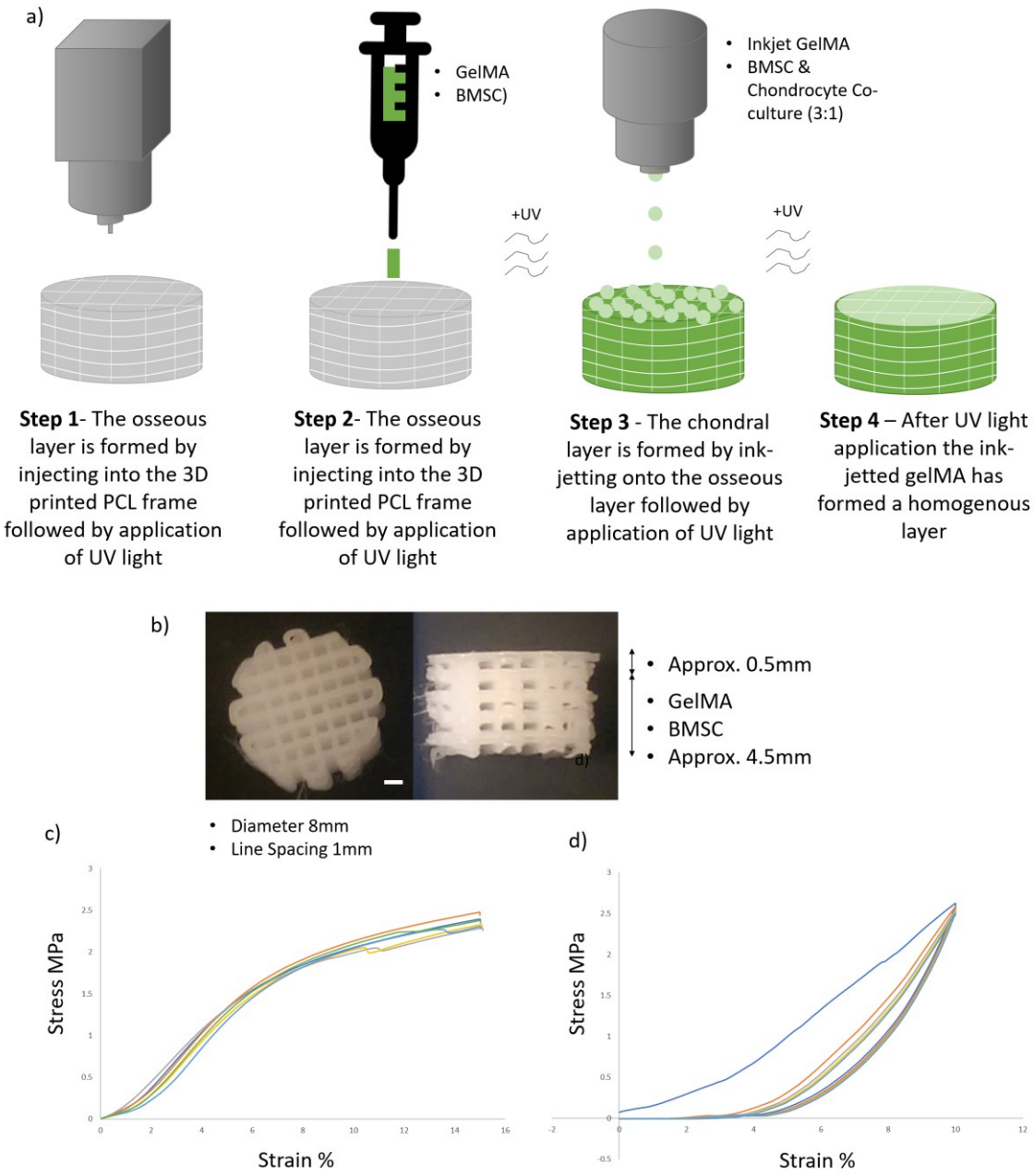

Figure 8-1| Summary of the printing process and mechanical characterisation: *a) the stages of forming the bi-layered construct, first the PCL frame is printed, then gelMA containing BMSC is injected into the scaffold and UV'ed for 10 minutes, followed by ink-jetting of the chondral layer, which is then UV'ed for 10 minutes to form a homogenous surface, b) Macroscopic image of the cylindrical PCL scaffold, scale bar =1mm, c) stress-strain curve, for 6 samples, d) representative cyclic loading curve, each colour represents another cycle.*

Cartilage ECM was synthesised by the co-culture of BMSCs and CC within the ink-jetted gelMA bioinks (Fig.8-2 a-e). sGAGs deposition was greater in the cartilage layer of the construct, as evidenced by the intensity of alcian blue staining (Fig.8-2 b c). Homogenous staining with picrosirius red for collagen was observed throughout the construct (Fig.8-2 d), with the chondral layer staining positive for collagen type II and the osseous layer staining more strongly for the hypertrophic marker collagen type X (Fig.8-2 e). There was no staining

for collagen type X in the chondral layer. The histological results were confirmed by the biochemical analysis, where significantly higher levels of sGAG were detected in the chondral layer (Fig.8-2 g), with equivalent levels of collagen deposited in both layers (Fig.8-2 h). DNA was significantly higher in the chondral layer (11043± 2234 ng) compared to the osseous layer (9344±91.61 ng) (Fig.8-2 f). There was a trend toward a higher calcium accumulation in the osseous layer, however it was not found to be significant (Fig.8-2 i).

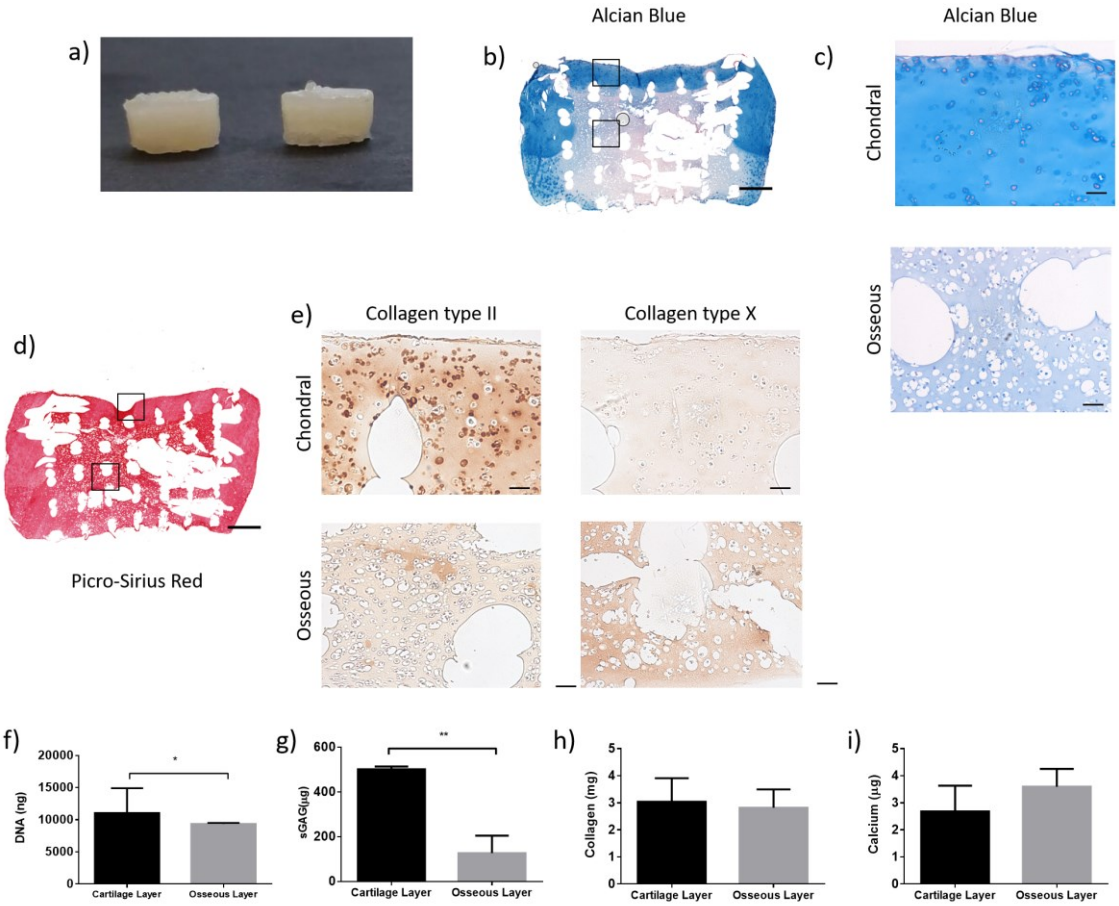

Figure 8-2| In-vitro analysis: *a) macroscopic image, b) sGAG deposition in the whole construct, scale bar 1mm c)magnified images of sections of either the chondral or the osseous layer, scale bar 100µm d) collagen deposition in the entire construct, scale bar 1mm e) deposition of immunohistochemical staining for collagen type II and X in chondral and osseous layers, scale bar 100µm, biochemical analysis for half the construct f) DNA, g) sGAG, h) collagen, i) calcium, *significance p<0.05, t-test.*

8.3.2 Tissue engineered anatomically accurate knee condyle

An anatomically accurate, bi-layered knee condyle was successfully engineered using multi-tool biofabrication techniques. The medial condyle of a rabbit was scanned using a microCT (Fig.8-3 a) and the section to be reproduced was isolated (Fig.8-3 b). The scan was converted to an STL file and 3D printed in an orthogonal fashion (Fig.8-3 c, d). The stem was attached to

the base of the prosthesis by melting the tip at 60 degrees. Similarly to before, BMSC laden gelMA was pipetted into the osseous layer (Fig.8-3 c, e) and the chondral layer was formed by ink-jetting a co-culture of BMSCs and CCs onto the surface of the implant (Fig.8-3 d, f). The pre-implanted construct underwent 4 weeks of *in vitro* priming and stained positive for sGAG and collagen type II prior to implantation. The BMSC in the osseous layer had synthesised hypertrophic cartilage as evidenced by collagen type II, X and sGAG deposition (Fig.8-3 h-k).

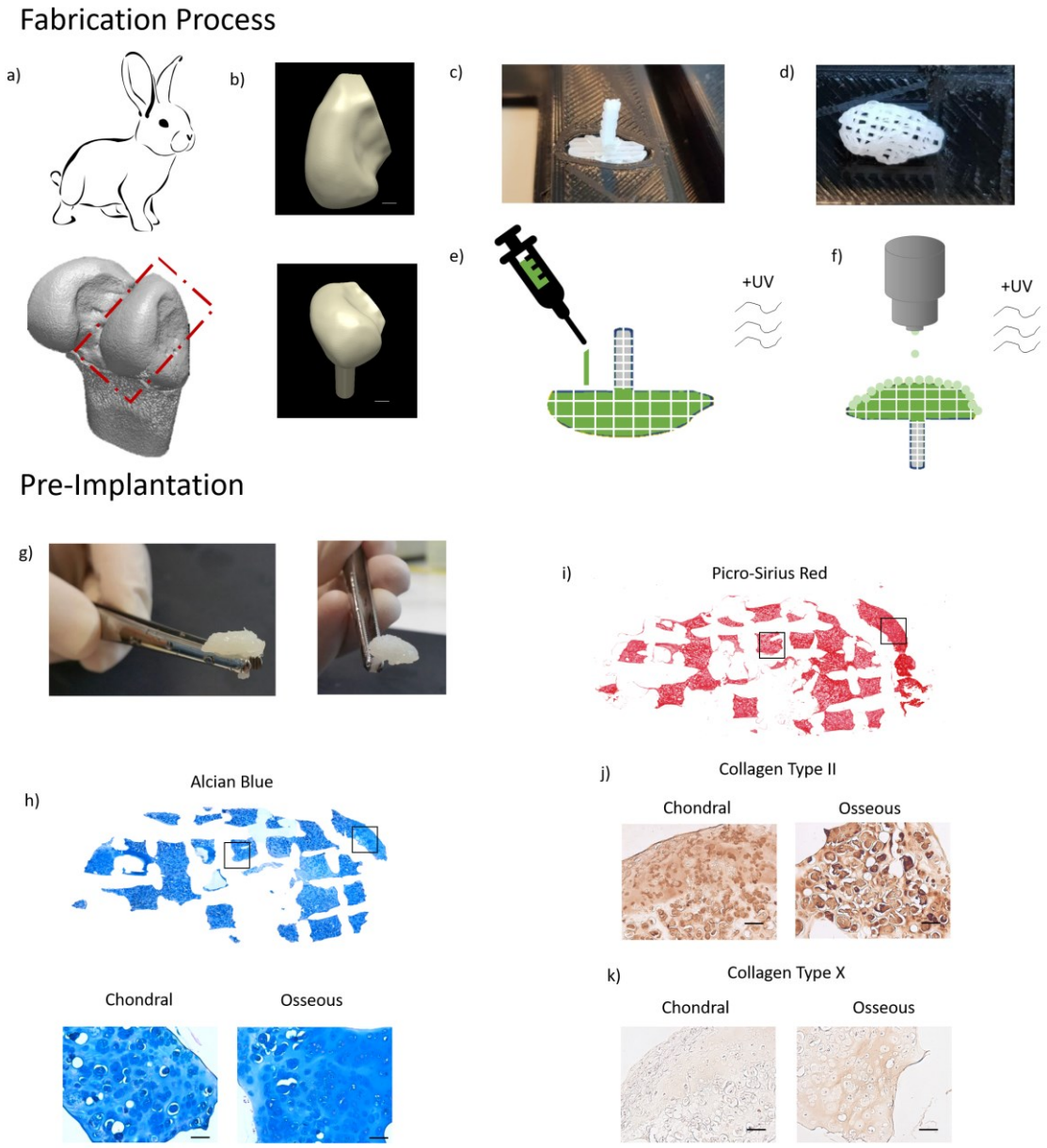

Figure 8-3|Fabrication process and pre-implantation analysis: *a) 3D reconstruction of the microCT scan of a rabbit knee b) 3D reconstruction of the condyle that was converted to an STL file for printing c) the printed scaffold in the mould prior to injection of BMSC laden gelMA d) printed scaffold in the mould prior to ink-jetting the chondral layer, e) schematic of forming the osseous layer f) schematic of forming the chondral layer g) macroscopic images of the construct after 4 weeks in culture, h) alcian blue staining showing deposition of sGAG with magnified images of sections from the two layers, scale bar =100µm, i) pricosirius red staining for collagen, j) collagen type II deposition and k) collagen type X in chondral and osseous layers, scale bar =100µm.*

8.3.3 *In vivo failure of anatomically accurate prosthesis*

The tissue engineered prosthesis fit well into the defect site (Fig.8-4 a). Mobility of the rabbits was assessed for 10 days after implantation. By day 7 all rabbits were weight bearing on the joint/limb which had undergone surgery. No limping was observed throughout the 3-month time period. However, upon sacrifice of the animals it was observed that 4/6 scaffolds had delaminated from the stem and were loose in the joint (Fig.8-4 c). The defect site was filled with a white tissue as indicated by the red arrow in figure 8-4 b. In two rabbits the scaffold no longer appeared whole and had lost its structure, see figure 8-4 d (red arrow). Again, mechanical failure appeared to be the cause of implant failure.

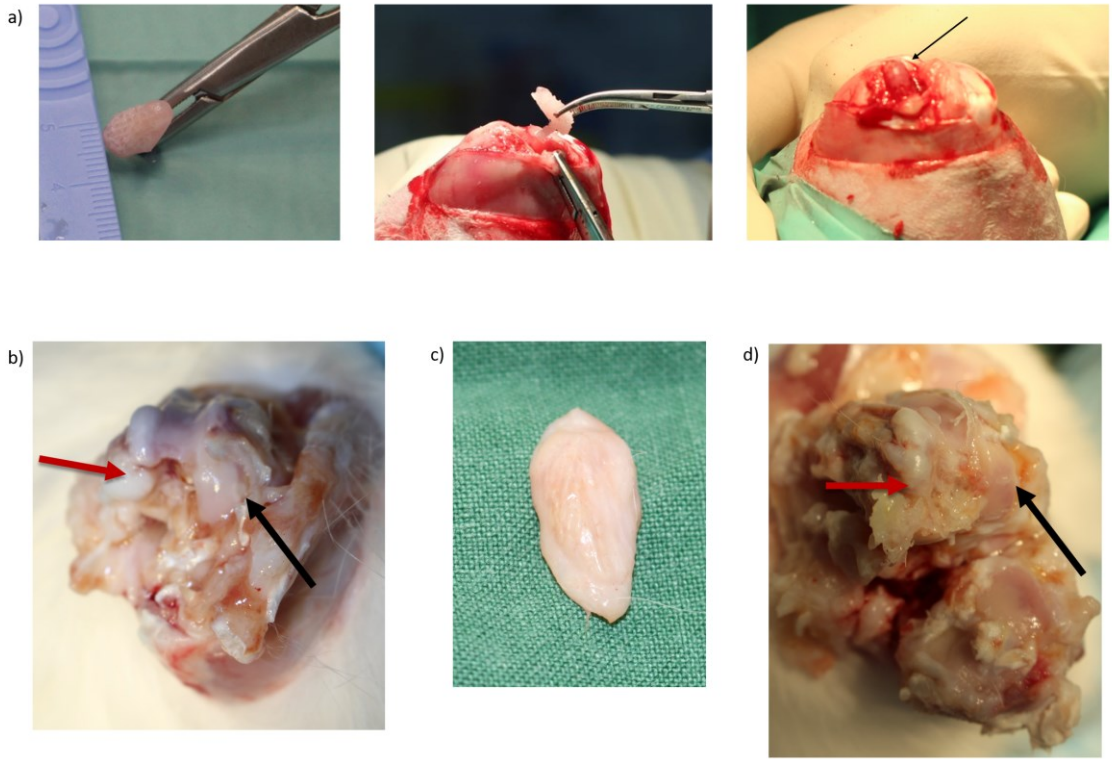

Figure 8-4| Scaffold implantation and post-implantation images: *a) image of the scaffold prior to implantation, black arrow shows the scaffold in the joint b) 3 months after implantation the repair was analysed, red arrow points to the repair tissue and the black arrow to the opposing condyle c) an implant which had been displaced in the joint d) red arrow points to a failed scaffold and the black again to the opposing condyle.*

8.4 Discussion

Tissue engineering an entire joint requires engineering a mechanically reinforced, fully integrated bone-articular cartilage construct. Herein a new method to 3D print an anatomically accurate knee condyle using multi-tool biofabrication techniques is described. Initially, a cylindrical construct was printed to demonstrate the concept and feasibility. Subsequently an implant mimicking the geometry of a rabbit condyle was printed using the geometrical information obtained from a CT scan of a rabbit knee. BMSC encapsulated in GelMA were used to engineer a hypertrophic cartilage tissue within the osseous layer, which was overlaid by a more phenotypically stable articular cartilage layer ink-jet printed onto the surface of the implant. To cover the curved surface of the scaled-up implant, GelMA containing a mixture of BMSCs and CCs was deposited in droplets on the uneven surface of the osseous region of the implant. *In vitro,* stable and hypertrophic cartilage formed within the implant in a spatially defined manner. The implant had a compressive strength deemed suitable for the loading environment in the rabbit knee, and a pilot study of a bioink/cell free PCL scaffold demonstrated that the construct was intact one week after implantation. However, three months after implantation of the scaled-up implant it was observed that the scaffolds had failed mechanically. In most cases it appeared that this was due to delamination of the body of the implant from the stem.

Ink-jetted GelMA containing chondrocytes and BMSCs facilitated the development of an articular cartilage layer on the curved surface of anatomically accurate, PCL reinforced implant. GelMA is widely used for cartilage tissue engineering applications as it supports both cell proliferation, migration and matrix production (Boere et al., 2014; Klotz et al., 2016; Li et al., 2016; Schuurman et al., 2013; Visser et al., 2015b; Yang et al., 2016). GelMA has also been combined with digested cartilage tissue in an attempt to promote tissue specific ECM production, although no significant improvement was observed over GelMA alone (Visser et al., 2015c). In the current study, a hyaline cartilage-like tissue staining positive for type II collagen and sGAG formed on both the on both a simple cylindrical geometry and on the curved surface of the knee condyle implant. This indicates that ink-jetting is a promising technique for depositing bioinks on the surface of scaled-up implants. Previously a PEG-gelMA bioink has been ink-jetted to form 3D constructs (Cui et al., 2012b; Gao et al., 2015). In this study PEG was recommended as a blend for gelMA as they reported difficulties in ink-jetting gelMA alone due to the viscosity (Gao et al., 2015). Here it is demontrated that gelMA can be ink-jetted, provided it is maintained at 37˚C. One potential limitation of inkjet printing is that that the cells may sediment in the bioink in the chamber and post-printing before the application of UV crosslinking (Cui et al., 2012b; Gao et al., 2015). In such cases layer by layer UV crosslinking could be utilised to address this problem (Cui et al., 2012b). In the present study, as rabbit

cartilage is only 0.3mm thick, cell sedimentation within the uncrosslinked ink was not an issue. GelMA is more commonly printed via extrusion based technology between 24.5 to 30˚C (Billiet et al., 2014; Hoch et al., 2013). One of the reasons why this approach was not chosen to deposit the cartilage layer is that ink-jetting enables more spatial control over smaller volumes of liquids (Cui et al., 2012a). There was the potential to use such extrusion based bioprinting to deposit the GelMA into the bone layer rather than to manually fill this region of the implant, but given the small size of the rabbit knee, achieving precise heights was challenging.

The mechanical properties of the PCL scaffold can be tailored by altering the line/filament spacing and needle gauge. The line spacing used was 1mm, however, other studies for whole joint applications have used narrower line spacings such as 0.2mm, 0.4mm and 0.6mm (Woodfield et al., 2009). Smaller line spaces increase the resulting mechanical properties, however it also increases the amount of bulk PCL material within the implant, potentially impeding tissue infiltration and bone repair. From the force-displacement curve it is apparent that the scaffold could withstand forces up to 100N in the elastic region. From the literature it is predicted that the medial condyle experiences peak forces of up to 77N (Grover et al., 2007). Whilst this simple compression comparison indicates that the scaffold would be stable *in vivo* it is clear that a more complex testing regime is required to better mimic the biomechanics of the knee. For example, the interface strength between the scaffold body and the stem should be assessed. A shear analysis should also be undertaken, as shear forces are high in the knee joint. Another potential consideration is to determine the coefficient of friction between the engineered condyle and the corresponding tibial plateau.

This study shows the potential of 3D multi-tool bioprinting techniques to engineer complex shaped bi-layered tissues by spatially controlling the deposition of the bioinks. Whilst significant alterations need to be made to the reinforcement frame, the general concept of engineering both articular cartilage and the subchondral bone in an anatomically accurate shape has been demonstrated. Going forward, there is also the potential for bi- or tri-layered PCL scaffolds. By varying the line spacing and filament diameter throughout the depth of the construct it would be possible to more closely mimic the mechanical properties of the articular cartilage, subchondral plate and bone.

8.5 Concluding Remarks

This study outlines a novel approach for regenerating whole joints by utilising 3D multi-tool bioprinting. It provides an insight into combining 3D printing and developmental tissue engineering strategies to engineer an anatomically accurate biological implant. The next chapter will discuss and elaborate on, the results presented in this thesis. It will also highlight the limitations, and advise on future work based on research questions which have stemmed from this thesis.

9 Discussion

9.1 Summary

The objective of this thesis was to develop a strategy to engineer scaled-up functional tissue engineered osteochondral implants for whole joint resurfacing. This thesis began by investigating whether a cartilage template engineered using BMSCs encapsulated in RGD γ-irradiated alginate could be used to regenerate a critically sized osteochondral defect *in vivo* by undergoing spatially defined endochondral ossification. The results showed that these developmentally inspired templates could support hyaline-like cartilage and bone formation, however it was hypothesised that by including a top cartilage layer specifically targeting articular cartilage repair, more robust regeneration could occur. Based on promising results reported in the literature (Acharya et al., 2012; Bian et al., 2011; Hendriks et al., 2007, 2010), it was hypothesised that such an articular cartilage layer could be engineered using a co-culture of chondrocytes and stem/stromal cells. Recognising that these grafts will need to be engineered using cells from osteoarthritic joints, this thesis next sought to identify suitable cell sources from OA. FPSCs and CCs derived from OA cartilage was found to undergo robust chondrogenesis when combined in a co-culture, especially in low oxygen conditions.

With a view to engineering mechanically functional constructs for repairing osteochondral defects, the next phase of this thesis investigated the optimal 3D printed polymer for reinforcing a cartilage template. PCL and PLA both supported high levels of cartilage-specific matrix synthesis and maintained their shape fidelity over time *in vitro,* whilst PLGA scaffolds were found to swell. PCL, however, had more stable mechanical properties and was chosen to reinforce the cartilage templates. Subcutaneous implantation demonstrated that chondrogenically primed PCL reinforced bi-layered cartilage templates, consisting of a top layer of FPSC and CCs and bottom layer of BMSC, were capable of supporting the development of an osteochondral tissue consisting of hyaline cartilage overlaying vascularised bone. Top layers formed with agarose were found to supress mineralisation more than those with RGD-γ-irradiated alginate. All bottom layers formed with RGD-γ-irradiated alginate supported bone formation. To assess the validity in a more representative environment, the bi-layered scaffold was implanted into a critical sized defect in a goat. Prior to undertaking the study, goat BMSC were optimised for chondrogenesis by altering the level of glucose and oxygen availability in the expansion and differentiation phases. The optimal condition was identified as expanding and differentiating at 5% O_2 in high glucose media. Cartilage repair using the reinforced bi-layered cartilage template was promising in the caprine model, however bone growth was

somewhat compromised. Finally, a 3D bioprinting strategy was implemented to develop an anatomically accurate tissue engineered knee prosthesis. Inkjet technology was used to deposit droplets of gelMA containing a chondrogenic co-culture on the curved surface of these scaled-up implants. While these implants ultimately failed mechanically *in vivo* they provide a framework for the development of biological implants suitable for whole joint resurfacing.

9.1.1 Cartilage templates for osteochondral defect repair

The thesis began by exploring whether cartilage templates could be used to regenerate osteochondral defects by mimicking the developmental process (Chapter 4). It has long been established that BMSC can undergo chondrogenesis *in vitro* through chemical stimulation (Coleman et al., 2007; Cunniffe et al., 2015; Daly et al., 2016b; Liu et al., 2008; Mackay et al., 1998; Ng et al., 2017). It has also been shown that they can become hypertrophic leading to mineralisation subcutaneously (Cunniffe et al., 2015; Daly et al., 2016a; Mesallati et al., 2015b). This study aimed to answer two questions, firstly, can a cartilage template engineered *in vitro* support spatial distribution of the osteochondral components *in situ* and secondly is RGD-γ-irradiated alginate a suitable biomaterial for this task? The alginate supported a very robust cartilage template after 32 days, with the entire construct rich in sGAG and collagen type II. Additionally, some pericellular staining for collagen type X was identified in the centre of the construct indicating the early stages of hypertrophy. *In vivo,* the bone repair in the rabbit condyle were not significantly different in the empty and the treated defects. One could view this as a positive result because in the literature empty defects have reported bone remodelling due to migration of the subchondral plate (Orth et al., 2012; Qui et al., 2003). This indicates that although the cartilage template is not accelerating bone growth compared to empty defects, it is also not acting as a significant barrier to repair. This opens-up scope for improvement, either by further increasing the degradability of the material or by accelerating endochondral bone repair. From the histological sections, it appeared that bone remodelling began at the periphery and the top of the construct and moved towards the centre. Residual alginate that was detected in two donors, was present inside the lower half of the 4x4mm original defect area. This indicates that material degradation and defect repair was accelerated more at the subchondral plate than in the deeper trabecular bone. Overall the cartilage repair was deduced to be superior in the treated groups compared to the control. It was not consistent repair, there was variability observed amongst animals. The results of this study provided strong support for the use of developmentally inspired templates for engineering osteochondral grafts.

9.1.2 Co-cultures for engineering hyaline cartilage

Inspired by the potential of cartilage templates to regenerate osteochondral defects, whilst recognising the limitations, an alternative template was designed, whereby the cartilage layer was engineered using different cells. Encouraged by the plethora of studies in the literature detailing that a co-culture of MSCs and CC results in a more stable cartilage (Bian et al., 2011; Hendriks et al., 2007; Hubka et al., 2014; Meretoja et al., 2012; Mesallati et al., 2015b; de Windt et al., 2014; Wu et al., 2011) this strategy was employed for engineering the chondral layer of a bi-layered cartilage template. Chapter 5 assessed if this concept was clinically feasible by determining the chondrogenic capacity of FPSCs and CCs isolated from diseased joints. Corresponding with the literature diseased CC could regain their capacity to synthesise sGAG and collagen type II (Caron et al., 2012; Jakob et al., 2001; Li et al., 2012; Tallheden et al., 2005). FPSCs alone were found to develop a fibro-cartilage phenotype staining positively for both collagen type I and II. The co-culture, especially when the FPSC were combined with freshly isolated chondrocytes had higher levels of sGAG and collagen type II and lower levels of collagen type I than FPSC alone. In addition, oxygen was found to regulate collagen type I production. This aligns with the literature on how low oxygen tension promotes a chondrogenic phenotype (Buckley et al., 2010b; Meyer et al., 2010; Murphy and Polak, 2004; Sheehy et al., 2012). Whilst freshly isolated chondrocytes were the most chondrogenic, they are not a feasible cell source (due to limited availability) for the overall goal of resurfacing an entire joint. Co-cultures of expanded and freshly isolated CCs with FPSCs promoted robust chondrogenesis. This is the first work in the literature describing chondrogenesis of a co-culture of FPSC and CC from diseased joints. To promote a more stable cartilage phenotype growth factor BMP-7 was added to the pellet culture media, however no increase in ECM was observed. This could be due to the low concentration of BMP-7, the literature describes usage of higher concentrations to yield a response (Gavenis et al., 2012; Lee et al., 2008). One study showed that BMP-7 alone was not conducive to support chondrogenesis of human BMSC (Weiss et al., 2010).

9.1.3 Strategies to mechanically reinforce engineered tissues

Chapter 6 investigated mechanically reinforcing the bi-layered scaffold for both mechanical support *in vivo* and to provide the skeletal shape of an implant. Firstly, 3D printed PCL, PLA and PLGA fibre networks were compared for their capacity to mechanically reinforce MSC laden hydrogels. A distinct advantage of PLGA is the tailorable degradation rate (based on the LA to GA ratio) (Guo et al., 2006; Pan and Ding, 2012; Shasteen and Choy, 2011). This is an attractive property, however it was discovered that this was coupled with fibre swelling

causing the loss of the two primary functions, shape and mechanical properties. PLA and PCL on the other hand retained their shape. However, after 28 days PLA had a significantly reduced Young's modulus compared to day 0. This is of concern for *in vivo* studies down the line, as the environment is unpredictable and may cause the degradation rate to accelerate. Having identified PCL as a suitable reinforcing network that did not negatively impact chondrogenesis of encapsulated BMSCs, bi-layered cartilage templates were fabricated consisting of either alginate or agarose (containing a co-culture of FPSCs and chondrocytes) in the chondral layer and alginate (containing BMSCs only) in the endochondral bone layer. To improve on the degradability of the alginate from chapter 4, the RGD-γ alginate was 1% oxidised (Bouhadir et al., 2001). Evaluation was conducted subcutaneously to determine the optimal chondral layer and the effect, if any, of the PCL reinforcement. As expected from the results in chapter 4, the RGD-γ-alginate supported mineral deposition and vasculature after just 6 weeks *in vivo*. The hypothesis was confirmed with mineral deposition being confined to the osseous regions of the implant, indicating that the co-culture in the overlying layer was supressing hypertrophy and endochondral ossification (Mesallati et al., 2015b). This spatial pattern of tissue development was confirmed by histological analysis which demonstrated that a bony tissue was beginning to form within the endochondral region of the biphasic implant. In contrast, a cartilaginous tissue rich in type II collagen developed in the chondral region of these biphasic implants. MicroCT analysis demonstrated that single-phase constructs had twice the level of mineralisation than the biphasic constructs with defined chondral regions. There was some evidence for the onset of mineralisation in the chondral region formed within alginate. Potentially, this was due to the degradability of the material or the induced by the calcium during crosslinking, equally hyaline cartilage should inhibit any mineralisation. Only one chondral region generated using agarose showed evidence of mineralisation. It was confined to the periphery of the PCL struts. It is potential that the gel had not fully covered the strut, leaving a space for host cells to invade. Importantly, the mechanical properties remained the same post-implantation, reinforcing its potential to mechanically reinforce tissues with properties appropriate for implantation into load bearing environments.

Having identified a technique to mechanically reinforce bi-layered cartilage templates, the next step of the thesis explored the templates' validity *in vivo* in a goat model (Chapter 7). Given the limited information in the literature concerning priming goat BMSC for chondrogenesis the first part of Chapter 7 explored the optimal expansion and differentiation conditions in pellet culture. Aligning with the findings in chapter 4 and the literature oxygen tension played a significant role in determining the fate of the cells (Buckley et al., 2010b; Schrobback et al., 2012; Sheehy et al., 2012; Thorpe et al., 2013b). This study, however, highlights the importance of oxygen and glucose in the expansion phase in addition to the

differentiation phase. 5% oxygen and high glucose in both conditions dictated the most robust chondrogenesis. The reinforced bi-layered cartilage template promoted variable hyaline-like repair on a donor-to-donor basis. The bone healing was poor, potentially due to poor implant integration or the lack of nutrient supply. As mentioned earlier, low oxygen plays a significant role directing MSCs toward a chondrogenic phenotype. It has been shown previously that the their exists an oxygen gradient within a hydrogel during *in vitro* priming, whereby, the ambient oxygen exists only at the periphery and it decreases with depth from the top and side surfaces (Buckley et al., 2012; Thorpe et al., 2013b). The top chondral layer of the bi-layer was placed face down in the well-plate during *in vitro* priming to take advantage of this affect. It has been shown, however, that a vast proportion of a 6mm cylindrical hydrogel maintained in 5% oxygen will be subjected to an oxygen tension of >1.5% (Buckley et al., 2012). This may have caused the central region of the osseous layer to become a more stable cartilage which was then unable to undergo hypertrophy *in vivo* (Liu et al., 2008).

9.1.4 Scaled-up biological implants for joint resurfacing

The final chapter focused on the ultimate goal of the thesis; scaling-up the reinforced cartilage templates to form a mechanically functional biological joint (Chapter 8). Owing in part to the difficulties of printing RGD-γ alginate (Daly et al., 2016a), and the degree of spreading which occurs when printing agarose (Daly et al., 2016b) gelMA was selected as the bioink. Previous chapters 6 and 7 had utilised a PCL frame designed to mimic the mechanical properties of articular cartilage. A much stronger frame is required to withstand the loads of an entire joint. This was achieved by modulating the line spacing and filament diameter (Moroni et al., 2006; Olubamiji et al., 2016; Visser et al., 2015a). The condyle was 3D printed using information from a microCT scan of a native condyle. In keeping with previous chapters, it was printed in lattice form. Using ink-jet technology, a co-culture encapsulated in gelMA was deposited over the curved surface of the condyle and subsequently crosslinked with UV light. The implant failed *in situ* in a rabbit model, most appearing as if they had delaminated from the stem. Previous studies have demonstrated that 3D printed PCL can be utilised for whole joint applications, specifically the meniscus and the humeral head (Lee et al., 2010, 2014). The meniscus had a similar structure the knee scaffold in this thesis, however it was sutured into place which presumably aided in maintaining congruency and preventing delamination (Lee et al., 2014). The humeral head study had a different 3D printed architecture whereby there were no pores on the periphery but there was an opening at top surface to allow nutrient diffusion and cell homing (Lee et al., 2010). Similar to the knee prosthesis it had a stem that press-fitted into the medullary cavity. The confinement of the internal PCL fibres potentially prevented delamination.

In summary, this thesis describes a novel approach for the regeneration of whole joints by utilising developmental processes to direct repair of both articular cartilage and bone. This work provides an insight into combining 3D printing and tissue engineering strategies to engineer an anatomically accurate biological joint.

9.2 Limitations and Future Directions

Only one time-point was analysed in the rabbit and goat osteochondral models. Although reduction is an important aspect of animal studies, it is difficult to ascertain the exact repair mechanism without earlier time-points. In lieu of more animals, future studies could label cells to track if the repair was due to the implanted cartilage template or due to host progenitor cells (Koga et al., 2006, 2008).

Chapter 5 identified a co-culture of FPSC and CC originating from OA joints as a suitable cell source for clinically relevant cartilage tissue engineering. Considering the osseous layer of the cartilage template is formed through chondrogenic priming of BMSC, the assessment of BMSC from diseased joints should potentially have been carried out, especially since they have been identified as having a reduced chondrogenic capacity (Murphy et al., 2002). Additionally suitability was determined via pellet culture, however, in the rest of the thesis hydrogels were used as cell carriers. Therefore the assessment of suitability should have been conducted in both environments. It was deemed that BMP-7 did not have any effect on the chondrogenic capacity of the co-culture with the caveat that only one concentration was assessed. Further, higher concentrations could have been included in the study to determine if there was an optimal concentration.

Chapter 6 and 7 both utilised PCL frames that were fabricated to mimic the mechanical properties of articular cartilage. The stiffness was constant throughout the depth however this is not representative of an actual osteochondral unit. The osseous layer would need to be much stiffer than the chondral layer. A combination of the scaffold in Chapter 8 with the one in Chapter 6 and 7 may have been more characteristic. Future work should improve on the PCL skeleton by co-depositing PCL of different filament thicknesses and line spacings to create a depth dependant mechanical profile. In addition, a clinically compliant human prosthesis would be much larger than those presented in the thesis. Nutrient diffusion in this case is a critical consideration, bioreactor culture could be used to enhance nutrient diffusion of tissue engineered cartilage templates (Santoro et al., 2010).

Chapter 7 analysed the effect of glucose and oxygen tension during expansion and differentiation of goat BMSCs on subsequent levels of chondrogenesis. A limitation of this study

was that only 3 donors were assessed; additional donors would have provided a more in-depth profile of the most potent factors effecting cell proliferation and chondrogenesis. Secondly, only specific chondrogeneic markers were analysed, however given that the cartilage template is designed for the osseous layer to undergo endochondral ossification, it would have been also beneficial to stain for collagen type X to determine the best conditions for engineering hypertrophic cartilage. Thirdly, levels of sGAG were much higher than collagen, which is different to articular cartilage which is richer in collagen than sGAGs. The sheer volume of sGAG being synthesised could have impeded the collagen production (Bian et al., 2009). Potentially the decision to focus primarily on the choosing the condition based on the highest levels of sGAG was pre-emptive. Further studies should focus on achieving similar ratios/levels of ECM as found in the native tissue.

The poor bone healing in the goat model was another serious limitation of this study. Due to the large size of the tissue engineered cartilage template, the oxygen levels in the centre of the construct would have been low and the density may have inhibited nutrient diffusion *in vivo,* potentially causing tissue necrosis. It is recommended that future studies incorporate channels into the osseous layer to support vascularisation and mineralisation *in situ* (Cunniffe et al., 2015; Sheehy et al., 2014, 2015b). In addition, since oxygen tension plays a significant role in the ECM synthesis of cells, the levels of oxygen in the construct should be assessed through computational modelling, thereby enabling the optimal geometry of the engineered tissue to be predicted. This would aide in ensuring that no part of a large construct would be at risk of necrosis. Future studies could investigate confining the chondral region in a mould to ensure that low oxygen is maintained in the entirety of the chondral region (Thorpe et al., 2013b) or by tailoring the glucose availability to influence a zonal matrix deposition (Spitters et al., 2014).

The primary limitation of Chapter 8 was the limited mechanical testing preformed on the PCL scaffold. A wider range of mechanical tests, including shear, tensile and long-term cyclic loading should have been carried out prior to implantation. In addition, the rabbits were allowed to move freely directly after surgery, therefore the scaffold was subjected to loads before integration between the scaffold and the underlying bone could occur. Future studies should focus enhancing the mechanical properties and to promote faster bone integration to stabilise the implant as quickly as possible. One method to increase the mechanical properties is to confine the PCL skeleton by printing a PCL 'shell' (Lee et al., 2010). This would result in porosity being removed from the periphery, however if this was combined with nutrient channels in the bone region, it may not be a limiting factor. Nutrient channels could be incorporated via a 'sacrificial bioink' strategy, whereby the bioink is printed in the desired channel architecture and subsequently washed away following cross-linking of the cell seeded

bioink (Jin et al., 2016; Kesti et al., 2015; Visser et al., 2013). A further approach could look to combine two polymeric supports, a PCL periphery with a porous lattice shaped PCL/PLGA centre. PLGA would provide temporary mechanical support whilst bone matrix is deposited by the cells, the PLGA would degrade leaving behind space for more bone matrix to be deposited. Other approaches should look to either bind growth factors and other osteogenic factors (such as BMP-2 or hydroxyapatite) to the polymer surface or to incorporate them into degrading microspheres for growth factor release to enhance the integration between the engineered cartilage template and the native host bone (Lee et al., 2014; Place et al., 2009; Poldervaart et al., 2013; Stevens et al., 2005). Finally, future studies could look to utilise the 'bone bioreactor' concept, where the chondrogenically primed prosthesis is placed *in vivo* ectopically, allowing a more mature cartilage-bone tissue to form (Stevens et al., 2005). The subsequent engineered implant may be more stable and more likely to integrate *in situ*.

9.3 Conclusions

- A tissue engineered cartilage template formed through *in vitro* priming of BMSC encapsulated in RGD-γ alginate hydrogels can stimulate better repair of an osteochondral defect *in vivo* compared to empty controls
- A co-culture of chondrocytes and FPSCs from OA affected human joints represent a promising population of cells for driving cartilage ECM synthesis, particularly for applications which require large cell numbers. When maintained in low oxygen they promote chondrogenesis in pellet culture
- Cartilage templates can be reinforced with 3D printed thermopolymers; PCL, PLA and PLGA. The degradation of PLGA *in vitro* causes the fibers to swell and lose shape and the mechanical properties significantly decrease
- PCL reinforced chondrogenically primed bi-layered cartilage templates, containing a co-culture of CC and MSCs on top of BMSC, spatially regulates mineralisation subcutaneously, leading to the development of a bi-layered tissue akin to an osteochondral unit
- Bi-layered cartilage templates can support donor dependent repair of hyaline tissue in the chondral region of an osteochondral defect in a large animal model, however significant improvements must be made to stimulate bone repair
- 3D multi-tool bioprinting can be used to print anatomically accurate whole joints containing spatially distributed bioinks. Spatial distribution of the top co-culture from the bottom bone layer can be achieved by utilising inkjet technology to deposit droplets of cell encapsulated GelMA
- Overall this thesis has demonstrated progressions toward biological joint resurfacing by highlighting the potential for developmentally inspired implants combined with a 3D printed polymer frame to generate the osteochondral unit. Future work, however, must address the limitations outlined in this thesis, primarily to improve upon the mechanical integrity of the 3D printed frame.

References

Abdel-Sayed, P., and Pioletti, D.P. (2015). Strategies for improving the repair of focal cartilage defects. Nanomedicine (Lond). *10*, 2893–2905.

Acharya, C., Adesida, A., Zajac, P., Mumme, M., Riesle, J., Martin, I., and Barbero, A. (2012). Enhanced chondrocyte proliferation and mesenchymal stromal cells chondrogenesis in coculture pellets mediate improved cartilage formation. J. Cell. Physiol. *227*, 88–97.

Ahern, B.J., Parvizi, J., Boston, R., and Schaer, T.P. (2009). Preclinical animal models in single site cartilage defect testing: a systematic review. Osteoarthr. Cartil. *17*, 705–713.

Ahmed, N., Dreier, R., Göpferich, A., Grifka, J., and Grässel, S. (2007). Soluble signalling factors derived from differentiated cartilage tissue affect chondrogenic differentiation of rat adult marrow stromal cells. Cell. Physiol. Biochem. *20*, 665–678.

Alford, J.W., and Cole, B.J. (2005). Cartilage Restoration, Part 1: Basic Science, Historical Perspective, Patient Evaluation, and Treatment Options. Am. J. Sports Med. *33*, 295–306.

Almeida, H. V., Liu, Y., Cunniffe, G.M., Mulhall, K.J., Matsiko, A., Buckley, C.T., O'Brien, F.J., and Kelly, D.J. (2014). Controlled release of transforming growth factor-β3 from cartilage-extracellular-matrix-derived scaffolds to promote chondrogenesis of human-joint-tissue-derived stem cells. Acta Biomater.

Almeida, H. V., Cunniffe, G.M., Vinardell, T., Buckley, C.T., O'Brien, F.J., and Kelly, D.J. (2015). Coupling Freshly Isolated CD44^{+} Infrapatellar Fat Pad-Derived Stromal Cells with a TGF-β3 Eluting Cartilage ECM-Derived Scaffold as a Single-Stage Strategy for Promoting Chondrogenesis. Adv. Healthc. Mater. *4*, 1043–1053.

Almeida, H.V., Mulhall, K.J., O'Brien, F.J., and Kelly, D.J. (2016). Stem cells display a donor dependent response to escalating levels of growth factor release from extracellular matrix-derived scaffolds. J. Tissue Eng. Regen. Med. 524–531.

Alsberg, E., Kong, H.J., Hirano, Y., Smith, M.K., Albeiruti, A., and Mooney, D.J. (2003). Regulating Bone Formation via Controlled Scaffold Degradation. J. Dent. Res. *82*, 903–909.

Amoako, A., Guntur, G., and Pujalte, A. (2014). Osteoarthritis in Young, Active, and Athletic Individuals. Clin Med Insights Arthritis Musculoskelet Disord *7*, 21–26.

An, Y.H., Webb, D., Gutowska, A., Mironov, V.A., and Friedman, R.J. (2001). Regaining chondrocyte phenotype in thermosensitive gel culture. Anat. Rec. *263*, 336–341.

Anderson, D.E., Markway, B., Weekes, K.J., McCarthy, H.E., and Johnstone, B. (2017). Physioxia

promotes the articular chondrocyte-like phenotype in human chondroprogenitor-derived self-organized tissue. Tissue Eng. Part A ten.TEA.2016.0510.

Ando, W., Tateishi, K., Katakai, D., Hart, D. a, Higuchi, C., Nakata, K., Hashimoto, J., Fujie, H., Shino, K., Yoshikawa, H., et al. (2008). In vitro generation of a scaffold-free tissue-engineered construct (TEC) derived from human synovial mesenchymal stem cells: biological and mechanical properties and further chondrogenic potential. Tissue Eng. Part A *14*, 2041–2049.

Andriacchi, T.P., Briant, P.L., Bevill, S.L., and Koo, S. (2006). Rotational Changes at the Knee after ACL Injury Cause Cartilage Thinning. Clin. Orthop. Relat. Res. *442*, 39–44.

Arthritis Ireland (2015). About Arthritis.

Athanasiou, K. a., Rosenwasser, M.P., Buckwalter, J. a., Malinin, T.I., and Mow, V.C. (1991). Interspecies comparisons of in situ intrinsic mechanical properties of distal femoral cartilage. J. Orthop. Res. *9*, 330–340.

Aufderheide, A.C., and Athanasiou, K.A. (2005). Comparison of scaffolds and culture conditions for tissue engineering of the knee meniscus. Tissue Eng. *11*, 1095–1104.

Aulthouse, A.L., Beck, M., Griffey, E., Sanford, J., Arden, K., Machado, M.A., and Horton, W.A. (1989). Expression of the human chondrocyte phenotype in vitro. In Vitro Cell. Dev. Biol. *25*, 659–668.

Aung, A., Gupta, G., Majid, G., and Varghese, S. (2011). Osteoarthritic chondrocyte-secreted morphogens induce chondrogenic differentiation of human mesenchymal stem cells. Arthritis Rheum. *63*, 148–158.

Awad, H. a., Wickham, M.Q., Leddy, H. a., Gimble, J.M., and Guilak, F. (2004). Chondrogenic differentiation of adipose-derived adult stem cells in agarose, alginate, and gelatin scaffolds. Biomaterials *25*, 3211–3222.

B.R., S., S.S., Y., H., J., S.H., L., D.Y., P., J.H., L., S.R., P., S.-H., P., and B.-H., M. (2015). Three dimensional plotted extracellular matrix scaffolds using a rapid prototyping for tissue engineering application. Tissue Eng. Regen. Med. *12*, 172–180.

Bahney, C.S., Jacobs, L., Tamai, R., Hu, D., Luan, T.F., Wang, M., Reddy, S., Park, M., Limburg, S., Kim, H.T., et al. (2016). Promoting Endochondral Bone Repair Using Human Osteoarthritic Articular Chondrocytes. Tissue Eng. Part A *22*, 427–435.

Bakker, a. C., van de Loo, F. a J., van Beuningen, H.M., Sime, P., van Lent, P.L.E.M., van der Kraan, P.M., Richards, C.D., and van den Berg, W.B. (2001). Overexpression of active TGF-beta-1 in the murine knee joint: Evidence for synovial-layer-dependent chondro-osteophyte formation.

Osteoarthr. Cartil. *9*, 128–136.

Barbero, A., Grogan, S., Schäfer, D., Heberer, M., Mainil-Varlet, P., and Martin, I. (2004). Age related changes in human articular chondrocyte yield, proliferation and post-expansion chondrogenic capacity. Osteoarthritis Cartilage *12*, 476–484.

Behrens, P., Bitter, T., Kurz, B., and Russlies, M. (2006). Matrix-associated autologous chondrocyte transplantation/implantation (MACT/MACI)-5-year follow-up. Knee *13*, 194–202.

Bekkers, J.E.J., Tsuchida, a. I., van Rijen, M.H.P., Vonk, L. a., Dhert, W.J. a., Creemers, L.B., and Saris, D.B.F. (2013a). Single-Stage Cell-Based Cartilage Regeneration Using a Combination of Chondrons and Mesenchymal Stromal Cells: Comparison With Microfracture. Am. J. Sports Med. *41*, 2158–2166.

Bekkers, J.E.J., Creemers, L.B., Tsuchida, A.I., van Rijen, M.H.P., Custers, R.J.H., Dhert, W.J.A., and Saris, D.B.F. (2013b). One-stage focal cartilage defect treatment with bone marrow mononuclear cells and chondrocytes leads to better macroscopic cartilage regeneration compared to microfracture in goats. Osteoarthr. Cartil. *21*, 950–956.

Bensaïd, W., Triffitt, J.T., Blanchat, C., Oudina, K., Sedel, L., and Petite, H. (2003). A biodegradable fibrin scaffold for mesenchymal stem cell transplantation. Biomaterials *24*, 2497–2502.

Benya, P.D., and Shaffer, J.D. (1982a). Dedifferentiated Chondrocytes Reexpress the Differentiated Collagen Phenotype When Cultured in Agarose Gels. Cell *30*, 215–224.

Benya, P.D., and Shaffer, J.D. (1982b). Dedifferentiated chondrocytes reexpress the differentiated collagen phenotype when cultured in agarose gels. Cell *30*, 215–224.

Benya, P.D., Padilla, S.R., and Nimni, M.E. (1978). Independent regulation of collagen types by chondrocytes during the loss of differentiated function in culture. Cell *15*, 1313–1321.

Bi, X., Li, G., Doty, S.B., and Camacho, N.P. (2005). A novel method for determination of collagen orientation in cartilage by Fourier transform infrared imaging spectroscopy (FT-IRIS). Osteoarthritis Cartilage *13*, 1050–1058.

Bian, L., Crivello, K.M., Ng, K.W., Xu, D., Williams, D.Y., Ateshian, G.A., and Hung, C.T. (2009). Influence of Temporary Chondroitinase ABC-Induced Glycosaminoglycan Suppression on Maturation of Tissue-Engineered Cartilage. Tissue Eng. Part A *15*, 2065–2072.

Bian, L., Zhai, D.Y., Mauck, R.L., and Burdick, J. a (2011). Coculture of human mesenchymal stem cells and articular chondrocytes reduces hypertrophy and enhances functional properties of engineered cartilage. Tissue Eng. Part A *17*, 1137–1145.

Billiet, T., Gevaert, E., De Schryver, T., Cornelissen, M., and Dubruel, P. (2014). The 3D printing of gelatin methacrylamide cell-laden tissue-engineered constructs with high cell viability. Biomaterials *35*, 49–62.

Blaeser, A., Duarte Campos, D.F., Puster, U., Richtering, W., Stevens, M.M., and Fischer, H. (2016). Controlling Shear Stress in 3D Bioprinting is a Key Factor to Balance Printing Resolution and Stem Cell Integrity. Adv. Healthc. Mater. *5*, 326–333.

Blaney Davidson, E.N., van der Kraan, P.M., and van den Berg, W.B. (2007). TGF-?? and osteoarthritis. Osteoarthr. Cartil. *15*, 597–604.

Blumer, M.J.F., Longato, S., and Fritsch, H. (2008). Structure, formation and role of cartilage canals in the developing bone. Ann. Anat. *190*, 305–315.

Bodle, J.C., Teeter, S.D., Hluck, B., Hardin, J.W., Bernacki, S.H., and Loboa, E.G. (2014). Age-related effects on the potency of human adipose derived stem cells: Creation and evaluation of superlots and implications for musculoskeletal tissue engineering applications. Tissue Eng. Part C Methods *20*, 1–43.

Boere, K.W.M., Visser, J., Seyednejad, H., Rahimian, S., Gawlitta, D., Van Steenbergen, M.J., Dhert, W.J.A., Hennink, W.E., Vermonden, T., and Malda, J. (2014). Covalent attachment of a three-dimensionally printed thermoplast to a gelatin hydrogel for mechanically enhanced cartilage constructs. Acta Biomater. *10*, 2602–2611.

van den Borne, M.P.J., Raijmakers, N.J.H., Vanlauwe, J., Victor, J., de Jong, S.N., Bellemans, J., and Saris, D.B.F. (2007). International Cartilage Repair Society (ICRS) and Oswestry macroscopic cartilage evaluation scores validated for use in Autologous Chondrocyte Implantation (ACI) and microfracture. Osteoarthr. Cartil. *15*, 1397–1402.

Bouhadir, K.H., Lee, K.Y., Alsberg, E., Damm, K.L., Anderson, K.W., and Mooney, D.J. (2001). Degradation of partially oxidized alginate and its potential application for tissue engineering. Biotechnol. Prog. *17*, 945–950.

Bowland, P., Ingham, E., Jennings, L., and Fisher, J. (2015). Review of the biomechanics and biotribology of osteochondral grafts used for surgical interventions in the knee. Proc. Inst. Mech. Eng. H. *229*, 879–888.

Brittberg, M., Lindahl, A., Nilsson, A., Ohlsson, C., Isaksson, O., and Peterson, L. (1994). Treatment of Deep Cartilage Defects in the Knee with Autologous Chondrocyte Transpantation. N. Engl. J. Med. *331*, 889–895.

Bryant, S.J., and Anseth, K.S. (2002). Hydrogel properties influence ECM production by chondrocytes photoencapsulated in poly(ethylene glycol) hydrogels. J. Biomed. Mater. Res. *59*,

63–72.

Buckley, C.T., Vinardell, T., Thorpe, S.D., Haugh, M.G., Jones, E., McGonagle, D., and Kelly, D.J. (2010a). Functional properties of cartilaginous tissues engineered from infrapatellar fat pad-derived mesenchymal stem cells. J. Biomech. *43*, 920–926.

Buckley, C.T., Vinardell, T., and Kelly, D.J. (2010b). Oxygen tension differentially regulates the functional properties of cartilaginous tissues engineered from infrapatellar fat pad derived MSCs and articular chondrocytes. Osteoarthr. Cartil. *18*, 1345–1354.

Buckley, C.T., Meyer, E.G., and Kelly, D.J. (2012). The influence of construct scale on the composition and functional properties of cartilaginous tissues engineered using bone marrow-derived mesenchymal stem cells. Tissue Eng. Part A *18*, 382–396.

Buckwalter, J. a., and Mankin, H. j. (1997). Articular cartilage : Part I. J. Bone Jt. Surgury *79*, 600–611.

van Buul, G.M., Villafuertes, E., Bos, P.K., Waarsing, J.H., Kops, N., Narcisi, R., Weinans, H., Verhaar, J.A.N., Bernsen, M.R., and van Osch, G.J.V.M. (2012). Mesenchymal stem cells secrete factors that inhibit inflammatory processes in short-term osteoarthritic synovium and cartilage explant culture. Osteoarthr. Cartil. *20*, 1186–1196.

Caron, M.M.J., Emans, P.J., Coolsen, M.M.E., Voss, L., Surtel, D.A.M., Cremers, A., van Rhijn, L.W., and Welting, T.J.M. (2012). Redifferentiation of dedifferentiated human articular chondrocytes: Comparison of 2D and 3D cultures. Osteoarthr. Cartil. *20*, 1170–1178.

Carroll, S.F., Buckley, C.T., and Kelly, D.J. (2014). Cyclic hydrostatic pressure promotes a stable cartilage phenotype and enhances the functional development of cartilaginous grafts engineered using multipotent stromal cells isolated from bone marrow and infrapatellar fat pad. J. Biomech. *47*, 2115–2121.

Chang, C.C., Boland, E.D., Williams, S.K., and Hoying, J.B. (2011). Direct-write bioprinting three-dimensional biohybrid systems for future regenerative therapies. J. Biomed. Mater. Res. - Part B Appl. Biomater. *98 B*, 160–170.

Chaudhuri, O., Gu, L., Klumpers, D., Darnell, M., Bencherif, S.A., Weaver, J.C., Huebsch, N., Lee, H., Lippens, E., Duda, G.N., et al. (2015). Hydrogels with tunable stress relaxation regulate stem cell fate and activity. Nat. Mater. *15*, 326–334.

Chen, S., Fu, P., Cong, R., Wu, H., and Pei, M. (2015). Strategies to minimize hypertrophy in cartilage engineering and regeneration. Genes Dis. *2*, 76–95.

Chen, S., Fu, P., Wu, H., and Pei, M. (2017). Meniscus, articular cartilage and nucleus pulposus:

a comparative review of cartilage-like tissues in anatomy, development and function. Cell Tissue Res.

Chen, W.H., Lai, M.T., Wu, A.T.H., Wu, C.C., Gelovani, J.G., Lin, C.T., Hung, S.C., Chiu, W.T., and Deng, W.P. (2009). In vitro stage-specific chondrogenesis of mesenchymal stem cells committed to chondrocytes. Arthritis Rheum. *60*, 450–459.

Chimene, D., Lennox, K.K., Kaunas, R.R., and Gaharwar, A.K. (2016). Advanced Bioinks for 3D Printing: A Materials Science Perspective. Ann. Biomed. Eng. *44*, 2090–2102.

Chu, C.R., Szczodry, M., and Bruno, S. (2010). Animal Models for Cartilage Regeneration and Repair. Tissue Eng. Part B Rev. *16*, 105–115.

Chubinskaya, S., Kumar, B., Merrihew, C., Heretis, K., Rueger, D.C., and Kuettner, K.E. (2002). Age-related changes in cartilage endogenous osteogenic protein-1 (OP-1). Biochim. Biophys. Acta - Mol. Basis Dis. *1588*, 126–134.

Chubinskaya, S., Hurtig, M., and Rueger, D.C. (2007). OP-1/BMP-7 in cartilage repair. Int. Orthop. *31*, 773–781.

Coleman, R.M., Case, N.D., and Guldberg, R.E. (2007). Hydrogel effects on bone marrow stromal cell response to chondrogenic growth factors. Biomaterials *28*, 2077–2086.

Costantini, M., Idaszek, J., Szöke, K., Jaroszewicz, J., Dentini, M., Barbetta, A., Brinchmann, J.E., and Święszkowski, W. (2016). 3D bioprinting of BM-MSCs-loaded ECM biomimetic hydrogels for in vitro neocartilage formation. Biofabrication *8*, 35002.

Cui, X., Boland, T., D'Lima, D.D., and Lotz, M.K. (2012a). Thermal inkjet printing in tissue engineering and regenerative medicine. Recent Patents Drug Deliv. Formul. *6*, 149–155.

Cui, X., Breitenkamp, K., Finn, M.G., Lotz, M., and D'Lima, D.D. (2012b). Direct Human Cartilage Repair Using Three-Dimensional Bioprinting Technology. Tissue Eng. Part A *18*, 1304–1312.

Cunniffe, G.M., Vinardell, T., Thompson, E.M., Daly, A.C., Matsiko, A., O'Brien, F.J., and Kelly, D.J. (2015). Chondrogenically primed mesenchymal stem cell-seeded alginate hydrogels promote early bone formation in critically-sized defects. Eur. Polym. J. *72*, 464–472.

Cunniffe, G.M., Gonzalez-Fernandez, T., Daly, A., Sathy, B.N., Jeon, O., Alsberg, E., and Kelly, D.J. (2017). Three-Dimensional Bioprinting of Polycaprolactone Reinforced Gene Activated Bioinks for Bone Tissue Engineering. Tissue Eng. Part A *23*, ten.tea.2016.0498.

Daly, A.C., Cunniffe, G.M., Sathy, B.N., Jeon, O., Alsberg, E., and Kelly, D.J. (2016a). 3D Bioprinting of Developmentally Inspired Templates for Whole Bone Organ Engineering. Adv. Healthc. Mater.

Daly, A.C., Critchley, S.E., Rensock, E.M., and Kelly, D.J. (2016b). A Comparison of Different Bioinks for 3D Bioprinting of Fibrocartilage and Hyaline Cartilage. Biofabrication *8*, 1–25.

Dang, P., Herberg, S., Varghai, D., Riazi, H., Varghai, D., McMillan, A., Awadallah, A., Phillips, L., Jeon, O., Nguyen, M., et al. (2017). Endochondral Ossification in Critical-Sized BoneDefects via Readily Implantable Scaffold-Free Stem Cell Constructs. Stem Cells Transl. Med. *6*, 1644–1659.

Darling, E.M., and Athanasiou, K. a. (2005). Rapid phenotypic changes in passaged articular chondrocyte subpopulations. J. Orthop. Res. *23*, 425–432.

Dawson, E., Mapili, G., Erickson, K., Taqvi, S., and Roy, K. (2008). Biomaterials for stem cell differentiation. Adv. Drug Deliv. Rev. *60*, 215–228.

DeForest, C. a., and Anseth, K.S. (2012). Advances in Bioactive Hydrogels to Probe and Direct Cell Fate. Annu. Rev. Chem. Biomol. Eng. *3*, 421–444.

Deorosan, B., and Nauman, E.A. (2011). The Role of Glucose, Serum, and Three-Dimensional Cell Culture on the Metabolism of Bone Marrow-Derived Mesenchymal Stem Cells. Stem Cells Int. *2011*, 1–12.

Deschepper, M., Oudina, K., David, B., Myrtil, V., Collet, C., Bensidhoum, M., Logeart-Avramoglou, D., and Petite, H. (2011). Survival and function of mesenchymal stem cells (MSCs) depend on glucose to overcome exposure to long-term, severe and continuous hypoxia. J. Cell. Mol. Med. *15*, 1505–1514.

Dewan, A.K., Gibson, M.A., Elisseeff, J.H., and Trice, M.E. (2014). Evolution of autologous chondrocyte repair and comparison to other cartilage repair techniques. Biomed Res. Int. *2014*.

Diaz-Romero, J., Nesic, D., Grogan, S., Heini, P., and Mainil-Varlet, P. (2005). Immunophenotypic Changes of Human Articular Chondrocytes During Monolayer Culture Reflect Bona Fide Dedifferentiation Rather Than Amplification of Progenitor Cells. J. Cell. Physiol. *202*, 731–742.

Ding, C., Qiao, Z., Jiang, W., Li, H., Wei, J., Zhou, G., and Dai, K. (2013). Regeneration of a goat femoral head using a tissue-specific, biphasic scaffold fabricated with CAD/CAM technology. Biomaterials *34*, 6706–6716.

Doorn, J., Moll, G., Le Blanc, K., van Blitterswijk, C., and de Boer, J. (2012). Therapeutic applications of mesenchymal stromal cells: paracrine effects and potential improvements. Tissue Eng. Part B. Rev. *18*, 101–115.

Dragoo, J.L., Samimi, B., Zhu, M., Hame, S.L., Thomas, B.J., Lieberman, J.R., Hedrick, M.H., and Benhaim, P. (2003). Tissue-engineered cartilage and bone using stem cells from human infrapatellar fat pads. J. Bone Joint Surg. Br. *85*, 740–747.

Drury, J.L., and Mooney, D.J. (2003). Hydrogels for tissue engineering: Scaffold design variables and applications. Biomaterials *24*, 4337–4351.

Drury, J.L., Dennis, R.G., and Mooney, D.J. (2004). The tensile properties of alginate hydrogels. Biomaterials *25*, 3187–3199.

Duan, B., Kapetanovic, E., Hockaday, L., and Butcher, J. (2014). 3D Printed Trileaflet Valve Conduits Using Biological Hydrogels and Human Valve Interstitial Cells. Acta Biomater. *10*, 1836–1846.

Duong, H., Wu, B., and Tawil, B. (2009). Modulation of 3D Fibrin Matrix Stiffness by Intrinsic Fibrinogen–Thrombin Compositions and by Extrinsic Cellular Activity. Tissue Eng. Part A *15*, 1865–1876.

Engler, A.J., Sen, S., Sweeney, H.L., and Discher, D.E. (2006). Matrix Elasticity Directs Stem Cell Lineage Specification. Cell *126*, 677–689.

Erickson, I.E., Huang, a. H., Sengupta, S., Kestle, S., Burdick, J. a., and Mauck, R.L. (2009). Macromer density influences mesenchymal stem cell chondrogenesis and maturation in photocrosslinked hyaluronic acid hydrogels. Osteoarthr. Cartil. *17*, 1639–1648.

Estes, B.T., Wu, A.W., and Guilak, F. (2006). Potent induction of chondrocytic differentiation of human adipose-derived adult stem cells by bone morphogenetic protein 6. Arthritis Rheum. *54*, 1222–1232.

Fan, H., Hu, Y., Zhang, C., Li, X., Lv, R., Qin, L., and Zhu, R. (2006). Cartilage regeneration using mesenchymal stem cells and a PLGA-gelatin/chondroitin/hyaluronate hybrid scaffold. Biomaterials *27*, 4573–4580.

Farrell, E., van der Jagt, O.P., Koevoet, W., Kops, N., van Manen, C.J., Hellingman, C. a, Jahr, H., O'Brien, F.J., Verhaar, J. a N., Weinans, H., et al. (2009). Chondrogenic priming of human bone marrow stromal cells: a better route to bone repair? Tissue Eng. Part C. Methods *15*, 285–295.

Fischer, J., Dickhut, A., Rickert, M., and Richter, W. (2010). Human articular chondrocytes secrete parathyroid hormone-related protein and inhibit hypertrophy of mesenchymal stem cells in coculture during chondrogenesis. Arthritis Rheum. *62*, 2696–2706.

Fithian, D.C., Kelly, M. a, and Mow, V.C. (1990). Material properties and structure-function relationships in the menisci. Clin. Orthop. Relat. Res. *252*, 19–31.

Fortier, L. a., Barker, J.U., Strauss, E.J., McCarrel, T.M., and Cole, B.J. (2011). The role of growth factors in cartilage repair. Clin. Orthop. Relat. Res. *469*, 2706–2715.

Freeman, F.E., and Kelly, D.J. (2017). Tuning Alginate Bioink Stiffness and Composition for

Controlled Growth Factor Delivery and to Spatially Direct MSC Fate within Bioprinted Tissues. Sci. Rep. *7*, 1–12.

Frenkel, S.R., Bradica, G., Brekke, J.H., Goldman, S.M., Ieska, K., Issack, P., Bong, M.R., Tian, H., Gokhale, J., Coutts, R.D., et al. (2005). Regeneration of articular cartilage - Evaluation of osteochondral defect repair in the rabbit using multiphasic implants. Osteoarthr. Cartil. *13*, 798–807.

Gannon, A.R., Nagel, T., Bell, A.P., Avery, N.C., and Kelly, D.J. (2015). Postnatal Changes To the Mechanical Properties of Articular Cartilage Are Driven By the Evolution of Its Collagen Network. Eur. Cell. Mater. *29*, 105–123.

Gao, G., Schilling, A.F., Hubbell, K., Yonezawa, T., Truong, D., Hong, Y., Dai, G., and Cui, X. (2015). Improved properties of bone and cartilage tissue from 3D inkjet-bioprinted human mesenchymal stem cells by simultaneous deposition and photocrosslinking in PEG-GelMA. Biotechnol. Lett. *37*, 2349–2355.

Gao, L.-L., Zhang, C.-Q., Gao, H., Liu, Z.-D., and Xiao, P.-P. (2014). Depth and rate dependent mechanical behaviors for articular cartilage: experiments and theoretical predictions. Mater. Sci. Eng. C. Mater. Biol. Appl. *38*, 244–251.

Garreta, E., Oria, R., Tarantino, C., Pla-Roca, M., Prado, P., Fernández-Avilés, F., Campistol, J.M., Samitier, J., and Montserrat, N. (2017). Tissue engineering by decellularization and 3D bioprinting. Mater. Today *0*.

Gavenis, K., Heussen, N., and Schmidt-Rohlfing, B. (2012). Effects of low concentration BMP-7 on human osteoarthritic chondrocytes: comparison of different applications. J Biomater Appl *26*, 845–859.

Gawlitta, D., Ph, D., Farrell, E., Malda, J., and Creemers, L.B. (2010). Modulating Endochondral Ossification. Tissue Eng Part B *16*, 385–395.

Gawlitta, D., van Rijen, M.H.P., Schrijver, E.J.M., Alblas, J., and Dhert, W.J.A. (2012). Hypoxia Impedes Hypertrophic Chondrogenesis of Human Multipotent Stromal Cells. Tissue Eng. Part A *18*, 1957–1966.

Gelber, A.C., Hochberg, M.C., Mead, L.A., Wang, N., and Wigley, F.M. (2000). Joint Injury in Young Adults and Risk for Subsequent Knee and Hip Osteoarthritis. Ann. Intern. Med. *133*, 321–328.

Genes, N.G., Rowley, J.A., Mooney, D.J., and Bonassar, L.J. (2004). Effect of substrate mechanics on chondrocyte adhesion to modified alginate surfaces. Arch. Biochem. Biophys. *422*, 161–167.

Gikas, P.D., Morris, T., Carrington, R., Skinner, J., Bentley, G., and Briggs, T. (2009). A correlation

between the timing of biopsy after autologous chondrocyte implantation and the histological appearance. J. Bone Joint Surg. Br. *91*, 1172–1177.

Gioe, T.J., Novak, C., Sinner, P., Ma, W., and Mehle, S. (2007). Knee arthroplasty in the young patient. Clin Orthop Relat Res *464*, 83–87.

Giovannini, S., Diaz-Romero, J., Aigner, T., Heini, P., Mainil-Varlet, P., and Nesic, D. (2010). Micromass co-culture of human articular chondrocytes and human bone marrow mesenchymal stem cells to investigate stable neocartilage tissue formation in vitro. Eur. Cell. Mater. *20*, 245–259.

Goldring, M. (2000). Osteoarthritis and cartilage: The role of cytokines. Curr. Rheumatol. Rep. *2*, 459–465.

Goldring, M.B., and Goldring, S.R. (2010). Articular cartilage and subchondral bone in the pathogenesis of osteoarthritis. Ann. N. Y. Acad. Sci. *1192*, 230–237.

Goldring, M.B., Tsuchimochi, K., and Ijiri, K. (2006). The control of chondrogenesis. J. Cell. Biochem. *97*, 33–44.

Gong, J.P., Katsuyama, Y., Kurokawa, T., and Osada, Y. (2003). Double-network hydrogels with extremely high mechanical strength. Adv. Mater. *15*, 1155–1158.

Gotterbarm, T., and Spector, M. (2005). High interindividual variability in the chondrogenic potential of goat bone marrow-derived mesenchymal stem cells. In 53rd Annual Meeting of the Orthopaedic Research Society, p. 462.

Grande, D., Southerland, S., Manji, R., Pate, D., Schwartz, R., and Lucas, P. (1995). Repair of articular cartilage defects using mesenchymal stem cells. *1*.

Grässel, S., and Lorenz, J. (2014). Tissue-Engineering Strategies to Repair Chondral and Osteochondral Tissue in Osteoarthritis: Use of Mesenchymal Stem Cells. Curr. Rheumatol. Rep. *16*, 1–16.

Grover, D.M., Chen, A. a., and Hazelwood, S.J. (2007). Biomechanics of the rabbit knee and ankle: Muscle, ligament, and joint contact force predictions. J. Biomech. *40*, 2816–2821.

Gudas, R., Kalesinskas, R.J., Kimtys, V., Stankevičius, E., Toliušis, V., Bernotavičius, G., and Smailys, A. (2005). A prospective randomized clinical study of mosaic osteochondral autologous transplantation versus microfracture for the treatment of osteochondral defects in the knee joint in young athletes. Arthrosc. - J. Arthrosc. Relat. Surg. *21*, 1066–1075.

Guo, T., TR, H., Lim, C., Gao, F., Gargava, A., Trachtenberg, J., Mikos, A., and Fisher, J. (2006). 3D printing PLGA: a quantitative examination of the effects of polymer composition and printing

parameters on print resolution. Biofabrication *9*.

Hardingham, T.E., and Fosang, A.J. (1992). Proteoglycans: many forms and many functions. FASEB J. *6*, 861–870.

Harris, J.D., Brophy, R.H., Siston, R. a., and Flanigan, D.C. (2010). Treatment of Chondral Defects in the Athlete's Knee. Arthrosc. - J. Arthrosc. Relat. Surg. *26*, 841–852.

Hendriks, J. a. a., Riesle, J., and van Blitterswijk, C. a. (2007). Co-culture in cartilage tissue engineering. J. Tissue Eng. Regen. Med. *1*, 170–178.

Hendriks, J. a. a., Miclea, R.L., Schotel, R., de Bruijn, E., Moroni, L., Karperien, M., Riesle, J., and van Blitterswijk, C. a. (2010). Primary chondrocytes enhance cartilage tissue formation upon co-culture with a range of cell types. Soft Matter *6*, 5080.

Hickey, T., Kreutzer, D., Burgess, D.J., and Moussy, F. (2002). Dexamethasone/PLGA microspheres for continuous delivery of an anti-inflammatory drug for implantable medical devices. Biomaterials *23*, 1649–1656.

Hiep, N.T., and Lee, B.T. (2010). Electro-spinning of PLGA/PCL blends for tissue engineering and their biocompatibility. J. Mater. Sci. Mater. Med. *21*, 1969–1978.

Hoch, E., Hirth, T., Tovar, G.E.M., and Borchers, K. (2013). Chemical tailoring of gelatin to adjust its chemical and physical properties for functional bioprinting. J. Mater. Chem. B *1*, 5675.

Hockaday, L., Kang, K., Colangelo, N., Cheung, P., Duan, B., Malone, E., Wu, L., Girardi, N., Bonassar, L., Lipson, H., et al. (2012). Rapid 3D printing of anatomically accurate and mechanically heterogeneous aortic valve hydrogel scaffolds. Biofabrication *4*.

Hoemann, C., Kandel, R., Roberts, S., Saris, D.B.F., Creemers, L., Mainil-Varlet, P., Méthot, S., Hollander, A.P., and Buschmann, M.D. (2011). International Cartilage Repair Society (ICRS) Recommended Guidelines for Histological Endpoints for Cartilage Repair Studies in Animal Models and Clinical Trials. Cartilage *2*, 153–172.

Holy, C.E., Cheng, C., Davies, J.E., and Shoichet, M.S. (2001). Optimizing the sterilization of PLGA scaffolds for use in tissue engineering. Biomaterials *22*, 25–31.

Homenick, C.M., De Silveira, G., Sheardown, H., and Adronov, A. (2011). Pluronics as crosslinking agents for collagen: Novel amphiphilic hydrogels. Polym. Int. *60*, 458–465.

Hu, J.C., and Athanasiou, K. a (2006). A self-assembling process in articular cartilage tissue engineering. Tissue Eng. *12*, 969–979.

Hu, D.P., Ferro, F., Yang, F., Taylor, A.J., Chang, W., Miclau, T., Marcucio, R.S., and Bahney, C.S.

(2017). Cartilage to bone transformation during fracture healing is coordinated by the invading vasculature and induction of the core pluripotency genes. Development *144*, 221–234.

Huang, C.-Y.C., Reuben, P.M., D'Ippolito, G., Schiller, P.C., and Cheung, H.S. (2004). Chondrogenesis of human bone marrow-derived mesenchymal stem cells in agarose culture. Anat. Rec. A. Discov. Mol. Cell. Evol. Biol. *278*, 428–436.

Hubka, K.M., Dahlin, R.L., Meretoja, V. V, Kasper, K., and Mikos, A.G. (2014). Enhancing Chondrogenic Phenotype for Cartilage Tissue Engineering: Monoculture and Co-culture of Articular Chondrocytes and Mesenchymal Stem Cells. Tissue Eng. Part B *20*, 1–50.

Hung, C.T., Lima, E.G., Mauck, R.L., Taki, E., LeRoux, M.A., Lu, H.H., Stark, R.G., Guo, X.E., and Ateshian, G.A. (2003). Anatomically shaped osteochondral constructs for articular cartilage repair. J. Biomech. *36*, 1853–1864.

Hunziker, E.B. (2002). Articular cartilage repair: Basic science and clinical progress. A review of the current status and prospects. Osteoarthr. Cartil. *10*, 432–463.

Hunziker, E.B., Kapfinger, E., and Geiss, J. (2007). The structural architecture of adult mammalian articular cartilage evolves by a synchronized process of tissue resorption and neoformation during postnatal development. Osteoarthr. Cartil. *15*, 403–413.

Igarashi, T., Iwasaki, N., Kasahara, Y., and Minami, A. (2010). A cellular implantation system using an injectable ultra-purified alginate gel for repair of osteochondral defects in a rabbit model. J. Biomed. Mater. Res. - Part A *94*, 844–855.

Ikenoue, T., Trindade, M.C.D., Lee, M.S., Lin, E.Y., Schurman, D.J., Goodman, S.B., and Smith, R.L. (2003). Mechanoregulation of human articular chondrocyte aggrecan and type II collagen expression by intermittent hydrostatic pressure in vitro. J. Orthop. Res. *21*, 110–116.

Imhof, H., Breitenseher, M., Kainberger, F., Rand, T., and Trattnig, S. (1999). Importance of subchondral bone to articular cartilage in health and disease. Top. Magn. Reson. Imaging. *10*, 180–192.

Indrawattana, N., Chen, G., Tadokoro, M., Shann, L.H., Ohgushi, H., Tateishi, T., Tanaka, J., and Bunyaratvej, A. (2004). Growth factor combination for chondrogenic induction from human mesenchymal stem cell. Biochem. Biophys. Res. Commun. *320*, 914–919.

Ingavle, G.C., Frei, A.W., Gehrke, S.H., and Detamore, M.S. (2013). Incorporation of Aggrecan in Interpenetrating Network Hydrogels to Improve Cellular Performance for Cartilage Tissue Engineering. Tissue Eng. Part A *19*, 1349–1359.

Iwakura, T., Sakata, R., and Reddi, a H. (2013). Induction of chondrogenesis and expression of

superficial zone protein in synovial explants with TGF-β1 and BMP-7. Tissue Eng. Part A *19*, 2638–2644.

Jackson, D.W., Lalor, P.A., Aberman, H.M., and Simon, T.M. (2001). Spontaneous Repair of Full-Thickness Defects of Articular Cartilage in a Goat Model A PRELIMINARY STUDY. J. Bone Jt. Surg. *83*, 53–64.

Jakob, M., Démarteau, O., Schäfer, D., Hintermann, B., Dick, W., Heberer, M., and Martin, I. (2001). Specific growth factors during the expansion and redifferentiation of adult human articular chondrocytes enhance chondrogenesis and cartilaginous tissue formation in vitro. J. Cell. Biochem. *81*, 368–377.

Jeon, O., and Alsberg, E. (2013). Photofunctionalization of Alginate Hydrogels to Promote Adhesion and Proliferation of Human Mesenchymal Stem Cells. Tissue Eng. Part A *19*, 1424–1432.

Jeon, O., Powell, C., Ahmed, S.M., and Alsberg, E. (2010). Biodegradable, photocrosslinked alginate hydrogels with independently tailorable physical properties and cell adhesivity. Tissue Eng. Part A *16*, 2915–2925.

Jeon, O., Powell, C., Solorio, L.D., Krebs, M.D., and Alsberg, E. (2011). Affinity-based growth factor delivery using biodegradable, photocrosslinked heparin-alginate hydrogels. J. Control. Release *154*, 258–266.

Jin, Y., Compaan, A., Bhattacharjee, T., and Huang, Y. (2016). Granular gel support-enabled extrusion of three-dimensional alginate and cellular structures. Biofabrication *8*, 25016.

Johnstone, B., Hering, T.M., Caplan, a I., Goldberg, V.M., and Yoo, J.U. (1998). In vitro chondrogenesis of bone marrow-derived mesenchymal progenitor cells. Exp. Cell Res. *238*, 265–272.

Jukes, J.M., Both, S.K., Leusink, A., Sterk, L.M.T., van Blitterswijk, C. a, and de Boer, J. (2008). Endochondral bone tissue engineering using embryonic stem cells. Proc. Natl. Acad. Sci. U. S. A. *105*, 6840–6845.

Julkunen, P., Harjula, T., Iivarinen, J., Marjanen, J., Seppänen, K., Närhi, T., Arokoski, J., Lammi, M.J., Brama, P. a., Jurvelin, J.S., et al. (2009). Biomechanical, biochemical and structural correlations in immature and mature rabbit articular cartilage. Osteoarthr. Cartil. *17*, 1628–1638.

Jungst, T., Smolan, W., Schacht, K., Scheibel, T., and Groll, J. (2016). Strategies and Molecular Design Criteria for 3D Printable Hydrogels. Chem. Rev. *116*, 1496–1539.

Kalson, N.S., Gikas, P.D., and Briggs, T.W.R. (2010). Current strategies for knee cartilage repair. Int. J. Clin. Pract. *64*, 1444–1452.

Kang, H.-W., Lee, S.J., Ko, I.K., Kengla, C., Yoo, J.J., and Atala, A. (2016). A 3D bioprinting system to produce human-scale tissue constructs with structural integrity. Nat. Biotechnol. *34*, 312–319.

Kanichai, M., Ferguson, D., Prendergast, P.J., and Campbell, V.A. (2008). Hypoxia promotes chondrogenesis in rat mesenchymal stem cells: A role for AKT and hypoxia-inducible factor (HIF)-1α. J. Cell. Physiol. *216*, 708–715.

Keeney, J.A., Eunice, S., Pashos, G., Wright, R.W., and Clohisy, J.C. (2011). What is the evidence for total knee arthroplasty in young patients?: A systematic review of the literature. Clin. Orthop. Relat. Res. *469*, 574–583.

Kesti, M., Eberhardt, C., Pagliccia, G., Kenkel, D., Grande, D., Boss, A., and Zenobi-Wong, M. (2015). Bioprinting Complex Cartilaginous Structures with Clinically Compliant Biomaterials. Adv. Funct. Mater. *25*, 7406–7417.

Khan, W.S., Adesida, A.B., and Hardingham, T.E. (2007). Hypoxic conditions increase hypoxia-inducible transcription factor 2alpha and enhance chondrogenesis in stem cells from the infrapatellar fat pad of osteoarthritis patients. Arthritis Res. Ther. *9*, R55.

Kim, J.Y., and Cho, D.W. (2009). Blended PCL/PLGA scaffold fabrication using multi-head deposition system. Microelectron. Eng. *86*, 1447–1450.

Kim, B.S., Kim, H., Gao, G., Jang, J., and Cho, D.-W. (2017). Decellularized extracellular matrix: a step towards the next generation source for bioink manufacturing. Biofabrication *9*, 34104.

Kim, I.L., Mauck, R.L., and Burdick, J.A. (2011). Hydrogel design for cartilage tissue engineering: A case study with hyaluronic acid. Biomaterials *32*, 8771–8782.

Kim, J., McBride, S., Tellis, B., Alvarez-Urena, P., Song, Y.-H., Dean, D.D., Sylvia, V.L., Elgendy, H., Ong, J., and Hollinger, J.O. (2012). Rapid-prototyped PLGA/β-TCP/hydroxyapatite nanocomposite scaffolds in a rabbit femoral defect model. Biofabrication *4*, 25003.

Kim, M.S., Ahn, H.H., Shin, Y.N., Cho, M.H., Khang, G., and Lee, H.B. (2007). An in vivo study of the host tissue response to subcutaneous implantation of PLGA- and/or porcine small intestinal submucosa-based scaffolds. Biomaterials *28*, 5137–5143.

Kim, Y.B., Lee, H., Yang, G.H., Choi, C.H., Lee, D.W., Hwang, H., Jung, W.K., Yoon, H., and Kim, G.H. (2016). Mechanically reinforced cell-laden scaffolds formed using alginate-based bioink printed onto the surface of a PCL/alginate mesh structure for regeneration of hard tissue. J.

Colloid Interface Sci. *461*, 359–368.

Klotz, B.J., Gawlitta, D., Rosenberg, A.J.W.P., Malda, J., and Melchels, F.P.W. (2016). Gelatin-Methacryloyl Hydrogels: Towards Biofabrication-Based Tissue Repair. Trends Biotechnol. *34*, 394–407.

Koga, H., Muneta, T., Ju, Y.-J., Nagase, T., Nimura, A., Mochizuki, T., Ichinose, S., von der Mark, K., and Sekiya, I. (2006). Synovial Stem Cells Are Regionally Specified According to Local Microenvironments After Implantation for Cartilage Regeneration. Stem Cells *25*, 689–696.

Koga, H., Muneta, T., Nagase, T., Nimura, A., Ju, Y.J., Mochizuki, T., and Sekiya, I. (2008). Comparison of mesenchymal tissues-derived stem cells for in vivo chondrogenesis: Suitable conditions for cell therapy of cartilage defects in rabbit. Cell Tissue Res. *333*, 207–215.

Koh, J.L., Wirsing, K., Lautenschlager, E., and Zhang, L.-O. (2004). The effect of graft height mismatch on contact pressure following osteochondral grafting: a biomechanical study. Am. J. Sports Med. *32*, 317–320.

Kon, E., Delcogliano, M., Filardo, G., Pressato, D., Busacca, M., Grigolo, B., Desando, G., and Marcacci, M. (2010). A novel nano-composite multi-layered biomaterial for treatment of osteochondral lesions: Technique note and an early stability pilot clinical trial. Injury *41*, 693–701.

Kon, E., Filardo, G., Di Matteo, B., Perdisa, F., and Marcacci, M. (2013). Matrix assisted autologous chondrocyte transplantation for cartilage treatment: A systematic review. Bone Joint Res. *2*, 18–25.

Korhonen, R.K., Laasanen, M.S., Töyräs, J., Rieppo, J., Hirvonen, J., Helminen, H.J., and Jurvelin, J.S. (2002). Comparison of the equilibrium response of articular cartilage in unconfined compression, confined compression and indentation. J. Biomech. *35*, 903–909.

Kreuz, P.C., Steinwachs, M., Erggelet, C., Lahm, A., Krause, S., Ossendorf, C., Meier, D., Ghanem, N., and Uhl, M. (2007). Importance of Sports in Cartilage Regeneration After Autologous Chondrocyte Implantation. Am. J. Sports Med. *35*, 1261–1268.

Krinner, A., Zscharnack, M., Bader, A., Drasdo, D., and Galle, J. (2009). Impact of oxygen environment on mesenchymal stem cell expansion and chondrogenic differentiation. Cell Prolif. *42*, 471–484.

Kronenberg, H.M. (2003). Developmental regulation of the growth plate. Nature *423*, 332–336.

Kundu, J., Shim, J.-H., Jang, J., Kim, S.-W., and Cho, D.-W. (2015). An additive manufacturing-based PCL-alginate-chondrocyte bioprinted scaffold for cartilage tissue engineering. J. Tissue

Eng. Regen. Med. *9*, 1286–1297.

Kurtz, S.M., Lau, E., Ong, K., Zhao, K., Kelly, M., and Bozic, K.J. (2009). Future young patient demand for primary and revision joint replacement: National projections from 2010 to 2030. Clin. Orthop. Relat. Res. *467*, 2606–2612.

Kutty, J.K., Cho, E., Soo Lee, J., Vyavahare, N.R., and Webb, K. (2007). The effect of hyaluronic acid incorporation on fibroblast spreading and proliferation within PEG-diacrylate based semi-interpenetrating networks. Biomaterials *28*, 4928–4938.

Lafont, J.. (2010). Lack of oxygen in articular cartilage: Consequences for chondrocyte biology. Int. J. Exp. Pathol. *91*, 99–106.

Lee, K.Y., and Mooney, D.J. (2001). Hydrogels for Tissue Engineering. Chem. Rev. *101*, 1869–1879.

Lee, K.Y., and Mooney, D.J. (2012). Alginate: Properties and biomedical applications. Prog. Polym. Sci. *37*, 106–126.

Lee, C.H., Marion, N.W., Hollister, S., and Mao, J.J. (2009). Tissue Formation and Vascularization in Anatomically Shaped Human Joint Condyle Ectopically in Vivo. Tissue Eng. Part A *15*, 3923–3930.

Lee, C.H., Cook, J.L., Mendelson, A., Moioli, E.K., Yao, H., and Mao, J.J. (2010). Regeneration of the articular surface of the rabbit synovial joint by cell homing: a proof of concept study. Lancet (London, England) *376*, 440–448.

Lee, C.H., Rodeo, S.A., Fortier, L.A., Lu, C., Erisken, C., and Mao, J.J. (2014). Protein-releasing polymeric scaffolds induce fibrochondrocytic differentiation of endogenous cells for knee meniscus regeneration in sheep. Sci. Transl. Med. *6*, 266ra171-266ra171.

Lee, C.R., Grodzinsky, A.J., and Spector, M. (2001). The effects of cross-linking of collagen-glycosaminoglycan scaffolds on compressive stiffness, chondrocyte-mediated contraction, proliferation and biosynthesis. Biomaterials *22*, 3145–3154.

Lee, J.J., Lee, S.J., Lee, T.J., Yoon, T.H., and Choi, C.H. (2013). Results of microfracture in the osteoarthritic knee with focal full-thickness articular cartilage defects and concomitant medial meniscal tears. Knee Surg. Relat. Res. *25*, 71–76.

Lee, S.Y., Nakagawa, T., and Reddi, a. H. (2008). Induction of chondrogenesis and expression of superficial zone protein (SZP)/lubricin by mesenchymal progenitors in the infrapatellar fat pad of the knee joint treated with TGF-β1 and BMP-7. Biochem. Biophys. Res. Commun. *376*, 148–153.

Leijten, J., Georgi, N., Moreira Teixeira, L., van Blitterswijk, C. a., Post, J.N., and Karperien, M. (2014). Metabolic programming of mesenchymal stromal cells by oxygen tension directs chondrogenic cell fate. Proc. Natl. Acad. Sci. *111*, 13954–13959.

Leijten, J.C., Georgi, N., Wu, L., van Blitterswijk, C.A., and Karperien, M. (2013). Cell sources for articular cartilage repair strategies: shifting from monocultures to cocultures. Tissue Eng. Part B. Rev. *19*, 31–40.

Leijten, J.C.H., Emons, J., Sticht, C., Van Gool, S., Decker, E., Uitterlinden, A., Rappold, G., Hofman, A., Rivadeneira, F., Scherjon, S., et al. (2012). Gremlin 1, frizzled-related protein, and dkk-1 are key regulators of human articular cartilage homeostasis. Arthritis Rheum. *64*, 3302–3312.

Levingstone, T.J., Ramesh, A., Brady, R.T., Brama, P.A.J., Kearney, C., Gleeson, J.P., and O'Brien, F.J. (2016). Cell-free multi-layered collagen-based scaffolds demonstrate layer specific regeneration of functional osteochondral tissue in caprine joints. Biomaterials *87*, 69–81.

Li, H., Davison, N., Moroni, L., Feng, F., Crist, J., Salter, E., Bingham, C.O., and Elisseeff, J. (2012). Evaluating Osteoarthritic Chondrocytes through a Novel 3-Dimensional In Vitro System for Cartilage Tissue Engineering and Regeneration. Cartilage *3*, 128–140.

Li, X., Chen, S., Li, J., Wang, X., Zhang, J., Kawazoe, N., and Chen, G. (2016). 3D culture of chondrocytes in gelatin hydrogels with different stiffness. Polymers (Basel). *8*.

Li, Z., Kupcsik, L., Yao, S.J., Alini, M., and Stoddart, M.J. (2010). Mechanical load modulates chondrogenesis of human mesenchymal stem cells through the TGF-β pathway. J. Cell. Mol. Med. *14*, 1338–1346.

Liu, K., Zhou, G.D., Liu, W., Zhang, W.J., Cui, L., Liu, X., Liu, T.Y., and Cao, Y. (2008). The dependence of in vivo stable ectopic chondrogenesis by human mesenchymal stem cells on chondrogenic differentiation in vitro. Biomaterials *29*, 2183–2192.

Liu, X., Sun, H., Yan, D., Zhang, L., Lv, X., Liu, T., Zhang, W., Liu, W., Cao, Y., and Zhou, G. (2010). In vivo ectopic chondrogenesis of BMSCs directed by mature chondrocytes. Biomaterials *31*, 9406–9414.

Liu, Y., Buckley, C.T., Almeida, H., Mulhall, K., and Kelly, D.J. (2014). Infrapatellar Fat Pad Derived Stem Cells Maintain Their Chondrogenic Capacity in Disease and can be used to Engineer Cartilaginous Grafts of Clinically Relevant Dimensions. Tissue Eng. Part A *20*, 1–36.

Lu, X.L., and Mow, V.C. (2008). Biomechanics of articular cartilage and determination of material properties. Med. Sci. Sports Exerc. *40*, 193–199.

Lu, L., Peter, S.J., D. Lyman, M., Lai, H.L., Leite, S.M., Tamada, J.A., Uyama, S., Vacanti, J.P., Robert

Langer, and Mikos, A.G. (2000). In vitro and in vivo degradation of porous poly(DL-lactic-co-glycolic acid) foams. Biomaterials *21*, 1837–1845.

Luo, L., Thorpe, S.D., Buckley, C.T., and Kelly, D.J. (2015). The effects of dynamic compression on the development of cartilage grafts engineered using bone marrow and infrapatellar fat pad derived stem cells. Biomed. Mater. *10*, 55011.

Mackay, A.M., Beck, S.C., Murphy, J.M., Barry, F.P., Chichester, C.O., and Pittenger, M.F. (1998). Chondrogenic Differentiation of Cultured Human Mesenchymal Stem Cells from Marrow. Tissue Eng. *4*, 415–428.

Madry, H., van Dijk, C.N., and Mueller-Gerbl, M. (2010). The basic science of the subchondral bone. Knee Surgery, Sport. Traumatol. Arthrosc. *18*, 419–433.

Malda, J., Visser, J., Melchels, F.P., Jüngst, T., Hennink, W.E., Dhert, W.J. a, Groll, J., and Hutmacher, D.W. (2013). 25th anniversary article: Engineering hydrogels for biofabrication. Adv. Mater. *25*, 5011–5028.

Malinin, T., and Ouellette, E.A. (2000). Articular cartilage nutrition is mediated by subchondral bone: A long-term autograft study in baboons. Osteoarthr. Cartil. *8*, 483–491.

Mandrycky, C., Wang, Z., Kim, K., and Kim, D.H. (2016). 3D bioprinting for engineering complex tissues. Biotechnol. Adv. *34*, 422–434.

Mansour, J.M. (2009). Biomechanics of Cartilage. In Kinesiology: The Mechanics and Pathomechanics of Human Movement, pp. 66–79.

Markway, B.D., Cho, H., and Johnstone, B. (2013). Hypoxia promotes redifferentiation and suppresses markers of hypertrophy and degeneration in both healthy and osteoarthritic chondrocytes. Arthritis Res. Ther. *15*, R92.

Marlovits, S., Hombauer, M., Truppe, M., Vècsei, V., and Schlegel, W. (2004). Changes in the ratio of type-I and type-II collagen expression during monolayer culture of human chondrocytes. J. Bone Joint Surg. Br. *86*, 286–295.

Martin, I., Miot, S., Barbero, A., Jakob, M., and Wendt, D. (2007). Osteochondral tissue engineering. J. Biomech. *40*, 750–765.

Martinez, M.A., Palanca, D., and Doblare, M. (2006). Why Lateral Meniscectomy Is More Dangerous Than Medial Meniscectomy . A Finite Element Study. J. Orthop. Res. *24*, 1001–1010.

Martinez-Diaz, S., Garcia-Giralt, N., Lebourg, M., Gómez-Tejedor, J.-A., Vila, G., Caceres, E., Benito, P., Pradas, M.M., Nogues, X., Ribelles, J.L.G., et al. (2010). In vivo evaluation of 3-dimensional polycaprolactone scaffolds for cartilage repair in rabbits. Am. J. Sports Med. *38*, 509–519.

Mauck, R.L., Yuan, X., and Tuan, R.S. (2006). Chondrogenic differentiation and functional maturation of bovine mesenchymal stem cells in long-term agarose culture. Osteoarthr. Cartil. *14*, 179–189.

McNickle, A.G., Provencher, M.T., and Cole, B.J. (2008). Overview of existing cartilage repair technology. Sports Med. Arthrosc. *16*, 196–201.

Melchels, F.P.W., Dhert, W.J. a., Hutmacher, D.W., and Malda, J. (2014). Development and characterisation of a new bioink for additive tissue manufacturing. J. Mater. Chem. B *2*, 2282.

Mendes, S.C., Tibbe, J.M., Veenhof, M., Bakker, K., Both, S., Platenburg, P.P., Oner, F.C., de Bruijn, J.D., and van Blitterswijk, C. a (2002). Bone tissue-engineered implants using human bone marrow. *8*, 911–920.

Meretoja, V. V., Dahlin, R.L., Kasper, F.K., and Mikos, A.G. (2012). Enhanced chondrogenesis in co-cultures with articular chondrocytes and mesenchymal stem cells. Biomaterials *33*, 6362–6369.

Mesallati, T., Buckley, C.T., and Kelly, D.J. (2013). A Comparison of Self-Assembly and Hydrogel Encapsulation as a Means to Engineer Functional Cartilaginous Grafts Using Culture Expanded Chondrocytes. Tissue Eng. Part C. Methods *20*, 1–41.

Mesallati, T., Buckley, C.T., and Kelly, D.J. (2014). Engineering articular cartilage-like grafts by self-assembly of infrapatellar fat pad-derived stem cells. Biotechnol. Bioeng. *111*, 1686–1698.

Mesallati, T., Buckley, C.T., and Kelly, D.J. (2015a). Engineering cartilaginous grafts using chondrocyte-laden hydrogels supported by a superficial layer of stem cells. J. Tissue Eng. Regen. Med.

Mesallati, T., Sheehy, E.. ., Vinardell, T., Buckley, C.T., and Kelly, D.J. (2015b). Tissue engineering scaled-up anatomically shaped osteochondral constructs for joint resurfacing. Eur. Cell. Mater. *30*, 163–186.

Meyer, E.G., Buckley, C.T., Thorpe, S.D., and Kelly, D.J. (2010). Low oxygen tension is a more potent promoter of chondrogenic differentiation than dynamic compression. J. Biomech. *43*, 2516–2523.

Middleton, J.C., and Tipton, A.J. (2000). Synthetic biodegradable polymers as orthopedic devices. Biomaterials *21*, 2335–2346.

Minas, T., Gomoll, A.H., Rosenberger, R., Royce, R.O., and Bryant, T. (2009). Increased Failure Rate of Autologous Chondrocyte Implantation After Previous Treatment With Marrow Stimulation Techniques. Am. J. Sports Med. *37*, 902–908.

Miot, S., Scandiucci de Freitas, P., Wirz, D., Daniels, A.., Sims, T.., Hollander, A.., Mainil-Varlet, P., Heberer, M., and Martin, I. (2006). Cartilage Tissue Engineering by Expanded Goat Articular Chondrocytes. J. Orthop. Res. *24*, 1078–1085.

Mithoefer, K., McAdams, T., Williams, R.J., Kreuz, P.C., and Mandelbaum, B.R. (2009). Clinical Efficacy of the Microfracture Technique for Articular Cartilage Repair in the Knee. Am. J. Sports Med. *37*, 2053–2063.

Mo, X.T., Guo, S.C., Xie, H.Q., Deng, L., Zhi, W., Xiang, Z., Li, X.Q., and Yang, Z.M. (2009). Variations in the ratios of co-cultured mesenchymal stem cells and chondrocytes regulate the expression of cartilaginous and osseous phenotype in alginate constructs. Bone *45*, 42–51.

Mobasheri, A., Rayman, M.P., Gualillo, O., Sellam, J., van der Kraan, P., and Fearon, U. (2017). The role of metabolism in the pathogenesis of osteoarthritis. Nat. Rev. Rheumatol. *13*, 302–311.

Moran, C.J., Ramesh, A., Brama, P.A.J., O'Byrne, J.M., O'Brien, F.J., and Levingstone, T.J. (2016). The benefits and limitations of animal models for translational research in cartilage repair. J. Exp. Orthop. *3*, 1.

Moroni, L., De Wijn, J.R., and Van Blitterswijk, C.A. (2006). 3D fiber-deposited scaffolds for tissue engineering: Influence of pores geometry and architecture on dynamic mechanical properties. Biomaterials *27*, 974–985.

Moroni, L., Boland, T., Burdick, J.A., De Maria, C., Derby, B., Forgacs, G., Groll, J., Li, Q., Malda, J., Mironov, V.A., et al. (2017). Biofabrication: A Guide to Technology and Terminology. Trends Biotechnol. 1–19.

Moskowitz, R.W., Davis, W., Sammarco, J., Martens, M., Baker, J., Mayor, M., Burstein, A.H., and Frankel, V.H. (1973). Experimentally Induced Degenerative Joint Lesions Following Partial Meniscectomy in the Rabbit. Arthritis Rheum. *16*, 397–405.

Moskowitz, R.W., Howell, D.S., Goldberg, V.M., Muniz, O., and Pita, J.C. (1979). Cartilage Proteoglycan Alterations In An Experimentally Induced Model Of Rabbit Osteoarthritis. Arthritis Rheum. *22*, 155–163.

Mouser, V.H.M., Melchels, F.P.W., Visser, J., Dhert, W.J.A., Gawlitta, D., and Malda, J. (2016). Yield stress determines bioprintability of hydrogels based on gelatin-methacryloyl and gellan gum for cartilage bioprinting. Biofabrication *8*, 35003.

Mow, V.C., and Guo, X.E. (2002). Mechano-electrochemical properties of articular cartilage: their inhomogeneities and anisotropies. Annu. Rev. Biomed. Eng. *4*, 175–209.

Mow, V.C., and Huiskes, R. (2005). Basic orthopaedic biomechanics & mechano-biology

(Philadelphia: Lippincott Williams & Wilkins).

Mow, V., Kuei, S., Lai, W., and Armstrong, C. (1980). Biphasic creep and stress relaxation of articular cartilage in compression: Theory and experiments. J. Biomech. Eng. *102*, 73–84.

Mow, V.C., Ratcliffe, A., and Poole, A.R. (1992a). Cartilage and diarthrodial joints as paradigms for hierarchical materials and structures. Biomaterials *13*, 67–97.

Mow, V.C., Ratcliffe, A., and Poole, A.R. (1992b). Cartilage and diarthrodial joints asa paradigms for hierarchical materials and structures. Biomaterials *13*, 67–97.

Mow, V.C., Wang, C.C., and Hung, C.T. (1999). The extracellular matrix, interstitial fluid and ions as a mechanical signal transducer in articular cartilage. Osteoarthr. Cartil. *7*, 41–58.

Murphy, C.L., and Polak, J.M. (2004). Control of Human Articular Chondrocyte Differentiation by Reduced Oxygen Tension. J. Cell. Physiol. *199*, 451–459.

Murphy, S. V, and Atala, A. (2014). 3D bioprinting of tissues and organs. Nat. Biotechnol. *32*, 773–785.

Murphy, J.M., Dixon, K., Beck, S., Fabian, D., Feldman, A., and Barry, F. (2002). Reduced chondrogenic and adipogenic activity of mesenchymal stem cells from patients with advanced osteoarthritis. Arthritis Rheum. *46*, 704–713.

Murphy, J.M., Fink, D.J., Hunziker, E.B., and Barry, F.P. (2003). Stem Cell Therapy in a Caprine Model of Osteoarthritis. Arthritis Rheum. *48*, 3464–3474.

Muschler, G.F., Nitto, H., Boehm, C. a., and Easley, K. a. (2001). Age- and gender-related changes in the cellularity of human bone marrow and the prevalence of osteoblastic progenitors. J. Orthop. Res. *19*, 117–125.

Mwale, F., Roughley, P., Antoniou, J., Alini, M., Hollander, A., Kirsch, T., and Stokes, I. (2004). Distinction between the extracellular matrix of the nucleus pulposus and hyaline cartilage: A requisite for tissue engineering of intervertebral disc. Eur. Cells Mater. *8*, 58–64.

Nair, L.S., and Laurencin, C.T. (2007). Biodegradable polymers as biomaterials. Prog. Polym. Sci. *32*, 762–798.

Nakagawa, Y., Suzuki, T., Kuroki, H., Kobayashi, M., Okamoto, Y., and Nakamura, T. (2007). The effect of surface incongruity of grafted plugs in osteochondral grafting: A report of five cases. Knee Surgery, Sport. Traumatol. Arthrosc. *15*, 591–596.

Naqvi, S.M., and Buckley, C.T. (2015a). Differential response of encapsulated nucleus pulposus and bone marrow stem cells in isolation and coculture in alginate and chitosan hydrogels.

Tissue Eng. Part A *21*, 288–299.

Naqvi, S.M., and Buckley, C.T. (2015b). Extracellular matrix production by nucleus pulposus and bone marrow stem cells in response to altered oxygen and glucose microenvironments. J. Anat. *227*, 757–766.

Naqvi, S.M., and Buckley, C.T. (2016). Bone Marrow Stem Cells in Response to Intervertebral Disc-Like Matrix Acidity and Oxygen Concentration. Spine (Phila. Pa. 1976). *41*, 743–750.

Nehrer, S., Spector, M., and Minas, T. (1999). Histologic analysis of tissue after failed cartilage repair procedures. Clin. Orthop. Relat. Res. 149–162.

Ng, J.J., Wei, Y., Zhou, B., Bernhard, J., Robinson, S., Burapachaisri, A., Guo, X.E., and Vunjak-Novakovic, G. (2017). Recapitulation of physiological spatiotemporal signals promotes in vitro formation of phenotypically stable human articular cartilage. Proc. Natl. Acad. Sci. *114*, 201611771.

Nichol, J.W., Koshy, S., Bae, H., Hwang, C.M., and Khademhosseini, A. (2010). Cell-laden microengineered gelatin methacrylate hydrogels. Biomaterials *31*, 5536–5544.

Norwegian National Advisory Unit on Arthoplasty and Hip Fractures (2017). Annual Report 2017.

O'Brien, F.J. (2011). Biomaterials & scaffolds for tissue engineering. Mater. Today *14*, 88–95.

Obradovic, B., Martin, I., Padera, R.F., Treppo, S., Freed, L.E., and Vunjak-Novakovic, G. (2001). Integration of engineered cartilage. J. Orthop. Res. *19*, 1089–1097.

Oliveira, S.M., Mijares, D.Q., Turner, G., Amaral, I.F., Barbosa, M. a, and Teixeira, C.C. (2009a). Engineering endochondral bone: in vitro studies. Tissue Eng. Part A *15*, 635–643.

Oliveira, S.M., Mijares, D.Q., Turner, G., Amaral, I.F., Barbosa, M. a, and Teixeira, C.C. (2009b). Engineering endochondral bone: in vivo studies. Tissue Eng. Part A *15*, 635–643.

Olubamiji, A.D., Izadifar, Z., Si, J.L., Cooper, D.M.L., Eames, B.F., and Chen, D.X. (2016). Modulating mechanical behaviour of 3D-printed cartilage-mimetic PCL scaffolds: influence of molecular weight and pore geometry. Biofabrication *8*, 25020.

Olvera, D., Daly, A., and Kelly, D.J. (2015). Mechanical Testing of Cartilage Constructs. Methods Mol. Biol. *1340*, 279–287.

Orth, P., Cucchiarini, M., Kaul, G., Ong, M.F., Gräber, S., Kohn, D.M., and Madry, H. (2012). Temporal and spatial migration pattern of the subchondral bone plate in a rabbit osteochondral defect model. Osteoarthr. Cartil. *20*, 1161–1169.

Orth, P., Rey-Rico, A., Venkatesan, J.K., Madry, H., and Cucchiarini, M. (2014). Current perspectives in stem cell research for knee cartilage repair. Stem Cells Cloning Adv. Appl. *7*, 1–17.

Ouyang, L., Yao, R., Zhao, Y., and Sun, W. (2016a). Effect of bioink properties on printability and cell viability for 3D bioplotting of embryonic stem cells. Biofabrication *8*, 35020.

Ouyang, L., Highley, C.B., Sun, W., and Burdick, J.A. (2016b). A Generalizable Strategy for the 3D Bioprinting of Hydrogels from Nonviscous Photo-crosslinkable Inks. Adv. Mater. 1604983.

Pan, Z., and Ding, J. (2012). Poly(lactide-co-glycolide) porous scaffolds for tissue engineering and regenerative medicine. Interface Focus *2*, 366–377.

Papalia, R., Buono, A. Del, Osti, L., and Denaro, V. (2011). Meniscectomy as a risk factor for knee osteoarthritis : a systematic review. Br. Med. Bull. *99*, 89–106.

Park, K.M., and Gerecht, S. (2014). Hypoxia-inducible hydrogels. Nat. Commun. *5*, 4075.

Park, J.S., Yang, H.N., Jeon, S.Y., Woo, D.G., Na, K., and Park, K.H. (2010). Osteogenic differentiation of human mesenchymal stem cells using RGD-modified BMP-2 coated microspheres. Biomaterials *31*, 6239–6248.

Park, S.H., Park, D.S., Shin, J.W., Kang, Y.G., Kim, H.K., Yoon, T.R., and Shin, J.W. (2012). Scaffolds for bone tissue engineering fabricated from two different materials by the rapid prototyping technique: PCL versus PLGA. J. Mater. Sci. Mater. Med. *23*, 2671–2678.

Paschos, N.K., Brown, W.E., Eswaramoorthy, R., Hu, J.C., and Athanasiou, K.A. (2014). Advances in tissue engineering through stem cell-based co-culture. J. Tissue Eng. Regen. Med.

Pati, F., Jang, J., Ha, D.-H., Won Kim, S., Rhie, J.-W., Shim, J.-H., Kim, D.-H., and Cho, D.-W. (2014). Printing three-dimensional tissue analogues with decellularized extracellular matrix bioink. Nat. Commun. *5*, 1–11.

Pelttari, K., Winter, A., Steck, E., Goetzke, K., Hennig, T., Ochs, B.G., Aigner, T., and Richter, W. (2006). Premature induction of hypertrophy during in vitro chondrogenesis of human mesenchymal stem cells correlates with calcification and vascular invasion after ectopic transplantation in SCID mice. Arthritis Rheum. *54*, 3254–3266.

Peterson, L., Brittberg, M., Kiviranta, I., Akerlund, E.L., and Lindahl, A. (2002). Autologous chondrocyte transplantation. Biomechanics and long-term durability. Am J Sport. Med *30*, 2–12.

Pittenger, M., Mackay, A., Beck, S., Jaiswal, R., Douglas, R., Mosca, J., Moorman, M., Simonetti, D., Craig, S., and Marshak, D. (1999). Multilineage potential of adult human mesenchymal stem

cells. Science *284*, 143–147.

Place, E.S., Evans, N.D., and Stevens, M.M. (2009). Complexity in biomaterials for tissue engineering. Nat. Mater. *8*, 457–470.

Plumb, M.S., and Aspden, R.M. (2005). The response of elderly human articular cartilage to mechanical stimuli in vitro. Osteoarthr. Cartil. *13*, 1084–1091.

Poldervaart, M.T., Wang, H., Van Der Stok, J., Weinans, H., Leeuwenburgh, S.C.G., Oner, F.C., Dhert, W.J.A., and Alblas, J. (2013). Sustained release of BMP-2 in bioprinted alginate for osteogenicity in mice and rats. PLoS One *8*.

Poole, C. a (1997). Articular cartilage chondrons: form, function and failure. J. Anat. *191*, 1–13.

Poole, R., Blake, S., Buschmann, M., Goldring, S., Laverty, S., Lockwood, S., Matyas, J., McDougall, J., Pritzker, K., Rudolphi, K., et al. (2010). Recommendations for the use of preclinical models in the study and treatment of osteoarthritis. Osteoarthr. Cartil. *18*, S10–S16.

Proffen, B.L., McElfresh, M., Fleming, B.C., and Murray, M.M. (2012). A comparative anatomical study of the human knee and six animal species. Knee *19*, 493–499.

Qui, Y.S., Shahgaldi, B.F., Revell, W.J., and Heatley, F.W. (2003). Observations of subchondral plate advancement during osteochondral repair: A histomorphometric and mechanical study in the rabbit femoral condyle. Osteoarthr. Cartil. *11*, 810–820.

Reyes, R., Pec, M.K., Sánchez, E., del Rosario, C., Delgado, A., and Évora, C. (2012). Comparative, osteochondral defect repair: Stem cells versus chondrocytes versus bone morphogenetic protein-2, solely or in combination. Eur. Cells Mater. *25*, 351–365.

Robins, J.C., Akeno, N., Mukherjee, A., Dalal, R.R., Aronow, B.J., Koopman, P., and Clemens, T.L. (2005). Hypoxia induces chondrocyte-specific gene expression in mesenchymal cells in association with transcriptional activation of Sox9. Bone *37*, 313–322.

Roemhildt, M.L., Coughlin, K.M., Peura, G.D., Fleming, B.C., and Beynnon, B.D. (2006). Material properties of articular cartilage in the rabbit tibial plateau. J. Biomech. *39*, 2331–2337.

Sabatino, M.A., Santoro, R., Gueven, S., Jaquiery, C., Wendt, D.J., Martin, I., Moretti, M., and Barbero, A. (2012). Cartilage graft engineering by co-culturing primary human articular chondrocytes with human bone marrow stromal cells. J. Tissue Eng. Regen. Med. *9*, 1394–1403.

Sailor, L.Z., Hewick, R.M., and Morris, E.A. (1996). Recombinant human bone morphogenetic protein-2 maintains the articular chondrocyte phenotype in long-term culture. J. Orthop. Res. *14*, 937–945.

Sandell, L.J., and Aigner, T. (2001). Articular cartilage and changes in arthritis. An introduction: cell biology of osteoarthritis. Arthritis Res. *3*, 107–113.

Santoro, R., Olivares, A.L., Brans, G., Wirz, D., Longinotti, C., Lacroix, D., Martin, I., and Wendt, D. (2010). Bioreactor based engineering of large-scale human cartilage grafts for joint resurfacing. Biomaterials *31*, 8946–8952.

Schaefer, L., and Schaefer, R.M. (2010). Proteoglycans: From structural compounds to signaling molecules. Cell Tissue Res. *339*, 237–246.

Schiavone Panni, A., Cerciello, S., Vasso, M., and Tartarone, M. (2009). Stiffness in total knee arthroplasty. J. Orthop. Traumatol. *10*, 111–118.

Schinkothe, T., Bloch, W., and Schmidt, A. (2008). In vitro secreting profile of human mesenchymal stem cells. Stem Cells Dev. *17*, 199–206.

Schnabel, M., Marlovits, S., Eckhoff, G., Fichtel, I., Gotzen, L., Vécsei, V., and Schlegel, J. (2002). Dedifferentiation-associated changes in morphology and gene expression in primary human articular chondrocytes in cell culture. Osteoarthr. Cartil. *10*, 62–70.

Schrobback, K., Klein, T.J., Crawford, R., Upton, Z., Malda, J., and Leavesley, D.I. (2012). Effects of oxygen and culture system on in vitro propagation and redifferentiation of osteoarthritic human articular chondrocytes. Cell Tissue Res. *347*, 649–663.

Schumacher, B.L., Block, J.A., Schmid, T.M., Aydelotte, M.B., and Kuettner, K.E. (1994). A Novel Proteoglycan Synthesized and Secreted by Chondrocytes of the Superficial Zone of Articular Cartilage. Arch. Biochem. Biophys. *311*, 144–152.

Schuurman, W., Khristov, V., Pot, M.W., van Weeren, P.R., Dhert, W.J. a, and Malda, J. (2011). Bioprinting of hybrid tissue constructs with tailorable mechanical properties. Biofabrication *3*, 21001.

Schuurman, W., Levett, P. a., Pot, M.W., van Weeren, P.R., Dhert, W.J. a, Hutmacher, D.W., Melchels, F.P.W., Klein, T.J., and Malda, J. (2013). Gelatin-methacrylamide hydrogels as potential biomaterials for fabrication of tissue-engineered cartilage constructs. Macromol. Biosci. *13*, 551–561.

Scotti, C., Tonnarelli, B., Papadimitropoulos, A., Scherberich, A., Schaeren, S., Schauerte, A., Lopez-Rios, J., Zeller, R., Barbero, A., and Martin, I. (2010). Recapitulation of endochondral bone formation using human adult mesenchymal stem cells as a paradigm for developmental engineering. Proc. Natl. Acad. Sci. U. S. A. *107*, 7251–7256.

Seung, H.H., Yun, H.K., Min, S.P., In, A.K., Jung, W.S., Woo, I.Y., Kyoung, S.J., Ki, D.P., Gyu, H.R., and

Lee, J.W. (2008). Histological and biomechanical properties of regenerated articular cartilage using chondrogenic bone marrow stromal cells with a PLGA scaffold in vivo. J. Biomed. Mater. Res. - Part A *87*, 850–861.

Shao, X., Goh, J., Hutmacher, D.W., Lee, H., and Zigang, G. (2006). Repair of Large Articular Osteochondral Defects Using Hybrid Scaffolds and Bone Marrow-Derived Mesenchymal Stem Cells in a Rabbit Model. Tissue Eng. *1539–1551*, 6.

Shasteen, C., and Choy, Y. Bin (2011). Controlling degradation rate of poly(lactic acid) for its biomedical applications. Biomed. Eng. Lett. *1*, 163–167.

Shearer, H., Ellis, M.J., Perera, S.P., and Chaudhuri, J.B. (2006). Effects of Common Sterilization Methods on the Structure and Properties of Poly(D,L Lactic-Co-Glycolic Acid) Scaffolds. Tissue Eng. *12*, 2717–2727.

Sheehy, E.J., Buckley, C.T., and Kelly, D.J. (2012). Oxygen tension regulates the osteogenic, chondrogenic and endochondral phenotype of bone marrow derived mesenchymal stem cells. Biochem. Biophys. Res. Commun. *417*, 305–310.

Sheehy, E.J., Vinardell, T., Toner, M.E., Buckley, C.T., and Kelly, D.J. (2014). Altering the architecture of tissue engineered hypertrophic cartilaginous grafts facilitates vascularisation and accelerates mineralisation. PLoS One *9*, 1–10.

Sheehy, E.J., Mesallati, T., Kelly, L., Vinardell, T., Buckley, C.T., and Kelly, D.J. (2015a). Tissue Engineering Whole Bones Through Endochondral Ossification: Regenerating the Distal Phalanx. Biores. Open Access *4*, 229–241.

Sheehy, E.J., Mesallati, T., Vinardell, T., and Kelly, D.J. (2015b). Engineering cartilage or endochondral bone: A comparison of different naturally derived hydrogels. Acta Biomater. *13*, 245–253.

Shim, J.-H., Jang, K.-M., Hahn, S.K., Park, J.Y., Jung, H., Oh, K., Park, K.M., Yeom, J., Park, S.H., Kim, S.W., et al. (2016). Three-dimensional bioprinting of multilayered constructs containing human mesenchymal stromal cells for osteochondral tissue regeneration in the rabbit knee joint. Biofabrication *8*, 14102.

Shim, J.H., Moon, T.S., Yun, M.J., Jeon, Y.C., Jeong, C.M., Cho, D.W., and Huh, J.B. (2012). Stimulation of healing within a rabbit calvarial defect by a PCL/ PLGA scaffold blended with TCP using solid freeform fabrication technology. J. Mater. Sci. Mater. Med. *23*, 2993–3002.

Shimomura, K., Ando, W., Tateishi, K., Nansai, R., Fujie, H., Hart, D.A., Kohda, H., Kita, K., Kanamoto, T., Mae, T., et al. (2010). The influence of skeletal maturity on allogenic synovial mesenchymal stem cell-based repair of cartilage in a large animal model. Biomaterials *31*,

8004–8011.

Shimomura, K., Moriguchi, Y., Ando, W., Nansai, R., Fujie, H., Hart, D., Gobbi, a, Kita, K., Horibe, S., Shino, K., et al. (2014). Osteochondral Repair Using a Scaffold-Free Tissue-Engineered Construct Derived from Synovial Mesenchymal Stem Cells and a Hydroxyapatite-Based Artificial Bone. Tissue Eng Part A *0*, 2291–2305.

Shiomi, T., Nishii, T., Tamura, S., Tanaka, H., Murase, K., Yoshikawa, H., and Sugano, N. (2012). Influence of medial meniscectomy on stress distribution of the femoral cartilage in porcine knees : a 3D reconstructed T2 mapping study. Osteoarthr. Cartil. *20*, 1383–1390.

van Sliedregt, A., Knook, M., Hesseling, S.C., Koerten, H.K., de Groot, K., and van Blitterswijk, C.A. (1992). Cellular reaction on the intraperitoneal injection of four types of polylactide particulates. Biomaterials *13*, 819–824.

Soltz, M. a., and Ateshian, G. a. (1998). Experimental verification and theoretical prediction of cartilage interstitial fluid pressurization at an impermeable contact interface in confined compression. J. Biomech. *31*, 927–934.

Sommerfeldt, D., and Rubin, C. (2001). Biology of bone and how it orchestrates the form and function of the skeleton. Eur. Spine J. *10*, 86–95.

Spiller, K.L., Maher, S.A., and Lowman, A.M. (2011). Hydrogels for the Repair of Articular Cartilage Defects. Tissue Eng. Part B Rev. *17*, 281–299.

Spitters, T.W.G.M., Mota, C.M.D., Uzoechi, S.C., Slowinska, B., Martens, D.E., Moroni, L., and Karperien, M. (2014). Glucose Gradients Influence Zonal Matrix Deposition in 3D Cartilage Constructs. Tissue Eng. Part A *20*, 3270–3278.

Sridhar, B. V., Brock, J.L., Silver, J.S., Leight, J.L., Randolph, M.A., and Anseth, K.S. (2015). Development of a cellularly degradable PEG hydrogel to promote articular cartilage extracellular matrix deposition. Adv. Healthc. Mater. *4*, 702–713.

Stevens, M.M., Marini, R.P., Schaefer, D., Aronson, J., Shastri, V.P., Stevens, M.M., Marini, R.P., Schaefersil, D., and Langer, R. (2005). In vivo Engineering of Organs : The Bone Bioreactor. PNAS *102*, 11450–11455.

Steward, A.J., Thorpe, S.D., Vinardell, T., Buckley, C.T., Wagner, D.R., and Kelly, D.J. (2012). Cell-matrix interactions regulate mesenchymal stem cell response to hydrostatic pressure. Acta Biomater. *8*, 2153–2159.

Sukegawa, A., Iwasaki, N., Kasahara, Y., Onodera, T., Igarashi, T., and Minami, A. (2012). Repair of Rabbit Osteochondral Defects by an Acellular Technique with an Ultrapurified Alginate Gel

Containing Stromal Cell-Derived Factor-1. Tissue Eng. Part A *18*, 934–945.

Sun, H., Mei, L., Song, C., Cui, X., and Wang, P. (2006). The in vivo degradation, absorption and excretion of PCL-based implant. Biomaterials *27*, 1735–1740.

Sweigart, M. a., Zhu, C.F., Burt, D.M., Deholl, P.D., Agrawal, C.M., Clanton, T.O., and Athanasiou, K. a (2004). Intraspecies and interspecies comparison of the compressive properties of the medial meniscus. Ann. Biomed. Eng. *32*, 1569–1579.

Tabriz, A.G., Hermida, M.A., Leslie, N.R., and Shu, W. (2015). Three-dimensional bioprinting of complex cell laden alginate hydrogel structures. Biofabrication *7*, 45012.

Takahashi, K., Kubo, T., Kobayashi, K., Imanishi, J., Takigawa, M., Arai, Y., and Hirasawa, Y. (1997). Hydrostatic pressure influences mRNA expression of transforming growth factor-beta 1 and heat shock protein 70 in chondrocyte-like cell line. J. Orthop. Res. *15*, 150–158.

Tallheden, T., Bengtsson, C., Brantsing, C., Sjögren-Jansson, E., Carlsson, L., Peterson, L., Brittberg, M., and Lindahl, A. (2005). Proliferation and differentiation potential of chondrocytes from osteoarthritic patients. Arthritis Res. Ther. *7*, R560-8.

Tanaka, T., Hirose, M., Kotobuki, N., Tadokoro, M., Ohgushi, H., Fukuchi, T., Sato, J., and Seto, K. (2009). Bone augmentation by bone marrow mesenchymal stem cells cultured in three-dimensional biodegradable polymer scaffolds. J. Biomed. Mater. Res. - Part A *91*, 428–435.

Teeple, E., Jay, G.D., Elsaid, K.A., and Fleming, B.C. (2013). Animal Models of Osteoarthritis: Challenges of Model Selection and Analysis. AAPS J. *15*, 438–446.

Thorpe, S.D., Nagel, T., Carroll, S.F., and Kelly, D.J. (2013a). Modulating Gradients in Regulatory Signals within Mesenchymal Stem Cell Seeded Hydrogels: A Novel Strategy to Engineer Zonal Articular Cartilage. PLoS One *8*.

Thorpe, S.D., Nagel, T., Carroll, S.F., and Kelly, D.J. (2013b). Modulating Gradients in Regulatory Signals within Mesenchymal Stem Cell Seeded Hydrogels: A Novel Strategy to Engineer Zonal Articular Cartilage. PLoS One *8*.

Tsuchiya, K., Chen, G., Ushida, T., Matsuno, T., and Tateishi, T. (2004). The effect of coculture of chondrocytes with mesenchymal stem cells on their cartilaginous phenotype in vitro. Mater. Sci. Eng. C *24*, 391–396.

Varghese, F., Bukhari, A.B., Malhotra, R., and De, A. (2014). IHC profiler: An open source plugin for the quantitative evaluation and automated scoring of immunohistochemistry images of human tissue samples. PLoS One *9*.

Varoni, E., Tschon, M., Palazzo, B., Nitti, P., Martini, L., and Rimondini, L. (2012). Agarose gel as

biomaterial or scaffold for implantation surgery: characterization, histological and histomorphometric study on soft tissue response. Connect. Tissue Res. *53*, 548–554.

Vieira, A.C., Vieira, J.C., Ferra, J.M., Magalhães, F.D., Guedes, R.M., and Marques, A.T. (2011). Mechanical study of PLA-PCL fibers during in vitro degradation. J. Mech. Behav. Biomed. Mater. *4*, 451–460.

Vinardell, T., Sheehy, E.J., Buckley, C.T., and Kelly, D.J. (2012a). A comparison of the functionality and in vivo phenotypic stability of cartilaginous tissues engineered from different stem cell sources. Tissue Eng. Part A *18*, 1161–1170.

Vinardell, T., Rolfe, B.A., Buckley, C.T., Meyer, E.G., Ahearne, M., Murphy, P., and Kelly, D.J. (2012b). Hydrostatic pressure acts to stabilize a chondrogenic phenotype in porcine joint tissue derived stem cells. Eur. Cells Mater. *23*, 121–132.

Visser, J., Peters, B., Burger, T.J., Boomstra, J., Dhert, W.J.A., Melchels, F.P.W., and Malda, J. (2013). Biofabrication of multi-material anatomically shaped tissue constructs. Biofabrication *5*, 35007.

Visser, J., Melchels, F.P.W., Jeon, J.E., van Bussel, E.M., Kimpton, L.S., Byrne, H.M., Dhert, W.J. a, Dalton, P.D., Hutmacher, D.W., and Malda, J. (2015a). Reinforcement of hydrogels using three-dimensionally printed microfibres. Nat. Commun. *6*, 6933.

Visser, J., Melchels, F.P.W., Jeon, J.E., van Bussel, E.M., Kimpton, L.S., Byrne, H.M., Dhert, W.J. a., Dalton, P.D., Hutmacher, D.W., and Malda, J. (2015b). Reinforcement of hydrogels using three-dimensionally printed microfibres. Nat. Commun. *6*, 6933.

Visser, J., Levett, P.A., te Moller, N.C.R., Besems, J., Boere, K.W.M., van Rijen, M.H.P., de Grauw, J.C., Dhert, W.J.A., van Weeren, P.R., and Malda, J. (2015c). Crosslinkable hydrogels derived from cartilage, meniscus, and tendon tissue. Tissue Eng. Part A *21*, 1195–1206.

Vos, T., Allen, C., Arora, M., Barber, R.M., Bhutta, Z.A., Brown, A., Carter, A., Casey, D.C., Charlson, F.J., Chen, A.Z., et al. (2016). Global, regional, and national incidence, prevalence, and years lived with disability for 310 diseases and injuries, 1990-2015: a systematic analysis for the Global Burden of Disease Study 2015. Lancet *388*, 1545–1602.

Wakitani, S., Goto, T., Pineda, S.J., Young, R.G., Mansour, J.M., Caplan, a I., and Goldberg, V.M. (1994). Mesenchymal cell-based repair of large, full-thickness defects of articular cartilage. J. Bone Joint Surg. Am. *76*, 579–592.

Wakitani, S., Goto, T., Young, R.G., Mansour, J.M., Ph, D., Goldberg, V.M., and Caplan, A.I. (1998). Defects with Allograft Articular Chondrocytes. Tissue Eng *4*, 429–444.

Walsh, D.A., Bonnet, C.S., Turner, E.L., Wilson, D., Situ, M., and McWilliams, D.F. (2007). Angiogenesis in the synovium and at the osteochondral junction in osteoarthritis. Osteoarthr. Cartil. *15*, 743–751.

Wang, C.C.-B., Deng, J.-M., Ateshian, G. a, and Hung, C.T. (2002). An automated approach for direct measurement of two-dimensional strain distributions within articular cartilage under unconfined compression. J. Biomech. Eng. *124*, 557–567.

Wang, J., Zhang, F., Tsang, W.P., Wan, C., and Wu, C. (2017). Fabrication of injectable high strength hydrogel based on 4-arm star PEG for cartilage tissue engineering. Biomaterials *120*, 11–21.

Wang, W., Li, B., Yang, J., Xin, L., Li, Y., Yin, H., Qi, Y., Jiang, Y., Ouyang, H., and Gao, C. (2010). The restoration of full-thickness cartilage defects with BMSCs and TGF-beta 1 loaded PLGA/fibrin gel constructs. Biomaterials *31*, 8964–8973.

Wang, X., Ye, K., Li, Z., Yan, C., and Ding, J. (2013). Adhesion, proliferation, and differentiation of mesenchymal stem cells on RGD nanopatterns of varied nanospacings. Organogenesis *9*, 280–286.

Wei, X., and Messner, K. (1999). Maturation-dependent durability of spontaneous cartilage repair in rabbit knee joint. J. Biomed. Mater. Res. *46*, 539–548.

Wei, J., Wang, J., Su, S., Wang, S., Qiu, J., Zhang, Z., Christopher, G., Ning, F., Cong, W., Noyes, F.R., et al. (2015). 3D printing of an extremely tough hydrogel. RSC Adv. *5*, 81324–81329.

Wei Xu, Xiaohong Wang, Yongnian Yan, Wei Zheng, Zhuo Xiong, Feng Lin, Rendong Wu, and Renji Zhang (2007). Rapid Prototyping Three-Dimensional Cell/Gelatin/Fibrinogen Constructs for Medical Regeneration. J. Bioact. Compat. Polym. *22*, 363–377.

Weiss, S., Hennig, T., Bock, R., Steck, E., and Richter, W. (2010). Impact of growth factors and PTHrP on early and late chondrogenic differentiation of human mesenchymal stem cells. J. Cell. Physiol. *223*, 84–93.

Whitney, G.A., Mera, H., Weidenbecher, M., Awadallah, A., Mansour, J.M., and Dennis, J.E. (2012). Methods for producing scaffold-free engineered cartilage sheets from auricular and articular chondrocyte cell sources and attachment to porous tantalum. Biores. Open Access *1*, 157–165.

Whitney, G.A., Kean, T.J., Fernandes, R.J., Waldman, S., Tse, M.Y., Pang, S.C., Mansour, J.M., and Dennis, J.E. (2017). Thyroxine Increases Collagen Type II Expression and Accumulation in Scaffold-Free Tissue-Engineered Articular Cartilage. Tissue Eng. Part A ten.tea.2016.0533.

de Windt, T.S., Hendriks, J. a. a., Zhao, X., Vonk, L. a., Creemers, L.B., Dhert, W.J. a., Randolph, M.

a., and Saris, D.B.F. (2014). Concise Review: Unraveling Stem Cell Cocultures in Regenerative Medicine: Which Cell Interactions Steer Cartilage Regeneration and How? Stem Cells Transl. Med. *3*, 723–733.

Wittenauer, R., Smith, L., and Aden, K. (2013). Priority Medicines for Europe and the World " A Public Health Approach to Innovation " Update on 2004 Background Paper Background Paper 6.12 Osteoarthritis. World Heal. Organ. 1–31.

Wolfram, U., and Schwiedrzik, J. (2016). Post-yield and failure properties of cortical bone. Bonekey Rep. *5*, 1–10.

Woodfield, T.B.F., Guggenheim, M., Von Rechenberg, B., Riesle, J., Van Blitterswijk, C.A., and Wedler, V. (2009). Rapid prototyping of anatomically shaped, tissue-engineered implants for restoring congruent articulating surfaces in small joints. Cell Prolif. *42*, 485–497.

Woodruff, M.A., and Hutmacher, D.W. (2010). The return of a forgotten polymer - Polycaprolactone in the 21st century. Prog. Polym. Sci. *35*, 1217–1256.

Worthley, D.L., Churchill, M., Compton, J.T., Tailor, Y., Rao, M., Si, Y., Levin, D., Schwartz, M.G., Uygur, A., Hayakawa, Y., et al. (2015). Gremlin 1 identifies a skeletal stem cell with bone, cartilage, and reticular stromal potential. Cell *160*, 269–284.

Wu, D.D., Burr, D.B., Boyd, R.D., and Radin, E.L. (1990). Bone and cartilage changes following experimental varus or valgus tibial angulation. J. Orthop. Res. *8*, 572–585.

Wu, L., Leijten, J.C.H., Georgi, N., Post, J.N., van Blitterswijk, C. a, and Karperien, M. (2011). Trophic effects of mesenchymal stem cells increase chondrocyte proliferation and matrix formation. Tissue Eng. Part A *17*, 1425–1436.

Wu, L., Leijten, J., Blitterswijk, C.A. Van, and Karperien, M. (2013). Fibroblast Growth Factor-1 Is a Mesenchymal Stromal Cell-Secreted Factor Stimulating Proliferation of Osteoarthritic Chondrocytes in Co-Culture. *22*, 2356–2367.

Wu, Y., Joseph, S., and Aluru, N.R. (2009). Effect of Cross-Linking on the Diffusion of Water , Ions , and Small Molecules in Hydrogels Effect of Cross-Linking on the Diffusion of Water , Ions , and Small Molecules in Hydrogels. Molecules 3512–3520.

Wylde, V., Dieppe, P., Hewlett, S., and Learmonth, I.D. (2007). Total knee replacement: Is it really an effective procedure for all? Knee *14*, 417–423.

Xin, X., Hussain, M., and Mao, J.J. (2007). Continuing differentiation of human mesenchymal stem cells and induced chondrogenic and osteogenic lineages in electrospun PLGA nanofiber scaffold. Biomaterials *28*, 316–325.

Yang, J., Zhang, Y.S., Yue, K., and Khademhosseini, A. (2016). Cell-laden hydrogels for osteochondral and cartilage tissue engineering. Acta Biomater.

Yao, S., Ph, D., Alini, M., Ph, D., Stoddart, M.J., Ph, D., Li, Z., Yao, S., Alini, M., and Stoddart, M.J. (2010). Chondrogenesis of human bone marrow mesenchymal stem cells in fibrin-polyurethane composites is modulated by frequency and amplitude of dynamic compression and shear stress. Tissue Eng. Part A *16*, 575–584.

Yoo, J.U., Barthel, T.S., Nishimura, K., Solchaga, L., Caplan, a I., Goldberg, V.M., and Johnstone, B. (1998). The chondrogenic potential of human bone-marrow-derived mesenchymal progenitor cells. J. Bone Joint Surg. Am. *80*, 1745–1757.

Yu, Y., Moncal, K.K., Li, J., Peng, W., Rivero, I., Martin, J. a, and Ozbolat, I.T. (2016). Three-dimensional bioprinting using self-assembling scalable scaffold-free “tissue strands” as a new bioink. Sci. Rep. *6*, 28714.

Yue, K., Trujillo-de Santiago, G., Alvarez, M.M., Tamayol, A., Annabi, N., and Khademhosseini, A. (2015). Synthesis, properties, and biomedical applications of gelatin methacryloyl (GelMA) hydrogels. Biomaterials *73*, 254–271.

Zhou, X., Nowicki, M., Cui, H., Zhu, W., Fang, X., Miao, S., Lee, S.-J., Keidar, M., and Zhang, L.G. (2017). 3D bioprinted graphene oxide-incorporated matrix for promoting chondrogenic differentiation of human bone marrow mesenchymal stem cells. Carbon N. Y. *116*, 615–624.

Zuk, P. (2001). Multilineage cells from human adipose tissue: implications for cell-based therapies. Tissue Eng. *7*, 211–228.

Supplementary Figures

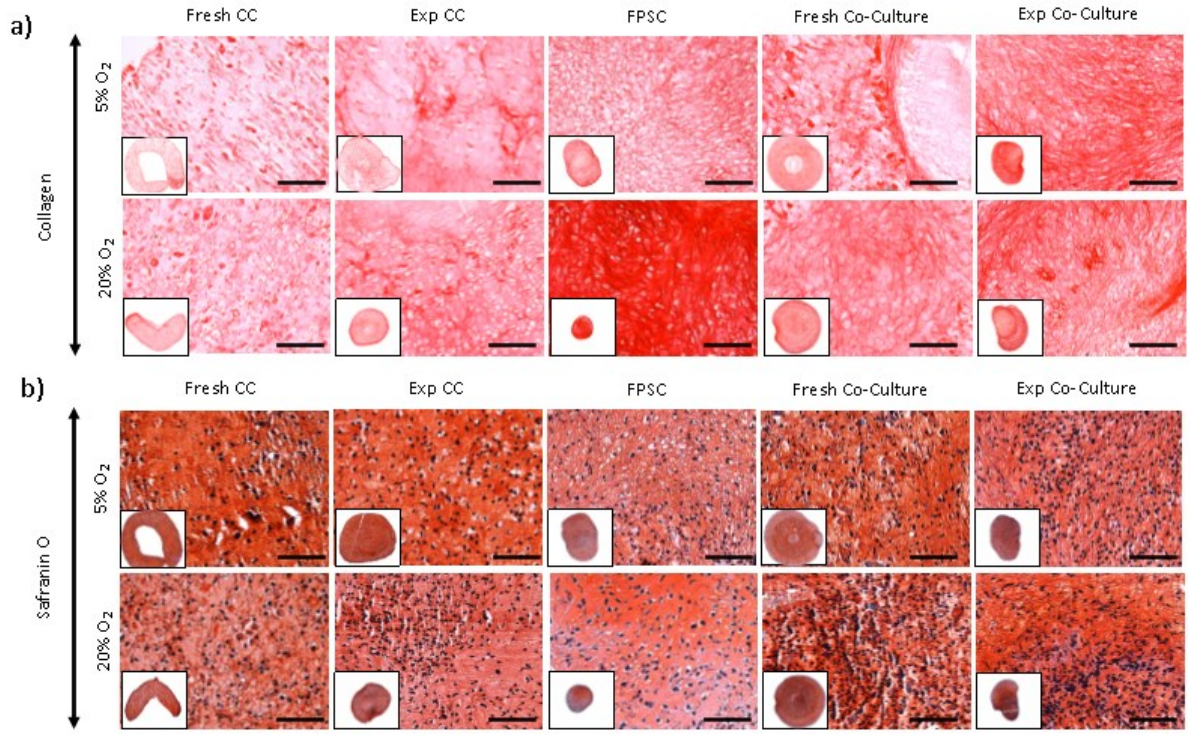

Figure S 1 |Histological staining from chapter 5: *a) Picro-sirius red for collagen b) safranin O for sGAG*

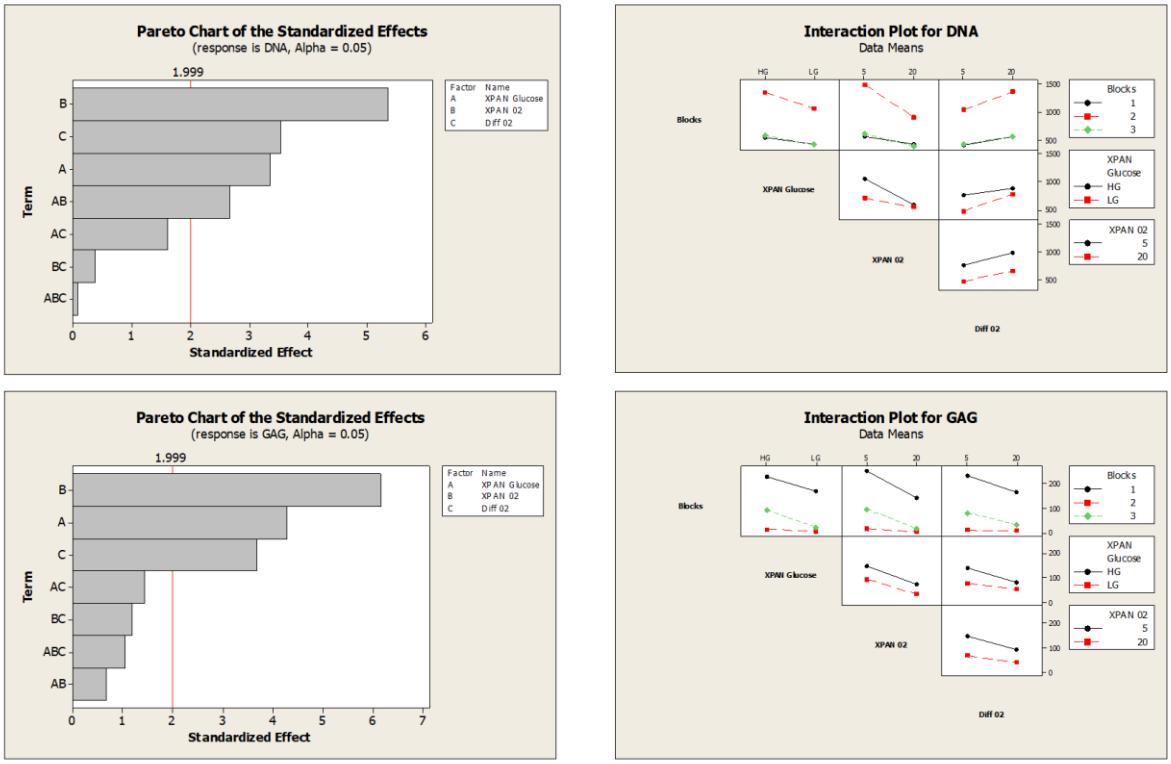

Figure S 2| From chapter7: Pareto charts for factors affecting DNA and sGAG for all 3 donors

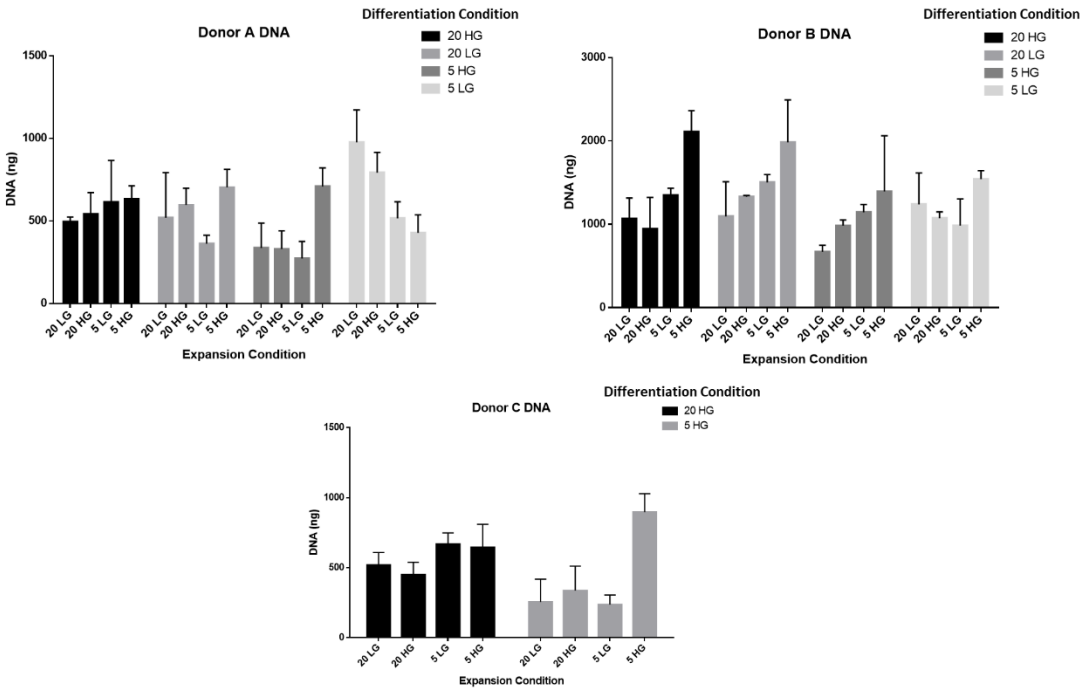

Figure S 3|From chapter 7: DNA values for individual donors

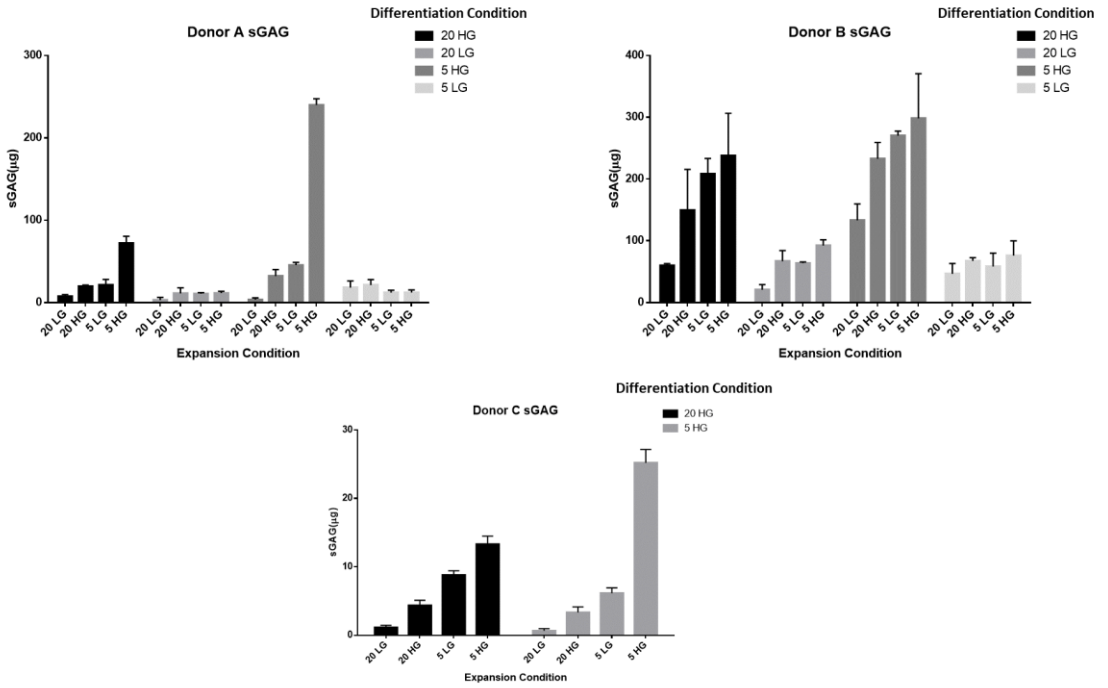

Figure S 4| From chapter 7: sGAG values for individual donors

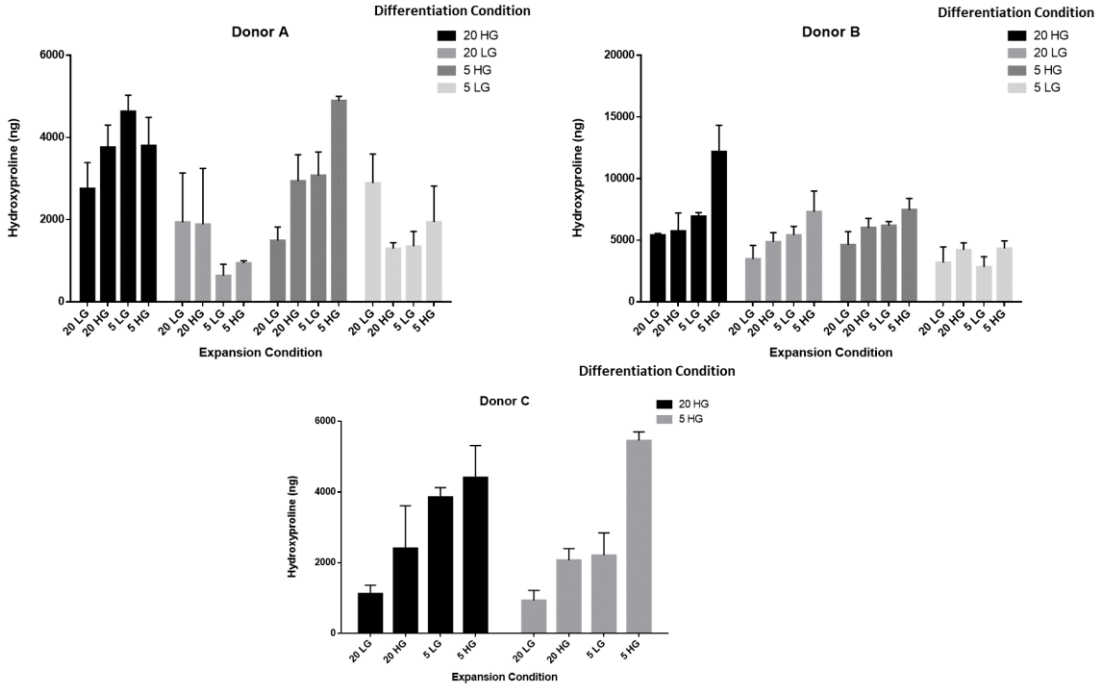

Figure S 5| From chapter 7: Hydroxyproline values for individual donors

d